ELECTROCRYSTALLIZATION OF CHROMIUM FROM MOLTEN SALTS

BY

José Tomás Vargas Valero, M.Sc., D.I.C.

A thesis submitted for the degree of Doctor of Philosophy in the University of London

Department of Metallurgy and Materials Science
Royal School of Mines
Imperial College of Science and Technology
London

1984

To Tatiana

ABSTRACT

The electrocrystallization of chromium on different foreign substrates in the LiCl-KCl eutectic melt at 450°C, was studied. The chromium, present in the electrolyte as chromium(II) ions, was introduced either by anodic dissolution of aqueous electrolytic chromium or by the addition of $CrCl_2$. The study was directed towards determining the relationship between the electrochemical parameters of the process and the mechanism of formation of the electrodeposit and its final morphology. The system was studied using electrochemical methods, sweep voltammetry and chronoamperometry, complemented with the characterization of the electrodeposits using microscopic techniques.

The electrocrystallization of chromium under potentiostatic conditions was found to occur according to the following steps: I) initial three-dimensional nuclei formation with growth controlled by the diffusion of chromium (II) ions in the melt, ii) termination of the nucleation stage and attaining of a final saturation nucleus density, iii) building up into a macrodeposit by the growth of initially formed nuclei. The electrolytic nucleation kinetics was well described according to the classical nucleation theory. The final saturation nucleus density was found to be limited by the growth of nucleation exclusion zones around the nuclei, which was in agreement with the obtaining of lower nucleus densities as the solute concentration increased.

Based on the determined mechanism of chromium electrocrystallization, adequate operating conditions for the electrodeposition of improved chromium coatings were selected, which resulted in the obtaining of coherent, crack-free, non-dendritic electrodeposits, which adhered well.

CONTENTS

Page

LIST OF FIGURES

LIST OF TABLES

MAJOR SYMBOLS

a^2	area of one atomic site, cm^2
A	instant area of deposition, cm^2
C	solute concentration, $mol.dm^{-3}$
C^s	solution concentration at the electrode surface, $mol.dm^{-3}$
$C_o(O,t)$	concentration of species O at the electrode surface, $mol.dm^{-3}$
$C_R(O,t)$	concentration of species R at the electrode surface, $mol.dm^{-3}$
D	diffusion coefficient of electrodepositing species, $cm^2.s^{-1}$
e	charge of the electron, C
E	potential applied to the electrode (w.r.t. reference electrode), V
E^o	formal potential of an electrode, V
$E^o_{M/M^{z+}}$	equilibrium potential of the infinite electrode M, V
E_p	peak potential, V
F	Faraday constant, $C.mol^{-1}$
$\Delta G(n_k)$	Gibbs free energy (per atom) of critical nuclei formation (homogeneous nucleation), μJ
$\Delta G_{2,k}$	Gibbs free energy (per atom) of two-dimensional critical nuclei formation, μJ
$\Delta G_{3,k}$	Gibbs free energy (per atom) of three-dimensional critical nuclei formation, μJ
i	current density $A.cm^{-2}$, $mA.cm^{-2}$

i_o	exchange current density, $A.cm^{-2}$
I,I(t)	current A, mA
$I_i(t)$	individual growth current to nucleus i, A, mA
I_p	peak current value in cyclic voltammetry, A, mA
I_o	steady state nucleation rate per unit area, $cm^{-2}.s^{-1}$
J	nucleation rate per centre, s^{-1}
J_o	steady state nucleation rate per centre, s^{-1}
k	Boltzmann constant, JK^{-1}
k^o	standard heterogeneous rate constant, $cm.s^{-1}$
M	molecular weight of depositing material
M'	constant defined by equation 2.76
n	number of atoms in the forming nucleus
n_k	number of atoms in the critical nucleus (homogeneous nucleation)
$n_{2,k}$	number of atoms in the two-dimensional critical nucleus
$n_{3,k}$	number of atoms in the three-dimensional critical nucleus
N,N(t)	number of nuclei at the time t
N_S	saturation nucleus density
r	radial distance from the centre of a spherical electrode, cm
r_o	radius of the spherical electrode, cm
R	molar gas constant, $J.mol^{-1}\ K^{-1}$
S	electrode surface (substrate), cm^{-2}
S(t)	substrate surface not covered by nucleation exclusion zones, cm^{-2}

t	time, s
t_N	length of nucleation pulse, s
t_G	length of growth pulse, s
t_{cl}	length of cleaning pulse, s
t_r	length of resting period, s
t_o	experimental induction time, s
T	absolute temperature, K
u	age of nucleus, s
v	linear potential scan rate, $V.s^{-1}$
x	distance, cm
z	valence number
z_o	initial number of nucleation centres
$z(t)$	number of nucleation centres at time t

Greek Symbols

α	transfer coefficient
β	adhesion, defined according to equation 2.34, $\mu J.cm^{-2}$
η	overpotential, V, mV
η_N	nucleation overpotential, V, mV
η_G	growth overpotential, V, mV
η_{cl}	cleaning overpotential, V, mV
η_r	resting overpotential, V, mV
μ_a	chemical potential (per atom) of ambient phase, μJ
μ_c	chemical potential (per atom) of the infinite crystal of deposited phase, μJ
$\Delta\mu$	supersaturation, μJ
ρ	density of deposited material, gr. cm^{-3}

σ	specific surface energy of the deposited material, $\mu J.cm^{-2}$
σ_s	specific surface energy of the substrate, $\mu J.cm^{-2}$
σ_i	specific surface energy of the substrate-deposit interphase, $\mu J.cm^{-2}$
$\Delta\sigma$	surface energy change, $\mu J.cm^{-2}$
τ	induction time, s
Φ	constant, defined by equation 2.59.
$\varphi_{1/2}$	work of separation of one atom from the infinite large crystal.
φ_i^*	work of separation of one atom from a complex of i atoms
φ_a	work of separation of one atom from the surface of the indifferent electrode
φ_v	work of separation of one atom from the two-dimensional complex of v atoms

1. INTRODUCTION

1.1. FOREWORD

The aim of the present work has been to obtain protective chromium electrodeposits from the molten LiCl-KCl eutectic in the context of a research programme directed towards the production of protective metal coatings on AGR fuel cans.

The AGR fuel cans in an advanced gas-cooled reactor are subjected to fluctuating temperatures which can reach up to $\sim 800^{o}C$ under CO_2 atmospheres containing small fractions of CO, CH_3 and H_2O. 20/25 niobium stabilized stainless steel, which is used as the fuel cladding alloy, suffers the deleterious effects of oxidation and carbon deposition reactions[1] under these conditions. The structural damage to the AGR fuel cans may have serious economic consequences, especially if the shortening of their serviceable life eventually becomes a limiting factor in the length of the reactor cycle.

One of the most effective methods for the protection of metals from corrosion appears to be the application of a protective layer of another metal which is resistant to the chemical and/or electrochemical activities of the medium concerned. The refractory metals, namely metals with a high melting point, generally have outstanding mechanical and anti-corrosive properties which make them suitable materials to be used as protective coatings. Chromium metal is especially suitable in the present case

as it offers good protection against oxidation and its presence has an inhibiting effect on the carbon deposition reaction[2]. In addition chromium is a refractory metal relatively cheap and readily available[3].

The protective action of chromium can only be fully utilized if the coatings obtained are both coherent and of good adherence, so that they provide a thorough coverage of the substrate. Chromium coatings with such characteristics are not easily obtained by conventional methods. On the one hand chromium electrodeposits from aqueous solutions are not free from porosity and cracks and protection in corrosive atmospheres is provided, at least in part, by the nickel undercoat on which the chromium is normally plated. They are unsuitable for use at high temperatures because they do not provide a uniform and reliable protection against oxidation[4,5]. On the other hand, the chromizing process leads to the formation of coatings which are protective, adherent and resistant to thermal shock[6]. Nevertheless, the high operating temperature involved in this method prohibits its use on AGR fuel cans as it would result in the recrystallization of the fuel cladding alloy[7].

In the present work an alternative method of obtaining protective coatings by the electrodeposition of chromium from molten salts has been studied, using the LiCl-KCl eutectic mixture as electrolyte. A process of this kind so far appears to offer promising characteristics.

1.2. THE ELECTRODEPOSITION OF METALS FROM MOLTEN SALTS

Besides the conventional methods of metal-plating, e.g. hot plating in molten salts or the electroplating from aqueous solutions, in the last two decades the possibility of electrolytic metal-plating in fused salts has been intensively studied both with traditional materials such as tin, zinc and aluminium and with others such as the refractory metals. The electrodeposition of metals in molten salts has a number of advantages in relation to the electrolytic operation and the characteristics of the deposit obtained, which have been extensively analysed[8-11]. They can be summarised in the following ways:

i) the high stability of these solvents[12-14] (large decomposition voltage) and their low gas solubility, reduce the incidence of side-reactions in the process so that electrolysis at high current efficiency can take place. This can be three or four times higher than in aqueous solutions[8].

ii) the electrodeposition reactions in molten salts usually show high exchange current densities[15] which, in addition to the use of high solute concentrations (molten salts are powerful solvents for inorganic materials[10]), enable the system to work at high deposition rates and with a better 'throwing power' (or ability to plate uniformly over an intricate surface[8,16,17]).

iii) Metallic coatings obtained by conventional electroplating commonly have flaws such as pinholes (porosity), and are susceptible to pitting of the underlying metal layers by galvanic action. Electrocoating from molten salts produces better anti-corrosion properties in the deposited metal[8], freedom from stress due to undisturbed crystal growth and thus high purity and ductility[9], and the ability to deposit thick films on a wide variety of substrates.

iv) The binding between the deposited metal and the base metal is improved due to a property common to many fused salts, that of dissolving the oxide films and moisture films from the substrate[9] (particularly in the case of fluoride melts). In addition, one is able to produce diffusion layers, whenever the temperature and the deposition rate are adjusted to the diffusion rate of the deposited metal into the substrate[18-21].

v) The good ionic conductivity ($2\text{-}9(\Omega cm)^{-1}$) for a molten solvent[22] ensures that, with good cell design, Joule heating in the cell can be used in a controlled way to provide the necessary heat input to the cell contents. The low cathodic overvoltages[23] are also a desirable factor from the point of view of energy efficiency.

vi) In comparison with hot dipping and gas or pack cementation processes, electrodeposition in molten salts has the possible advantage of independent control over the rate of metal deposition[24-30] by changing the cathode

current density or the deposition potential, or the rate of metal diffusion into the substrate, e.g. by changing the temperature. This means an increased ability to obtain the desired structural and morphological characteristics in the final deposit.

vii) The refractory metals cannot be deposited in aqueous solutions (except chromium) since a) their electrodeposition potentials are more negative than hydrogen, b) by taking up oxygen from the environment they become protected by oxide films, c) their metallic ions are often converted to stable oxy-cations, or they undergo redox reactions with water[11]. The molten salts with their wide voltage span for operation, and their ability to offer an oxide-free solvent, constitute an ideal solvent for the electro-deposition of refractory metals, and numerous available processes confirm this view[31].

An electrolytic operation in molten salts also has some disadvantages to be considered. Usually the operation has to be carried out under an inert atmosphere as the hydrolysis of the hygroscopic salts employed[32-34] as solute or solvent can cause difficulties in a large scale operation, therefore the use of more sophisticated and expensive equipment is necessary. Also an expensive purification of the melt is necessary either initially or during the operation to ensure its long-term range stability[9]. More resistant, and usually more expensive, electrical and insulating materials for the cell components are required[35], considering the high solvent power of

molten salts which can act as an active corrosive media especially at high temperatures of operation. The high temperatures can also have detrimental effects on the substrate either through quick surface attack or by changing its internal structure. As the electrodeposition in molten salts usually occurs under mass transfer control, the deposits arise in a dendritic form[36] unless special precautions are taken. The obtaining of dendritic deposits in molten salts introduce a major inconvenience: as the dendritic deposit occlude solidified melt a major drag-out of salts occurs and an additional leaching-type operation is needed afterwards to separate the pure metal[36]. In addition, dendritic deposits mean that the cathodes are dimensionally unstable which may lead to lower current efficiencies and even, in extreme cases, to shorting the cell[37,38]. Of course if the electrodeposition is intended to produce protective metal coatings, dendritic deposits must be avoided. The electrodeposition under conditions of mass transfer can be avoided by the introduction of a slow irreversible step in the cathodic reduction to metal as in the case of the Mellors-Sendderoff process in fluorides[39].

Powdery deposits can also arise in electrodeposition in molten salts which originate in secondary electrode processes either involving disproportionation reactions near the surface or chemical reactions between deposited alkali metals and metal ions away from the electrode surfaces[10].

For practical purposes and especially when considering the possibility of a large scale process, a series of additional properties and attributes are necessary in a molten bath, such as low vapour pressure, low melting point, low viscosity, non-corrosion and the ability to be readily-purified, non-polluting (non-toxic), and inexpensive. So in spite of the very wide range of molten inorganic solvents, the choice of suitable solvents and solutes to be used in an electrolytic operation can be confined to the alkali and alkaline earth halides and their mixtures with aluminium halides[22]. In practice a great part of the basic research and development of electroplating operations in molten salts has been focused until now on the use of chlorides and fluorides melts[40].

1.3. ELECTROREFINING OF CHROMIUM IN MOLTEN SALTS

The electrolysis of chromium in molten salt baths has been carried out successfully with the object of electrorefining various impure chromium materials. The production of 99.8% pure chromium containing 0.12% oxygen was reported by Horizon Inc.,[41] using $KCrF_3$-NaCl electrolyte at 750°C and an inert atmosphere. High-purity chromium product containing 0.01% oxygen and 0.002% nitrogen was prepared by electrorefining aqueous electrolytic chromium in helium-atmosphere cells equipped with graphite liners, using an NaCl-$CrCl_2$ electrolyte at 800°C[42]. A NaCl-KCl melts at 950°C was used for the same purpose[43] and a product was obtained with a quality comparable to that of chromium produced by the iodine process. Other chromium materials

such as its carbides and aluminothermically-reduced forms have been electrorefined in NaCl-$CrCl_2$, KCl-LiCl-$CrCl_2$ melts and NaCl-$CrCl_2$ melts respectively, obtaining chromium efficiently and with good purity[44,45].

LiCl-KCl mixtures have been used with positive results for electrorefining electrolytic chromium obtained in aqueous solutions. Working in a LiCl-KCl eutectic mixture at 450°C, under an inert atmosphere and using $CrCl_3$ as solute, aqueous electrolytic chromium was refined with a current efficiency of 88%[46]. It was shown that the impurity content was greatly reduced; dissolved oxygen and nitrogen, which are the main impurities in the starting material, were reduced from 0.1% to 0.02% for oxygen and from 0.05% to 0.0005% for nitrogen.

An improved molten salt electrolytic refining process was developed for the preparation of high-purity chromium, using a KCl-LiCl-$CrCl_2$ electrolyte[47]. After testing other chloride mixtures such as KBr-NaBr-$CrCl_2$, $BaCl_2$-KCl-NaCl-$CrCl_2$, the electrorefining data indicated that the KCl-LiCl-$CrCl_2$ electrolyte was superior to the others with respect to lower operating temperature, higher cathode/current efficiency, higher cell conductivity and less electrolytic dragout with deposits. Chromium of greater than 99.99% purity was prepared by electro-refining commercial aqueous electrolytic chromium in electrolytes containing 22% and 45% $CrCl_2$, at 520°C under a helium atmosphere. The applied initial current density was of 40-210 $A.ft^{-2}$ and the average current efficiency

and chromium recovery were 96% and 99%, respectively. Table 1.1 shows the analysis of feed material and refined chromium in these experiments. The quality of the chromium obtained in this way was comparable to that of chromium prepared commercially by the iodide refining process[48]: the hydrogen and oxygen content on the iodide-refined chromium was lower than that presented here for the electrorefined chromium, but the reverse was true for the carbon and nitrogen content of the metal. The deposit always presented a highly dendritic structure and no attempts were made to control the morphology of the final deposit.

1.4. ELECTROCHEMISTRY OF CHROMIUM IN THE LiCl-KCl EUTECTIC

Chromium (III), chromium (II) and chromium (0) were studied in LiCl-KCl eutectic at 450°C for solutions over a concentration range of 1×10^{-2} to 5×10^{-2} M, using polarography[49]. It was shown that chromium (II) is the stable specie over the potential range of -0.3 to -1.5 V, that chromium (III) is an oxidant at potentials more negative than -0.3 V and that chromium metal is the stable species in the potential region negative to -1.5 V (potentials with respect to Pt/Pt 0.001 M). The process of chromium electrodeposition was found to be reversible and to occur without alloy formation.

Potentiostatic measurements were carried out[50] and the following standard potentials were determined using Pt/Pt(II) 1 M as reference electrode:

TABLE 1.1. Analysis of chromium feed material and refined chromium (ppm) in LiCl-KCl-$CrCl_2$ melts.[47]

	22% $CrCl_2$ electrolyte		45% $CrCl_2$ electrolyte	
	Feed material	Product	Feed material	Product
Aluminium	<5	*	<5	*
Carbon	70	<5	5	<5
Copper	<5	<5	*	*
Hydrogen	48	1	113	1
Iron	10	10	10	<10
Magnesium	8	6	10	8
Manganese	5	<5	5	5
Nickel	5	<5	<5	<5
Nitrogen	130	2	2	2
Oxygen	640	13	1180	18
Silicon	<10	*	<10	*

*Below detection limits of emission spectrography.

E^{o} Cr(II)/Cr(0) = -1.425 V

E^{o} Cr(III/Cr(II) = -0.525 V

The couple Cr(II/Cr(0) gives rise to experimental Nernst plots in agreement with the theoretical ones for n=2, but for the case of Cr(III)/Cr(II) the corresponding n value was greater than one. Other measurements also using potentiostatic techniques[51] determined E^{o} Cr(III)/Cr(II) = -0.5392 (ref. Pt/Pt(II)1M), and the value obtained for the Nernst slope was in better agreement with the theoretical one for n=1. In this case the solutions of known Cr(III)/Cr(II) ratios were prepared by cathodic reduction of Cr(III) or anodic oxidation of Cr(II) at constant potential, while in the former case (ref. 50) a constant current method was used. The couple Cr(III)/Cr(0) was found to exhibit unstable equilibrium potentials[52] because of the oxidizing effect of the Cr(III) ion which attacks the metal.

Different aspects of the reduction of chromium (III) ions to metal have been studied. According to coulometric studies on the anodic dissolution of chromium metal, the electrolytic oxidation of chromium (II) and the reduction of chromium (III), together with experiments on the stoichiometric reaction between chromium (III) and chromium metal, the electrolytic reduction of chromium (III) was found to have two steps[49]. Using linear sweep voltametry the steps involved in the reduction of chromium (III) ions were found to be:[53]

$$Cr^{+3} + e \rightarrow Cr^{+2} \qquad 1.1$$

$$Cr^{+2} + 2e \rightarrow Cr^{o} \qquad 1.2$$

These reactions were seen to occur reversibly only up to a sweep rate of 1 $V.sec^{-1}$. The diffusion coefficient of the chromium (III) ions in the melt was found to be 0.4×10^{-5} $cm^2.sec^{-1}$ at 450°C. In another sweep voltametric study, carried out at 500°C on a vitreous carbon electrode, the following reaction scheme was proposed[54]:

$$Cr^{+3} + e \underset{}{\overset{\text{fast}}{\rightleftharpoons}} Cr^{+2} \qquad 1.3$$

$$Cr^{+2} + Cl^{-} \rightleftharpoons CrCl_2 \qquad 1.4$$

$$Cr^{+2} + 2e^{-} \rightleftharpoons Cr^{o} \qquad 1.5$$

If the potential is varied slowly enough, an appreciable portion of the Cr^{+2} will react with chloride ions according to reaction 1.4. Rapid changing of the potential, or maintaining the potential at a value negative to that required for reaction 1.5, will result in virtually all the Cr^{+3} being reduced to the metal, since this reaction is kinetically faster than the chemical one. From chronopotentiometric experiments carried out at 500°C in chromium (II) solutions[55,56], the electroreduction of chromium (II) ions was found to be irreversible and rate-controlled by charge transfer. Absorption was also found to be involved in the reduction step, its effect being more pronounced at chromium (II) concentrations higher than approximately 3.5×10^{-2} M, where the exchange current was enhanced. The diffusion coefficient for Cr(II) ions was found to be 1.5×10^{-5} $cm^2.sec^{-1}$.

1.5. CHROMIUM COATINGS FROM $CrCl_2$-LiCl-KCl MELTS

The $CrCl_2$-LiCl-KCl melt is a promising system in which to investigate the electrodeposition of protective chromium coatings as it has advantages in respect to the electrolytic operation and the properties of the chromium obtained .

The use of $CrCl_2$-LiCl-KCl melts allows an operation at relatively low temperatures (400-600^{o}C) which minimises the volatilization from the bath, facilitates the choice of the corrosion-resistant materials for the electrolytic cell and parts, and reduces the heating requirement. Operation at low temperature is also desirable in the present case as the recrystallisation of the fuel cladding alloy during the coating process is prevented. The consumption of electricity per unit of deposited chromium is low as chromium is in the melt in the oxidation state +2 (compared with +3 or +6 in aqueous solutions) and the efficiency of the deposition is nearly 100%. The high solubility of $CrCl_2$ in the system allows the use of a wide range of chromium (II) ion concentrations and a more flexible choice of convenient electrodeposition conditions.

The high-purity chromium obtainable from the $CrCl_2$-LiCl-KCl melts has improved mechanical properties such as low ductile-brittle fracture transition[57], high ductility[58,59] and, because of its low oxygen content, lower hardness[60]. A material with these characteristics seems suitable to form coatings which adapt well to the

substrate topography and are better able to absorb the stresses produced in the substrate-deposit discontinuity when subject to wide temperature changes. In addition the structure of this chromium is likely to be crack-free and of low porosity, which are the main disadvantages of deposits obtained from aqueous solutions. This is because the phenomenon which originates this kind of structures, i.e. codeposition of hydrogen and oxygen[60-63], can be completely prevented in this case.

1.6. AIMS OF THIS WORK

The electrocrystallization aspects of the electrodeposition of chromium in the LiCl-KCl-$CrCl_2$ melts have not yet been analysed. On the one hand the electrometallurgical studies on electrorefining have been directed towards obtaining a high-purity product, but no attempt was made to improve the morphology of the deposit, which is generally highly dendritic. On the other hand, the electrochemical studies, carried out mainly in the LiCl-KCl eutectic, have focused attention basically on the characterization of the kinetics and mechanisms of the electroreduction.

The present work was directed to the study of the mechanism of formation of the chromium electrodeposit, its interdependence with the associated electrode process and its influence on the final morphology of the deposit. The emphasis put here in clarifying the electrogrowth mechanism was justified considering the applied context

of this study, in which the production of chromium electrocoatings of specific morphological characteristics was desired. The study was mainly focused on the mechanism of the initial stages of the electrocrystallization of chromium under potentiostatic conditions, on foreign substrates, employing $CrCl_2$-(LiCl-KCl eutectic) melts at 450^{o}C. The study was approached combining the use of electrochemical methods - chronoamperometry and sweep-voltametry - with the characterisation of the structure of the deposit by means of microscopical observations.

2. ELECTROLYTIC GROWTH OF METALS

2.1. GENERALITIES

In the process of metal electrodeposition on a foreign substrate there are two distinct stages. At the start of the plating process the deposition of the metal will occur on an electrode surface of a different material with formation of nuclei of the new phase and their growth into crystals with the characteristic lattice of the electroplating metal. Once the electrode is fully covered by an initial layer of this metal the deposition will continue as the thickening of this initial layer into a macroscopic deposit; this stage corresponds to an M/M^{n+} electrode. In terms of charge or deposition time, the plating process consists almost entirely of the latter process, but the initial stages are especially important since they determine the structure of the initial layer and thereby influence the structure of the final electroplate and its properties.

The overall transformation, from metal ion in the solution to metal atom in the deposit lattice, is a complex process of phase growth which involves a process of at least four stages (see Figure 2.1.): a) mass transport of the metal ion to the electrode surface, either by diffusion, convection or migration; b) electroreduction of the metal ion in the double layer and formation of an adatom; c) diffusion of the adatoms across the electrode surface; and d) incorporation of adatoms into growing sites.

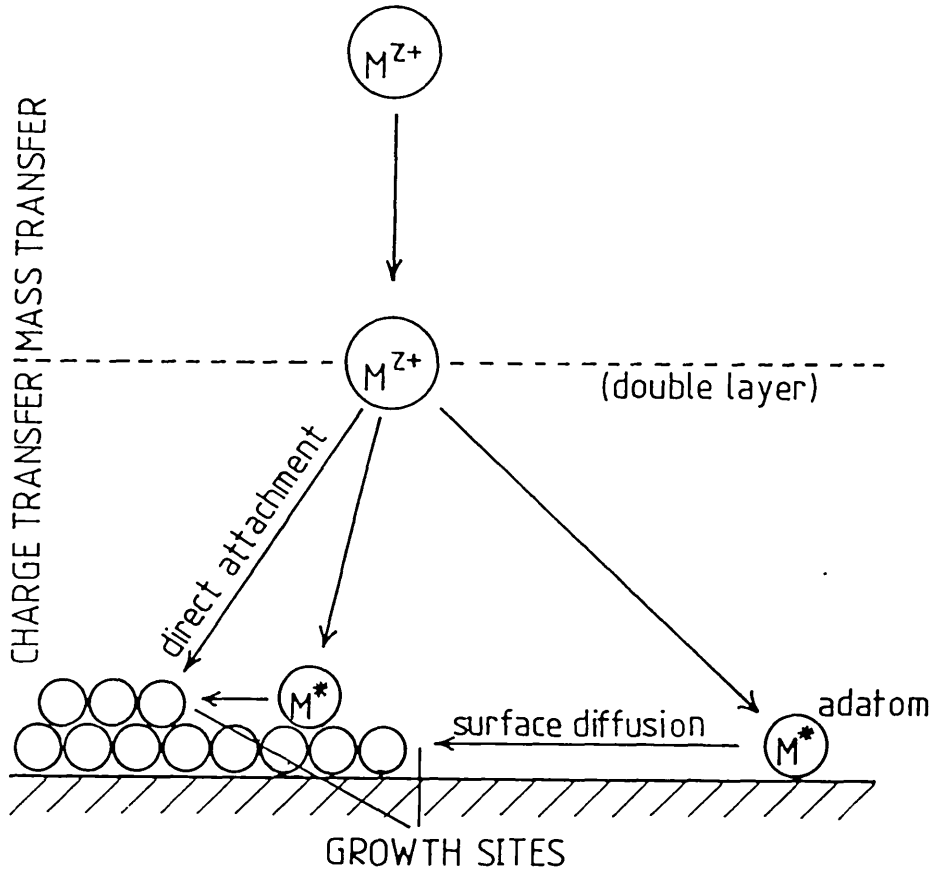

FIGURE 2.1. Schematic diagram showing possible reaction paths for the electrogrowth of metals on a foreign substrate

The electrochemical reduction of the metal ion, represented as the equation:

$$M^{z+} + ze \rightarrow M^{o} \qquad 2.1$$

is just one of the various stages involved in the global process of electrocrystallization.

The adatoms, formed either on the substrate surface or on the deposit surface, diffuse across the surface and incorporate in energetically stable sites where they interact with several other atoms in the growing lattice. Of the sites which are possible in a perfect crystal lattice, incorporation will be most favourable at kink sites (where the atom can interact with three neighbours), although some incorporation will also take place at edge sites (two neighbours). The adatoms are also likely to interact with each other forming new stable clusters, or just redissolve into the solution.

The early stages of electrocrystallization on a foreign substrate usually involve a nucleation mechanism. When a constant potential is applied on the substrate it has been observed that, after an initial induction period, the number of nuclei increase linearly with time at a rate dependent on the overpotential and,at a sufficient length of time,reach a saturation or maximum number. The formation of the initial layer of deposited metal thus involves the simultaneous processes of growth and formation of nuclei, and its structure will depend to some extent on the relative rates of these two competitive

processes. A continuous initial deposit may be attained either through the direct coverage of the substrate by newly created nuclei (path a, Figure 2.2) or, if the termination of the nucleation process occurs before, by growing and coalescence of the nuclei originally formed (path b, Figure 2.2). In addition the nuclei may present different morphologies and their structure may develop various degrees of epitaxy with the substrate. All these factors will determine the characteristics of the initial layers and, to a large extent, the properties of the deposit such as adherence and the degree of coverage (throwing power). The path followed during the early stages of electrogrowth will be related to the conditions of deposition, the relative rates of the intermediate stages involved (see Figure 2.1) and the type of interaction between the substrate and the deposited metal.

Electrocrystallization is a particular case of phase transformation and its theoretical description has relied heavily on ideas derived from studies of other phase transformations, especially vapour deposition. The general theory of phase transformation can be used to describe the electrolytic growth if the basic kinetic and thermodynamic parameters of the process are expressed in the corresponding electrochemical quantities. The fundamental aspects of this theory are here described, together with its application to the description of the initial stages of electrogrowth.

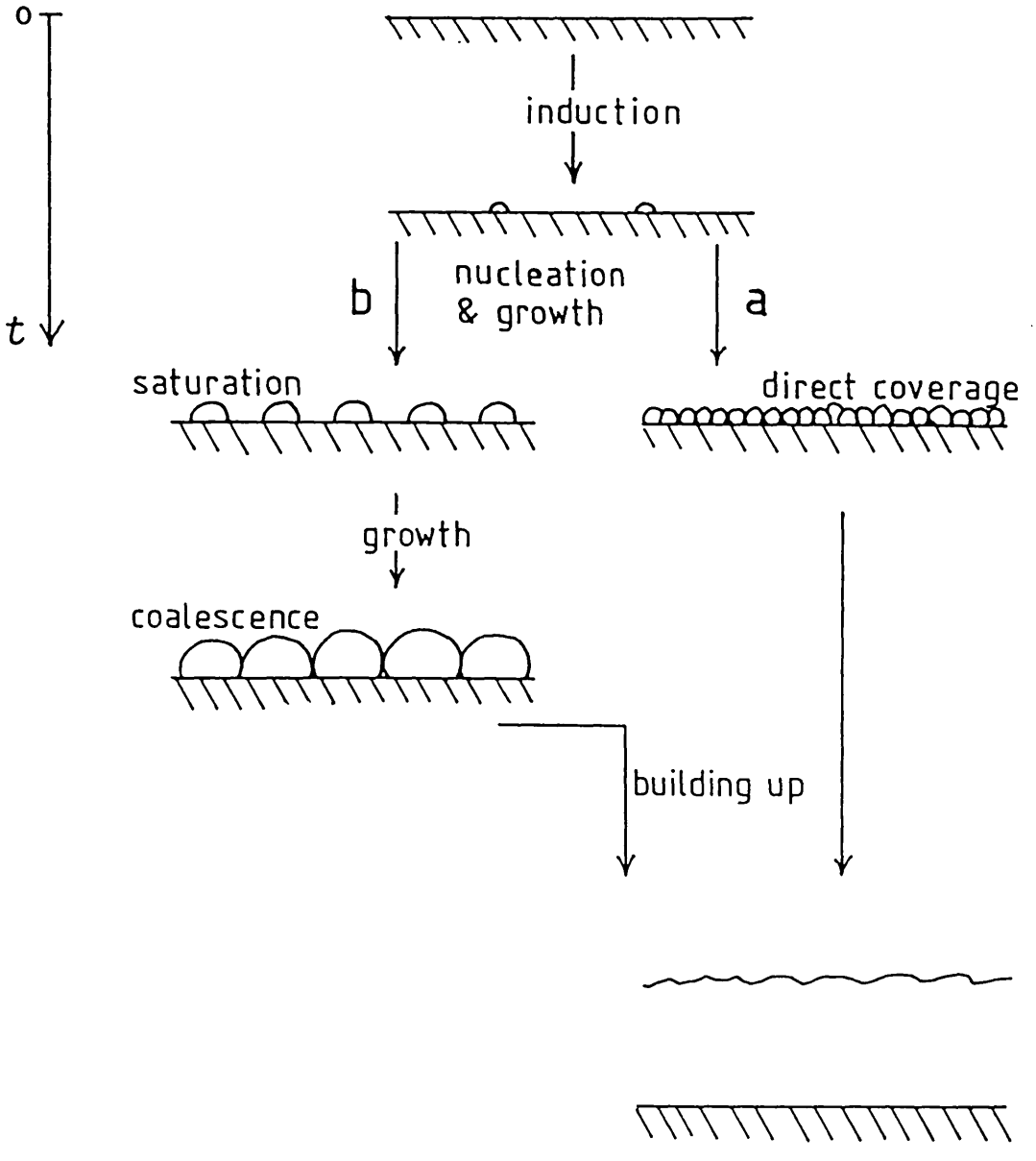

FIGURE 2.2. Scheme showing two possible growth paths followed during the formation of an electrodeposit on a foreign substrate under potentiostatic conditions.

2.2. CLASSICAL THEORY OF NUCLEATION

2.2.1. Thermodynamical Theory

The phase transformation begins with the formation and growth of discrete clusters of the new phase. The Gibbs free energy of a cluster consists of two terms[64].

$$G = G_{bulk} + G_{surface} \qquad 2.2$$

Considering for the sake of simplicity a cluster consisting of a simple cubic crystal of n atoms ($n^{1/3}$ per edge) G(n) is given by the expression

$$G(n) = n\ \mu_c + 6n^{2/3} a^2 \sigma \qquad 2.3$$

where μ_c is the chemical potential (per atom) of the infinite crystal phase, a^2 is the area occupied by one atom on the face of the crystal and σ is the specific surface free energy of the crystal-ambient phase boundary. For sufficiently small clusters G(n) is higher than the Gibbs free energy $n\mu_a$ of an equivalent number of atoms belonging to the ambient phase, in spite of the fact that μ_c is lower than the chemical potential μ_a of the ambient metastable phase. This is related to the increase of the Gibbs free energy of the cluster due to the formation of a new interphase boundary (second term in 2.3). The difference $\Delta\mu = \mu_a - \mu_c$ represents the supersaturation existing in the system which acts as a driving force for the phase change to occur.

The Gibbs free energy change:

$$\Delta G(n) = -n\,\Delta\mu + 6n^{2/3}.a^2\sigma \qquad 2.4$$

is dependent on the cluster size and initially increases, reaches a maximum and then decreases. The maximum occurs at a 'critical' size of the nucleus determined by:

$$\partial\Delta G/\partial n = 0 = -\Delta\mu + 4n_k^{-1/3}a^2\sigma \qquad 2.5$$

i.e.:

$$n_k = (4a^2\sigma/\Delta\mu)^3 \qquad 2.6$$

The cluster of size n_k is a critical nucleus and the quantity:

$$\Delta G(n_k) = 32(a^2\sigma)^3/\Delta\mu^2 \qquad 2.7$$

is usually referred to as the Gibbs free energy of critical nucleus formation. Since the critical nucleus of size n_k satisfies the condition:

$$\partial\Delta G/\partial n = \partial G/\partial n - \mu_a = 0 \qquad 2.8$$

the chemical potential of the critical nucleus

$$\mu(n_k) = \partial G(n_k)/\partial n \qquad 2.9$$

is equal to the chemical potential μ_a of the metastable phase. The equilibrium between the critical nucleus and the bulk supersaturated phase is unstable since any deviations of the cluster size from the value n_k leads to its spontaneous growth or decay. The chemical potential of the clusters of size $n < n_k$ is higher than μ_a and therefore

they tend to decay. On the other hand the chemical potential of the clusters of size $n > n_k$ is lower than μ_a and their growth is thermodynamically favoured.

2.2.2. Kinetic Theory

Since fluctuation theory can be applied to the region where ΔG is increasing, $\Delta G(n_k)$ will appear as a free energy of activation in expressions for the nucleation rate constant. The statistical probability of formation of a critical nucleus is proportional to $\exp(-\Delta G(n_k)/kT)$ and thus the nucleation rate can be expressed by[65]

$$Jo = Kn \exp(-\Delta G(n_k)/kT) \qquad 2.10$$

A quantitative expression for the pre-exponential factor has been derived[66-69] which is expressed as:

$$Kn = c_k \, w_k \, Z \qquad 2.11$$

where c_k is the equilibrium concentration of critical clusters, w_k is the rate at which monomers impinge on the surface of a critical cluster and Z is a 'non-equilibrium factor' usually referred to as the Zeldovich factor[69].

When a system is subjected to a constant super-saturation, a certain period of time is required to reach a steady state nucleation rate. A time interval is necessary to create a stationary size distribution of embryos of the stable phase[69-72]. The problem of evaluating the non-steady state nucleation rate J(t) has been solved using different assumptions[70,73,74],

but usually the following expression is accepted as the most precise solution[75-77]:

$$J(t) = Jo[1 + 2 \sum_{n=1}^{\infty} (-1)^n \exp(-n^2 t/\tau)] \qquad 2.12$$

Here τ is the non-stationary time lag, known as well as induction and relaxation time and it is defined[77,78] as the time necessary for J(t), the non-steady nucleation rate, to reach a value corresponding to Jo/4. From equation 2.12 it can be deduced that J(t) approaches Jo when $t \geq 5\tau$. The induction time has been evaluated to be[76]:

$$\tau = \varkappa kT/\lambda_k w_k \qquad 2.13$$

Since:

$$\lambda_k = -(\partial^2 \Delta G(n)/\partial n^2)_{n_k} \qquad 2.14$$

the induction time takes the form:

$$\tau = \varkappa' kT\sigma^3/\Delta\mu^4 w_k \qquad 2.15$$

The number of nuclei N as a function of time is given by:

$$N(t) = \int_o^t J(t)dt \qquad 2.16$$

Thus on integrating equation 2.12, the following expression is obtained:

$$N(t) = Jo[t-\pi\tau/6-2\tau \sum_{n=1}^{\infty} (-1)^n/n^2 .\exp(-n^2 t/\tau)] \qquad 2.17$$

when $t > 5\tau$ $N(t)$ can be approximated by a straight line defined by:

$$N(t) = Jo(t - \pi^2\tau/6) \qquad 2.18$$

which allows τ to be determined from an experimental N/t curve.

2.3. MECHANISM OF ELECTROGROWTH

When the phase transformation occurs on a substrate the process of formation and growth of the new phase is fundamentally modified by the surface activity of the inert solid. Heterogeneous nucleation is more favourable than homogeneous nucleation as the presence of the substrate lowers the energetic barrier for critical nuclei formation. In the case of formation of deposits the interaction deposit-substrate plays an important role in defining the mechanism of the phase formation process.

2.3.1. Types of Growth

Three fundamentally different types of growth have been observed during the early stages of thin film formation[79-81] (see Figure 2.3): a) Frank van der Merwe mechanism (FM) or layer by layer growth, b) Stranski-Krastnov mechanism (SK), original formation of a mono- or polymolecular layer without nucleation, which then

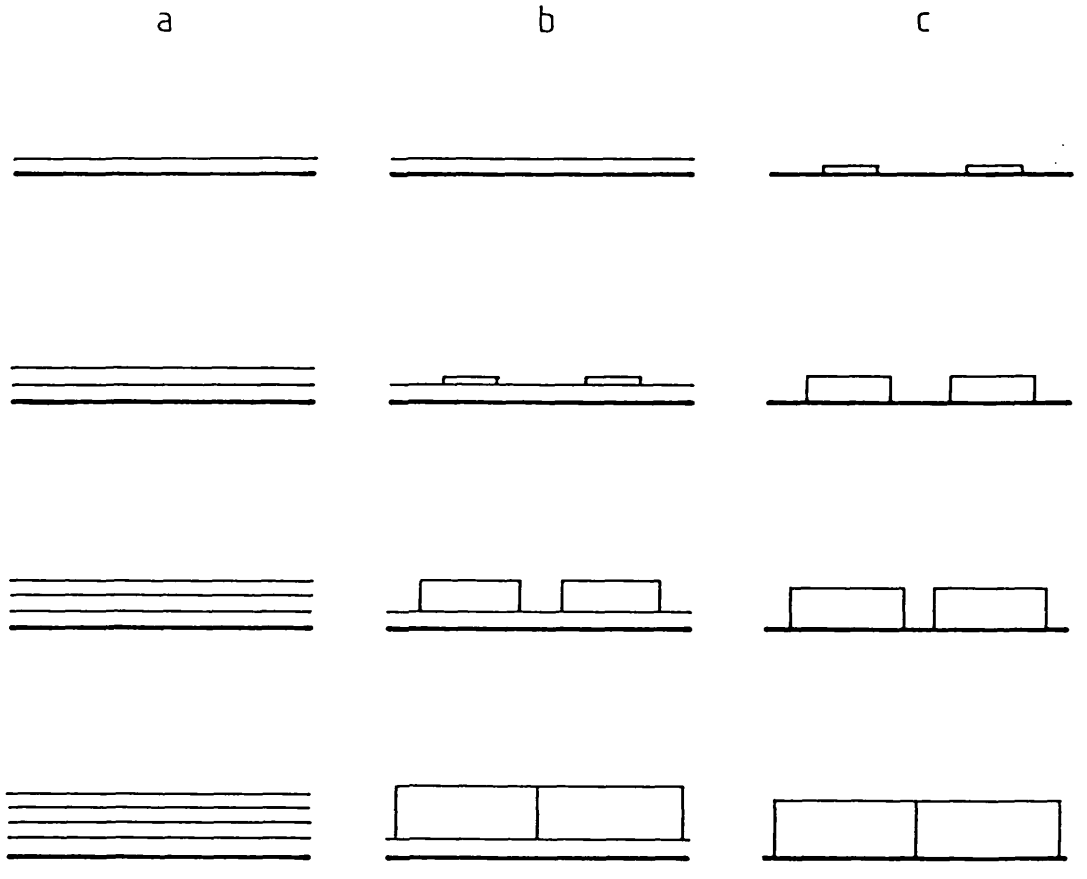

FIGURE 2.3. Basic mechanisms of film growth:
a) Frank van der Merwe mechanism, b) Stranski-Krastanov mechanism, c) Vol mer-Weber mechanism.

leads to the formation of three dimensional nuclei, and c) the Volmer-Weber mechanism (VW), that is the formation of three dimensional nuclei directly on the foreign substrate.

On the basis of thermodynamic analysis Bauer[79] established that if no chemical reaction, no alloying or other change on the surface takes place, the mechanism of film growth is only governed by the interrelation of the specific surface energies of the substrate, σ_s, the deposit, σ, and the substrate-deposit interphase, σ_i, expressed as the surface energy change $\Delta\sigma$:

$$\Delta\sigma = \sigma + \sigma_i - \sigma_s \qquad 2.19$$

When $\Delta\sigma = 0$ the growth occurs under the FM mechanism, which only occurs for materials of the same composition as the substrate. The growth on foreign substrates, on the other hand, should occur according to the S-K mechanism when $\Delta\sigma < 0$ or to the V-W mechanism when $\Delta\sigma > 0$, that is when the deposited material is relatively more strongly bound to the substrate, or to itself, respectively.

However, some additional experimental data concerning the deposition of fcc metals on to fcc metals[82,83] and on to ionic crystals[84] show a transition from island growth (IG) to layer growth (LG) as the saturation increases. This has led to extend the approach of Bauer and to explain the role of the supersaturation $\Delta\mu$

in the mechanism of growth of thin films, on the basis of classical nucleation theory[85-91]. Sufficiently general conclusions on the dependence of the Gibbs free energies of formation of two- and three-dimensional nuclei can be drawn by analysing the simplest case of formation of a cubic cluster on a structureless substrate. When the cluster is large enough the specific surface free energies σ, σ_i, σ_s can be used. If we take a cluster having a height of h atoms and a square base of m atoms per edge (see Figure 2.4), then according to the classical nucleation theory the free energy of formation of a cluster of the new phase is given by

$$\Delta G = -\Delta\mu . m^2 . h + m^2 . a^2 . \sigma + 4\, m . h . a^2 \sigma' + m^2 a^2 \sigma_i - m^2 . a^2 . \sigma_s \qquad 2.20$$

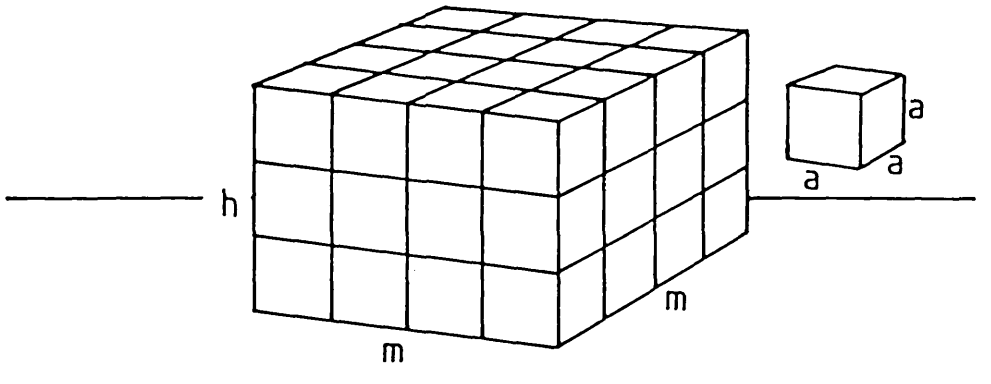

FIGURE 2.4. Representation of the basic three-dimensional cluster.

Assuming for simplicity that the surface energy is the same for every face of the cluster, $\sigma' = \sigma$, and replacing the expression 2.19 for $\Delta\sigma$, equation 2.20 can be rewritten as

$$\Delta G = -\Delta\mu\, m^2\, h + m^2\, a^2\, \Delta\sigma + 4h\, m\, a^2\sigma \qquad 2.21$$

Clearly the condition $\Delta\sigma = 0$ characterises their own substrate; then $\sigma_s = \sigma$ and $\sigma_i = 0$ because of the absence of the interphase deposit/substrate. At $\Delta\sigma < 0$ the substrate even promotes the formation of the cluster and thus the second term in 2.21 is negative too. When $\Delta\sigma > 0$, however, the substrate is inhospitable and a higher supersaturation must be imposed for the presence of the additional positive term $m^2.a^2.\Delta\sigma$ to be compensated. Due to statistical fluctuations two- and three-dimensional clusters of arbitrary dimensions can appear on the substrate and the stable cluster will have the shape that offers the lowest energy barrier to its formation.

By definition the critical three-dimensional nucleus is that cluster which grows in thermodynamic equilibrium and whose height h_k, and edge m_k, satisfy the conditions:

$$(\partial \Delta G)/\partial m)_{h_k, m_k} = (\partial \Delta G/\partial h)_{h_k, m_k} = 0 \qquad 2.22$$

which results in the Gibbs-Thompson equations:

$$m_k = 4\, a^2\, \sigma/\Delta\mu \qquad 2.23$$

$$\text{and} \quad h_k = 2\, a^2\, \Delta\sigma/\Delta\mu \qquad 2.24$$

Therefore the cluster equilibrium shape is characterized by

$$h_k/m_k = \Delta\sigma/2\sigma \qquad 2.25$$

known as the formula of Kaischew[92], and the number of atoms in the critical nucleus will be in this case:

$$n_{3,k} = m_k^2 . h_k = 32a^6\sigma^2\Delta\sigma/\Delta\mu^3 \qquad 2.25$$

Replacing 2.23 and 2.24 in 2.22, the following expression for ΔG_{3k} is obtained:

$$\Delta G_{3,k} = 16\ a^6\sigma^2\Delta\sigma/\Delta\mu^2 \qquad 2.26$$

which corresponds to the Gibbs free energy of formation of the critical three-dimensional nucleus.

In the case of two-dimensional nucleation $h_k = 1$ and the nucleus is that cluster whose edge m_k satisfies the condition:

$$(\partial\Delta G/\partial m)_{1,m_k} = 0 \qquad 2.27$$

which leads in this case to

$$m_k = 2a^2\sigma/(\Delta\mu - a^2\Delta\sigma) \qquad 2.28$$

The number of atoms in the critical nucleus is now

$$n_{2,k} = m_k^2 = 4a^4\sigma^2/(\Delta\mu - a^2\Delta\sigma)^2 \qquad 2.29$$

and the Gibbs free energy of formation of the critical two-dimensional nucleus is thus

$$\Delta G_{2,k} = 4a^4\sigma^2/(\Delta\mu - a^2\Delta\sigma) \qquad 2.30$$

The formation of two- or three-dimensional nuclei will be preferential depending on the relative values of $\Delta G_{2,k}$ and $\Delta G_{3,k}$ for the given surface energy change $\Delta\sigma$ and the applied supersaturation. When $\Delta G_{2,k} = \Delta G_{3,k}$, a critical supersaturation $\Delta\mu_{cr}$ is defined

$$\Delta\mu_{cr} = 2a^2\Delta\sigma \qquad 2.31$$

and the following criteria may thus be written to define which kind of growth is preferred:

$$\Delta\sigma - \Delta\mu/2a^2 > 0 \text{ (three-dimensional nucleation)} \qquad 2.32$$

$$\Delta\sigma - \Delta\mu/2a^2 < 0 \text{ (two-dimensional nucleation)} \qquad 2.33$$

The dependence of the Gibbs free energies of formation of two- and three-dimensional nuclei on the supersaturation for the three different possible surface energy relations is shown schematically in Figure 2.5. It is evident that when the surface energy change $\Delta\sigma$ is positive and

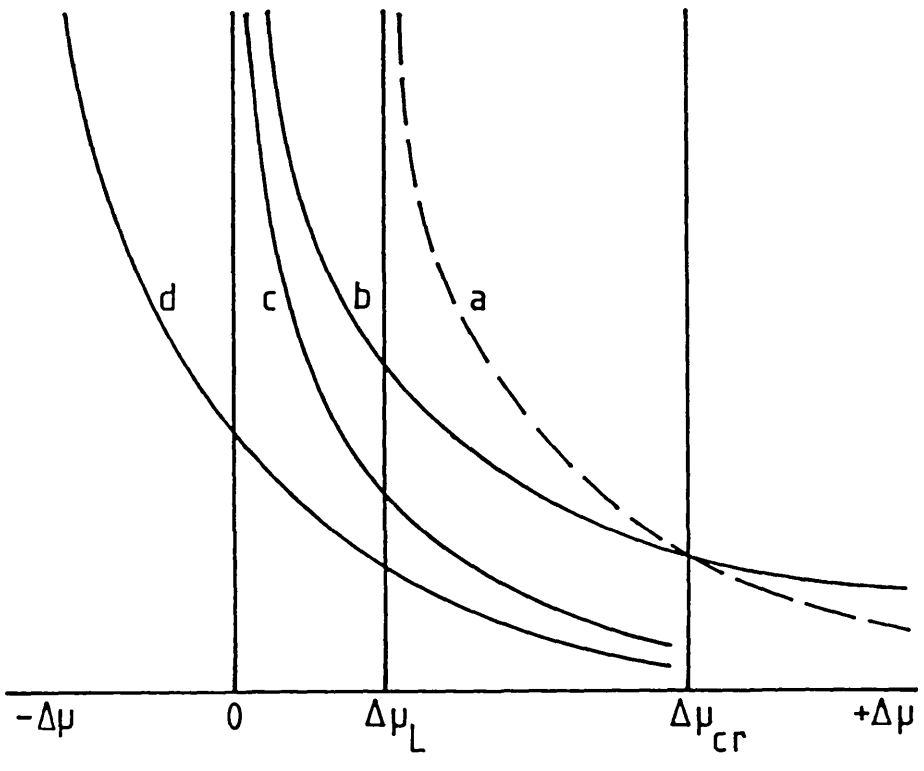

FIGURE 2.5. Dependence of Gibbs free energies on formation of three-dimensional nuclei ($\Delta G_{3,k}$) and two-dimensional nuclei ($\Delta G_{2,k}$), on the supersaturation $\Delta\mu$, for different surface energy relations:
a) $\Delta G_{2,k}$, $\Delta\sigma>0$; b) $\Delta G_{3,k}$, $\Delta\sigma>0$; c) $\Delta G_{2,k}$, $\Delta\sigma=0$;
d) $\Delta G_{2,k}$, $\Delta\sigma<0$.

$\Delta\mu<\Delta\mu_{cr}$ then three-dimensional nucleation (island growth) is energetically favoured, and if $\Delta\sigma$ is positive and $\Delta\mu > \Delta\mu_{cr}$, two-dimensional nucleation takes place. Obviously when the surface energy change is zero or negative, the supersaturation term cannot reverse the sign of the inequality 2.33 so the two-dimensional nucleation is always favourable (layer growth).

Within this theoretical consideration the Stranski-Krastanov mechanism appears to consist of two successive stages: layer growth under condition 2.33 and then island growth under condition 2.32. The occurrence of this growth mode depends on some particular properties of the given system such as the sign and the value of the lattice misfit[88]. For instance, if the misfit is negative and condition 2.33 holds for the first layer the latter will be dilated to fit the substrate. The surface energy of the new substrate will be smaller than that of the bulk deposit. Taking into account the interfacial energy due to the misfit it becomes clear that a positive surface energy change will accompany the next step of the deposition. If now $\Delta\mu < \Delta\mu_{cr}$ three-dimensional nuclei could be formed on top of the first layer. The deposition of Cu on (111)-Au[93] may be considered an example.

Sometimes it is convenient to express the above criterion as a function of β, the adhesion energy per unit area of the deposit-substrate interphase[94,95]. As β is given by

$$\beta = \sigma + \sigma_s - \sigma_i \qquad 2.34$$

the surface energy change can be written as:

$$\Delta\sigma = 2\sigma - \beta \qquad 2.35$$

and the criterion defining the type of nucleation (2.31 and 2.32) becomes

$$(2\sigma-\beta) - \Delta\mu/2a^2 > 0 \qquad 2.36$$

$$(2\sigma-\beta) - \Delta\mu/2a^2 < 0 \qquad 2.37$$

The Gibbs free energy of formation of three-dimensional nuclei is now:

$$\Delta G_{3k} = 16(a^2\sigma)^3 (2\sigma-\beta)/\Delta\mu^2 \qquad 2.38$$

and the number of atoms in the critical nucleus

$$n_{3k} = 64(a^2\sigma)^3 (1-\beta/2\sigma)/\Delta\mu^3 \qquad 2.39$$

ΔG_{3k} can be related to $\Delta G(n_k)$ (eqn. 2.7) by the expression

$$\Delta G_{3k} = \Delta G(n_k)(1 - \beta/2\sigma) \qquad 2.40$$

which shows that the Gibbs free energy of critical nucleus formation on a substrate is considerably smaller than the corresponding quantity for homogeneous nucleation

and decreases with the increase of interaction between the nucleus and the substrate.

When $\beta = 2\sigma$, which characterizes the substrate, or $\beta > 2\sigma$, then two-dimensional nucleation occurs and the Gibbs free energy of formation of the critical nuclei is in this case:

$$\Delta G_{2k} = 4a^4\sigma^2/(\Delta\mu - a^2(2\sigma-\beta)) \qquad 2.41$$

and the number of atoms in the critical nucleus is given by

$$n_{2k} = 4a^2\sigma^2/[\Delta\mu - a^2(2\sigma-\beta)] \qquad 2.42$$

The above criterion is in good agreement with experimental data in the case of vacuum deposition of metal films[82,83,96] and it has been extended considering the influence of the substrate structure of the substrate[85,89]

The kinetic factor was also taken into account as having an effect on the determination of the structure of the deposit, e.g. the idea that different times are required for the subsequent layers to be filled[90] or the rate of formation of nuclei with different numbers of layers which can then lead to the transformation of two-dimensional nuclei into nuclei with n^{th} layers[97]. An extreme situation is the formation of an amorphous deposit which may also occur when the rate of deposition

is too high for the adatoms to reorientate in the equilibrium structure[81].

The former considerations, developed on the basis of the classical nucleation theory, have provided a theoretical explanation of the different kind of growth observed in thin film formation which can also be applied to the case of electrogrowth. The supersaturation which acts as a driving force in the creation of the new phase is replaced in the electrolytic case by the additional electrical potential difference appearing at the substrate-ambient phase boundary, which is represented as the overpotential η(volts). Considering the cathodic reaction 2.1, the overpotential has a negative value which is expressed as:

$$\eta = E - E^{o}_{M/M^{z+}} \qquad 2.43$$

where E is the actual potential applied to the electrode and $E^{o}_{M/M^{z+}}$ is the corresponding equilibrium potential of the infinite electrode of M. The gain in electrochemical potential per atom transferred to the electrodeposit is $-z\eta e$, z being the valency of the depositing ion and e the elementary electric charge, provided the metal ions are in equilibrium with the metal substrate and with the nucleus. The supersaturation thus becomes[98]

$$\Delta\mu = -z.\eta.e \qquad 2.44$$

Therefore the Gibbs free energy of critical nucleus formation in the electrolytic case can be expressed as[88,95,99,100]

$$\Delta G_{2,k} = 4a^4\sigma^2 / (z|\eta|e - a^2(2\sigma - \beta) \qquad 2.45$$

$$\Delta G_{3,k} = 32(a^2\sigma)^3 (1-\beta/2\sigma)/z^2\eta^2e^2 \qquad 2.46$$

and similarly the number of atoms in the critical nucleus.

$$n_{2,k} = 4a^4\sigma^2/[z|\eta|e - a^2(2\sigma-\beta)]^2 \qquad 2.47$$

$$n_{3,k} = 64(a^2\sigma)^3 (1-\beta/2\sigma)/(z|\eta|e)^3 \qquad 2.48$$

It is obvious that in the electrolytic case when the surface energy change is zero or positive ($2\sigma \geq \beta$), an overpotential is required for electrodeposition to occur (nucleation overpotential). When the surface energy change is negative ($\beta > 2\sigma$) the interaction of the deposited material with the foreign substrate is stronger than its interaction with itself, i.e. the electrochemical potential of the monolayer formed on the substrate is lower than the electrochemical potential of the infinite crystal $E^{o}_{M/M^{z+}}$. In this case then the formation of the first monolayer occurs even when the applied potential E is more positive than $E^{o}_{M/M^{z+}}$. a phenomenon known as underpotential deposition.

2.3.2. Electronucleation Kinetics

The fundamental expression for the steady-state nucleation rate (eqn. 2.10), is also applicable to the case of electrodeposition on a substrate [101,102]. In this case the rate is expressed as:

$$Jo = z_o D_k Z \exp(-\Delta G^*/kT) \qquad 2.49$$

where the quantities have the following meaning: z_o is the number of sites on the substrate where nucleation can proceed, Z is the Zeldovich factor, D_k is the flux of ambient phase particles to the critical nucleus surface and ΔG^* is the Gibbs free energy of heterogeneous nucleus formation.

The flux of ambient phase particles, D_k, is a kinetic quantity depending substantially on the mechanism of critical nucleus formation. In the case of direct attachment of ions D_k is usually expressed as:

$$D_k = S_k M_i \qquad 2.50$$

S_k being the surface area of the critical nucleus and M_i the number of ion impingements per cm^2 per sec. It is interesting to note that M_i does not depend on the 'curvature' of the critical nucleus[103] and can be expressed by the cathodic current to the flat interphase boundary:

$$M_i = (i_o/ze) \exp(\alpha ze\eta/kT) \qquad 2.51$$

where i_o is the exchange current density ($A.cm^{-2}$) and α is the transfer coefficient.

In the surface diffusion mechanism the following expression for D_k is adequate:

$$D_k = z_1 L_k D_s / \ell \qquad 2.52$$

Here L_k is the length of the critical nucleus periphery, D_s is the surface diffusion coefficient, ℓ is the jump distance in surface diffusion and z_1 the number of single atoms adsorbed on the substrate, expressed here by a quasi-equilibrium Nernst equation:

$$z_1 = z_1^o \exp[ze\eta/kT] \qquad 2.53$$

z_1^o being the equilibrium adatom concentration.

The work for heterogeneous nucleus formation corresponds to the Gibbs free energy of formation of two- or three-dimensional nuclei which, in the electrolytic case, has been expressed as a function of the overpotential. It is well known that a rigorous derivation of ΔG^* has to consider the dependence of σ on the size of the cluster[104,105] and in the electrolytic case the situation is additionally complicated since the surface energies σ, σ_i and σ_s depend on the electrode potential. The consideration of all these effects however would lead to an expression for Jo which could hardly be used for a simple interpretation of experimental results. The

factor $\sigma^3(1-\beta/2\sigma)$ in equation 2.46 is usually assumed to be a constant, and this approximation has proved justified possibly because of the very narrow overpotential intervals within which electrolytic nucleation is normally investigated[106].

Since unfortunately there are no data for the specific surface energy of metals in electrolytic solutions (either aqueous or molten salts), the equations developed based on the classical model cannot predict the value of the nucleation rate under a given overpotential. The real value of the electronucleation models is in the establishment of the overpotential dependence of the nucleation rate so that the theoretical expressions for Jo can be used to interpret the experimental data, thus providing information concerning the type of nucleation involved and the interfacial energies of the system, which could hardly be obtained by other methods. The stationary rate of formation of two- and three-dimensional nuclei can thus be expressed in a more general way. For the case of two-dimensional nucleation as:

$$J_o = K_n \exp(K_2'/\eta-\eta_x) \qquad 2.54$$

where:

$$K_2' = b\sigma^2 \qquad 2.55$$

b being a geometrical factor depending on the shape of the critical nucleus, and:

$$\eta_x = a^2 (2\sigma - \beta) ze \qquad 2.56$$

For the case of three-dimensional nucleation as:

$$J_o = K_n \exp(-K_2/\eta^2) \qquad 2.57$$

where:

$$K_2 = c\sigma^3 \Phi / z^2 e^2 \qquad 2.58$$

c being a geometrical factor depending on the shape of the three-dimensional critical nucleus, and:

$$\Phi = (1 - \beta/2\sigma) \qquad 2.59$$

Clearly the pre-exponential term in the expression of Jo also depends exponentially on the overpotential and can also be transformed into a more convenient form for the interpretation of the experimental results and expressed as:

$$K_n = K \theta \qquad 2.60$$

Here θ expresses the overvoltage dependence of the pre-exponential term which in the case of a surface diffusion mechanism is given by,

$$\theta = \exp(ze\eta/kT) \qquad 2.61$$

and in the case of a direct attachment mechanism by:*

$$\theta = \exp(\alpha z e \eta / kT) \qquad 2.62$$

2.3.3. Atomistic Theory of Nucleation

The classical nucleation theory presents some limitations arising from the thermodynamic treatment which assigns macroscopic properties such as surface and surface energy to very small clusters. This approximation is good at relatively low supersaturations but becomes less realistic as the applied supersaturation increases and the critical nucleus contains only a few atoms. In that case neither the use of the surface energy, nor the division of the cluster free energy into one volume and one surface term can be justified.

The above contradiction, which is in fact more clearly distinguishable in heterogeneous phase formation, was successfully overcome in the case of the condensation of metal vapours or substrates with the aid of the atomistic theory of nucleation[106-109]. Here the basis of the theoretical discussions is given by the concept of a critical nucleus whose formation governs the phase transition, but macroscopic thermodynamic concepts are now replaced by a kinetic model which considers the frequencies of attachment and detachment of single atoms from clusters with different numbers of atoms.

---

* θ does not include the overpotential dependence of z_0 which, if existing, could be determined only experimentally for each concrete case.

The application of the classical theory may also be limited to interpret the kinetics of electrochemical nucleation which occur at high overpotentials where the critical nuclei are very small. In a recent theoretical study, the atomistic approach was successfully applied to electrolytic nucleation on foreign substrates[110,111] and the steady-state nucleation rate was expressed according to the different mechanism of formation of the critical complex. If direct attachment of ions from the electrolyte is assumed, then the rate of nucleation is expressed by:

$$Jo = K \exp(-\Phi(n)/kT) \exp[(n+1-\alpha)\, ze\eta/kT] \qquad 2.63$$

where n is the number of atoms in the critical nucleus and $\Phi(n)$ represents the difference in the energy of n atoms when they are part of an infinitely large crystal on the one hand when they form an independent three-dimensional complex on the substrate on the other. It is expressed as:

$$\Phi(n) = n\varphi_{\frac{1}{2}} - \sum_{1}^{n} \varphi_i^* \qquad 2.64$$

For the formation of the critical complex by a mechanism of surface diffusion, the steady state rate of nucleation is given by:

$$Jo = K'' \exp(-\xi(n)/kT) \exp[(n+1)ze\eta/kT] \qquad 2.65$$

In this equation:

$$\xi(n) = n\varphi_{\frac{1}{2}} - n\varphi_a - \sum_{1}^{n} \varphi_v \qquad 2.66$$

is a measure of the difference in energy of n atoms when they are part of an infinitely large three-dimensional crystal on the one hand, and when they form an independent two-dimensional complex on the foreign substrate on the other.

When the complexes are formed on active sites on the substrate the nucleation rate is given by:

$$Jo = K'''\exp(-\Phi'(n)/kT)\ \exp[(n+1)ze\ /kT] \qquad 2.67$$

Here $\Phi'(n)$ has the same sense as $\Phi(n)$ in equation 2.63, but it refers to a complex formed on an active centre.

The linear dependence of the logarithm of the steady state rate on the overpotential provides a method to estimate the number of atoms in a critical complex directly from the slope of the straight line, and sharp changes of slope are to be expected if the different critical sizes are sufficiently small. Unfortunately the theoretical equations 2.63, 2.65 and 2.67 are practically indistinguishable from one another as the exponential terms show the same direct dependence on the overpotential. The difference between the three mechanisms appears mainly in the pre-exponential factors which cannot be treated quantitatively because of the presence in them of quantities inaccessible to direct experimental determination.

The connection between the classical and the atomistic models of electrolytic nucleation has been investigated showing that the equations describing the nucleation rate in the framework of the atomistic theory turn into the classical expression at low supersaturations[112,113].

2.3.4. Saturation Nucleus Density

It has been experimentally shown that the number N of nuclei formed electrolytically on inert electrodes at constant overpotential increases linearly after an initial induction period[114]. After a sufficient length of time it reaches saturation or a maximum number which is independent of time[115,116]. The saturation nucleus density increases with the overpotential applied and is strongly dependent on the concentration of the electrolyte and the state of the electrode surface. The termination of the process of nucleation can be explained through different mechanisms which can influence the final saturation nucleus density and simultaneously define the function of N with respect to time.

With very few exceptions the structure of an electrode is not uniform and the activity of the surface varies from site to site. For a single crystal substrate without surface films or impurities, the active sites can be closely identified with the equilibrium surface structure, i.e. of steps and kinks[117,118,119]. For a polycrystalline substrate, grain boundaries and edges will act as preferred sites[120]. If a film is present on the substrate, holes

in the film may act as preferential centres for nucleation[121,122]. Kaischew and Mutaftschiew[116] explained the phenomenon of nuclei saturation numbers on the basis of these energetic inhomogeneities of the substrate. They assumed that the active centres have different activity, or different critical overpotential, with respect to the formation of nuclei. The higher the activity, the lower the critical overpotential of a given centre and the greater the probability of nuclei forming on it. Nuclei can be formed on those centres whose critical overpotential is lower than or equal to that applied to the electrolytic cell from outside. Thus the saturation nucleus density would be determined by the number of centres active under the experimental conditions, i.e. at the overpotential imposed from outside. The higher the overpotential the greater the number of weaker active sites taking part in the nucleation process and hence the greater the saturation nucleus density.

The existence and growth of "exclusion" zones of nucleation (or 'deactivated' zones) around the growing nucleus have been also mentioned as an explanation of the phenomenon of saturation[115,116]. The phenomenon resembles that observed in the case of vapour deposition on to foreign substrates. After some time the zones overlap to cover the substrate exposed for nucleation, terminating the nucleation process, and the saturation nucleus density is reached. In the case of vapour condensation on a substrate the saturation nucleus density

has been calculated on the basis that the nucleation and growth is controlled by the two-dimensional diffusion to the growing centres[123-125]. A stable cluster acts as a sink for adatoms, depleting their concentration in its vicinity and thereby decreasing the nucleation probability in a zone around the nucleus ('capture area'). The saturation nucleus density has been expressed in general terms as:

$$N_s = A'(J/D_s)^{r'} \qquad 2.68$$

where J is the deposition rate, i.e. the rate at which adatoms are introduced into the system, D_s is the surface diffusion coefficient for adatoms on the substrate, and A' and r' are constants which vary according to the specific assumptions of the models.

In the case of electrolytic nucleation the mechanism of formation and kinetics of growth of the exclusion zones have been studied for mercury electrodeposition on platinum electrodes from $Hg(NO_3)_2$ solutions[126,127]. The phenomenon was related to the drop of overpotential within the electrolyte around the growing nuclei, due either to ohmic drop[126] or concentration changes[127].

In general, in electrolytic nucleation on a foreign substrate, both aspects, i.e. the depletion of active centres and the growth of exclusion zones, could be responsible for the reaching of a saturation nucleus density. The possibility of these two factors influencing

the kinetics of the process can be deduced directly from the definition of the nucleation rate

$$dN(t)/dt = J\, z(t) = IS(t) \qquad 2.69$$

where N(t) is the nuclei number at t, z(t) is the number of active centres unoccupied by nuclei up to moment t, $J(sec^{-1})$ is the nucleation rate per centre, $S(t)(cm^2)$ is the substrate surface area not covered by nucleation exclusion zones up to moment t, and I $(cm^{-2}.sec^{-1})$ is the nucleation rate per unit area. It is obvious that the saturation condition $(dN/dt)_{t\to\infty} = 0$ is fulfilled when $z(t\to\infty) = 0$, i.e. when all the centres are occupied by nuclei, or when $S(t\to\infty) = 0$, i.e. when the surface area is fully covered by nucleation exclusion zones.

The problem of deriving the dependence of the number of nuclei on time in a supersaturated system has been solved in the general case[128,129] using the probability mathematical formalism of Kolmogoroff[130], under the following assumptions: i) nuclei are formed on active centres only, ii) nucleation exclusion zones arise and grow around the growing nuclei and iii) there is no coalescence of stable nuclei. On the basis of that theory the specific case of the electrolytic formation of metallic nuclei under potentiostatic conditions on the surface of ideally polarizable electrodes was considered[131,132]. The physical model was based on the following assumptions: nuclei are formed on active

centres randomly located on the surface of an inert electrode with area S. An arbitrary continuous activity distribution z(a) for the centres is accepted, with the activity varying from a_s for a defect-free surface to a maximum of a_m. The corresponding critical overpotentials are denoted by E_s and E_m, being $E_s > E_m$. If the externally applied overpotential E is lower than E_m it is obvious that a nucleation process with an observable rate will not take place. Nucleation exclusion zones arise round the growing nuclei owing to a drop in overpotential below a certain critical value with respect to nucleation and the radii of the zones will have a size dependent on the critical overpotential E_a of the centre. This becomes clearer if one assumes that the nucleation exclusion zone radius is determined by the intersection of the profile E(x,t) of the overpotential around the growing nucleus (x being the distance) and the critical overpotential E_a of the corresponding active centre (see Figure 2.6). Thus, if the overpotential E(x) is lower than E_a the corresponding centre will be deactivated and will not take part in the process. Considering also the case of time-independent steady state nucleation $J_o(E_a)$, the following general expression for the number of nuclei was given[131].

$$N(t) = \int_o^E \int_o^t z(E_a) J_o(E,E_a) \exp\{-J_o(E,E_a)\tau - M' \int_o^\tau \frac{S'(E_a,t')}{S}\, dt'\} d\tau dE_a \qquad 2.70$$

where:

$$S'(E_a,t') = \pi\{\int_{t'}^{t} c(E_a) k(\tau - t')\, d\tau\}^2 \qquad 2.71$$

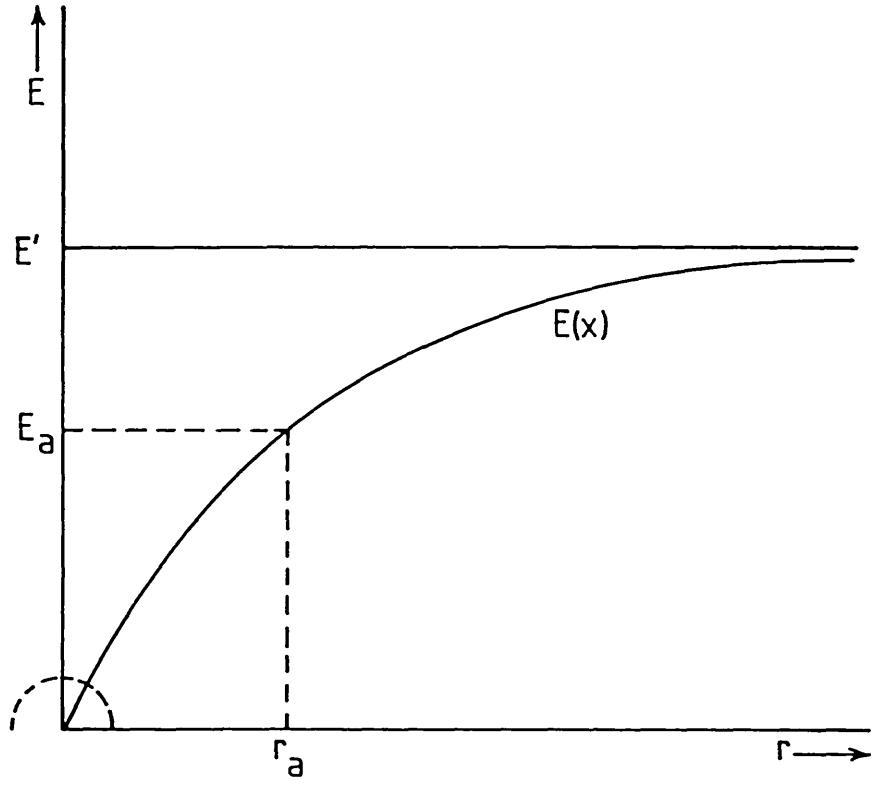

FIGURE 2.6. Schematic representation of the potential distribution in the electrolyte in the presence of a growing centre. The nucleation exclusion zone is determined by the intercept of the overpotential profile E(x) with the corresponding critical overpotential E_a.

is the area of a nucleation exclusion zone at moment t spreading around a nucleus formed at moment t' < t at a rate:

$$v(E_a,t) = c(E_a)k(t) \qquad 2.72$$

and:

$$M' = \int_o^E z(E_a)J(E,E_a)dE_a \qquad 2.73$$

Equation 2.70 represents a curve starting with a slope:

$$(dN/dt)_{t=0} = M' \qquad 2.74$$

reaching after a sufficient interval of time ($t\to\infty$) a constant value, the saturation nucleus density N_s.

In the case of centres of equal activity a_o or equal critical overpotential E_o, equation 2.70 has the form:

$$N(t) = z_o J_o \int_o^t \exp\{ -J_o\tau - z_o J \int_o^\tau \frac{S'(t')}{S} dt' \} d\tau \qquad 2.75$$

where $z_o = z(E_o)$ is the number of centres. The initial slope is now:

$$(dN/dt)_{t=0} = M' = z_o J_o = I_o S \qquad 2.76$$

The limiting case controlled by the active centres is obtained from equation 2.75 under the condition

$S'(t') = 0(v(E_a,t) = 0)$, giving

$$N(t) = z_o\{1-\exp(-J_o t)\} \qquad 2.77$$

and here N_s is equal to the number of active centres z_o. A similar expression is also obtained by direct integration of the first order law of nucleus formation[133,134], given by:

$$dN/dt = J_o\, z(t) \qquad 2.78$$

An expression similar to 2.77 must also hold if the centres have different activities. Using the generalized theorem of the mean value in the integral calculation this can be written in the form

$$N(t) = z(E)\{[1 - \exp -J_o(\bar{E}_a)t\}] \qquad 2.79$$

where $z(E) = N_s$ is given by:

$$N_s = \int_o^E z(E_a)dE_a \qquad 2.80$$

and E_a occupies some mean value in the interval (O,E).

The limiting case controlled by the growth of nucleation exclusion zones can be deduced from eqn. 2.70 substituting $J(E_a)$ from eqn. 2.69. Under the condition $z(E_a)\to\infty$ (the number of active centres is sufficiently large and their influence on the course of the process

is negligible), assuming a case of equal activity centres and introducing the zone growth law in the explicit form:

$$v(E_a,t) = c(E_a)q.t^{q-1} \qquad 2.81$$

where q is an arbitrary exponent, one finally obtains:

$$N(t) = N_s\ \gamma\left\{\Gamma\left(\frac{2q+2}{2q+1}\right)\ \frac{M't}{N_s}\right\} \qquad 2.82$$

where N_s is given by

$$N_s = \left\{\frac{(2q+1)S}{\pi c^2}\right\}^{1/2q+1}\ \Gamma\left(\frac{2q+2}{2q+1}\right)M',^{2q/2q+1} \qquad 2.83$$

$\Gamma(q)$ and $\gamma\ (x,q)$ being the complete gamma function and the incomplete gamma function, respectively.

Applying the generalized theorem of the mean value a similar expression for the case of different activity centres is obtained.

The above equations are valid for the case of a negligible small induction period. If the nucleation stage presents a considerable time lag all the previous equations can be used by simply substituting t by $t-t_o$, t_o being taken as the onset.

For the sake of confronting results with the different controlling mechanisms, it is convenient to express eqn. 2.77 and 2.82 in terms of the dimensionless coordinates $y = N(t)/N_s$ and $x = M'(t-t_o)/N_s$, obtaining respectively

$$y = 1-\exp(-x) \tag{2.84}$$

and

$$y = \gamma\left\{\Gamma\left(\frac{2q+2}{2q+1}\right)x\right\} \tag{2.85}$$

In the case when N_s is determined by the overlapping of nucleation exclusion zones with a constant rate of growth $q = 1$ or $q = 1/2$, then equation 2.85 becomes

$$y = 3\Gamma^{-1}\left(\frac{1}{3}\right)\int_0^{x\Gamma(4/3)} \exp(-t^3)dt \tag{2.86}$$

and

$$y = \operatorname{erf}\left\{x\Gamma\left(\frac{3}{2}\right)\right\} \tag{2.87}$$

respectively.

3. THE STUDY OF ELECTROGROWTH

3.1. GENERALITIES

The study of the process of electrogrowth offers one special advantage in relation to the study of other phase transformations, which is the ability to control accurately the degree of supersaturation applied to the system by controlling the electrical potential i.e. the overpotential, imposed on the substrate undergoing the deposition. By means of a potentiostat a constant overpotential can be imposed at will, changed instantly or varied arbitrarily with time, while the resulting current is measured. Alternatively under galvanostatic conditions the process can be forced to take place at a determined rate while the resulting overpotential is recorded during the process.

Various aspects of the process of electrogrowth have been characterized by using either sweep voltammetry[135,136] galvanostatic methods[137-139], galvanostatic-potentiostatic step methods[140], potential step methods[141-145] or different combinations of them[146-152]. The potential step method is very powerful and it has been the most widely used, especially in studies of electrochemical nucleation[141-151]. A variation of this technique, the double-potential step, permits even the determination of nucleation kinetics by direct counting of the nuclei formed at different stages of the process, which is "frozen" at will during its development[77,152-155]. A technique like this, involving direct nuclei counting, can be used only as an ancillary

method in the present study due to the limitations in interchanging electrodes imposed by working with a sealed system at high temperatures.

A potentiostatic current-time plot contains considerable information on the mechanism of the electrogrowth process. The metal electrodeposition takes place by a faradaic process and the observed current is a direct measurement of the morphological changes occurring at the electrode surface. If electrochemical nucleation is involved, a current-time plot may contain information on the nucleation rate and the mechanism of growth of the individual nuclei or crystallites. If $I_i(t)$ designates the individual growth current to the nucleus i, then the total current in a system of N discrete nuclei before the onset of overlap can be expressed as

$$I(t) = \sum_{1}^{N} I_i(t) \qquad 3.1$$

If the processes of nucleation and growth occur simultaneously the resulting current has a more complex form. In general, if the growth current of a single nucleus of age u is written as

$$I(u) = f_1(u) \qquad 3.2$$

and the nucleation law, expressing the number of nuclei at any time during the process of nucleation, is written as

$$N(t) = f_2(t) \qquad 3.3$$

then the overall current before the onset of overlap is given by the convolution expression[133]

$$I(t) = \int_0^t f_1(u) \left(\frac{df_2(t)}{dt}\right) du \qquad 3.4$$

This corresponds to the sum of the individual nuclei currents integrated over all nuclear births occurring in the interval of time from 0 to t. The nucleation law will be described according to the expressions described in Section 2.3.4.

Potentiostatic current-time relations for the growth of nuclei under different conditions have been deduced[156,157]. Different crystallite morphologies have been considered: one dimensional as in the case of needles, two-dimensional as in the case of patches or platelets, or three-dimensional as in the case of crystalline forms, and different deposition regimes where the rate determining step is either the incorporation of adatoms at the growing point or the mass transfer of depositing ions by diffusion or migration to the growing point. This latter regime is more likely to be the controlling step in the case of electrogrowth in molten salts, given the relatively fast charge transfer kinetics usually found in these systems[15].

The next two sections contain respectively a summary of the theory of chronoamperometry and its application

to the determination of potentiostatic current-time relationships for electrogrowth involving a nucleation stage.

3.2 CHRONOAMPEROMETRY

Chronoamperometry is an electrochemical technique in which the working electrode is subjected to a step functional change of potential while the resultant current is measured as a function of time or potential. The development of a quantitative treatment of a step experiments demands the creation of a theory that can predict, quantitatively, the current-time response function in terms of the experimental parameters of time, potential, concentration, mass transfer coefficients, kinetics parameters and so on.

A controlled potential experiment for the case of the general electrode reaction:

$$O + ze \rightarrow R \qquad 3.5$$

can be treated in general by invoking the current-potential characteristic:

$$i = zFAk^{o}[C_{o}(o,t)\exp(-\alpha z\eta) - C_{R}(o,t)\exp(1-\alpha)z\eta] \qquad 3.6$$

in conjunction with Fick's laws, which can give the time-dependent surface concentrations $C_{o}(o,t)$ and $C_{R}(o,t)$.

This approach is nearly always difficult and sometimes fails to yield closed-form solutions, but several special cases can provide simpler mathematical approaches. Two will be particularly applicable in the present study: a) Large-amplitude potential changes: when the potential is stepped to the mass-transfer controlled region, the concentration of the electroactive species is nearly zero at the electrode surface and the current is totally controlled by mass transfer. The electrode kinetics no longer influence the current, hence the general i-E characteristic is not needed at all. For this case i is independent of E. b) For very rapid electrode kinetics the general i-E relation 3.6 collapses to a relation of the Nernst form:

$$E = E^{o'} + \frac{RT}{zF} \ln \frac{C_o(o,t)}{C_R(o,t)} \qquad 3.7$$

Again the kinetic parameters k^o and α are not involved and the mathematical treatment is greatly simplified. In this way the concentration of electroactive species near the electrode surface can be calculated and the mathematical treatment used in case a) can be extended to intermediate overpotentials at which $C_o(o,t) = C_o \neq 0$.

3.2.1. Solution of the diffusion equation

In the case of metal deposition R is insoluble and then only the diffusion equations related to the oxidized form species O has to be considered. A sufficiently general

expression of the resulting current during a step potential experiment is obtained from the solution of the semi-infinite spherical diffusion equations. The Fick's second law becomes in this case[158]:

$$\frac{\partial C(r,t)}{\partial t} = D[\frac{\partial^2 C(r,t)}{\partial r^2} + \frac{2}{r}\frac{\partial C(r,t)}{\partial r}] \qquad 3.8$$

Here r is the radial distance from the electrode centre and now C(r,t) represents the concentration of oxidized species. The boundary conditions are:

$$C(r,o) = C \quad (r > r_o) \qquad 3.9$$

$$\lim_{r\to\infty} C(r,t) = C \qquad 3.10$$

$$C(r_o,t) = C^s \quad (t > o) \qquad 3.11$$

where r_o is the radius of the electrode. From the solution of the diffusion equation, the distribution of electroactive species near the electrode turns out to be

$$C(r,t) = C-(C-C^s)\frac{r_o}{r}\,\mathrm{erfc}(\frac{r-r_o}{2D^{\frac{1}{2}}t^{\frac{1}{2}}}) \qquad 3.12$$

According to the Fick's first law the current to the electrode is related to the flux of electroactive species by the equation:

$$I = zFAD[\frac{\partial C(r,t)}{\partial r}]_{r=r_o} \qquad 3.13$$

The expression for the resulting current is then:

$$I = zFAD(C-C^S)\left(\frac{1}{(\pi Dt)^{\frac{1}{2}}} + \frac{1}{r_o}\right) \qquad 3.14$$

The surface concentration C^S obtained at an applied overpotential is given by the Nernst equation

$$C^S = C \exp zF\eta/RT \qquad 3.15$$

Replacing in eq. 3.14 one finally obtains

$$I = zFADC(1-\exp zF\eta/RT)\left(\frac{1}{(\pi Dt)^{\frac{1}{2}}} + \frac{1}{r_o}\right) \qquad 3.16$$

When $r_o = \infty$ the electrode is planar and the expression for the current becomes:

$$I = zFAC(1-\exp -zF\eta/RT)\left(\frac{D}{\pi t}\right)^{\frac{1}{2}} \qquad 3.17$$

For very small r_o's the steady state term in equation 3.16 becomes predominant and the expression of the current reduces to

$$I = zFACD(1-\exp zF\eta/RT)/r_o \qquad 3.18$$

For high overpotentials, where $C_s \simeq 0$, the overpotential term tends to zero and corresponding equations for the different cases can be obtained from equations 3.16, 3.17, 3.18, giving respectively

$$I = zFADC(1/(\pi Dt)^{\frac{1}{2}} + 1/r_o) \qquad 3.19$$

$$I = zFAC(D/\pi t)^{\frac{1}{2}} \qquad 3.20$$

known as Cottrell equation; and

$$I = zFACD/r_o \qquad 3.21$$

3.3. GROWTH OF NUCLEI UNDER DIFFUSION CONTROL

In general the instantaneous current to a nucleus growing under diffusion control can be expressed as

$$I_1(t) = A(t).i(t) \qquad 3.22$$

Here A(t) is the growing area of the nucleus at the time t and i(t) is the instantaneous nuclear current density which can be evaluated for a given nuclear geometry according to the corresponding diffusional equations.

Assuming that the solute is transported to the surface of a hemispherical nucleus of radius r by planar diffusion, the nuclear current density is given by equation 3.20 and the total current is:

$$I_1(t) = (2\pi r^2)\ zFC\ (D/\pi t)^{\frac{1}{2}} \qquad 3.23$$

The current can be also related to the growth of the hemisphere according to:

$$I_l(t) = \frac{zF\rho}{M} \frac{dV}{dt} = \frac{zF\rho}{M} \left(\frac{dV}{dr}\right)\left(\frac{dr}{dt}\right) \qquad 3.24$$

where $dV/dr = 2\pi r^2$. Hence integrating

$$r = \frac{2CM}{\rho} \left(\frac{Dt}{\pi}\right)^{\frac{1}{2}} \qquad 3.25$$

and it follows that[159]:

$$I_l(t) = zF\pi(2DC)^{3/2} M^{\frac{1}{2}} t^{\frac{1}{2}}/\rho^{\frac{1}{2}} \qquad 3.26$$

The assumption of linear mass transfer is adequate for the case of short times when the extent of the diffusion zones is relatively small. Given the smallness of the nuclei the growing current has also been described in terms of localized spherical diffusion[147]. In this case the nuclear current density is expressed according to equation 3.21 and the instantaneous current to a hemispherical nucleus of radius $\underline{r}$ takes the form:

$$I_l(t) = 2zF\pi rDC \qquad 3.26'$$

As before the current can be related to the size and therefore to the radius of the nucleus through the quantity of charge required to form it (eqn. 3.24), and it follows that:

$$I_l(t) = zF\pi M^{\frac{1}{2}} (2DC)^{3/2} M^{\frac{1}{2}} t^{\frac{1}{2}}/\rho^{\frac{1}{2}} \qquad 3.27$$

A similar expression can be obtained for low overpotentials, starting from equation 3.18, that is

$$I_1(t) = z F \pi M^{\frac{1}{2}} (2DC)^{3/2} (1-\exp(-zF\eta/RT)^{3/2} t^{\frac{1}{2}}/\rho^{\frac{1}{2}} \qquad 3.28$$

That equation 3.27(or 3.28) is still an approximation follows from the application of 3.21 (or 3.18) which is true only for a fixed value of $\underline{r}$ and not for a growing hemisphere. A more precise expression for the current has been obtained by applying a more general expression for mass transfer to a small hemisphere the radius of which is also a function of time, by using numerical simulation[143]. This was found to differ from equation 3.21 only by a factor 1.04 which is well inside the range of accuracy expected in these experiments.

The hemispherical model is also applicable when the nucleus has different morphologies, not necessarily spherical. In fact as the depletion zones around the growing nucleus advance radially much more rapidly than its perimeter the mass transfer flux immediately adopts a hemispherical symmetry at the focus of which the nucleus acts just as a point sink.

The expression for the nuclei growth current obtained under both assumptions, planar and hemispherical diffusion, show the same linearity in $t^{\frac{1}{2}}$ but with a markedly different proportionality factor and concentration dependence. The validity of equation 3.27 over equation 3.26 has been ratified by visual counting of nuclei[143] and by confirming the $I\text{-}C^{3/2}$ dependence[160].

If there are N_o nuclei instantly formed at the start of the process, then the total current before the overlap of the individual diffusion zones can be expressed simply as:

$$I(t) = N_o.I_1(t) \qquad 3.29$$

If nucleation and growth occur simultaneously the resulting current before overlap can be obtained from the convolution expression 3.4, which can be integrated under the condition of steady nucleation rate obtained at the start of the nucleation process (see equation 2.76). Replacing

$$dN/dt = I_o.S \qquad 3.30$$

and applying equation 3.27 in which the variable $\underline{t}$ has been replaced by $\underline{u}$, the integration of equation 3.4 gives:

$$I(t) = 2\ I_o.S.zF\pi\ M^{\frac{1}{2}}(2CD)^{3/2}\ t^{3/2}/3\rho^{\frac{1}{2}} \qquad 3.31$$

An expression for the current for low values of overpotential can be similarly obtained by using equation 3.28 instead, resulting in

$$I(t)=2I_o.S.zFM^{\frac{1}{2}}(2CD)^{3/2}(1-\exp(-ZF\eta/RT))^{3/2}t^{3/2}/3\rho^{\frac{1}{2}} \qquad 3.32$$

4. EXPERIMENTAL

4.1. EQUIPMENT

The experimental work with a molten salt electrochemical system requires the use of highly purified melts and the operation under a protective atmosphere so to carry out the present research the design and construction of an adequate experimental system was necessary. A general layout of the system built is shown in Figure 4.1 and a brief description of the elements composing the different units is as follows.

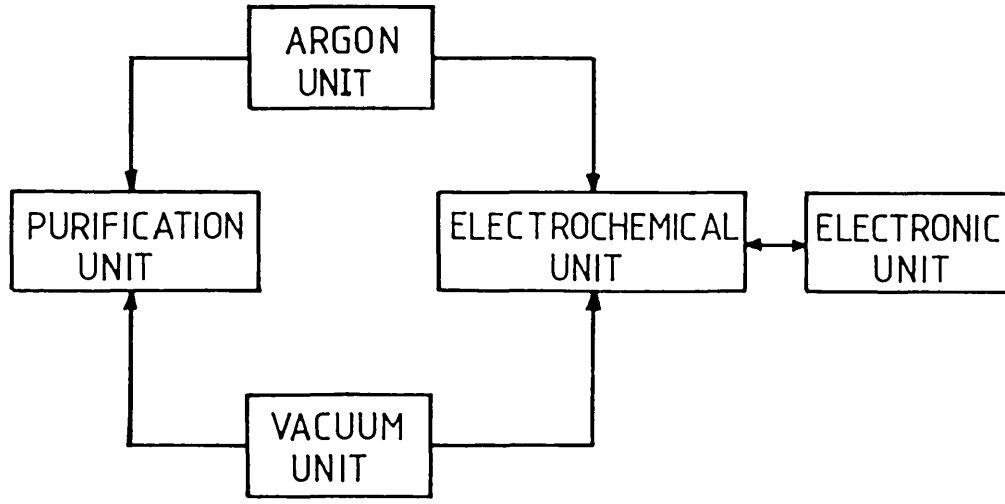

FIGURE 4.1. A schematic diagram showing the main units of the experimental system.

4.1.1. Vacuum system

The vacuum was produced by an oil vapour diffusion pump (Edwards ED1), backed by a high speed rotary vacuum pump (Edwards ED200). When necessary the diffusion pump could be isolated from the circuit by means of two isolation valves (Edwards SC10 speedivalves), allowing the direct use of the rotary pump. Volatile compounds sporadically produced could be removed from the vacuum system by a liquid nitrogen-cooled trap. The vacuum was measured by means of a Pirani-type system consisting of a gauge head (Edwards Pirani G5C-1) and a control unit (Edwards Pirani 8/1) with range $10\text{-}10^{-3}$ torr.

4.1.2. Argon system

The gas source was a BOC high-purity argon cylinder (99.999%). Before feeding the electrochemical cell or purification unit the argon passed through a molecular sieve column for extra desiccation and through high-temperature copper wool ($400^{o}C$) to eliminate any traces of oxygen.

4.1.3. Melt purification unit

The purification cell (Figure 4.2) was made of a vertical pyrex tube; 7.5 cms in diameter and 61 cms in height, which contained two pyrex vessels in juxtaposition,

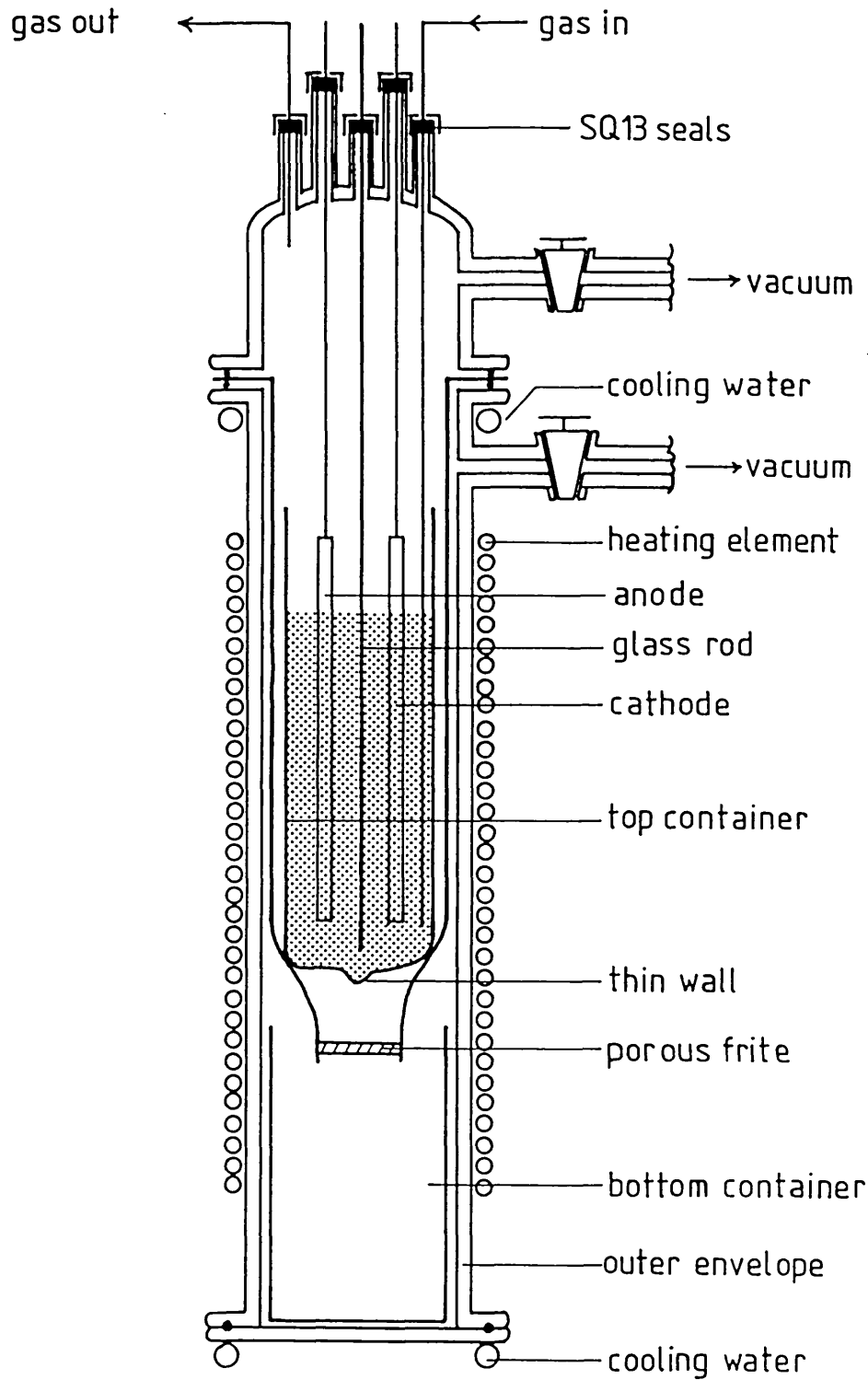

FIGURE 4.2. Purification unit.

with a porous frit No.4 in between. The top lid design allowed the introduction of electrodes, devices for gas bubbling, etc., as the specific purification method demanded. By breaking the thin bottom layer of the top vessel the melt could finally be filtered and poured into the bottom vessel. After solidification and cooling the mixture was transferred to a dry box and kept over P_2O_5. The purification unit could treat a batch of 0.6 kg.

4.1.4. Electrochemical unit

This included the electrolytic cell itself and the furnace. The vertical furnace was made of an alumina tube 15 cms O.D., 61 cms in height and 1.3 cms in thickness. It had two heating zones made of 18 SWG Kanthal winding, 26 Ω each. These two zones could be connected in series, in parallel or to independent power sources according to the specific temperature profile required. In the current operation the power supply and temperature control was provided from a Eurotherm unit, model PID/SCR/10A/PC/ 0-1000°C. The thermal isolation was obtained by using a silica wool cover contained in an aluminium external shell, 58 cms in diameter and 1 mm thick. The furnace provided a constant temperature region of ∿15 cms length where the electrolytic bath was placed.

The electrochemical cell (see Figure 4.3) consisted of an outer pyrex envelope, 80 cms O.D. and 35 cms high, in the bottom of which rested the vessel (17 cm height,

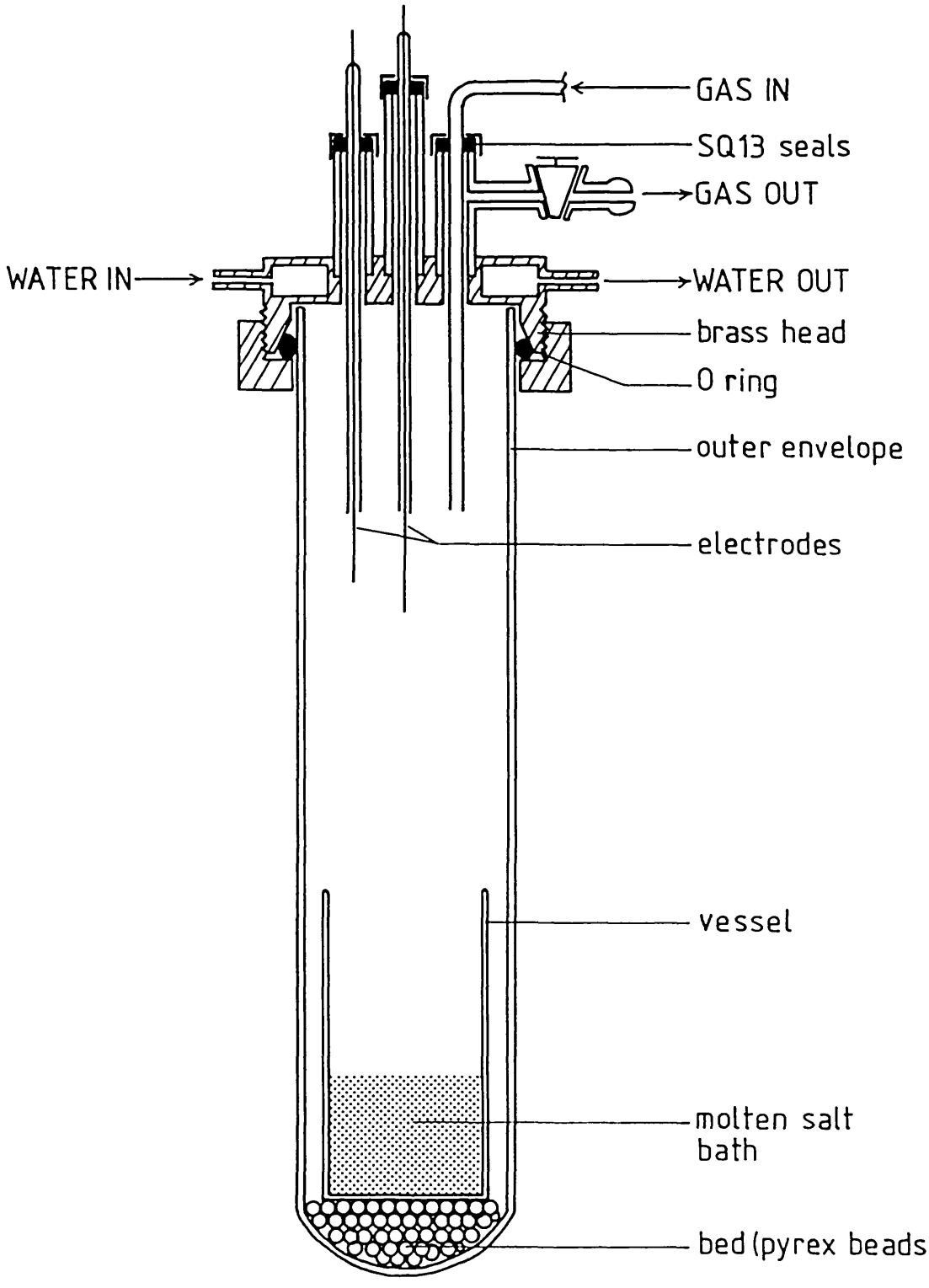

FIGURE 4.3. Electrochemical cell

6.5 cm diam.), with molten salt bath. The cell was capped by a water-cooled brass head whose design enabled the introduction and interchange of electrodes, the feeding of chemicals, gas bubbling, etc., without contamination by the outside atmosphere. The cell could operate under vacuum or argon atmosphere. The temperature was measured with a chromel-alumel thermocouple put inside a closed tube with a tip inserted in the melt.

The large size of the furnace permitted also the use of much larger electrolytic cells which could be required for the study of some process aspects of molten salts electrodeposition at bench scale.

4.1.5. Electronic unit

This unit included the instrumentation required for the application of different potential functions to the working electrodes in the electrochemical cell and the measuring and registration of their responses.

A basic diagram of the experimental system used for the application of controlled potential techniques is shown in Figure 4.4. A potentiostat has a control of the overvoltage across the working electrode-counter-electrode pair and it adjusts this voltage in order to maintain the potential difference between the working and the reference electrode (which it senses through a high-impedance feedback loop), in accord with the programme

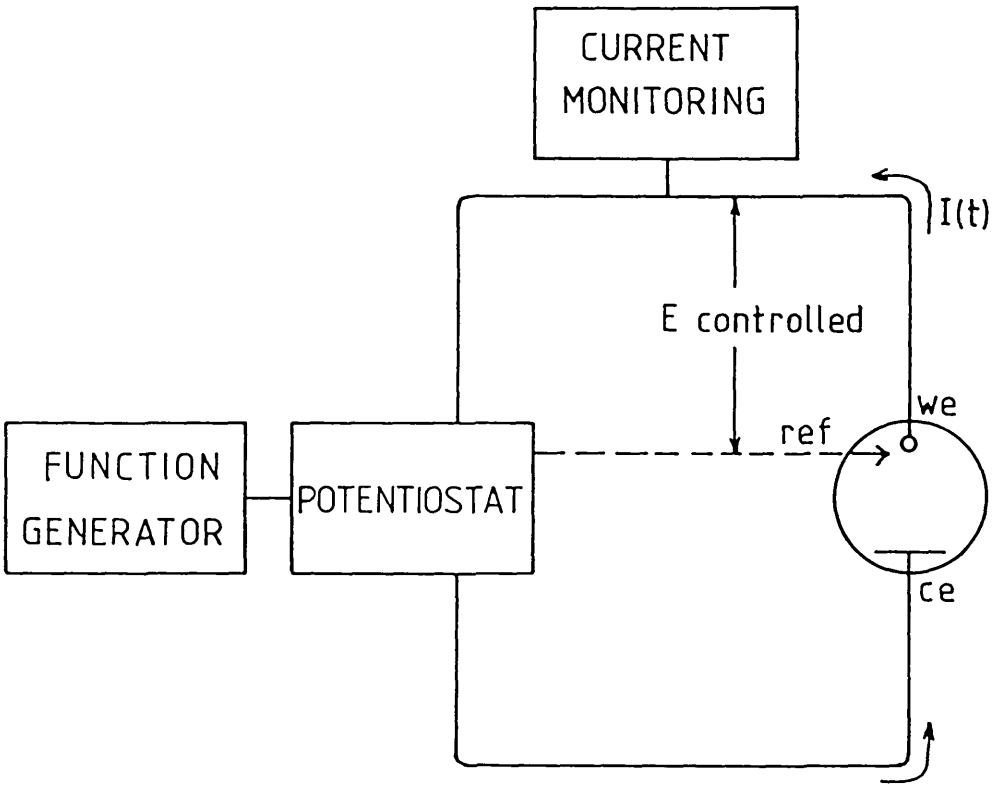

FIGURE 4.4. Experimental arrangement for controlled potential experiments.

supplied by a function generator.

The following instruments were used to generate the potential function: a potentiostat control amplifier working model PCA 72M (or L), a sweep generator model 175 Universal Programmer (Princenton Applied Research). A gated integrator and DVH Bentham Hi-tek, a Data-lab transient recorder DL905, digital voltmeter DVM44 Advanced Instruments, a Tektronic oscilloscope, an XY/t recorder Bryans 2900, and a X-t recorder Servoscribe 1S, were used to record and/or store the response of the system.

4.2. CHEMICALS AND MATERIALS

The grade and supplier of the chemicals and materials used in the reported experiments are shown in Table 4.1.

The commercial AGR fuel element cladding is fabricated from double vacuum-melted niobium stabilized 20% Cr/25%/Ni stainless steel (see specification in Table 4.2), which is heat-treated (930^{o}C/1 hour) to yield a grain size in the range 0.015 to 0.02 mm. The material was supplied as coupon specimens cut from a standard A.G.R. fuel can, their dimensions being 10 mm by 10 mm, 0.33-0.41 mm wall thickness, one side presenting square ribs (0.23-0.31 mm) at 1.90-2.16 mm intervals.

TABLE 4.1. Chemicals and Materials

Chemical and Gases	Grade and/or dimensions	Supplier
Silver chloride	ANALAR	B.D.H.Chemicals Ltd.
Lithium chloride	anhydrous, GPR	B.D.H.Chemicals Ltd.
Potassium chloride	ANALAR	B.D.H.Chemicals Ltd.
Chromous chloride	anhydrous, 98%	Alfa Ventron Ltd.
Chlorine	technical grade, 99.5%	B.O.C. Special Gases
Argon	high purity	B.O.C. Special Gases
Electrode Materials		
Platinum	0.05 mm foil, 99.99%	Englehard Ltd.
Copper	0.1 mm foil, 99.999%(elect)	-
Stainless steel	0.05 mm foil, EN58B	C.J.A. Stainless Ltd.
Tungsten	2.4 mm diam. rod, 99.9%	B.O.C. Murex
Chromium	electrolytic flake, 99.999%	
Aluminium	0.77 mm wire, 99.9%	B.D.H. Chemicals Ltd.
	6 mm rod, spec. pure	

TABLE 4.2. AGR fuel element cladding

Element	Weight %	
	Minimum	Maximum
Cr	19	21
Ni	24	26
Mn	0.55	0.85
Si	0.45	0.75
Nb	8x(C+N)	0.80
C+N	0.04	0.08
S+P	-	0.02 each
Ti,Zr,Al	-	0.05 each
Co	-	0.010 (average)
Ta	-	0.020 (average)
B		0.0005 (average)
Fe	(Balance)	

4.2.1. Electrodes

4.2.1.1. Working electrodes

Platinum, copper, EN58B stainless steel, tungsten and AGR fuel element cladding were the various substrates used here in the study of different aspects of the electrocrystallization of chromium. The characteristics of the materials used are described in Table 4.1.

In the case of materials obtained as foils (platinum, copper, EN58B stainless steel) flag microelectrodes were cut giving rectangular edges with areas between 0.2-0.5 cm^2. The electrical contact was provided either by a long narrow strip of foil left at one corner of the rectangle as in the case of copper and stainless steel, or by spot welding a 0.1 mm wire of the same material, as in the case of platinum electrodes. The platinum electrodes were flame polished by heating in a reducing flame until bright red and dipping into 12 M HCl; the process was repeated several times and finally the electrodes were washed with distilled water, acetone, and then dried. Copper and EN58B flags were cleaned in chloroform and dried. The electrode areas of the flat microelectrodes were determined geometrically.

Tungsten micro-electrodes were made from 2.4 mm diameter rods sealed into silica glass. Electrical contact to the tungsten was made by silver soldering a length of copper wire to one end of the tungsten rod. The section exposed to the solution was ground flat and polished up to 1 μm on diamond wheels, to give a mirror-like surface.

The AGR fuel element cladding coupons were made into two kinds of electrodes. Flag microelectrodes which were made in a similar way to copper microelectrodes (see above) and large flag electrodes made of the whole original coupon from which a thin strip of material was separated to serve as the electrical contact (~2 cm^2 area).

The fuel cladding material was initially treated anodically at room temperature in a solution of H_2SO_4 sp. gr. 1.53, applying 6 V between the anode and a lead electrode of similar area, for 1 minute. This treatment has been used before for other stainless steels as a method to improve the adherence of chromium deposits obtained from aqueous solutions[161].

4.2.1.2. Counterelectrodes

Chromium counter electrodes were made out of one or two chromium flakes forming an anode with 2-3 cm^2 as a total area. The electric contact was made with 0.1 mm diameter Pt-13% Rh wire spot welded to one extreme of the flakes which was kept over the melt during the experiment.

Graphite counter electrodes were made of graphite rods cut in lengths of approximately 4 cms. The electrical contact was made through one of the sections screwed to a 2.2 mm diameter stainless steel rod. The graphite was previously boiled in diluted HCl solutions for cleaning purposes and to get rid of small graphite particles, which could contaminate the melt and interfere with the measurements.

Aluminium counterelectrodes were made of aluminium wire wound in order to produce a high surface electrode, placed in a separate pyrex compartment. The electrical contact with the melt was made through a melt bridge with glass wool. This kind of electrode was used in the anodic dissolution of chromium and was designed in order to minimize the interaction between the freshly formed lithium and the chromium (II) ions in the melt. As is well known the lithium metal incorporates easily into the aluminium producing then low activity lithium alloys[162,163].

4.2.1.3. Reference electrodes.

The Ag/0.5 M AgCl couple was used for the reference electrode. This consisted of a silver wire immersed in the solution of silver chloride in purified LiCl-KCl eutectic (see Section 4.3.2. below), contained in a pear-shaped glass bulb with a thin wall end. At the temperature of the experiment the thin glass wall is sufficiently conducting, presumably through the migration of alkali metal ions and acts as a suitable membrane[164].

A chromium reference electrode was also used to measure the Cr/Cr^{+2} potential. It was made similar to the chromium counter electrode but using only one small piece of chromium flake.

4.2.1.4. Melt purification electrodes.

The electrodes used in the purification of the melt were made of graphite rod (anode) and of aluminium rod (cathode); of 15 cm length each, which were screwed at the top end to 2.2 mm diameter stainless steel rods, respectively, for electrical contact.

4.3. EXPERIMENTAL PROCEDURE

4.3.1. Preparation of glassware

All glassware and cell components which were contacted with the melt, i.e. crucible, reference bulb, gas bubblers, etc., were soaked for at least 24 hrs in 1:1 concentrated sulphuric to nitric acid bath. They were then thoroughly washed with distilled water, acetone and then dried in an oven.

4.3.2. Melt purification

Lithium chloride-potassium chloride eutectic mixtures (LiCl:KCl = 41.5:58.5 mol%) require special preparation and handling. Purification of this melt is necessary owing to the presence of heavy metals and organic materials in the commercially available salts. Also important is the removal of the water content from the mixture, strongly attached to the highly deliquescent lithium chloride, which hydrolyse and contaminate the melt according to:

$$Cl^- + H_2O \rightarrow HCl\uparrow + OH^- \qquad 4.1$$

Alkaline contamination of the melt is undesirable because the electrode reaction.

$$OH^- + e \rightarrow 1/2\ H_2 + O^{2-} \qquad 4.2$$

can interfere with the electrode processes to be studied. Furthermore the alkaline environment leads to further contamination by the corrosive attack on glass components and may result in the precipitation of some solutes as insoluble species. There are several available methods for the purification of the LiCl-KCl eutectic and they have been critically reviewed[165].

The LiCl-KCl eutectic mixture used in these studies was purified according to the following procedure: the salt mixture was initially desiccated at high vacuum under a slow increase of temperature until the molten state was reached. Then the temperature of the melt was raised to 450°C and chlorine gas was bubbled through during approximately 2 hrs. At this stage chlorine would remove any alkaline contamination resulting from the hydrolysis of the melt occasioned by any residual water, according to the reaction[166]:

$$2OH^- + 2Cl_2 \rightarrow O_2\uparrow + 2HCl\uparrow + 2Cl^- \qquad 4.3$$

The melt was then cleaned of chlorine by flushing with argon during 5 hrs approximately. The melt was then

electrolysed under vacuum by applying 2.5 V between a graphite electrode (anode) and an aluminium electrode (cathode) for 24 hrs, in order to remove the heavy metals. The melt was finally filtered through a No. 4 glass filter removing in this way any suspended solid particles, such as graphite, which could have originated from the decomposition of the organic impurities contained in the original chemicals or been detached from the anode during the process. The final purified mixture after solidification and cooling was quickly transferred to a dry box under argon, where it was kept in a desiccator under P_2O_5.

4.3.3. Preparation of electrochemical cell

After the cell was assembled it was placed in a lifting support stand, connected to the vacuum line and degassed overnight under a vacuum of 10^{-3} torr or less. The cell was then filled with purified argon and transferred to the dry box where the crucible was loaded with purified melt and chromous chloride, both weighed in an analytical balance placed in the dry box. A few grams of 0.5 M AgCl mixture were also added to the glass bulb of the reference electrode. The closed cell was taken out of the dry box, reconnected to the vacuum line and evacuated overnight as before. The cell was then lowered into the furnace which was at 450^{o}C, and it was still maintained under vacuum up to 6-7 hours after the molten state was reached. An argon atmosphere was then introduced in the cell, the melt was bubbled for at least

24 hrs to guarantee a thorough dissolution of the $CrCl_2$ and then it was left to settle for at least 1 day, until a transparent deep green solution could be observed through the crucible walls. The electrodes, which during all this preparation were over 10 cms above the melt, were now immersed in the electrolyte, and the electrochemical measurements could then be initiated, after 1 hr at least.

In some experiments chromous chloride was not initially added to the crucible but chromium (II) ions were introduced later by anodic dissolution of chromium electrolytic flakes. In this case a three electrode system was also used, the chromium flake as working electrode, the Ag/0.5 M AgCl couple as reference electrode and aluminium wire as counterelectrode (cathode).

All the electrodes which had been introduced into the cell when this was originally assembled were kept inside during the whole experiment, with the exception of the working electrodes which could be exchanged. During the exchange operation the possible contamination with air was minimized by keeping a high Argon exit flow through the corresponding opened SQ13, while the electrodes were quickly interchanged. Immediately afterwards the cell was subjected to high vacuum for approximately 5 min, in order to evacuate the system of any moisture or air adsorbed on the fresh working electrode.

4.3.4. Electrochemical experiments

Electrochemical studies of the electrocrystallization of chromium were carried out on microelectrodes made of different materials and at various chromium (II) ion concentrations. The studies were based mainly on the use of two controlled potential techniques: linear sweep voltammetry and the potential step method (chronoamperometry).

The diagram in Figure 4.5a shows the wave form applied in the sweepvoltammetry experiments and the diagram in Figure 4.5b shows the characteristic shape of the current-time response obtained with this case.

The diagram in Figure 4.6a shows the waveform applied in a basic potential step experiment and the diagram in Figure 4.6b shows the typical plot of current decay obtained. Sometimes, according to the requirements of the experiment, more complex potential step waveforms were applied which will be described in the corresponding sections below.

4.3.5. Characterization of chromium electrodeposits

Chromium electrodeposits obtained on different substrates and under different electrodeposition conditions were characterized. In this case, after the corresponding working electrode was removed from the electrolytic cell, it was immediately washed in running hot water to remove the melt retained on the deposit surface, then rinsed in distilled water and acetone and finally dried and kept in sealed flasks.

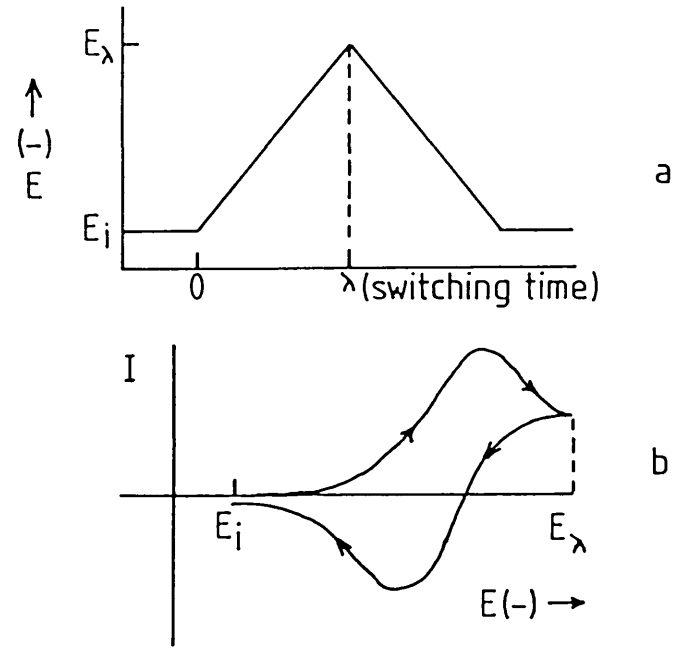

FIGURE 4.5. a) Cyclic potential sweep, b) Typical resulting voltammogram.

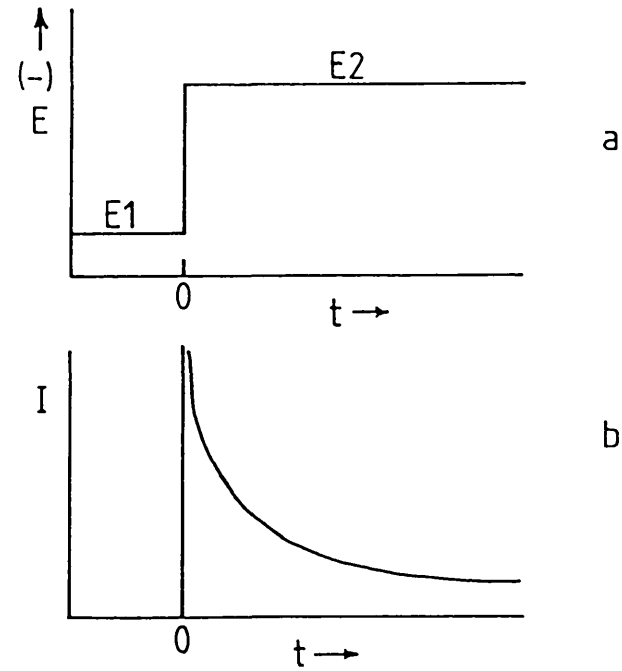

FIGURE 4.6. a) Waveform for a step experiment, b) Typical resulting current-time curve for a diffusional-limited rate process.

In the case of SEM observations the electrodes were used directly, without the need for additional preparation. In the case of profile morphology characterization and measurements of microhardness on chromium macrodeposits, it was necessary to obtain a cross section of the electrode. For this the electrode was vertically mounted, at high temperature, in a cylindrical bakelite mould and then polished to 1 μ.

Optical microscopic micrographs were obtained using a Reichert Mef II Inversion Microscope. In the case of microhardness measurements this system was complemented with a Reichert Micro-hardness Tester.

Scanning electron micrographs were obtained using a scanning microscope JSM-T200 Joel Technics Ltd. or a Stereocan 600, Cambridge.

The X-ray diffraction data of the chromium deposited was obtained using a Phillip X-ray generator with a cobalt target. Chromium powder for this analysis was obtained by grinding dendritic electrodeposits.

The adherence of chromium macrodeposits was tested with a Sebastian Adherence Tester (Quad Group), whose design is based on a modification of the original method of E.A. Ollard . This instrument measures adherence by simply measuring the force necessary to detach the coating from the substrate. The coating is vertically pulled out with a stud of known area, stuck on the deposit surface (see Figure 4.7). The pulling force, produced

with a tensile testing machine, is slowly increased from zero until reaching the detaching point, which is recorded. The stud-deposit surface link is made with a thermosetting resin which is polymerized at 150°C.

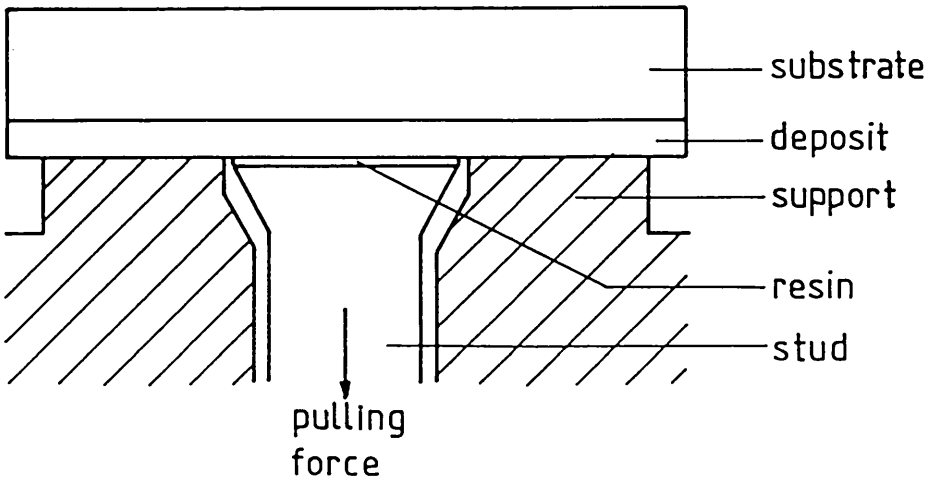

FIGURE 4.7. Detail of adherence tester.

To use this instrument the deposits have to be produced on completely flat surfaces, so that a good contact between the support and coating surface is established and any distortion due to internal stress created during the test is minimized.

5. NUCLEATION PHENOMENA IN THE ELECTROCRYSTALLIZATION OF CHROMIUM

5.1 CHARACTERIZATION OF THE SYSTEM

5.1.1 Sweep Voltammetry

The system under study was initially characterized by sweep voltammetry. Figure 5.1 shows a typical sweep voltammogram obtained at a sweep rate of 0.1 V sec^{-1} using a tungsten microelectrode. Two reversible waves were observed when scanning the LiCl-KCl-$CrCl_2$ system: a small pair of waves on the anodic side at approximately +0.2 V and a large pair on the cathodic side at approximately -0.7 V. These potentials correspond to the reduction of Cr(III) to Cr(II) and of Cr(II) to Cr(o), respectively. Studies of similar cyclic voltammograms obtained in the LiCl-KCl-$CrCl_3$ system at 500°C confirmed the number of electrons associated with each of these waves[54].

The waves corresponding to the Cr(II)/Cr(o) pair show the typical shape associated with a deposition/dissolution process on an inert substrate[135,147,150]. The current on the cathodic branch instead of increasing smoothly with the overpotential change, rises abruptly when the peak potential is approached resulting in a sharp shaped cathodic peak. An equally sharp fall in current occurs after the anodic peak and this is consistent with the stripping of a finite quantity of metal deposit from the electrode surface. The rising part of the cathodic peak is too steep and too cathodic of the reversible Cr(II)/Cr(o) potential to be considered the result of a simple diffusion controlled

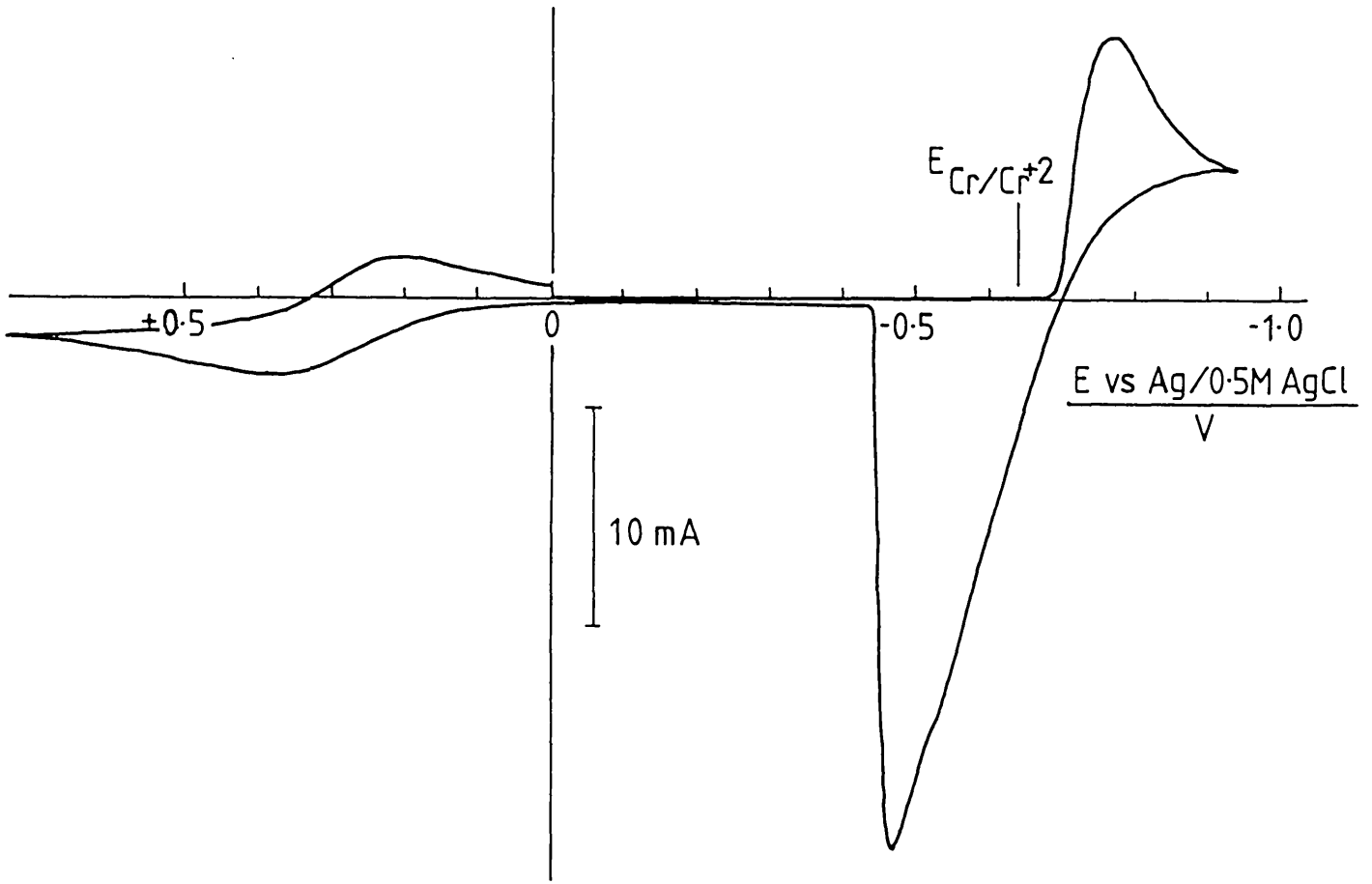

FIGURE 5.1. Sweep voltammogram for the $CrCl_2$-$(LiCl\text{-}KCl)_{eut}$ system: tungsten, 0.0452 cm^2, C = 0.931 $mol.dm^{-3}$, v = 0.1 $V.s^{-1}$

process. This delay in starting the cathodic process is related to the initial resistance involved in the formation of the new chromium phase. The nature of this phenomenon is more dramatically shown in cyclic voltammograms obtained at very low sweep rates such as that of Figure 5.2 which corresponds to a sweep rate of 1 mV sec^{-1}. It can be seen that the formation of the chromium deposit on the inert substrate requires the application of an extra overpotential related to the extra work necessary for the initial creation of critical chromium nuclei. Once this barrier is overcome the current rises sharply and enters a diffusion controlled regime. The reversible anodic wave shows some displacement to the left this time related to the extra work necessary to dissolve the chromium nuclei.

Sweep voltammograms were obtained at different chromium (II) ion concentrations and on different substrates, some typical ones being shown in Figures 5.3, 5.4. They all presented basically the same characteristics except for the case of less noble materials where the detection of the Cr(III)/Cr(II) wave was prevented by the onset of the anodic wave related to the dissolution of the substrate (see Fig. 5.4). The waves corresponding to the Cr(II)/Cr(o) transformation showed in every case the typical characteristics related to the nucleation phenomenon. Nevertheless the substrate determined to some extent the characteristics of the waves obtained as was clearly observed from slow sweep rate voltammograms,

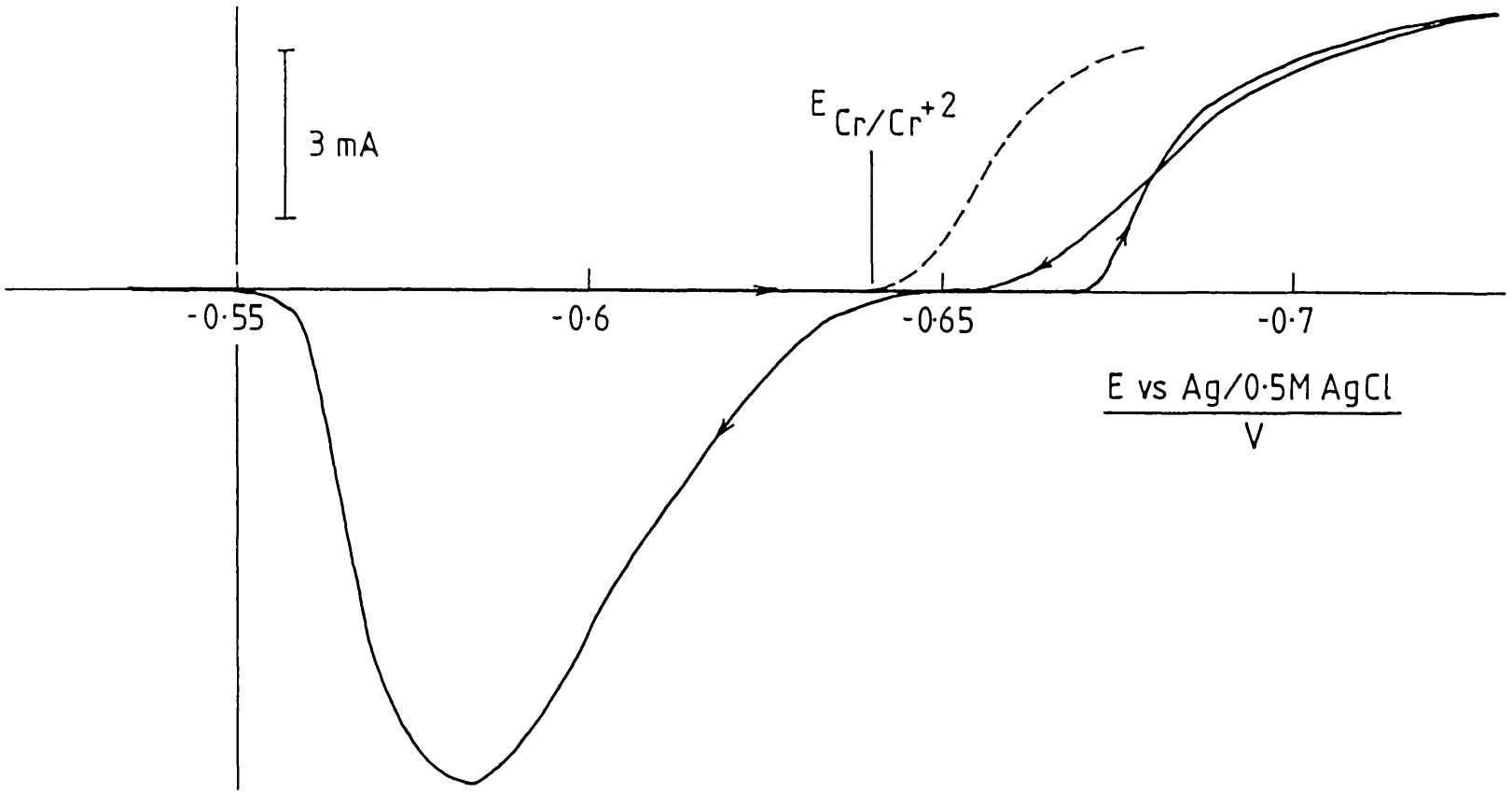

FIGURE 5.2. Low sweep rate voltammogram obtained on tungsten. Conditions as Figure 5.1, but v = 1 $mV.s^{-1}$

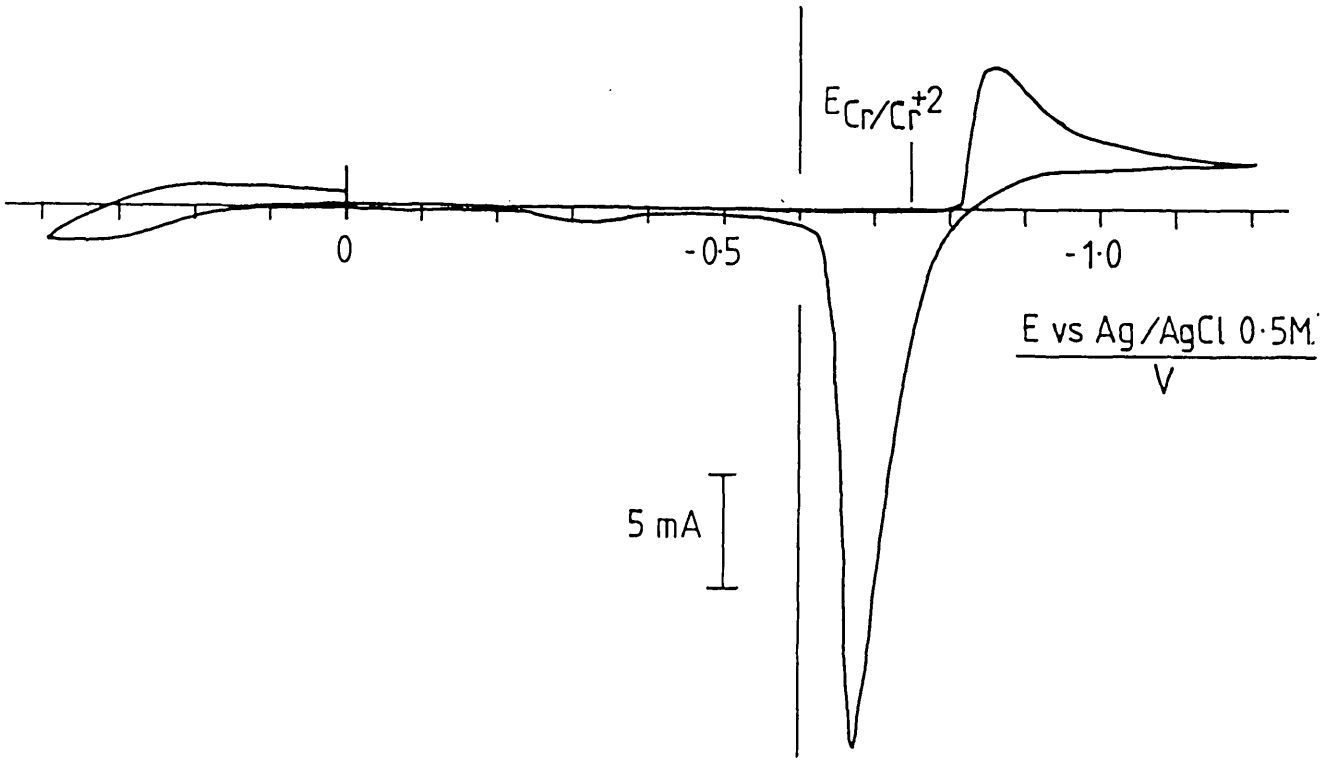

FIGURE 5.3. Sweep voltammogram for the $CrCl_2$-$(LiCl\text{-}KCl)_{eut}$ system: platinum, 0.387 cm^2, C = 0.039 $mol.dm^{-3}$, v = 0.1 $V.s^{-1}$.

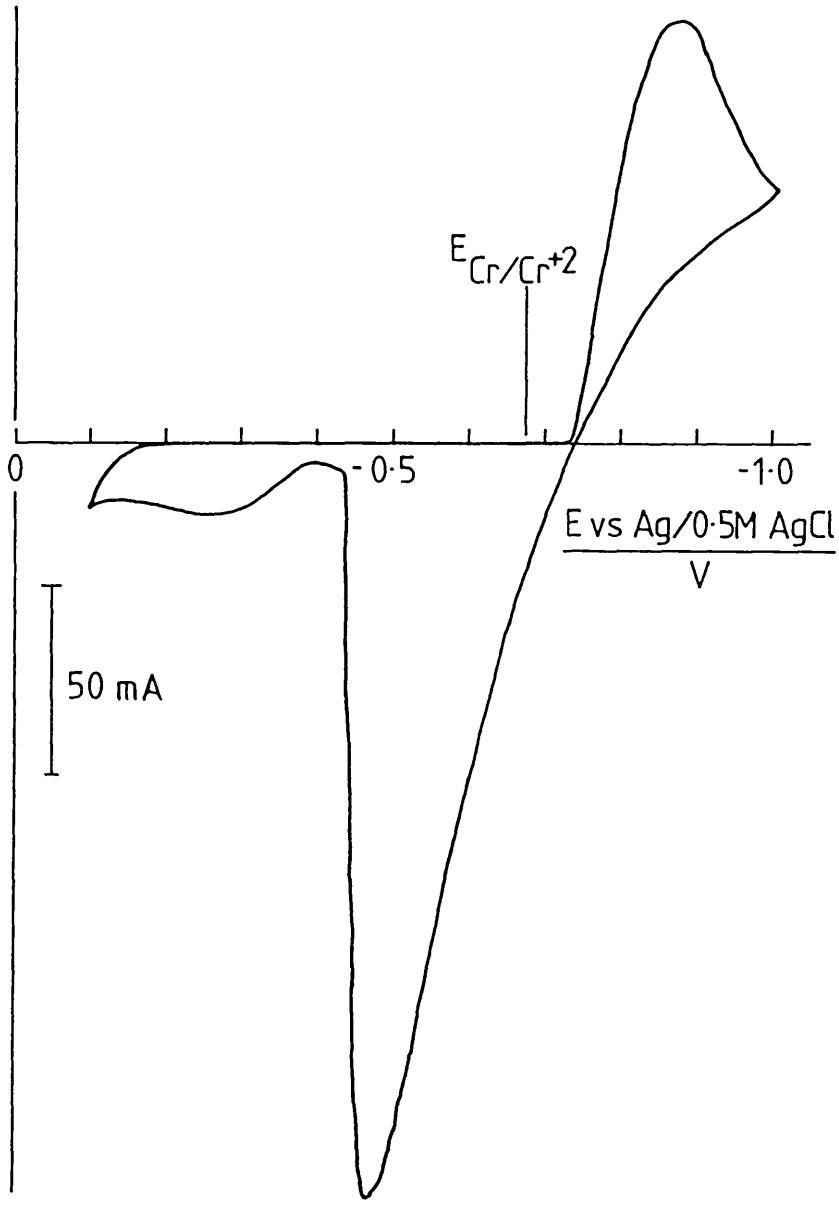

FIGURE 5.4. Sweep voltammogram for the $CrCl_2$-$(LiCl-KCl)_{eut}$ system: Nb stabilized 20/25 stainless steel, 0.7 cm^2, C = 0.346 $mol.dm^{-3}$, v = 0.1 $V.s^{-1}$.

as can be seen in Figure 5.5 where the overvoltage necessary to start the chromium electrodeposition varies for the different substrates. This change is in agreement with the nature of the work of critical nuclei formation, which depends on the interaction deposit-substrate manifested as "wettability" or adhesion (β). According to Figure 5.4 among the substrates considered, tungsten presents the lower resistance to the start of chromium nucleation indicating that the chromium-tungsten interaction is the highest in this case.

When studying the variation with sweep rate of cathodic peak potential the involvement of nucleation is revealed just as some additional kinetic factor which causes the system to deviate from the simple reversible behaviour[168]. As the sweep rate increases, the cathodic peak moves towards cathodic values and the displacement does not follow any simple relationship, as is shown in Figure 5.6. On the other hand, as is shown in Figure 5.7, I_p does not vary linearly with $v^{\frac{1}{2}}$ as expected for a simple diffusion controlled process.

Sweep voltammograms obtained in metal deposition on inert substrates have typically shown a deviation with respect to the reversible behaviour. On the one hand this has been related to the discrepancy between the theoretical model which assumes for the depositing metal an activity equal to one from the onset of the deposition, and the actual evolution of the activity during the early stages of deposition[168,169]. On the

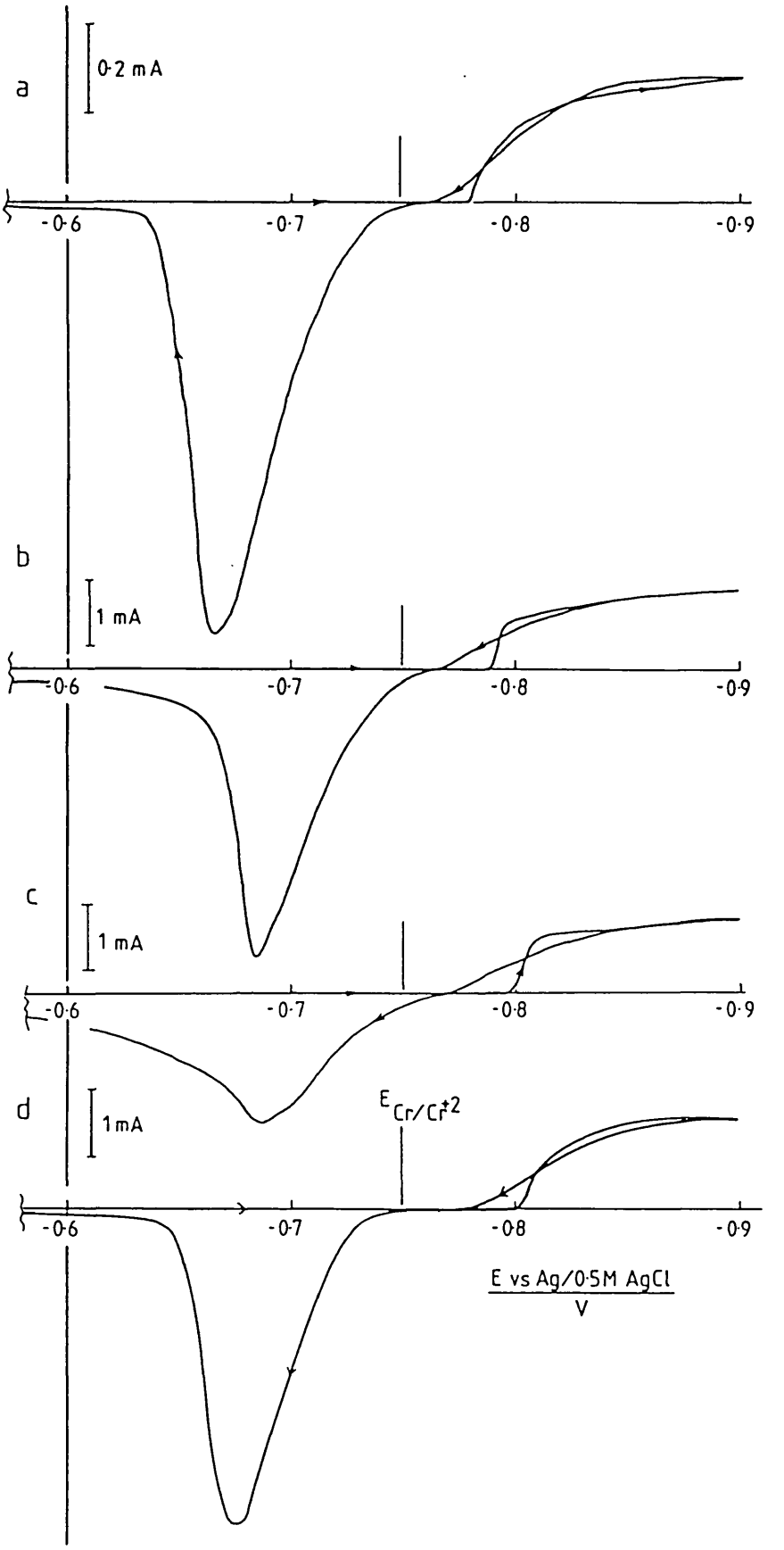

FIGURE 5.5. Effect of the substrate on the chromous ion reduction wave: C = 0.039 mol.dm^{-3}, v = 1 mV.s^{-1}.
a) tungsten, 0.0452 cm^2, b) Nb stabilized 20/25 stainless steel, 0.30 cm^2, c) EN 58B stainless steel, 0.28 cm^2, d) platinum, 0.387 cm^2.

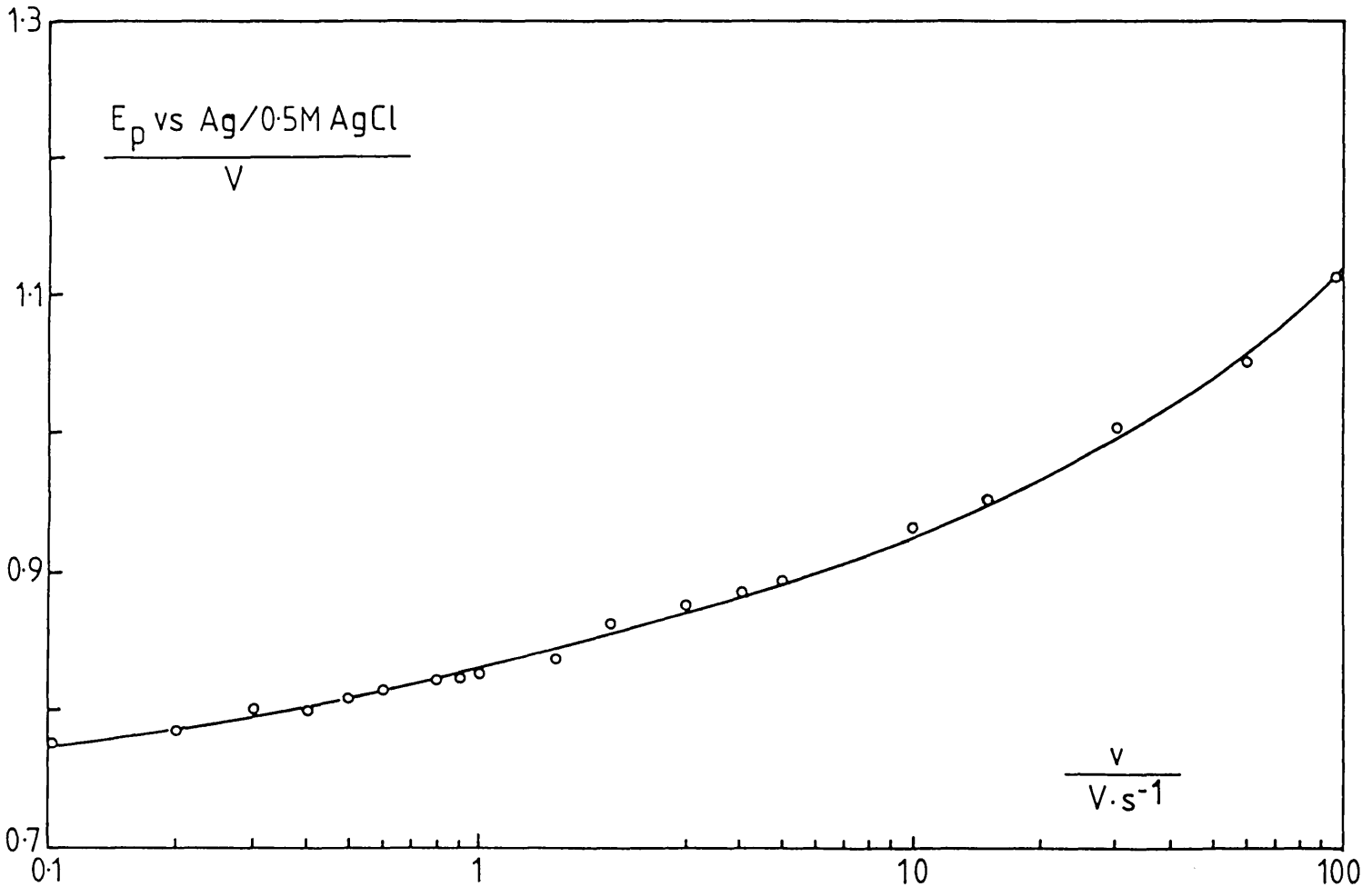

FIGURE 5.6. Dependence of E_p on the sweep rate for the reduction of chromous ions on tungsten: 0.0452 cm^2, C = 0.346 $mol.dm^{-3}$.

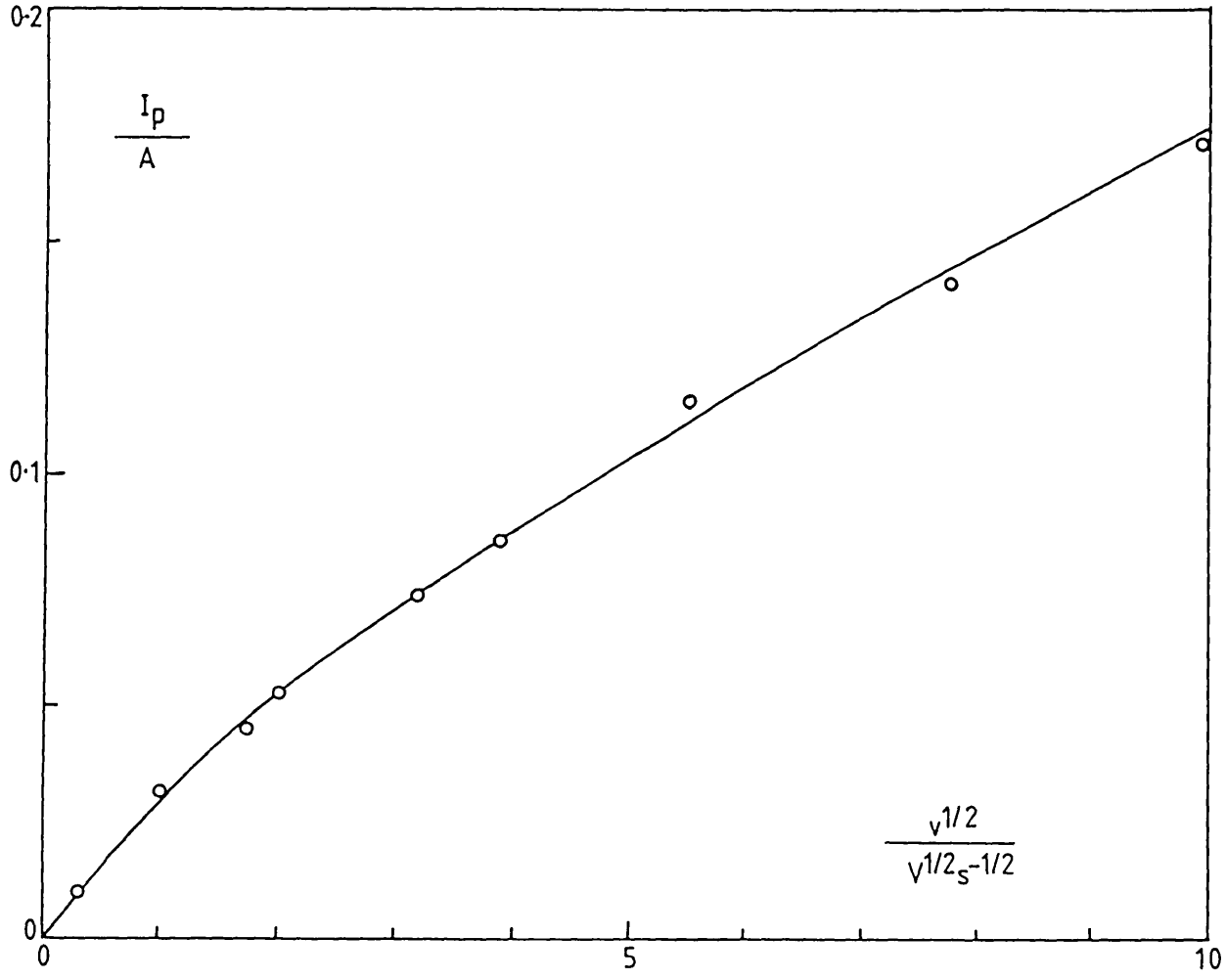

FIGURE 5.7. Dependence of I_p on the sweep rate for the reduction of chromous ions. Conditions as Figure 5.6.

other hand the involvement of a nucleation phenomenon as originating this deviation has been later also recognized[147]. In fact sweep voltammetry provides a useful initial criterion for characterizing a metal deposition reaction and can reveal the involvement of a nucleation stage. However it is not useful to define the nature of the nucleation in more depth. A thorough theoretical treatment considering nucleation should make allowances for different mechanisms which can control the various stages involved, that is induction, nucleation kinetics and saturation. Every one of these stages is potential dependent and the determination of the sweep voltammetric behaviour would involve in this situation a very complex mathematical problem which has not been attempted yet.

5.1.2. Potential Step Method

The involvement of a well defined nucleation stage in the formation of the chromium deposit is clearly revealed in the characteristics of potentiostatic current-time plots obtained at different overpotentials, different chromium (II) ion concentrations and on various substrates (see Figures 5.8,5.9). Instead of the typical current decay according to $t^{-\frac{1}{2}}$ expected for a simple diffusion controlled process, the curves show a more complex development associated with the morphological changes occurring on the electrode surface during the formation

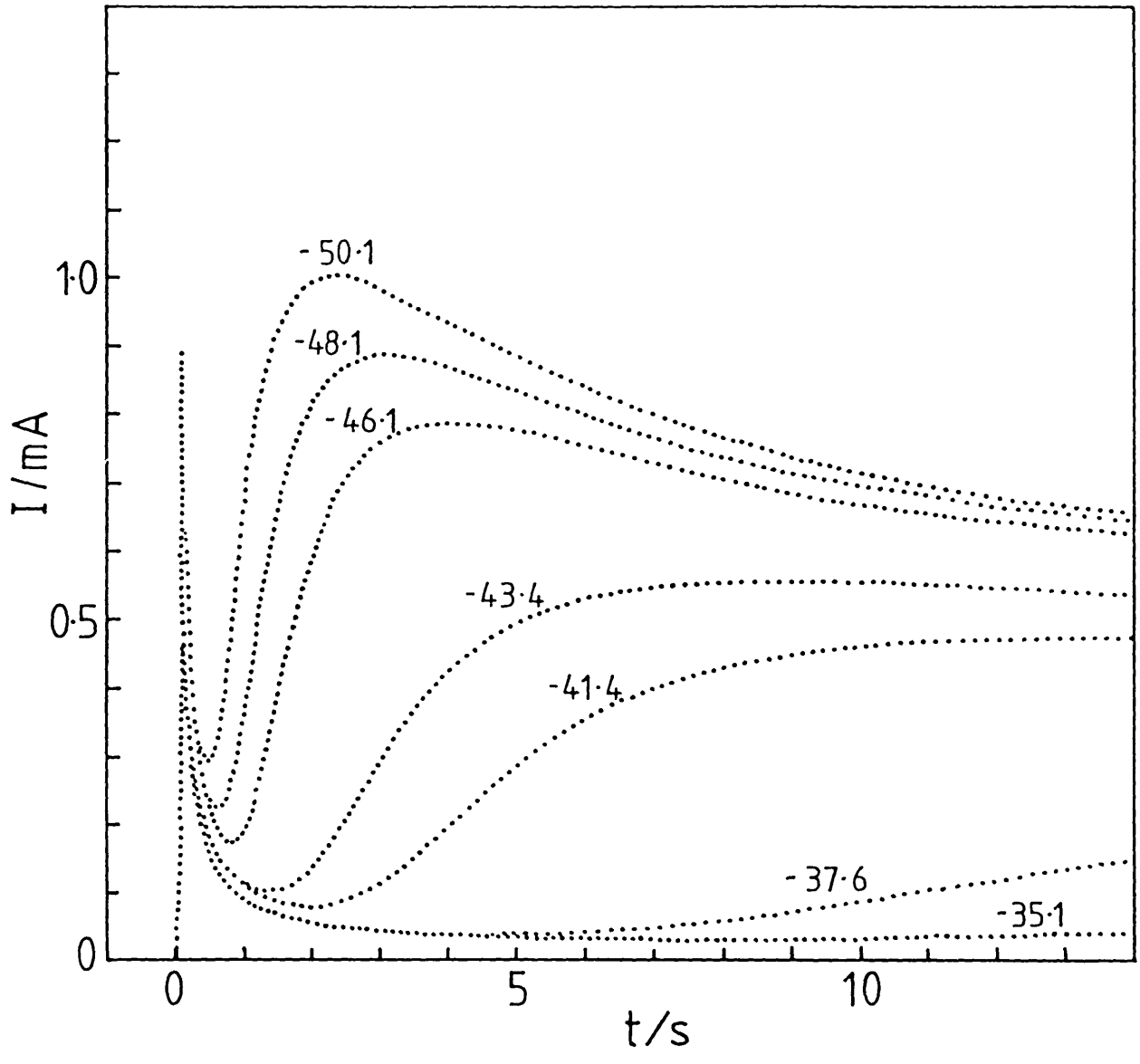

FIGURE 5.8a. Potentiostatic current transients for the electrodeposition of chromium on Nb stabilized 20/25 stainless steel: 0.30 cm^2, C = 0.039 $mol.dm^{-3}$ (overpotentials indicated in mV).

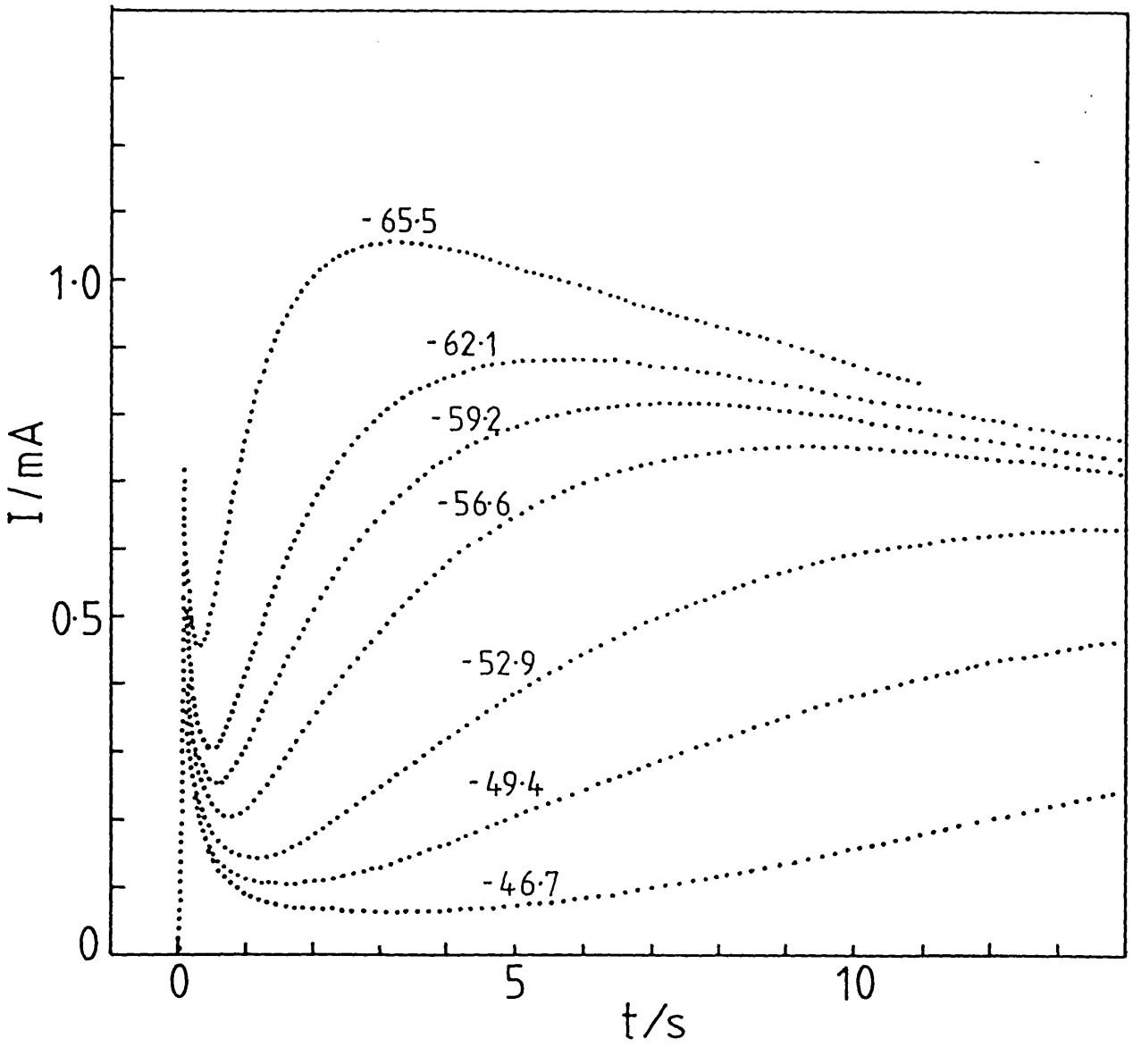

FIGURE 5.8b. Potentiostatic current transients for the electrodeposition of chromium on EN 58B stainless steel: 0.28 cm^2, C = 0.039 $mol.dm^{-3}$.

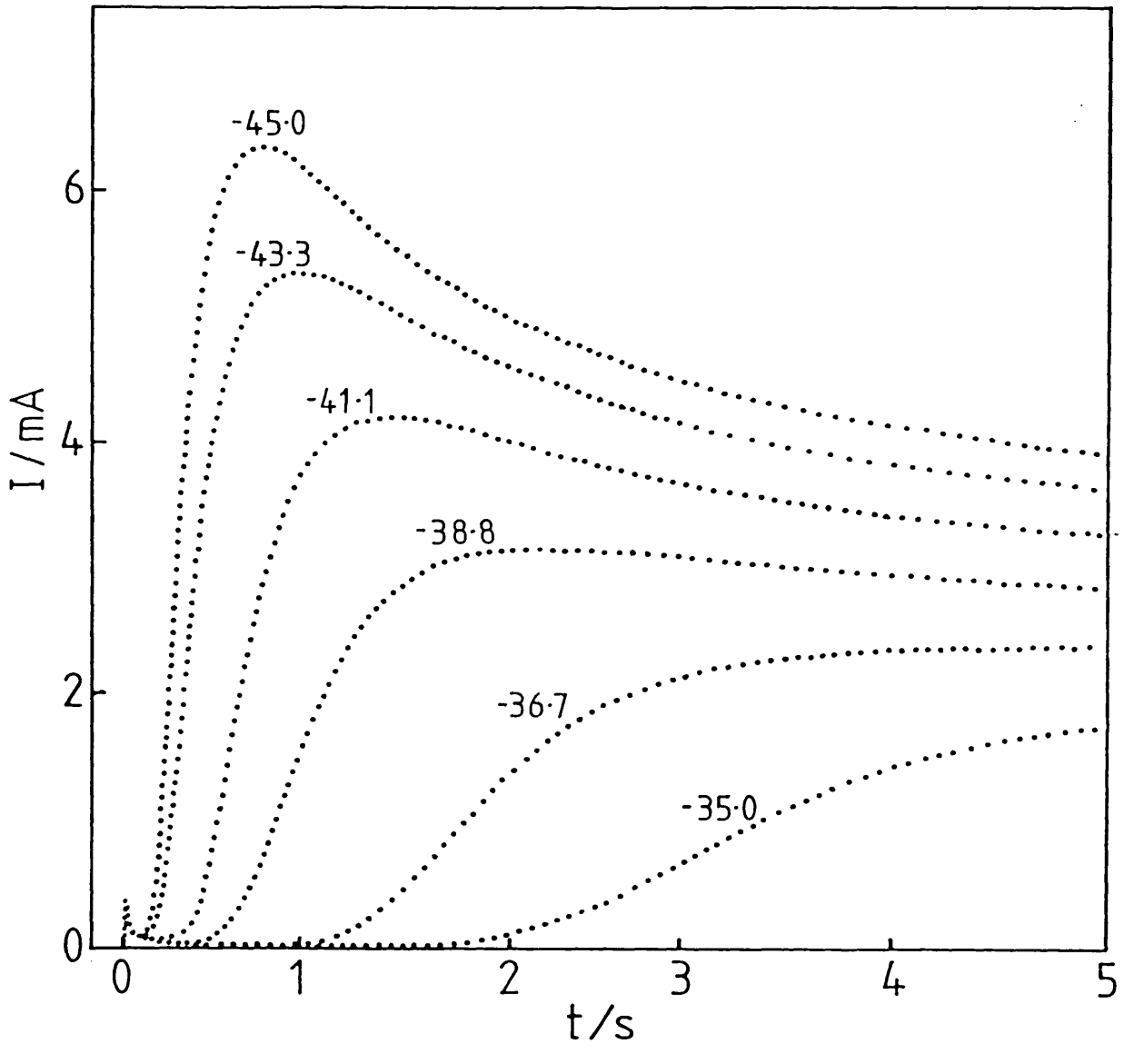

FIGURE 5.9a. Potentiostatic current transients for the electrodeposition of chromium on tungsten: 0.0452 cm^2, C = 0.931 $mol.dm^{-3}$.

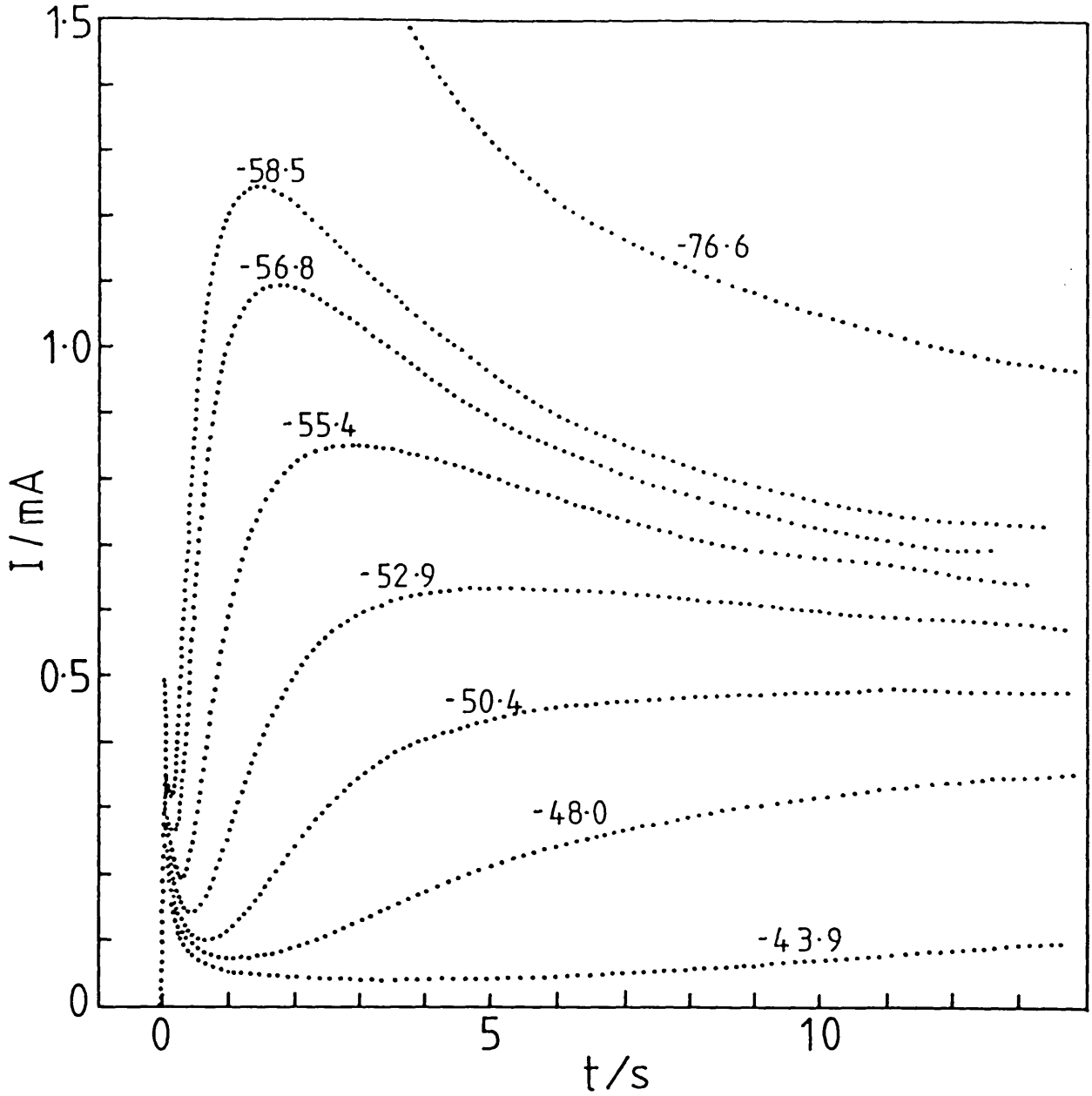

FIGURE 5.9b. Potentiostatic current transients for the electrodeposition of chromium on platinum: 0.4 cm^2, C = 0.039 $mol.dm^{-3}$.

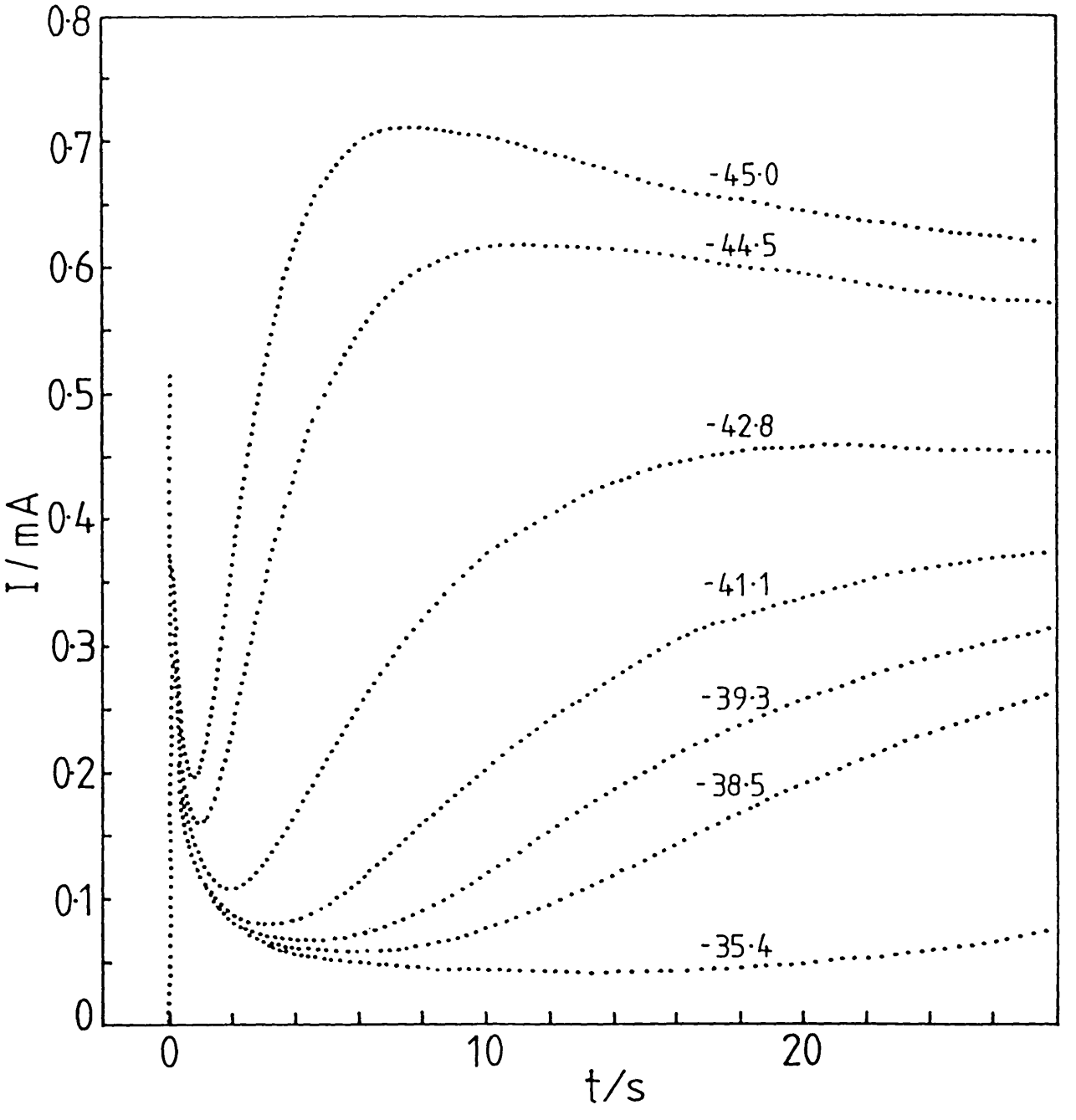

FIGURE 5.9c. Potentiostatic current transients for the electrodeposition of chromium on copper: 0.59 cm^2, C = 0.039 $mol.dm^{-3}$.

of the deposit. After an initial high current which is related to double layer charging and initial cluster formation, the current decays during the induction time and then increases again this time due to the formation and growth of discrete and stable nuclei which increase the deposition area. As the nucleation process is arrested and the individual diffusional zones of each nucleus begin to overlap, forming eventually a uniform diffusional plane parallel to the substrate surface, the current reaches accordingly a maximum and then decays following the usual $t^{-\frac{1}{2}}$ dependence.

The I-t curves are very dependent on the over-potential applied which is in agreement with the nature of the nucleation phenomenon. At low overpotentials, not sufficient enough to reach an appreciable rate of nuclei formation, the current plot shows after the initial peak just a continuous decay, at least in the range of the experiment. At higher overpotentials the rising zone of the current related to nuclei formation appears and this became steeper with increasing overpotential as the number of nuclei created augments. At very high overpotentials the nucleation stage becomes too quick to be detected by direct plotting on an X-Y recorder and just the usual diffusional $t^{-\frac{1}{2}}$ decay is observed. Nevertheless, measurements of the potentiostatic I-t transients obtained at high overpotentials with the aid of a transient recorder always revealed the characteristic rising current zone related to the nucleation stage.

5.1.3. SEM Observations on the Deposit

The involvement of nucleation in the initial stages of formation of the chromium electrodeposit was also verified through the direct observation of deposits formed at potentiostatic conditions during short times. The scanning electromicrographs in Figure 5.10 show different aspects of the early stages of chromium deposition on different substrates, and each of them typically reveals the presence of three-dimensional nuclei. The expected nuclei density increase with increasing applied overpotential can be observed for the case of EN 58B stainless steel in Figure 5.11 which shows the aspect of deposits obtained after 100 s at different overpotentials.

5.1.4. Conclusions

The electrocrystallization of chromium shows a well defined stage of nucleation. This phenomenon is critical in the mechanism of formation of the chromium electrodeposit as its occurrence persists all over the range of chromium (II) ion concentrations used ($0.03-1.61\ mol.dm^{-3}$) at every overpotential applied and on every substrate here considered. The characterization of its nature appears then as a condition *sin equa non* to understand the morphological aspects presented by the chromium deposits.

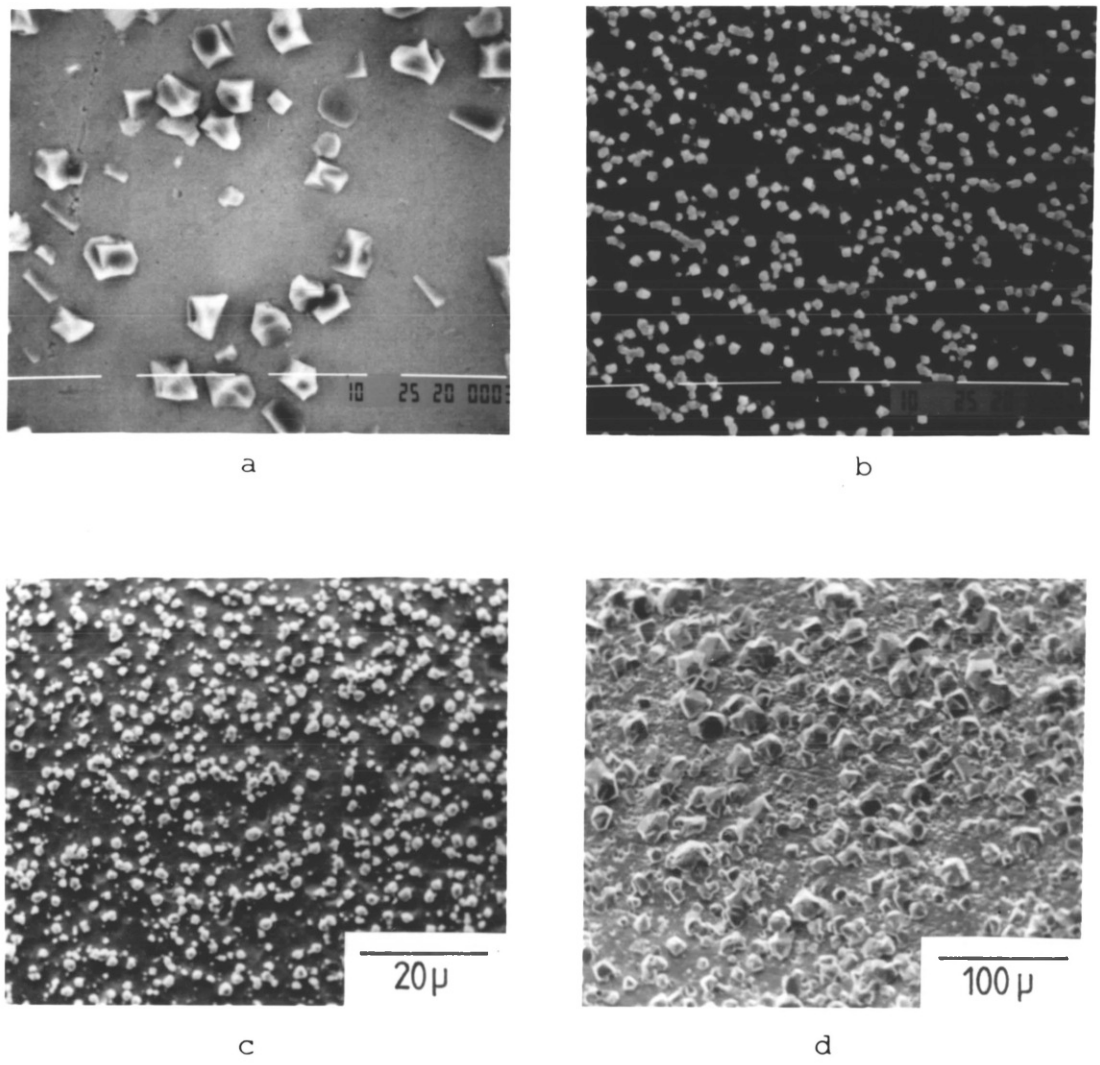

FIGURE 5.10. Scanning electron micrographs of chromium electrodeposits obtained on different substrates, showing the characteristic nucleated morphology. a) tungsten, b) platinum, c) EN 58B stainless steel, d) 20/25 Nb stabilized stainless steel.

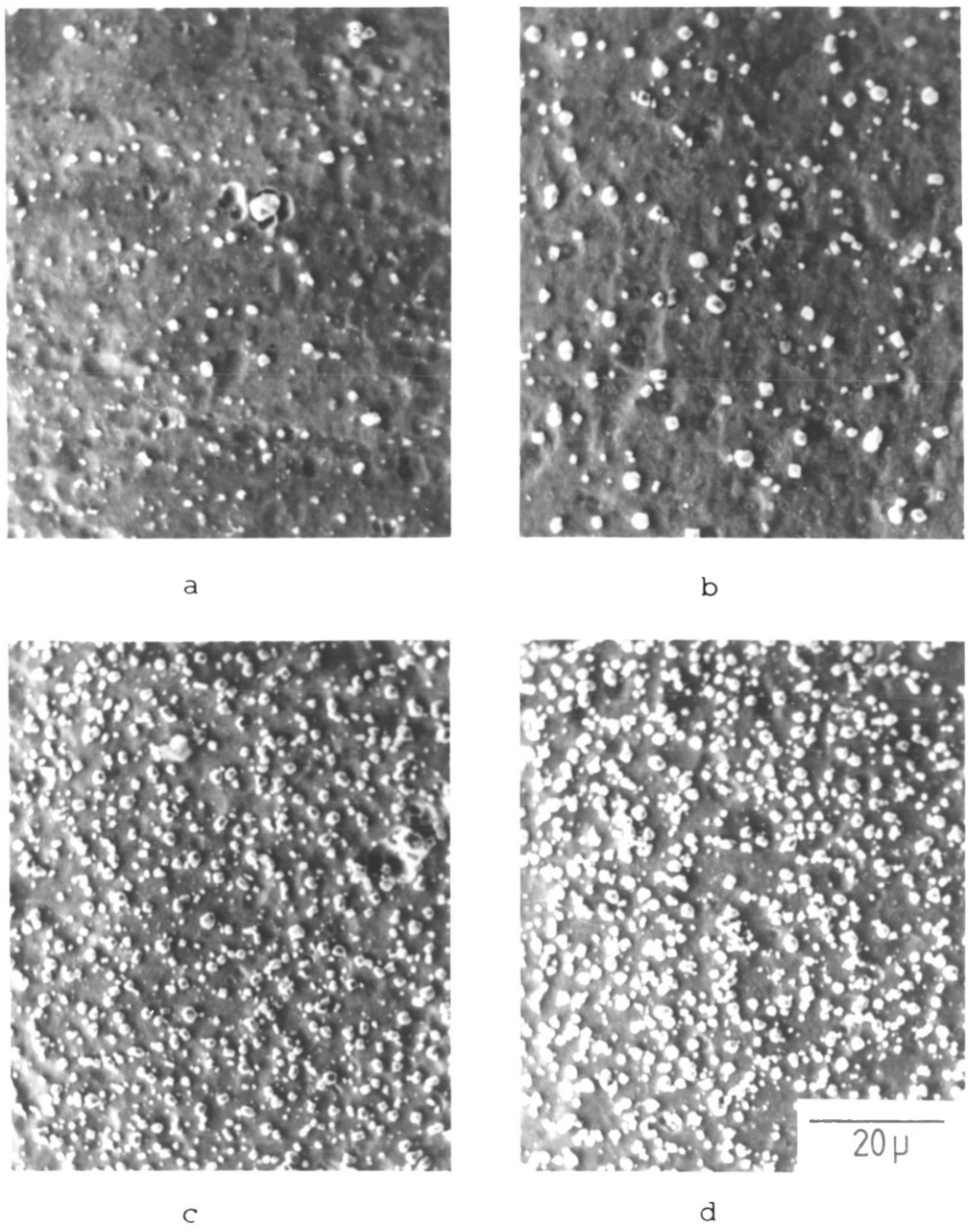

FIGURE 5.11. Scanning electron micrographs showing the increase of the final nuclei density with increasing overpotential. Deposition time: 100 s. Working electrode: EN 58B stainless steel. C=0.039 mol dm^{-3}. a) η =-0.045 V, b) η =-0.054 V, c) η =-0.064 V, d) η =-0.074 V.

5.2. ELECTROCHEMICAL NUCLEATION KINETICS

5.2.1. The determination of potentiostatic I-t transients

The study of the process of chromium electronucleation under potentiostatic conditions required the determination of reproducible and reliable I-t transients. This was not a straightforward achievement and therefore the design of a specific procedure was necessary, which was selected considering the following experimental observations:

a) If after the application of a potential pulse the electrode was returned to an overpotential just slightly anodic, then in the next transient with an identical pulse the characteristic rising region would not be obtained (see Figure 5.12). This indicated that under those conditions the formed deposit was not necessarily dissolved and a much more anodic overpotential was required to thoroughly clean the electrode surface and then to obtain reproducible responses. The anodicity of the cleaning potential (η_{cl}) was restricted first by the dissolution potential of the substrate and second by the decomposition potential of the electrolyte.

b) Once a potential step was applied, the cleaning potential η_{cl} had to be applied immediately afterwards. If instead the cleaning potential was applied after a few minutes of resting of the electrode, then the next transient obtained with an identical potential would show a much steeper slope indicating a dramatic

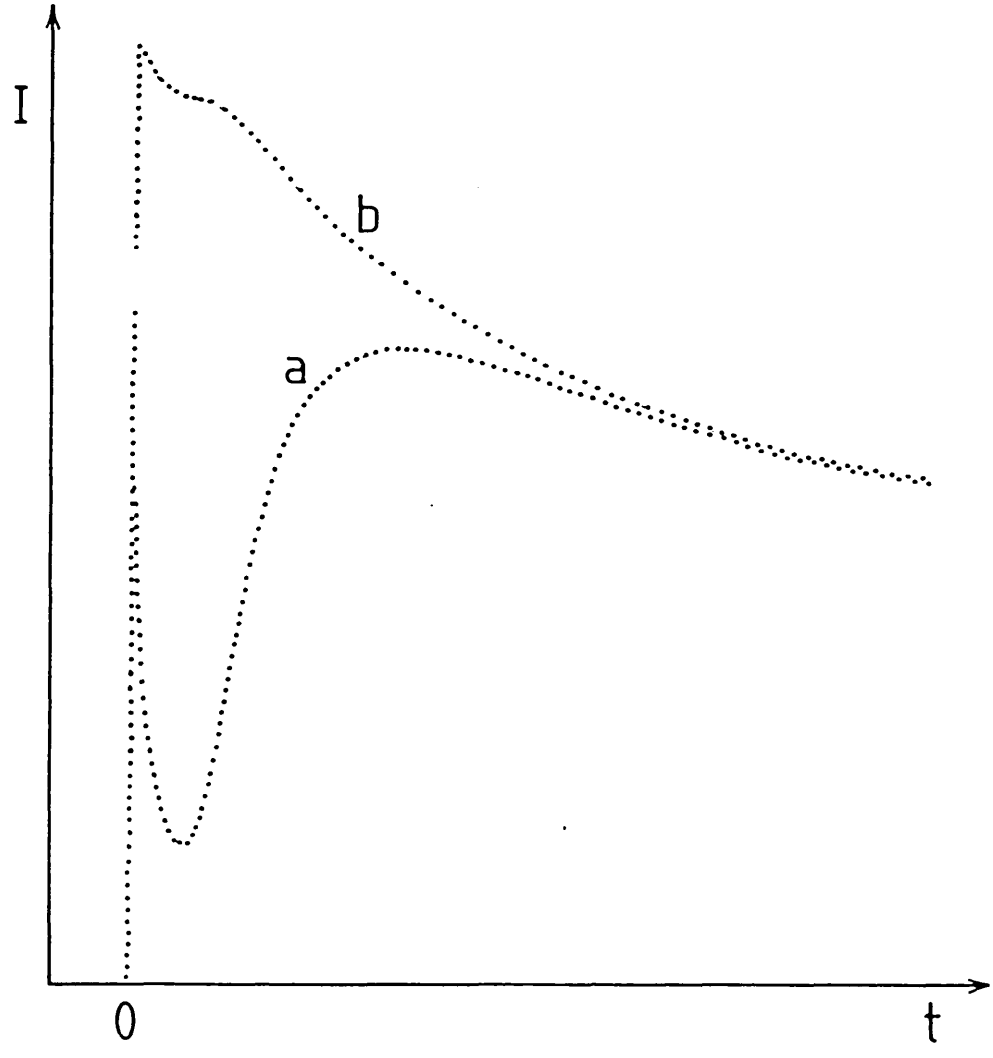

FIGURE 5.12. Effect of insufficient cleaning on the reproducibility of successive potentiostatic current transients. a) Initial transient, b) next transient, obtained at the same overpotential, but without applying previously an adequate cleaning overpotential.

increase of the substrate activity. This change could be attributed to some surface alloy formation between the substrate and the chromium nuclei. At the working temperature just the first atomic layers of the substrate may have been involved in this transformation, but these are the ones which determine the characteristics of the nucleation. When the surface transformation occurred, it seemed to be quite stable and in those cases even the application of a very positive cleaning potential would not produce a return to the original properties of the substrate.

c) Before obtaining an I-t transient it was found convenient to apply a rest potential slightly anodic with respect to the chromium (II)/chromium (o) reversible potential, in order to stabilize the system and minimize the initial deposition of some impurities which could affect the activity of the substrate.

The cycle of potential steps finally selected is shown in Figure 5.13 with the corresponding current transients obtained. The cleaning pulse η_{cl} took a value typically in the range +0.3, +0.7 V (w.r.t. $E_{Cr^{+2}/Cr^{o}}$) and it was applied for a time sufficient to bring the anodic current to zero, usually in the order of 0.5 to 2 min. The rest potential η_r usually took a value between +15 and +100 mV and it was applied for 5 to 10 seconds. If after the cleaning potential the electrode was left to rest for some time in open circuit then, before applying the next cathodic step, it was

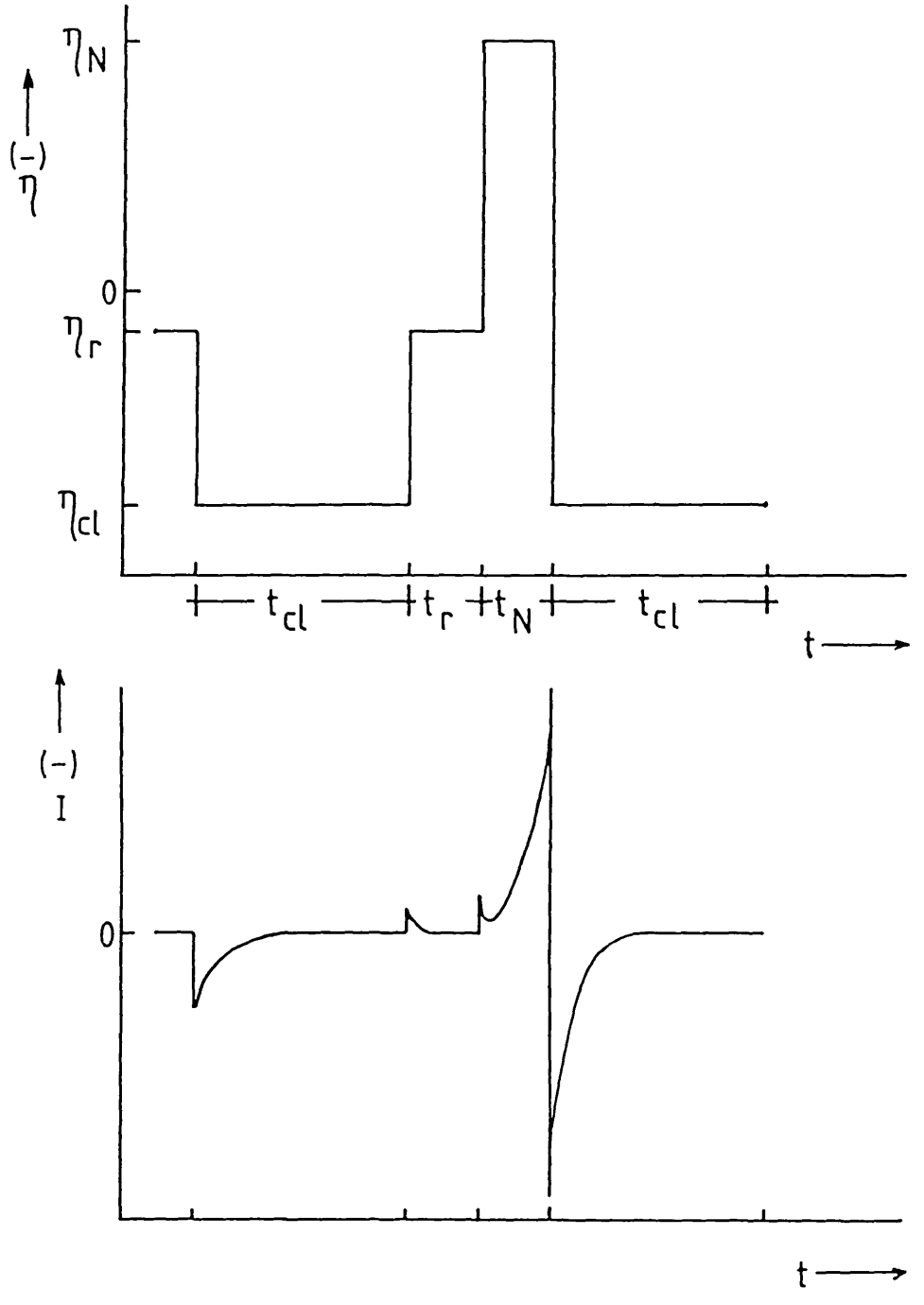

FIGURE 5.13. a) Step waveform applied in the chromium electronucleation studies, b) Typical current response.

found to be advisable to repeat the cycle from the beginning. In general the activity of an electrode evolved slightly with time due perhaps to some ageing, adsorption of impurities, etc. Therefore it was convenient to perform the electrochemical measurements with electrodes recently introduced into the melt.

The selected procedure permitted the obtaining of reproducible potentiostatic current-time transients.

5.2.2. Characteristics of the potentiostatic I-t transients

The rising sections of the potentiostatic current-time transients were analyzed in order to initially characterize the nature of the nucleation process. Plots of logI-logt corresponding to potentiostatic transients obtained on tungsten at 0.042 mol.dm^{-3} chromium (II) concentration, are shown in Figure 5.14a. The plots obtained at different overpotentials followed a similar pattern presenting a well defined middle section with a slope 3/2. According to the previous theory (see Section 3.3) this value for the slope indicates that the rising region of the current transients had its origin in the simultaneous processes of formation and growth of three-dimensional chromium nuclei, their growth being controlled by the diffusion of chromium (II) ions from the melt. After the middle section the slope of the curves in Figure 5.16 continually decayed until reaching a slope with a value of 1/2. This is consistent

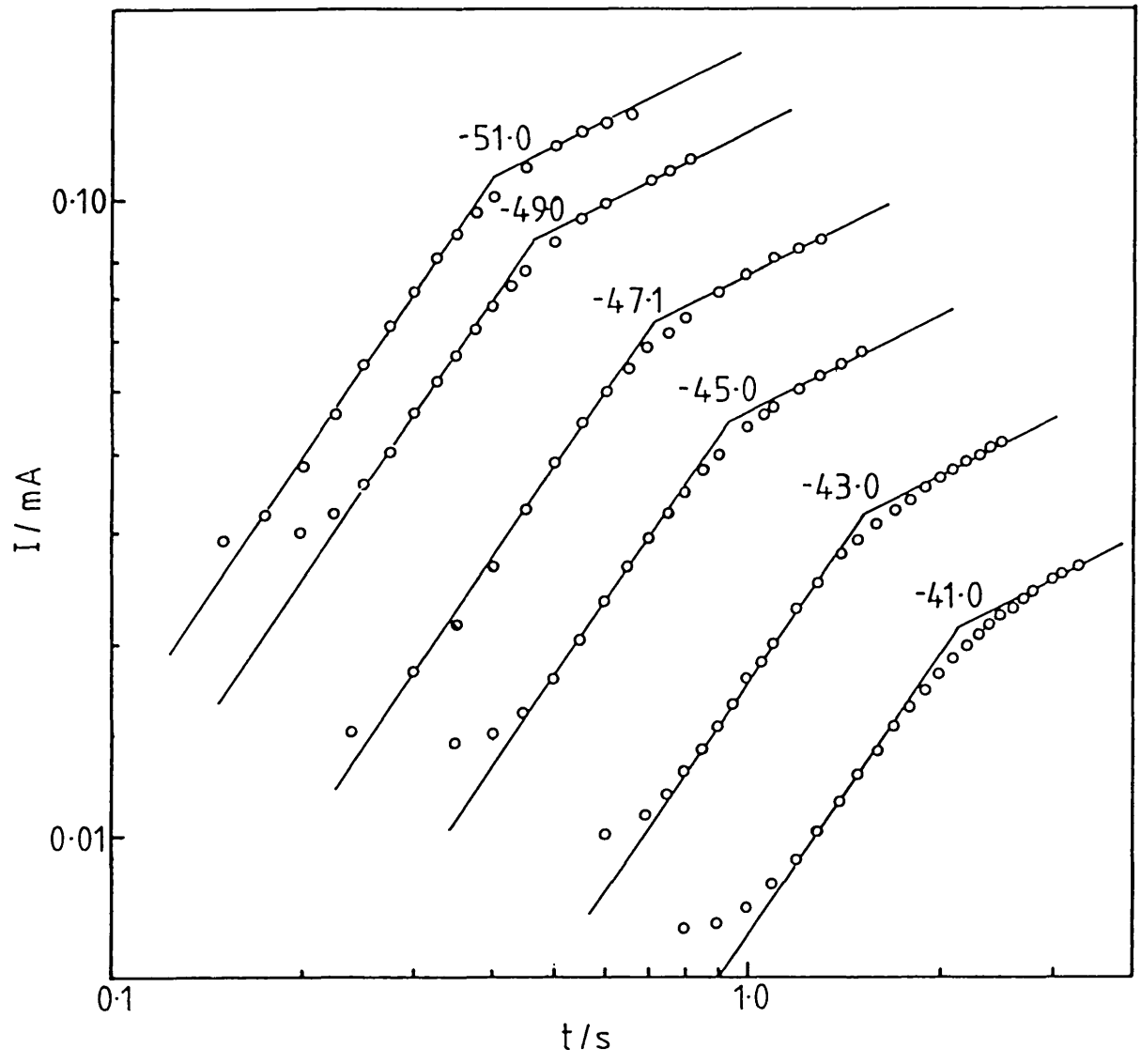

FIGURE 5.14a. Log I-log t plots for the potentiostatic current transients obtained on tungsten: 0.0452 cm^2, C = 0.042 $mol.dm^{-3}$ (overpotentials indicated in mV).

with the model for instantaneous nucleation, and indicates that here the nucleation process has practically stopped and the current is fundamentally due to the growth of the nuclei formed in the initial stage.

The characterization of potentiostatic current-time transients was extended to higher chromium (II) ion concentrations and to different substrates. Plots of log I-log t corresponding to transients obtained on tungsten at 0.346, 0.931, 1.487 mol.dm^{-3} chromium (II) ion concentrations are shown in Figures 5.14 b,c,d respectively. Plots of log I-log t for the case of a platinum microelectrode at a 0.346 mol.dm^{-3} concentration are shown in Figure 5.14e. It can be observed that even with the wide range of concentrations considered ($\sim$20 times), the log I-log t plots show a fairly consistent pattern and always present a well defined linear section related to the simultaneous growth and formation of nuclei. Nevertheless, the application of the model of nucleation and growth controlled by diffusion is more restricted as the chromium (II) ion concentration increases. At 0.346 mol.dm^{-3} there is still a defined range of overpotentials where the plots log I-log t have a slope equal to 3/2. However at low overpotentials the slope tends to increase, a fact that can be related to a displacement of the growth control from diffusion in the solution towards some mechanism of attachment on the nuclei surface[157]. On the other hand as the overpotential increases, the intermediate

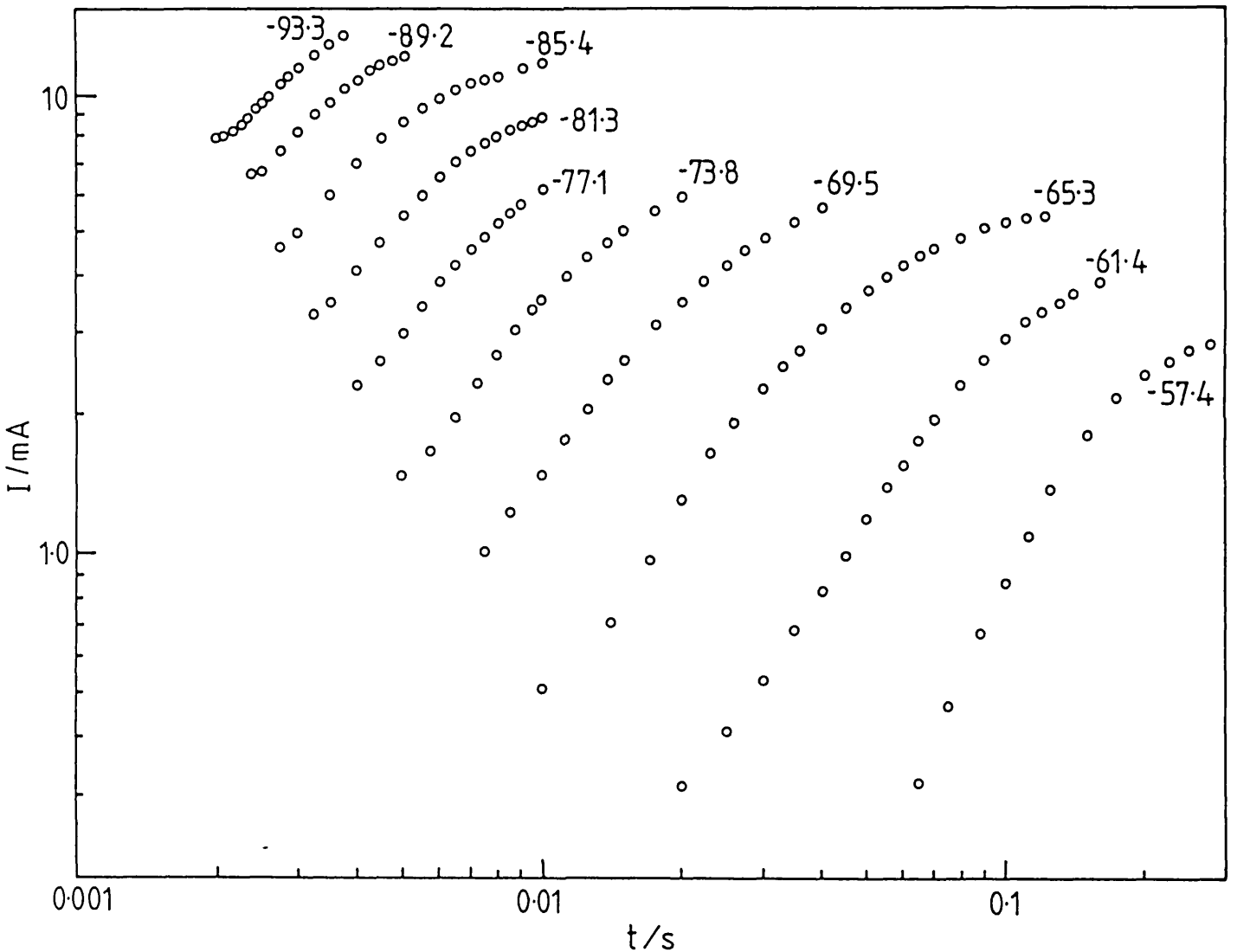

FIGURE 5.14b. As Figure 5.14a, with C = 0.346 mol.dm^{-3}

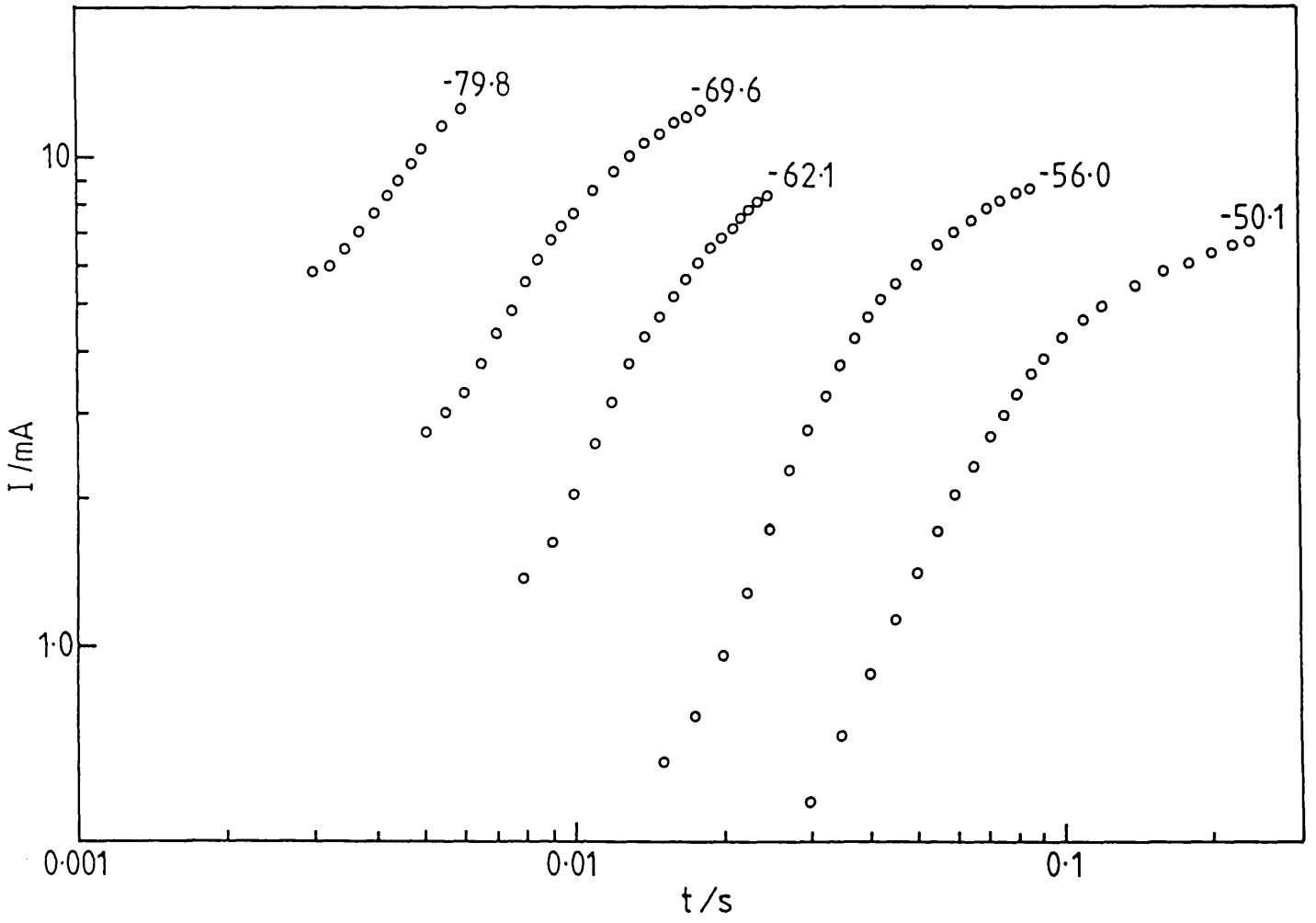

FIGURE 5.14c. As Figure 5.14a, with C = 0.931 mol.dm^{-3}

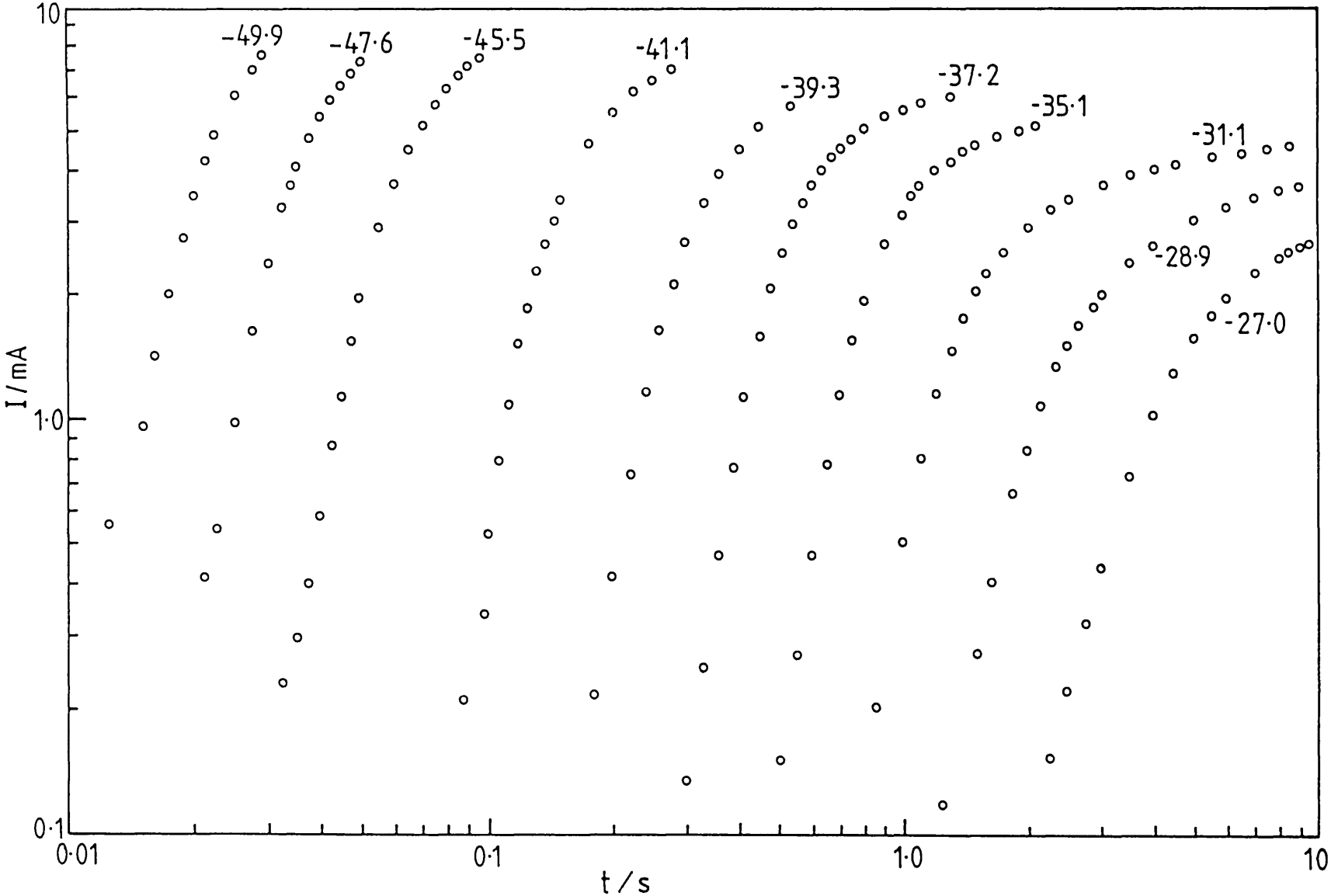

FIGURE 5.14d. As Figure 5.14a, with C = 1.487 mol.dm^{-3}

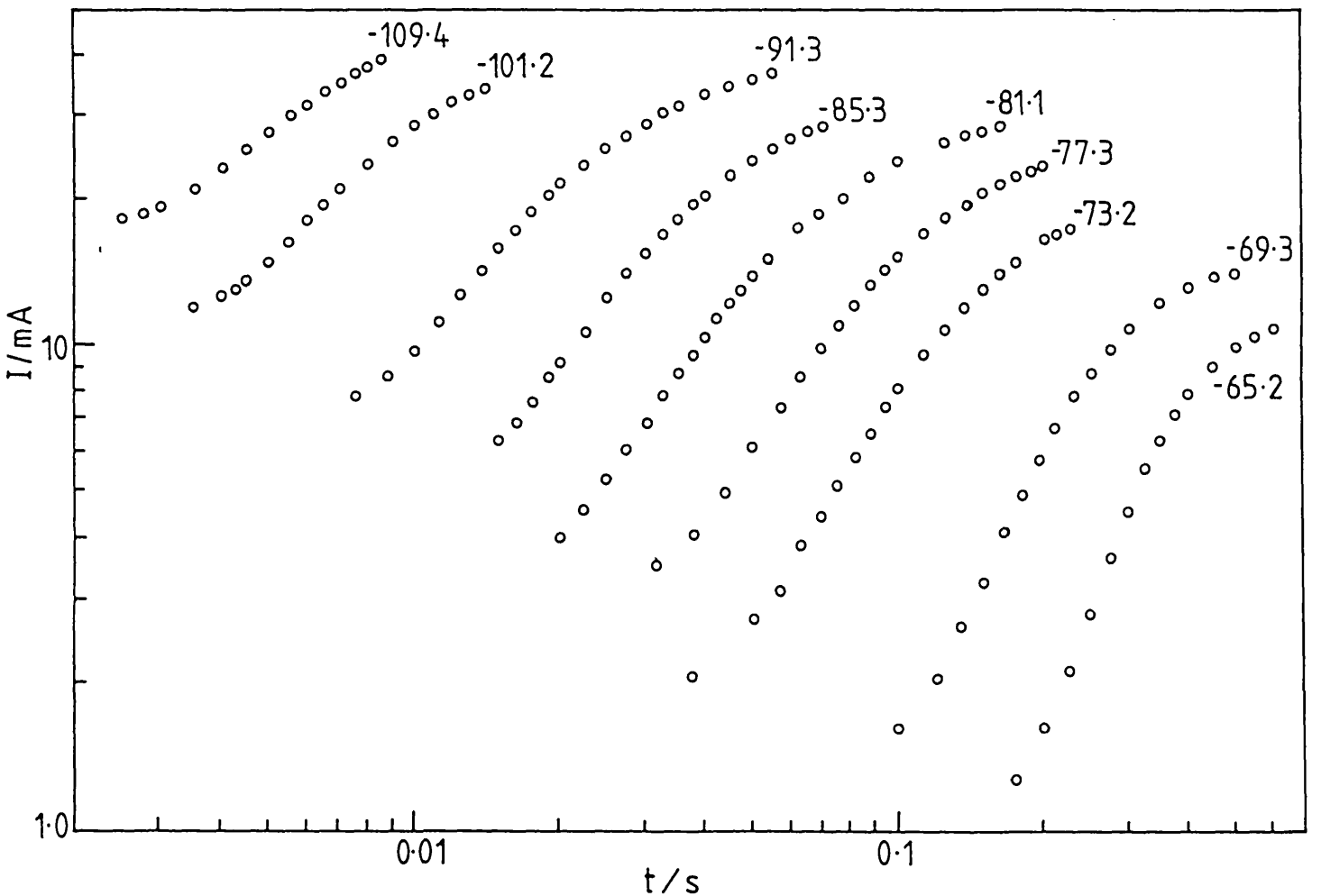

FIGURE 5.14e. Log I-log t plots for the potentiostatic current transients obtained on platinum: 0.245 cm^2, 0.346 $mol.dm^{-3}$.

part of the log I-log t plots is less defined and its slope tends to decay rapidly with time. At higher overpotentials there is not a defined region where the linear development of nucleation can be detected and the process of nuclei saturation seems to be superimposed from the start of the transient. A range of overpotentials where the growth of nuclei occurred under diffusion control still appeared in the experiments at concentrations of 0.931 $mol.dm^{-3}$ (Figure 5.14c), but at 1.487 $mol.dm^{-3}$ it could not be detected at all. At this high concentration the log I-log t plots showed an unusually high slope at every overpotential, indicating that in this case a control mechanism of a different nature becomes predominant.

5.2.3. Determination of the steady-state nucleation rate

Potentiostatic current-time transients obtained under conditions of diffusion control have typically shown the $I-t^{\frac{1}{2}}$ linear dependence corresponding to instantaneous nucleation[143-145,147-149,151] except in the low overpotential region where the involvement of progressive nucleation has been also detected[149]. In the conditions studied the electrochemical nucleation of chromium consistently showed a well defined progressive stage of nucleation and the current-time transients here obtained conveyed the information necessary to

characterize the kinetics of this process.

The expression for the current to a single nucleus growing under mass transfer control and assuming a hemispherical diffusive flux is given by[147]

$$I_1(t) = zF\pi\ M^{\frac{1}{2}}(2CD)^{3/2}(1-\exp z\eta F/RT)^{3/2}t^{\frac{1}{2}}/\rho^{\frac{1}{2}} \qquad 5.1$$

If nucleation and growth occur simultaneously, assuming there is no overlap of diffusion zones, the resulting current is given by[98]

$$I = \int_0^t I_1(u)(dN/dt)_{t=t-u}\ du \qquad 5.2$$

where u is the age of the nucleus and N is the number of nuclei at any time during the process of nucleation. It has been experimentally observed that under potentiostatic conditions the number of nuclei grows linearly with time before reaching a final saturation number[114,116]. For the linear region we can then write

$$dN/dt = S.I_o \qquad 5.3$$

where S is the area of the electrode in cm^2 and I_o represents the steady state nucleation rate expressed in nuclei.sec^{-1}.cm^{-2}. Substutiting $\underline{u}$ for $\underline{t}$ in the expression 5.1, the resulting current obtained by integrating 5.2 is:

$$I = 2\, I_o.S.z\pi M^{\frac{1}{2}}(2CD)^{3/2}(1-\exp(-z\eta F/RT))^{3/2}\, t^{3/2}/3\rho^{\frac{1}{2}} \qquad 5.4$$

This expression can be applied here to calculate the steady-state nucleation rate of chromium at those overpotentials for which the $I-t^{3/2}$ linear relation is fulfilled. Differentiating I with respect to $t^{3/2}$ in equation 5.4 and then rearranging, the steady-state nucleation rate I_o turns out to be

$$I_o = (dI/dt^{3/2})/[K_3(1-\exp(-z\pi F/RT))^{3/2}S] \qquad 5.5$$

where

$$K_3 = 2.S.z.F\pi M^{\frac{1}{2}}(2CD)^{3/2}/3\,\rho^{\frac{1}{2}} \qquad 5.6$$

In the present case z = 2, M = 52, ρ = 7.2 $gr.cm^{-3}$ and T = $723^{o}K$. A value for the diffusion coefficient $D = 1.29 \times 10^{-5}\ cm^2.s^{-1}$ was calculated from the $I-t^{-\frac{1}{2}}$ transients obtained for relatively high overpotential steps (see Appendix I). This value compares well with others reported by previous workers[56,170,171] and is typical for a divalent transition metal ion in this chloride media[170].

The value of $dI/dt^{3/2}$ was evaluated at each overpotential from Figures 5.15 a-d and the corresponding values for the steady-state nucleation rate were calculated according to eqn. 5.5, being shown in Table 5.1.

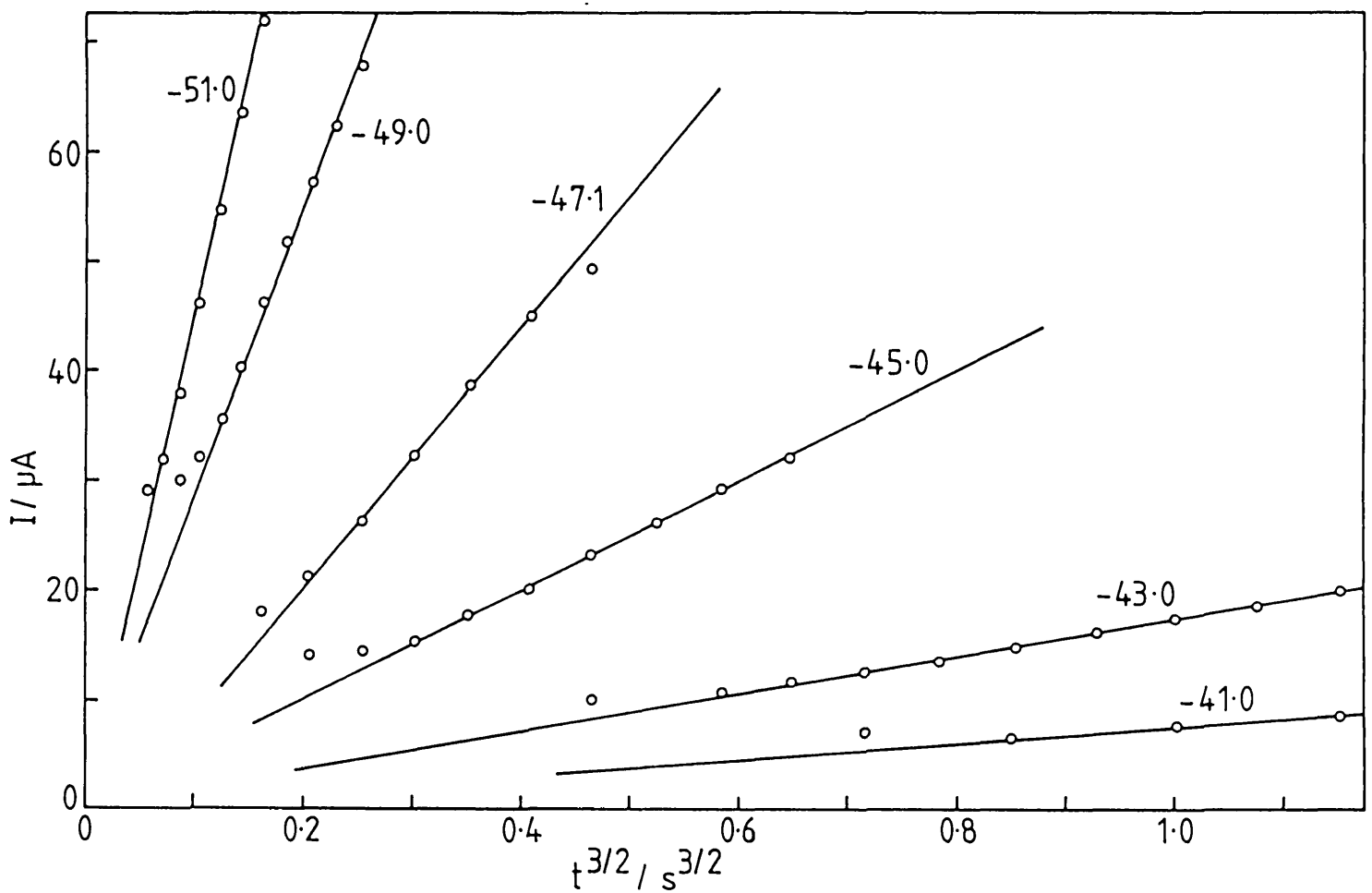

FIGURE 5.15a. I-$t^{3/2}$ plots. Data from Figure 5.14a.

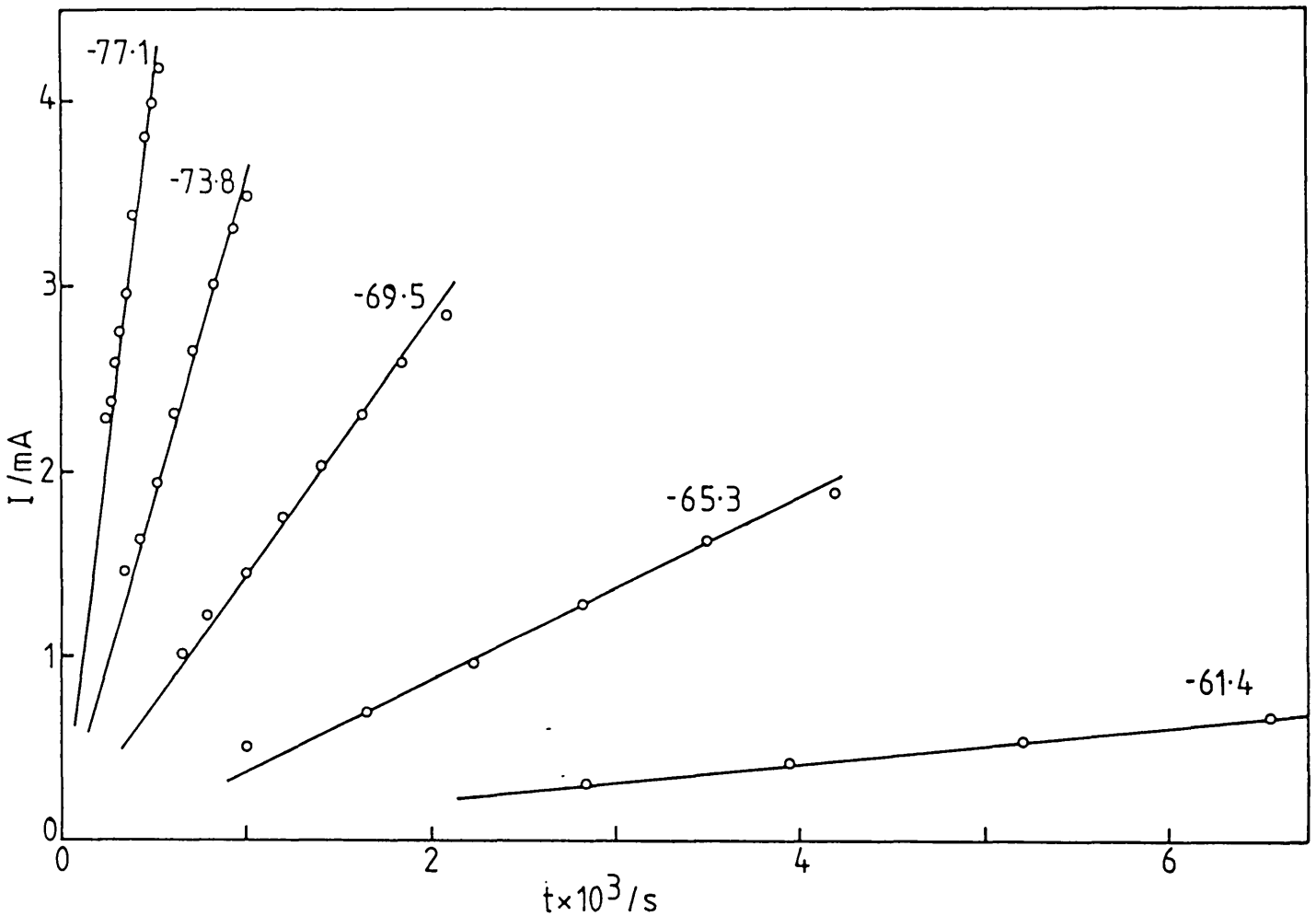

FIGURE 5.15b. I-$t^{3/2}$ plots. Data from Figure 5.14b.

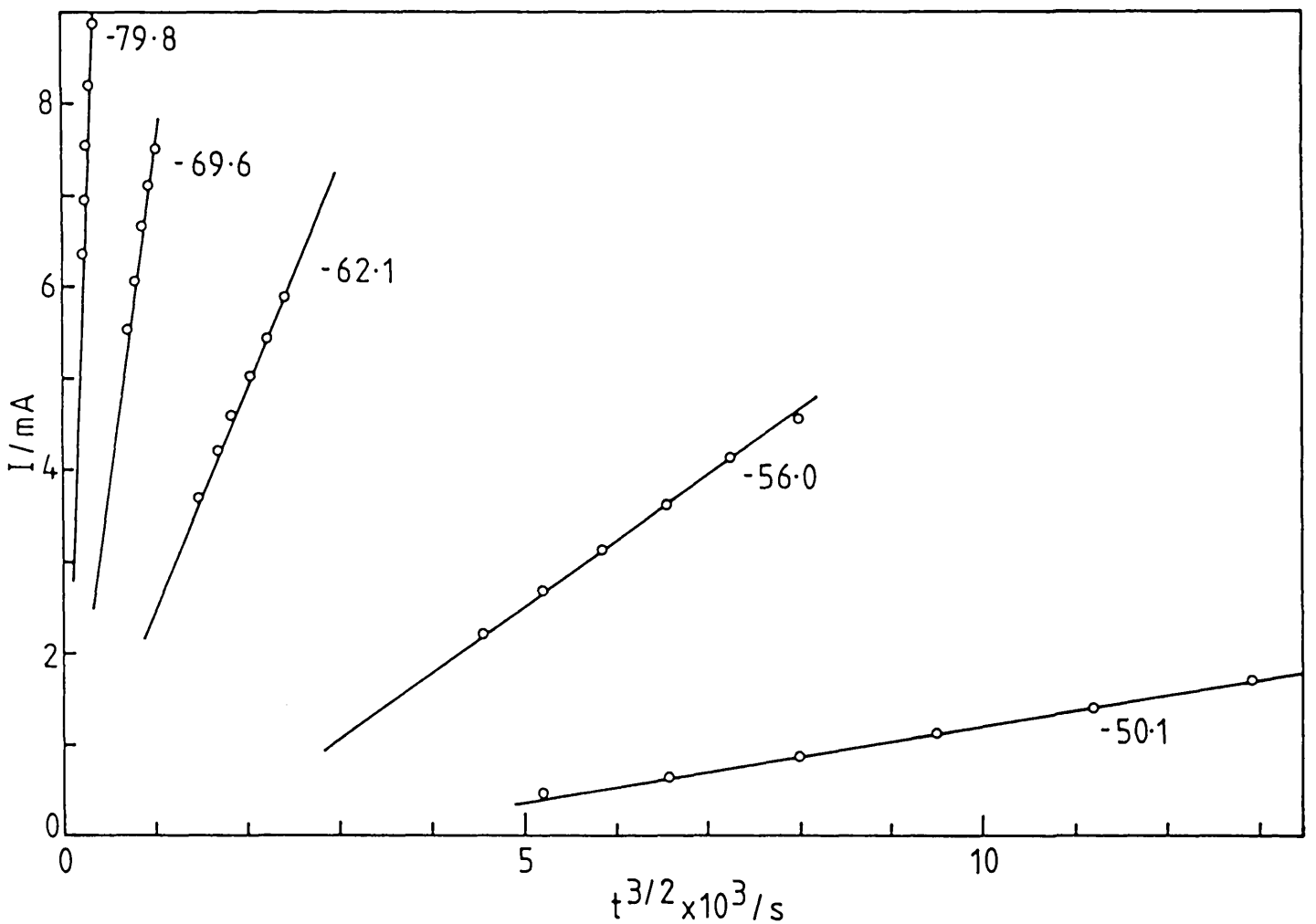

FIGURE 5.15c. I-$t^{3/2}$ plots. Data from Figure 5.1 c.

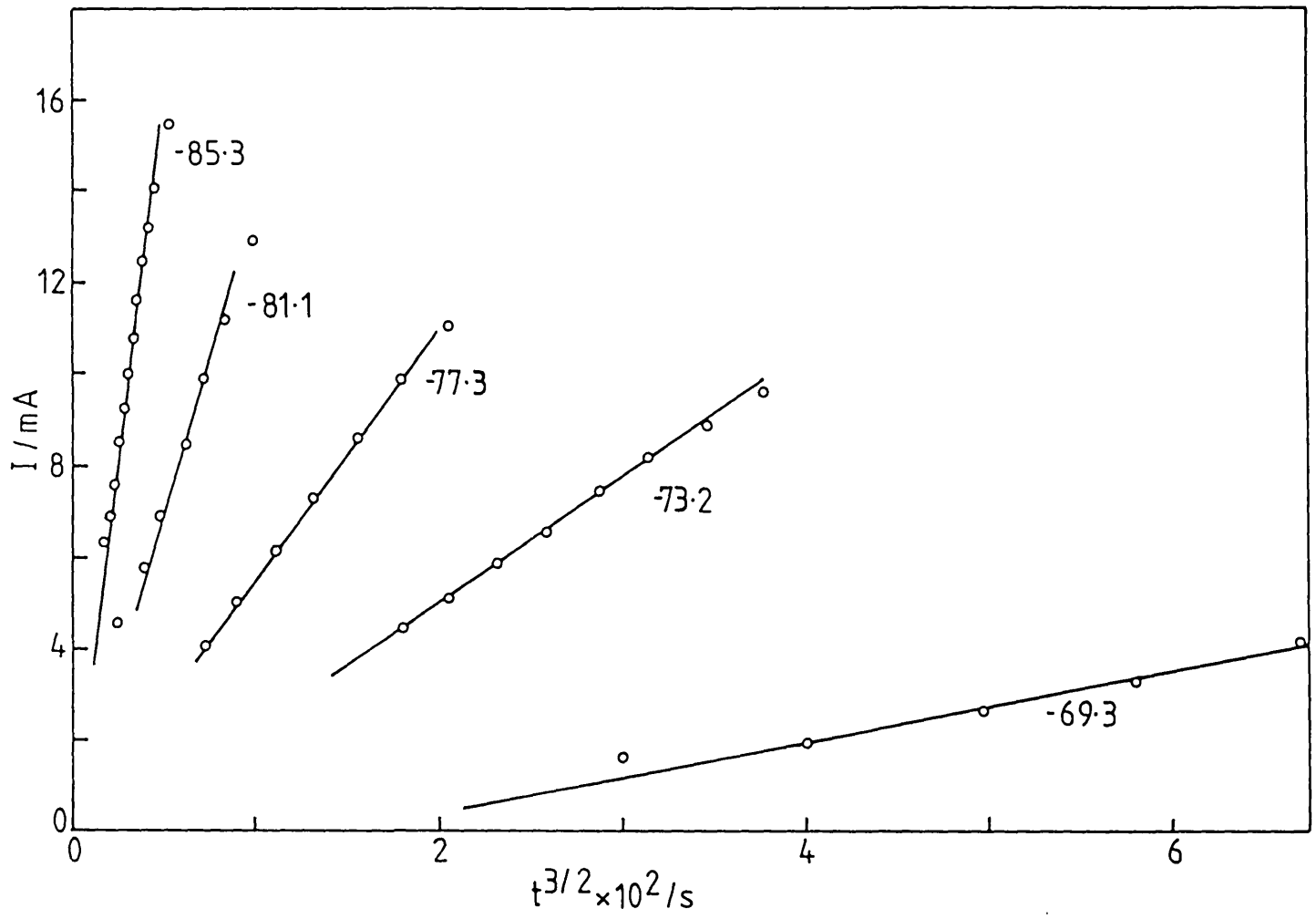

FIGURE 5.15d. I-$t^{3/2}$ plots. Data from Figure 5.1 e.

TABLE 5.1. Values of the steady state nucleation rate of chromium and related parameters.

$\frac{C}{mol.dm^{-3}}$	$\frac{\eta \times 10^{3}}{V}$	$\frac{I_o}{nuclei.sec.^{-1}cm^{-2}}$	$n_{3,k}$	$n_{2,k}$	n_k	Others
	41	4.66×10^{3}	18	18	15	3D
	43	1.18×10^{4}	16	15	15	$K_2 = -0.01992V^2$
0.042	45	3.40×10^{4}	14	14	12	$\sigma\Phi^{1/3} = 13.8 \mu J.cm^{-2}$
	47.1	7.77×10^{4}	12	12	12	2D
	49	1.67×10^{5}	11	11	8	$K_2' = -0.476V$
	51	2.87×10^{5}	9	10	8	$\sigma = 31.2\ \mu J.cm^{-2}$
						$\beta = 56.2\ \mu J.cm^{-2}$
	61.4	2.71×10^{6}	11	12	11	3D
	65.3	1.20×10^{7}	9	10	7	$K_2 = -0.04217V^2$
0.346	69.5	3.26×10^{7}	8	8	7	$\sigma.\Phi^{1/3} = 17.7\ \mu J.cm^{-2}$
	73.8	8.36×10^{7}	7	6	7	2D
	77.1	1.81×10^{8}	6	6	7	$K_2' = -0.4722$ V
						$\sigma = 31.1\ \mu J.cm^{-2}$
						$\beta = 48.9\ \mu J.cm^{-2}$
	50.1	8.41×10^{5}	11	9	7	3D
	56.0	3.23×10^{6}	8	7	7	$K_2 = -0.02259$
	62.1	1.35×10^{7}	6	6	4	$\sigma.\Phi^{1/3} = 14.4\ \mu J.cm^{-2}$
0.931	69.6	4.02×10^{7}	4	4	3	2D
	79.8	1.47×10^{8}	3	3	3	$K_2' = -0.48$
						$\sigma = 31.33\ \mu J.cm^{-2}$
						$\beta = 57.28\ \mu J.cm^{-2}$
(substrate: tungsten)						
	69.3	2.94×10^{5}	10	9	10	3D
	73.2	1.03×10^{6}	8	8	6	$K_2 = -0.05163$
	77.3	2.21×10^{6}	7	7	6	$\sigma.\Phi^{1/3} = 18.9\ \mu J.cm^{-2}$
0.346	81.1	5.19×10^{6}	6	6	6	2D
	85.3	1.23×10^{7}	5	6	6	$K_2' = -0.475$
						$\sigma = 31.18\ \mu J.cm^{-2}$
						$\beta = 46.47\ \mu J.cm^{-2}$

(substrate: platinum)

5.2.4. Comparison of the experimental data and the classical models of nucleation

According to the classical theory the steady state rate for three-dimensional electrochemical nucleation, expressed as I_o according to eqn. 2.76, obeys a relation of the form:

$$I_o = K_1 \exp(-K_2/\eta^2) \qquad 5.7$$

The work of formation of the three-dimensional critical nucleus is given by the expression (see Section 2.3)

$$\Delta G_{3,k} = 32\ a^6 \sigma^3 \Phi / z^2 e^2 |\eta|^2 \qquad 5.8$$

and the number of atoms in the critical nucleus is

$$n_{3,k} = 64(a^2\sigma)^3\ \Phi/(z|\eta|e)^3 \qquad 5.9$$

where

$$\Phi = 1 - \beta/2\sigma \qquad 5.10$$

On the other hand K_2 is connected with the work of nucleus formation by the equation

$$K_2/\eta^2 = \Delta G_{3,k}/kT \qquad 5.11$$

therefore

$$K_2 = 32\ a^6 \sigma^3 \Phi / z^2 e^2 kT \qquad 5.12$$

and

$$n_{3,k} = K_2(2KT/ze|\eta|^3) \qquad 5.13$$

In Figures 5.16a-d the data of I_o are plotted in coordinates ln I_o/η^{-2} and a good linearity is obtained at the various experimental conditions. The values for K_2 according to these figures together with values for $\sigma\Phi^{1/3}$ and $n_{3,k}$ are shown in Table 5.1.

On the other hand the classical theory also predicts the possibility of formation of two-dimensional nuclei on a foreign substrate. In this case the steady-state nucleation rate I_o obeys a relation of the form

$$I_o = K_1' \exp (K_2'/\eta - \eta_x) \qquad 5.14$$

The work of formation of the two-dimensional critical nucleus is (see Section 2.3):

$$\Delta G_{2,k} = 4a^4\sigma^2/ze[\eta - a^2(2\sigma - \beta)/ze] \qquad 5.15$$

and it is formed by a number of atoms given by

$$n_{2,k} = 4a^4\sigma^2/z^2e^2[\eta - a^2/ze(2\sigma - \beta)]^2 \qquad 5.16$$

On the other hand K_2' is connected with $\Delta G_{2,k}$ according to

$$K_2'/\eta - \eta_x = \Delta G_{2,k}/kT \qquad 5.17$$

from which

$$K_2' = 4a^2\sigma^2/zekT \qquad 5.18$$

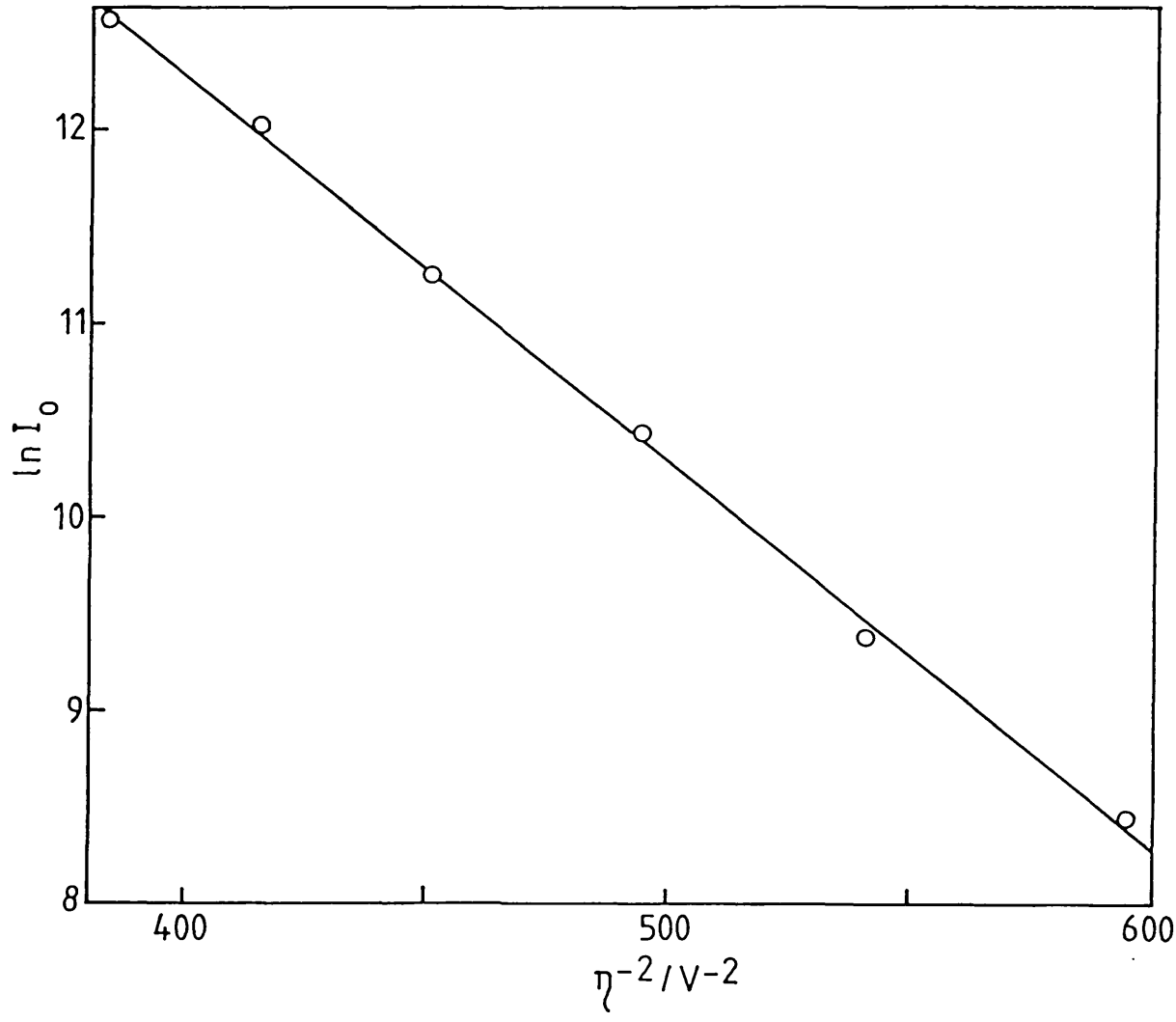

FIGURE 5.16a. Test of equation 5.7: tungsten, C = 0.042 mol.dm^{-3}

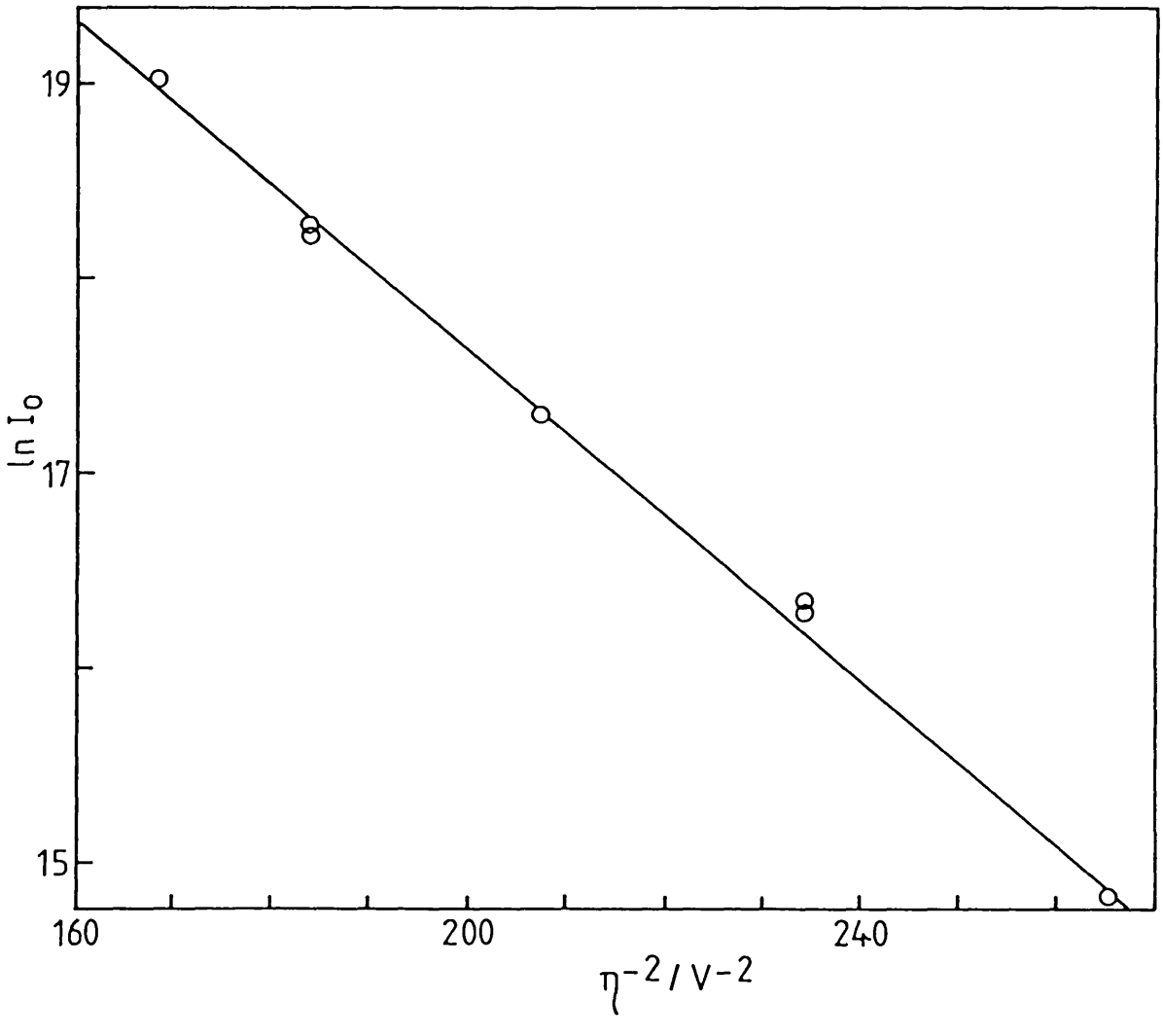

FIGURE 5.16b. Test of equation 5.7: tungsten, C = 0.346 mol.dm^{-3}.

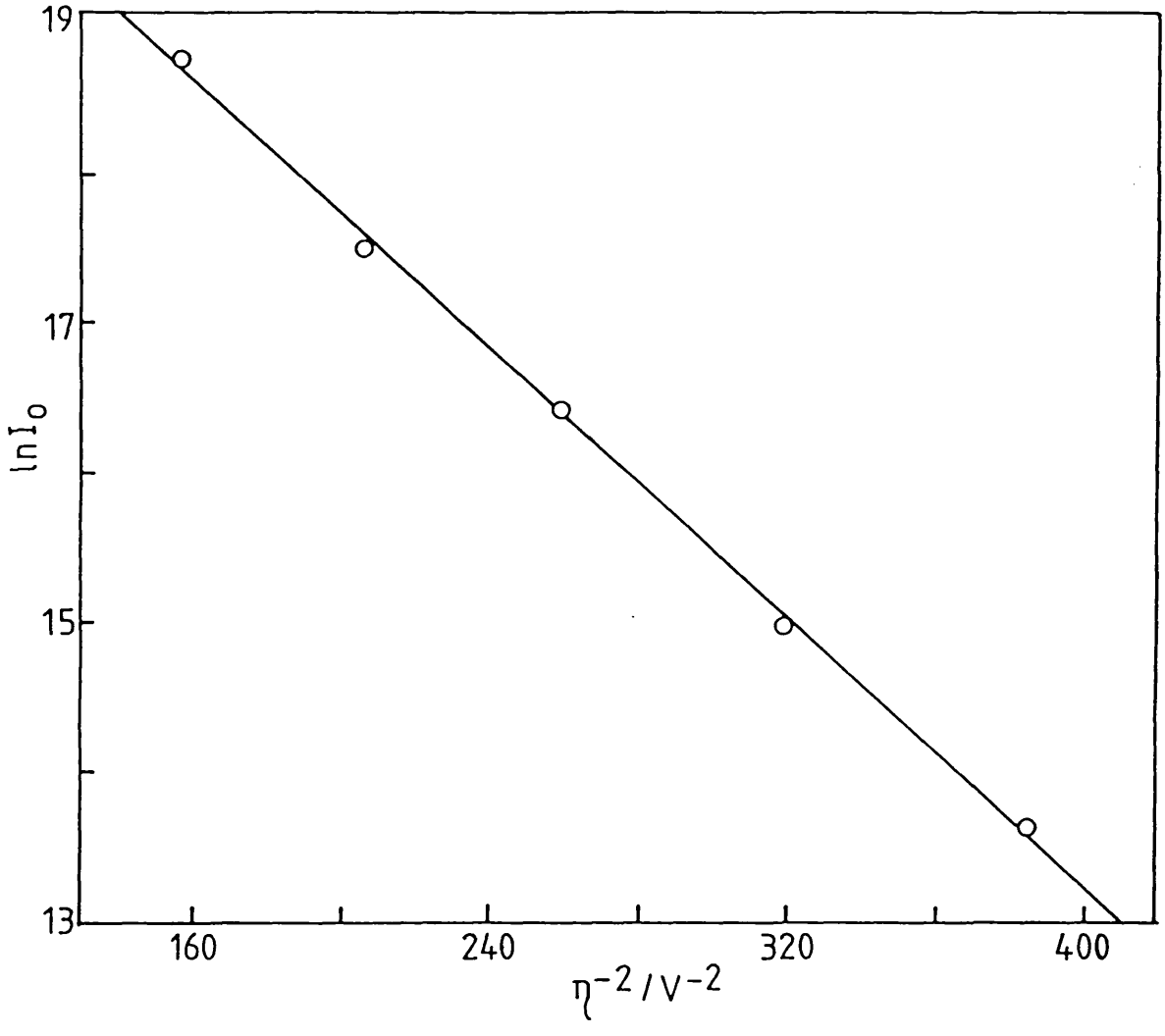

FIGURE 5.16c. Test of equation 5.7: tungsten, C = 0.931 mol.dm^{-3}.

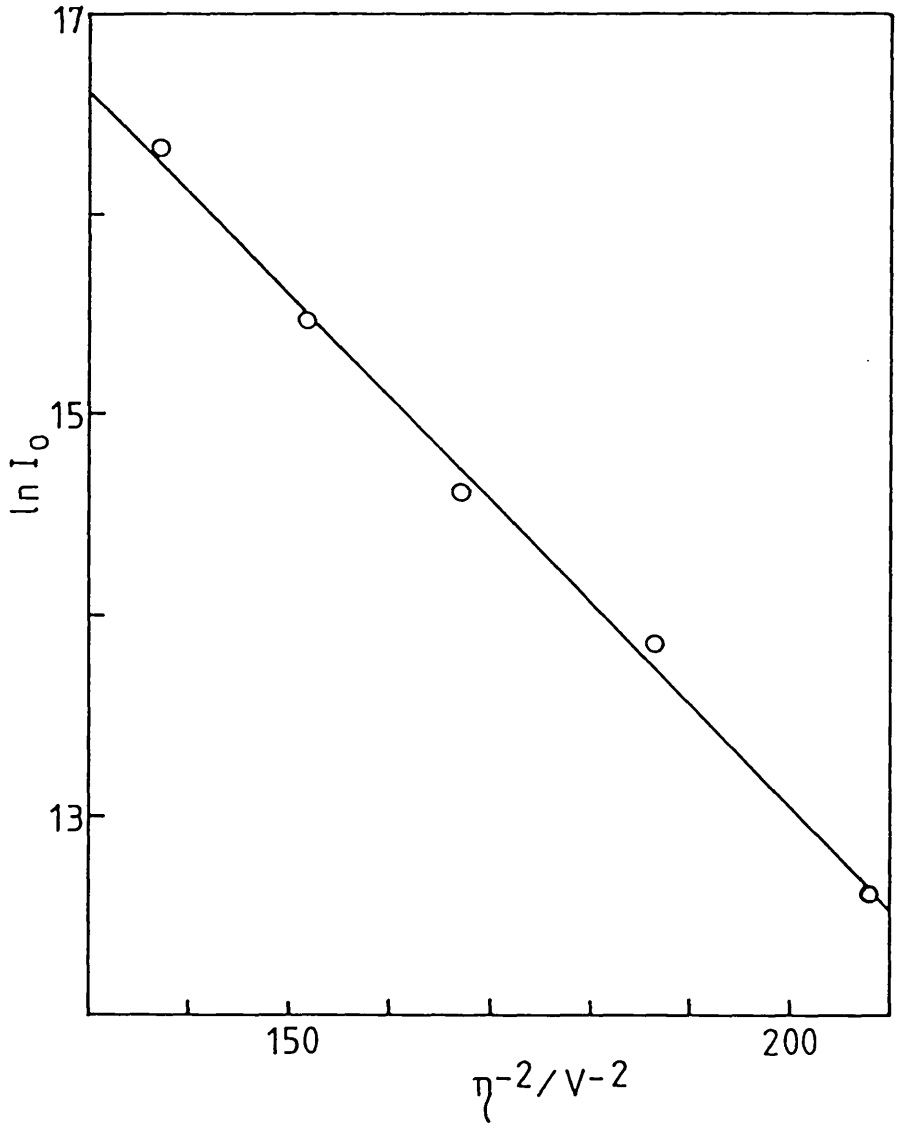

FIGURE 5.16d. Test of equation 5.7: platinum, C = 0.346 mol.dm^{-3}

then

$$\eta_x = a^2/ze\ (2\sigma-\beta) \qquad 5.19$$

and $n_{2,k}$ can be expressed as

$$n_{2,k} = K_2'\ kT/ze(\eta-\eta_x)^2 \qquad 5.20$$

In Figures 5.17a-d the experimental data are now compared with the classical model for two-dimensional nucleation and plotted in coordinates $\ln J_o/\eta-\eta_x$. The value of η_x was determined originally for one case (Figure 5.17a) by trying different values and choosing the one which produced the best fit of the data with a straight line, according to a statistical criterion[172]. The value of K_2' so obtained was then used to determine η_x in the other cases (Figs. 5.17b,c,d). Values of σ and β can be determined in this case and they are shown in Table 5.1, together with values of $n_{2,k}$.

The comparison of the data with the classical theory of nucleation shows a good qualitative agreement in terms of both the two and three-dimensional cases. In addition, the interpretation of the electrochemical nucleation of chromium according to both models is consistent. The values of K_2 and K_2' obtained for nucleation on tungsten electrodes do not change significantly in the wide range of chromium (II) ion concentrations considered, which is consistent with the nature of the exponential term defined in the classical theory.

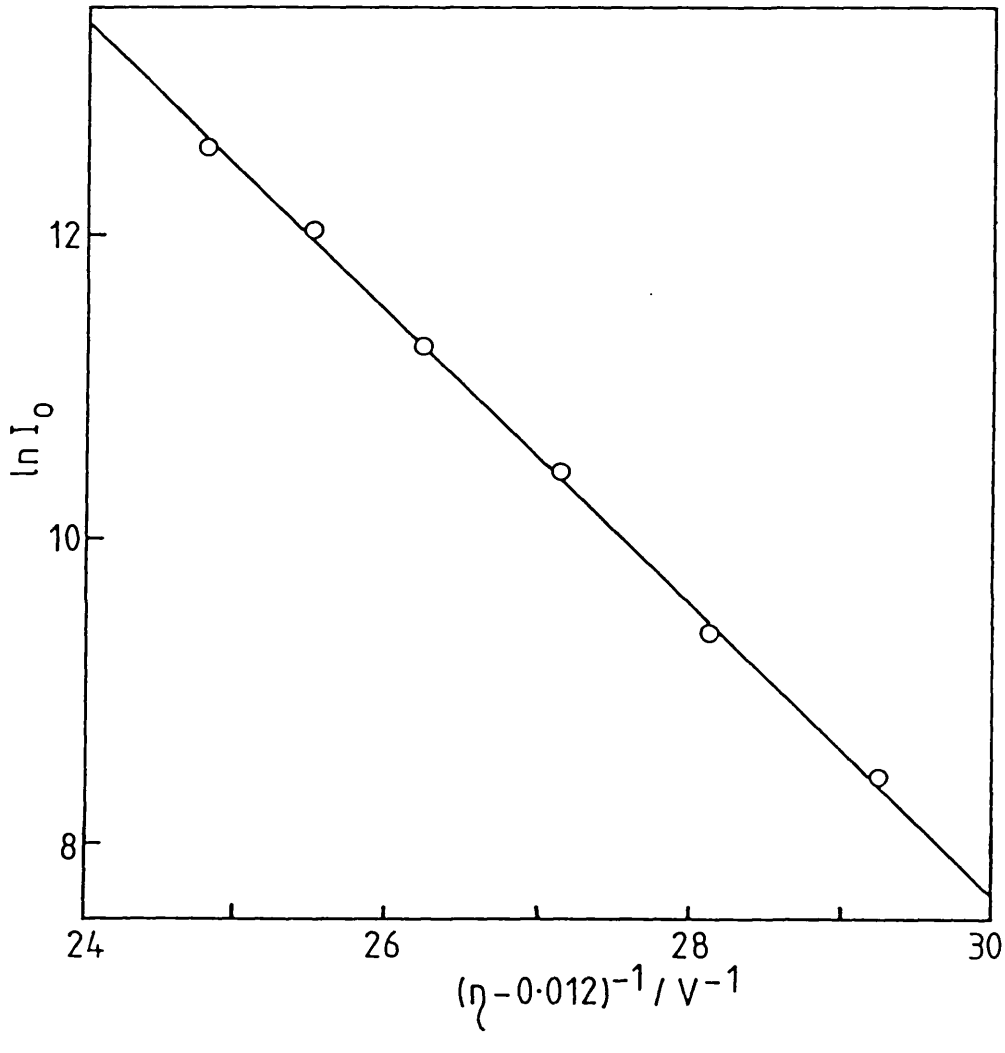

FIGURE 5.17a. Test of equation 5.14: tungsten, $C = 0.042$ mol.dm^{-3}.

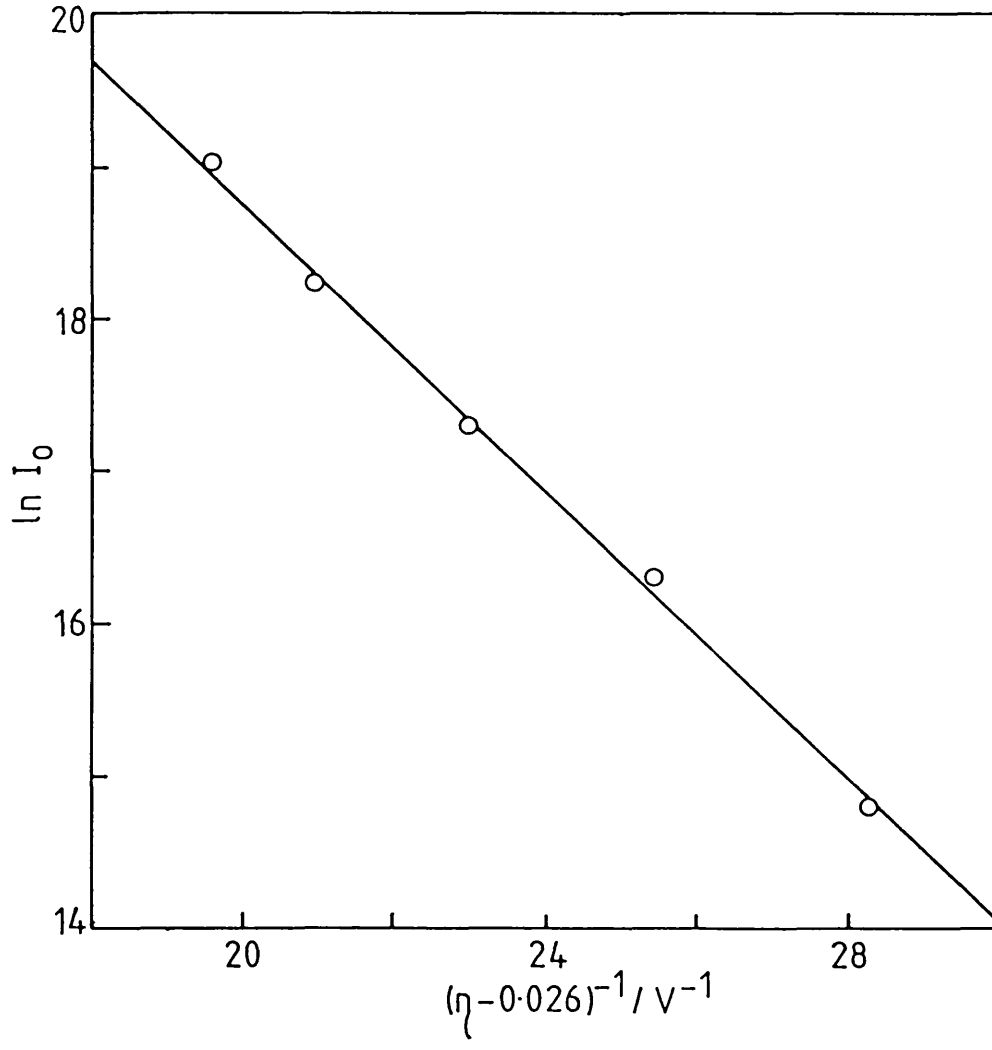

FIGURE 5.17b. Test of equation 5.14: tungsten, $C = 0.346$ mol.dm^{-3}.

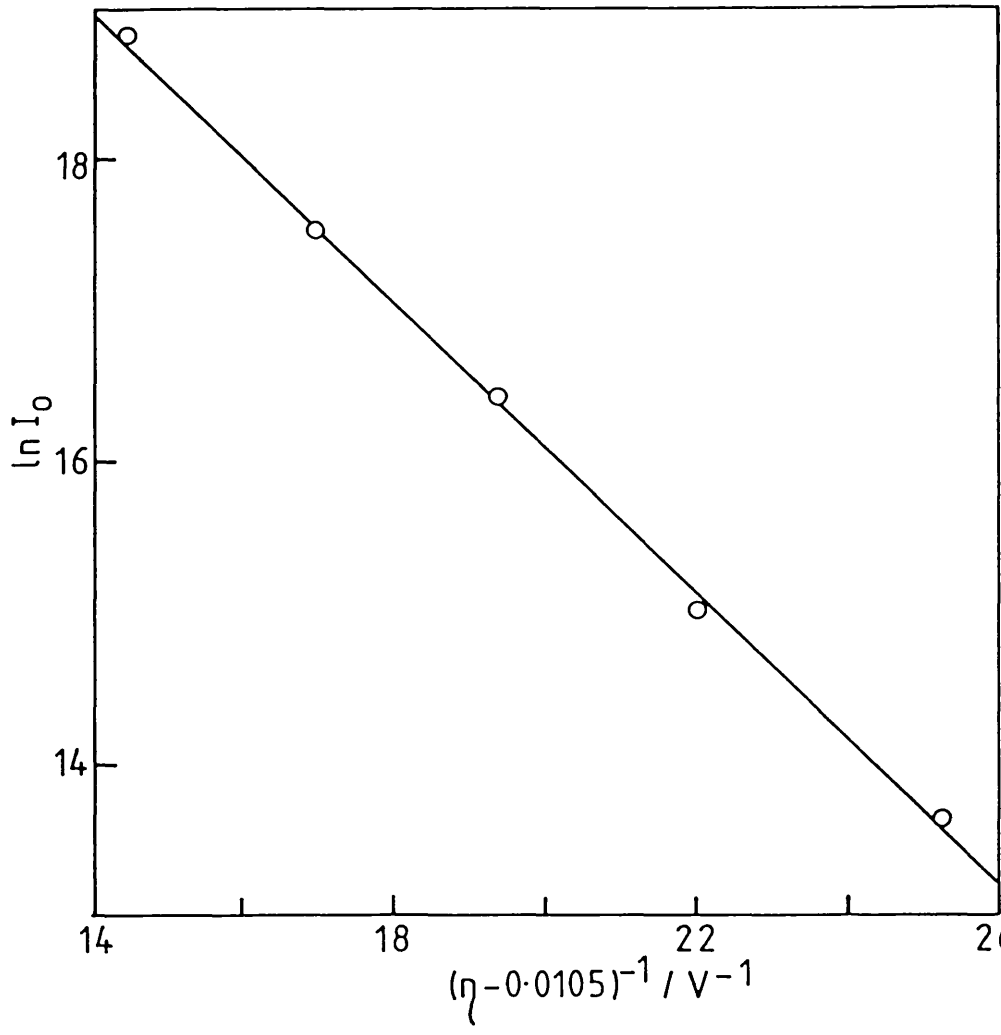

FIGURE 5.17c. Test of equation 5.14: tungsten, C = 0.931 mol.dm^{-3}

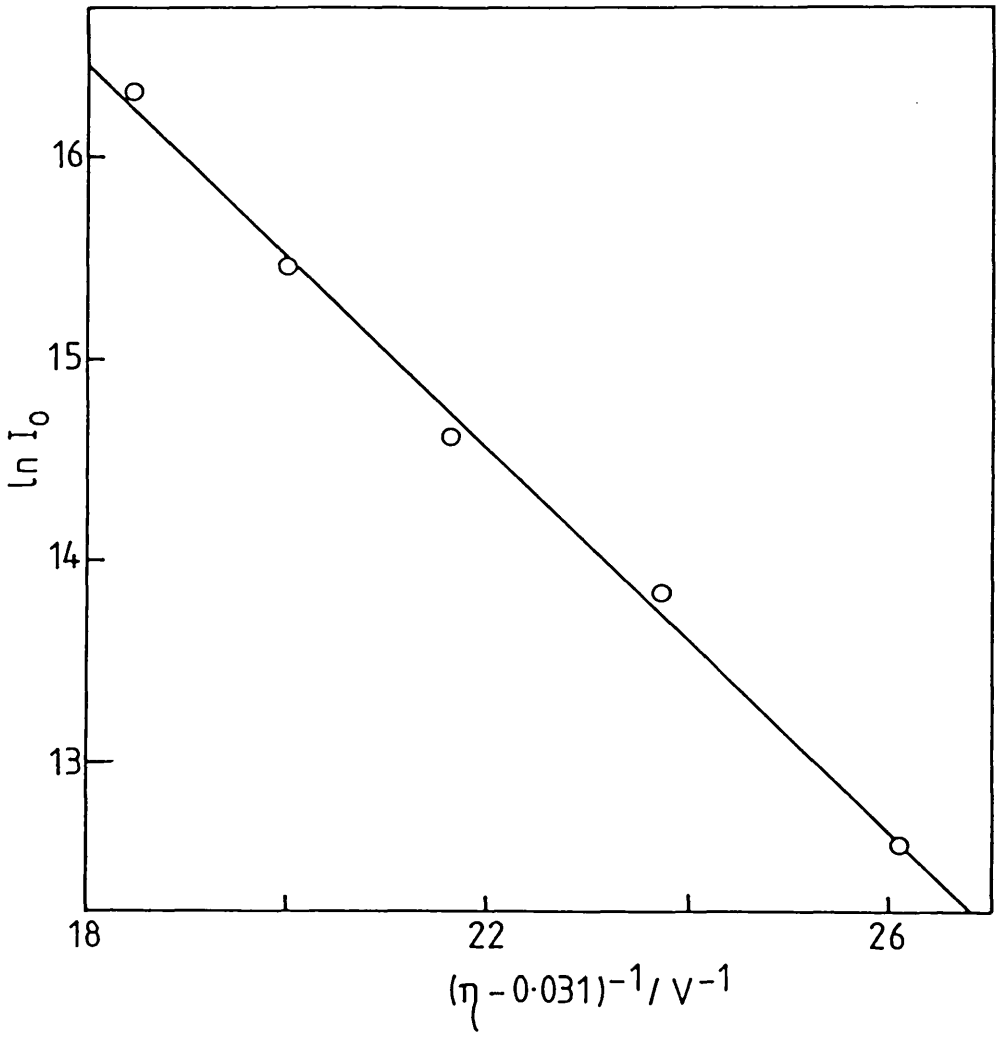

FIGURE 5.17d. Test of equation 5.14: platinum, C = 0.346 mol.dm^{-3}.

The low values assigned to Φ using σ and β obtained in terms of the two-dimensional model, correspond to the low values of K_2 obtained in the three-dimensional case, and so do their respective variations or different electrodes. In addition, the evaluation of the number of atoms in the critical nucleus gave similar values according to both models.

The small values obtained for the number of atoms in the critical nucleus explain to some extent the superposition of the two variants of the classical model in describing here the experimental data. In fact, the difference between the work of formation associated with clusters with two or three-dimensional configurations decreases as the size of the nucleus decreases, and both models converge when the critical nucleus contains just a few atoms. A selection of one of the models could be attempted based on the comparison of the absolute values of deviation. However, these are so small that practically in both cases satisfactory qualitative agreement exists between the theoretical model and the experiment. This lack of definition can be partially attributed to the fact that the data were obtained in a relatively small range of overpotentials. This is due to the restrictions of the method of measurement used here.

Additional evidence giving an insight into the nature of the critical nucleus was obtained by applying the criterion which defines, according to the classical

theory, the conditions for occurrence of two or three-dimensional nucleation (see Section 2.3). For the electrochemical case this is expressed in the following form

$$(2\sigma - \beta) - z\eta e/2a^2 > 0 \quad 3D \qquad 5.21$$

$$(2\sigma - \beta) - z\eta e/2a^2 < 0 \quad 2D \qquad 5.22$$

This criterion was checked based on the values of σ and β from Table 5.1 and it was found that in every experiment the conditions for the occurrence of two-dimensional nucleation were fulfilled. The possibility of initial formation of two-dimensional critical nuclei is not necessarily contradictory to the evidence of the scanning electromicrographs, which basically showed the presence of three-dimensional nuclei. In fact the observed nuclei are the result of the subsequent process of growth which obeys different mechanisms. In addition nuclei formation involving two-dimensional clusters can evolve later to three-dimensional growth as occurring under the Stranski-Krastanov mechanism[79].

The classical model for three-dimensional nucleation has been applied in interpreting several cases of electrochemical nucleation in aqueous systems at room temperature[111,122,150-154]. In the present study the value obtained for the exponential term K_2 is two orders of magnitude lower with respect to values obtained in the aqueous systems. This is consistent too with the

comparatively lower values of overvoltage which were required in the present system for the electrochemical nucleation to proceed. A low value of K_2 indicates a lower energetic barrier associated with the process of critical nuclei formation and seems to be a characteristic related to the nature of this process in molten salts. Values of K_2 of the same order of magnitude have been obtained in the KNO_3-$NaNO_3$ eutectic at 316°C in the electrochemical nucleation of silver on platinum[173] and in the LiCl-KCl eutectic at 410°C in the electrochemical nucleation of copper on graphite and vitreous carbon[145].

The form of equation 5.11 predicts a reduction of K_2 as the temperature increases, but the change of temperature in passing from an aqueous to a molten salts system does not account on its own for a two orders of magnitude fluctuation. On the other hand a large difference between the values of σ in aqueous and molten salts is not expected and the only available data, obtained from capillarity studies with liquid metals, show quite similar values in both systems[174,178]. The low magnitude of the term K_2 can be regarded better in terms of the diminution of the coefficient Φ. This can be related to an increase of the deposit-substrate interaction inherent in the high temperatures used in the molten salts which results in the occurrence of better adhesion or "wettability" between the two metals. This tendency was confirmed by evaluating Φ in terms of σ and β values

obtained from the interpretation of the nucleation data in terms of the two-dimensional model. In the present case values for Φ in the range 0.09-0.25 were obtained, which is relatively close to zero, value expected when the depositing material bonds to a substrate as strong as to itself. Some additional evidence in this direction was obtained from scanning electromicrographs which showed flattened shapes in chromium nuclei at very early stages of development (see Figure 5.18). According to the Kaischiev relation[90] the ratio between the height h and the width n in a three-dimensional nucleus of equilibrium shape is expressed as:

$$\frac{h}{n} = \frac{\Delta\sigma}{\sigma} = \frac{2\sigma-\beta}{\sigma} \qquad 5.23$$

The low h/n ratio associated with the observed crystallites is consistent with low values of $(2\sigma-\beta)$ and shows a good deposit-substrate contact. Finally the comparatively high adhesion observed in chromium macro-electrodeposits obtained on Nb 20/25 stainless steel (see Section 6.3.3 below) point also in this direction and this appears to be a macroscopic feature consistent with the characteristics of the initial nucleation stage.

The average value of K_2 obtained in the case of the electrochemical nucleation of chromium on tungsten electrodes (0.028) was smaller than the corresponding value obtained in the case of nucleation on platinum (0.052), indicating that the chromium-tungsten interaction

a

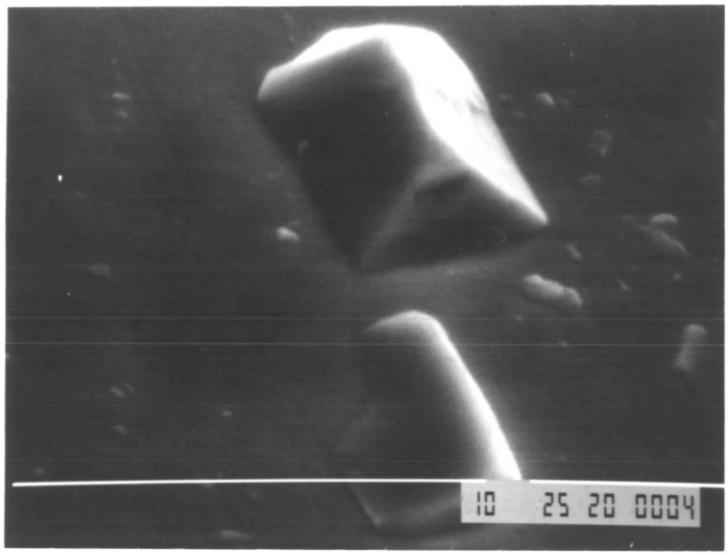

b

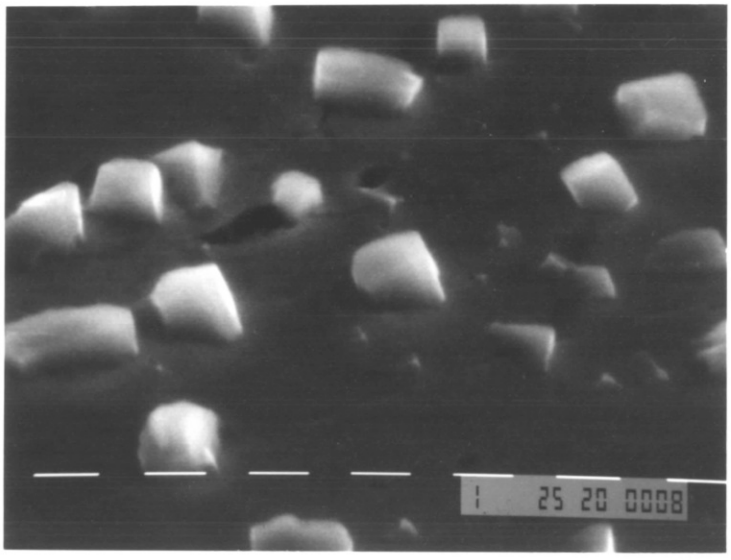

FIGURE 5.18. Scanning electron micrographs showing the morphology of chromium nuclei during early stages of development. a) Substrate: tungsten, C=0.931 mol dm^{-3}, η_N=-0.044 V, t_N=5 s. b) Substrate: platinum, C=1.487 mol dm^{-3}, η_N=-0.6 V, t_N=0.2 s.

is comparatively stronger. On the other hand the data on adherence obtained according to the two-dimensional model was consistent with this tendency giving an average $\beta = 54.1\ \mu J.cm^{-2}$ for chromium-tungsten and $\beta = 46.5\ \mu J.cm^{-2}$ for chromium-platinum. Therefore, according to the dependence of the work of critical nuclei formation expressed as

$$\Delta G_{3k} = \Delta G(\eta_k)(1-\beta/2\sigma) \qquad 5.24$$

tungsten facilitates more than platinum the electrochemical nucleation of chromium in the $LiCl-KCl-CrCl_2$ system. This is in agreement with the tendency observed in sweep voltammograms obtained at low sweep rates, where the overpotential necessary to reach the onset of nucleation was smaller for tungsten than for platinum (see Figure 5.4).

According to the data on electrochemical nucleation of chromium obtained on tungsten at different chromium(II) ion concentrations, the steady state nucleation rate shows a slight increase with the increase of concentration. Nevertheless the available data are not sufficient enough to be conclusive in this sense as the slight variations observed could be more due to variations of the substrate activity than to the influence of the chromium (II) ion concentration. The concentration dependence of the nucleation rate has been studied before for the electrochemical nucleation of silver

from aqueous solutions[141,153]. A slight dependence could be detected only when the process was studied over a very wide range of silver ion concentrations[153]. The dependence of the nucleation rate on concentration implies a mechanism of critical nuclei formation which involves the direct attachment of ions from the solution into the critical nuclei, opposed to a surface diffusion mechanism where the process is concentration independent.

5.2.5. Validity of the classical model

The number of atoms in the critical nucleus of chromium determined according to the classical theory is relatively small in every case. This result poses the question of the possibility of a correct quantitative interpretation of the experimental data on the basis of the classical theory. In fact the macroscopic concepts of surface and surface energy involved in this theory lose, to some extent, their physical meaning for clusters consisting of a few atoms. As far as the quantities K_2 and K_2' are concerned no precise information can be obtained from the magnitudes of their experimental values since their theoretical expression involve two unknown parameters, σ and β.

An additional criterion to judge the validity of the classical model in the present case, can be obtained with a quantitative comparison of the same data with the atomistic theoretical model of nucleation

which has the advantage that it does not use any macroscopic quantities for characterizing the critical nucleus. According to the atomistic theory the steady state rate of electrochemical nucleation I_o should obey a relation of the form:

$$I_o = K_1'' \exp K_2'' \eta \qquad 5.25$$

For the case of the formation of clusters by the direct attachment of ions from solution the value of K_2'' corresponds to

$$K_2'' = (n_k + 1 - \alpha)ze/kT \qquad 5.26$$

The exponential term in this case varies with the number of atoms of the critical nucleus so a plot of $\ln I_o/\eta$ should show linear sections of decreasing slope as the overpotential increases. In Figures 5.19a-d the data are now plotted in coordinates $\ln I/\eta$ and the values of n_k evaluated for each linear section, assuming $\alpha = 0.5$, are shown in Table 5.1. It can be seen that the numbers of atoms obtained do not differ significantly from the numbers obtained according to the classical model, a fact that clarifies the qualitative agreement existing between the experimental data and the classical model.

There is an apparent contradiction as the data can be well interpreted in terms of both the atomistic and the classical theory, a fact that has been also

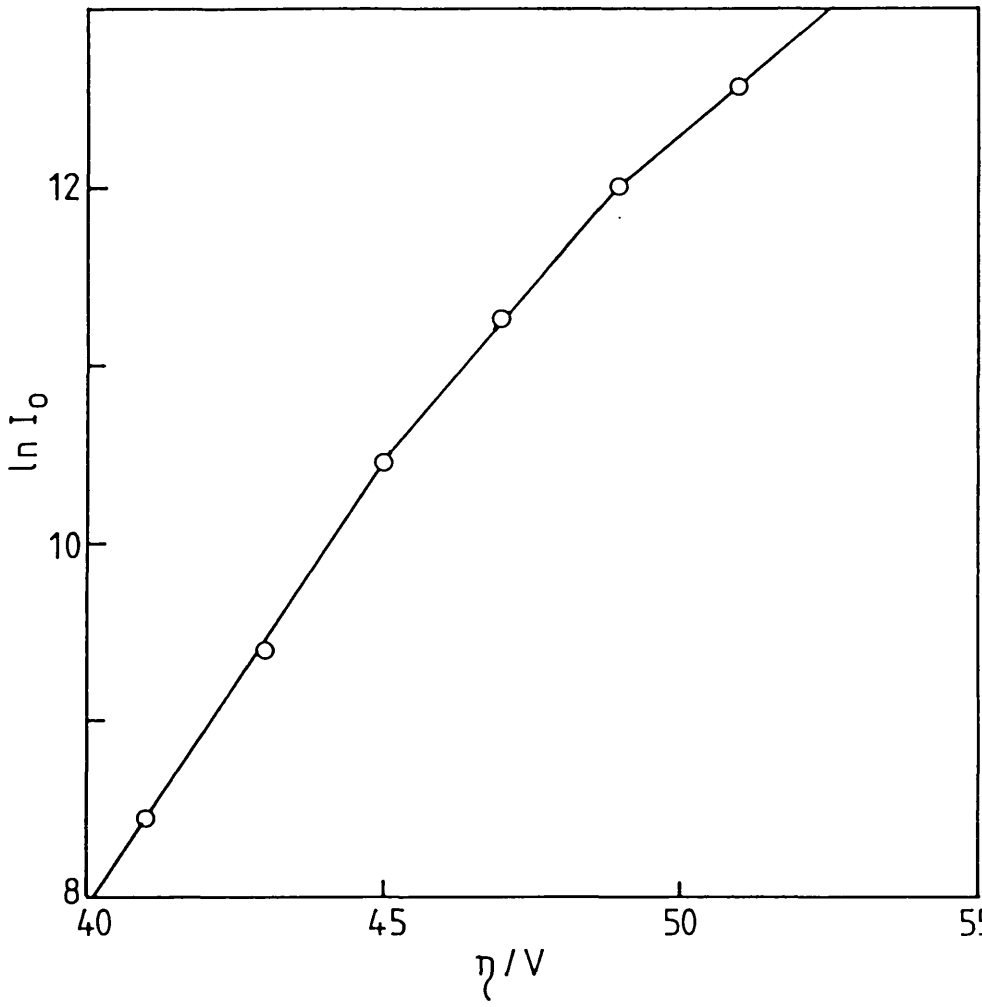

FIGURE 5.19a. Test of equation 5.25: tungsten, C = 0.042 mol.dm^{-3}

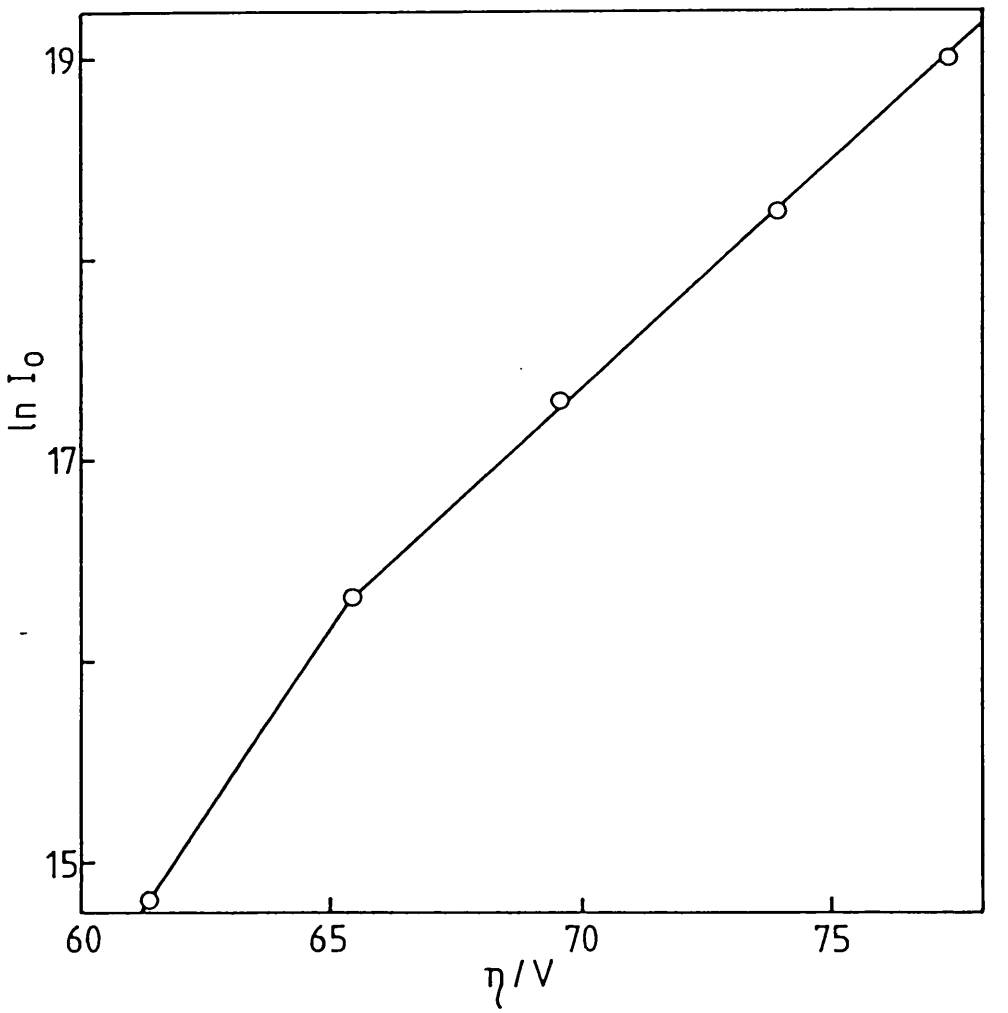

FIGURE 5.19b. Test of equation 5.25: tungsten, $C = 0.346\ mol.dm^{-3}$

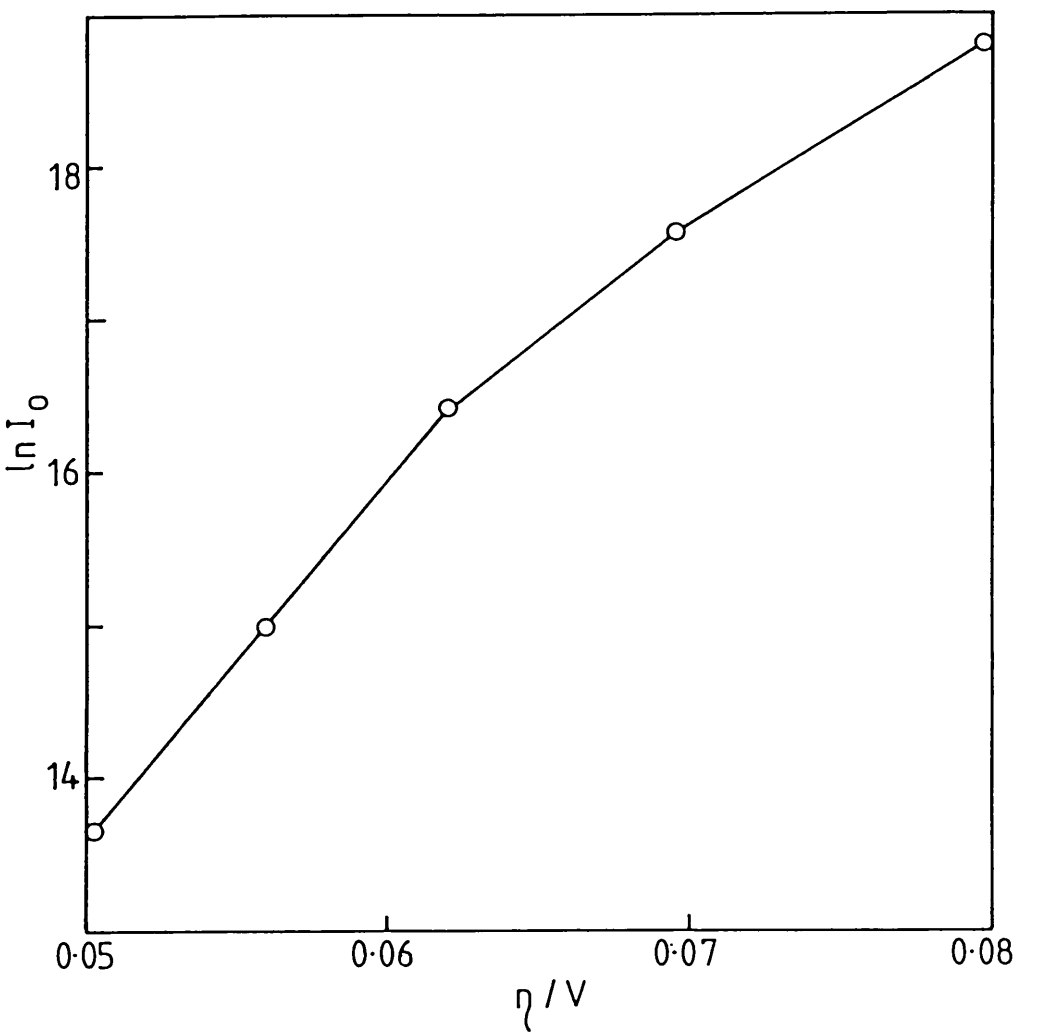

FIGURE 5.19c. Test of equation 5.25: tungsten, C = 0.931 mol.dm^{-3}.

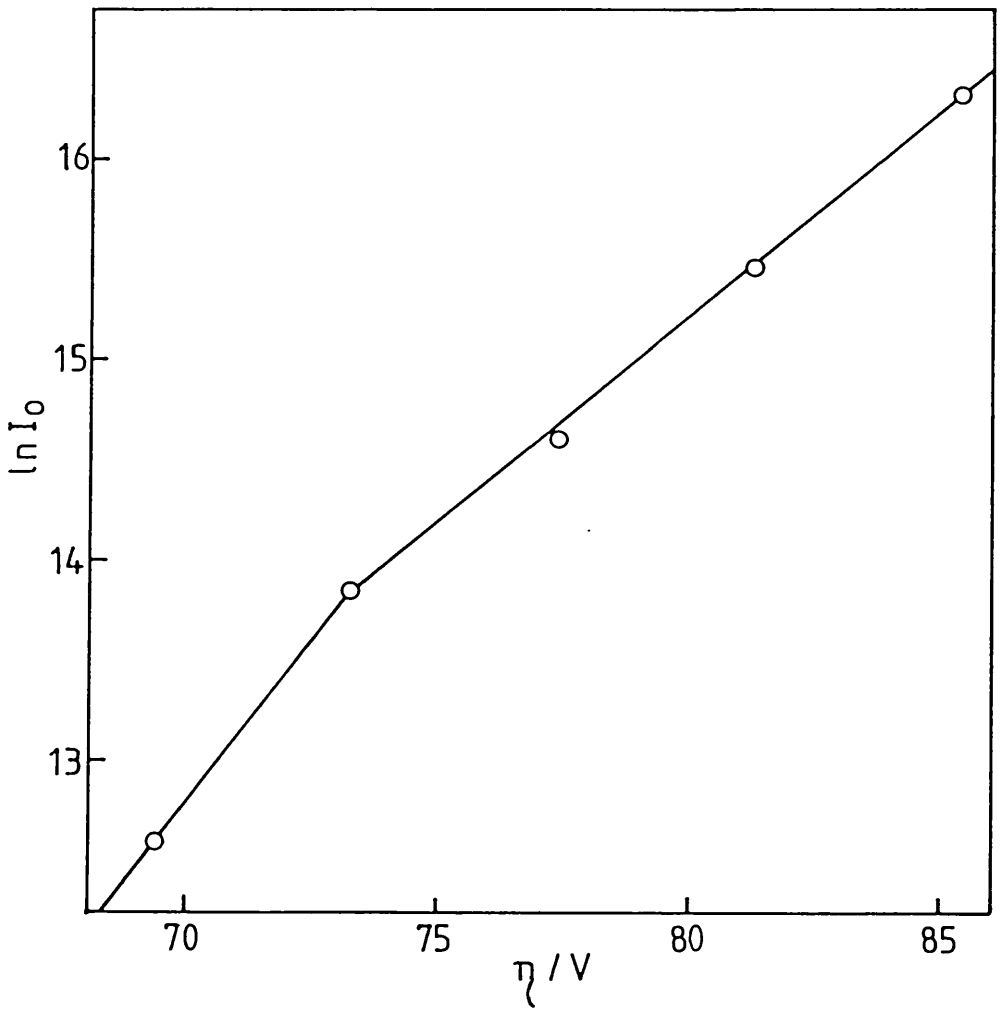

FIGURE 5.19d. Test of equation 5.25: platinum, $C = 0.346\ mol.dm^{-3}$.

observed in other systems[111,153]. In fact in general terms the two models describe the kinetics of the nucleation process in two limiting cases, at high and low supersaturations respectively. It has been demonstrated, however, that at low supersaturations the equations of the atomistic theory turn into the classical expression[112,113] and this approximation seems to be applicable at the low overpotentials at which the electrochemical nucleation of chromium occurs.

5.3 MECHANISM OF SATURATION NUCLEUS DENSITY

5.3.1. Introduction

It has been experimentally observed that the process of electrochemical formation of chromium nuclei ceases after a certain length of time with the production of a final saturation nucleus density (SND). The value of SND to be obtained is an important aspect to control in the process of electrocrystallization of chromium as it is closely related to the ability of reaching a good initial coverage of the substrate. This initial nucleated "layer" will also constitute the root of the whole electrodeposit and its characteristics will determine to a great extent the subsequent steps of electrogrowth. It is necessary to look in more detail at the nature of the saturation phenomenon in the present system and, therefore, to obtain a better control of this stage of the electrodeposit formation.

The termination of the nucleation process can be explained through different mechanisms which determine the final saturation nucleus density and, simultaneously, define the kinetics of the nucleation process and, consequently, the characteristics of the N(t) function (see Section 2.3.4). An insight into the mechanism of saturation can be obtained, therefore, by analysing the resulting N-t curve characteristics of each system.

The usual form for determining the variation of number of nuclei vs. time has been by using a double pulse method which involves the direct counting of nuclei formed at different times during the process[152,155]. A method like this which implies the frequent counting of nuclei in situ is impracticable in the present study which involves working with a molten salt bath at high temperatures in a sealed system under argon. The counting of nuclei can be carried out on electrodes once removed from the cell, but this can be done just sporadically as the interchange of electrodes from the cell has to be minimized in order to avoid the contamination of the bath. Therefore in the present case it is necessary to develop a method which permits us to characterize the variation of the number of nuclei exclusively from the electrochemical response obtained during the electrochemical nucleation stage.

5.3.2. Derivation of N-t curves

The potentiostatic current-time transients obtained during the electrochemical nucleation of chromium can be used, with some assumptions, as a base to obtain an explicit description of the number of nuclei at any time during the process. The development of an adequate method is necessary for that purpose.

When nucleation and growth occurs simultaneously, the total deposition current, before overlapping, can be expressed according to the convolution expression

$$I(t) = \int_0^t I_1(u)(dN/dt)_{t=t-u}\, du \qquad 5.27$$

where u is the age of the nuclei. By deconvoluting this equation, discretizing, and then deriving a convenient algorithm, N(t) can be evaluated by a numerical integration technique from the values of I(t) experimentally obtained. The I-t data can be divided into k equally spaced time intervals t between t=o and t=t (see Figure 5.20a), so that

$$t = k\Delta t \qquad 5.28$$

The nuclei formed at the interval j are designated by $\Delta N(j\Delta t)$ (see Figure 5.20b). It is assumed that the nuclei formed in each time interval Δt form instantaneously at the start of the period so that the age of the nuclei $\Delta N(j\Delta t)$ at the time $k\Delta t$ can be expressed as

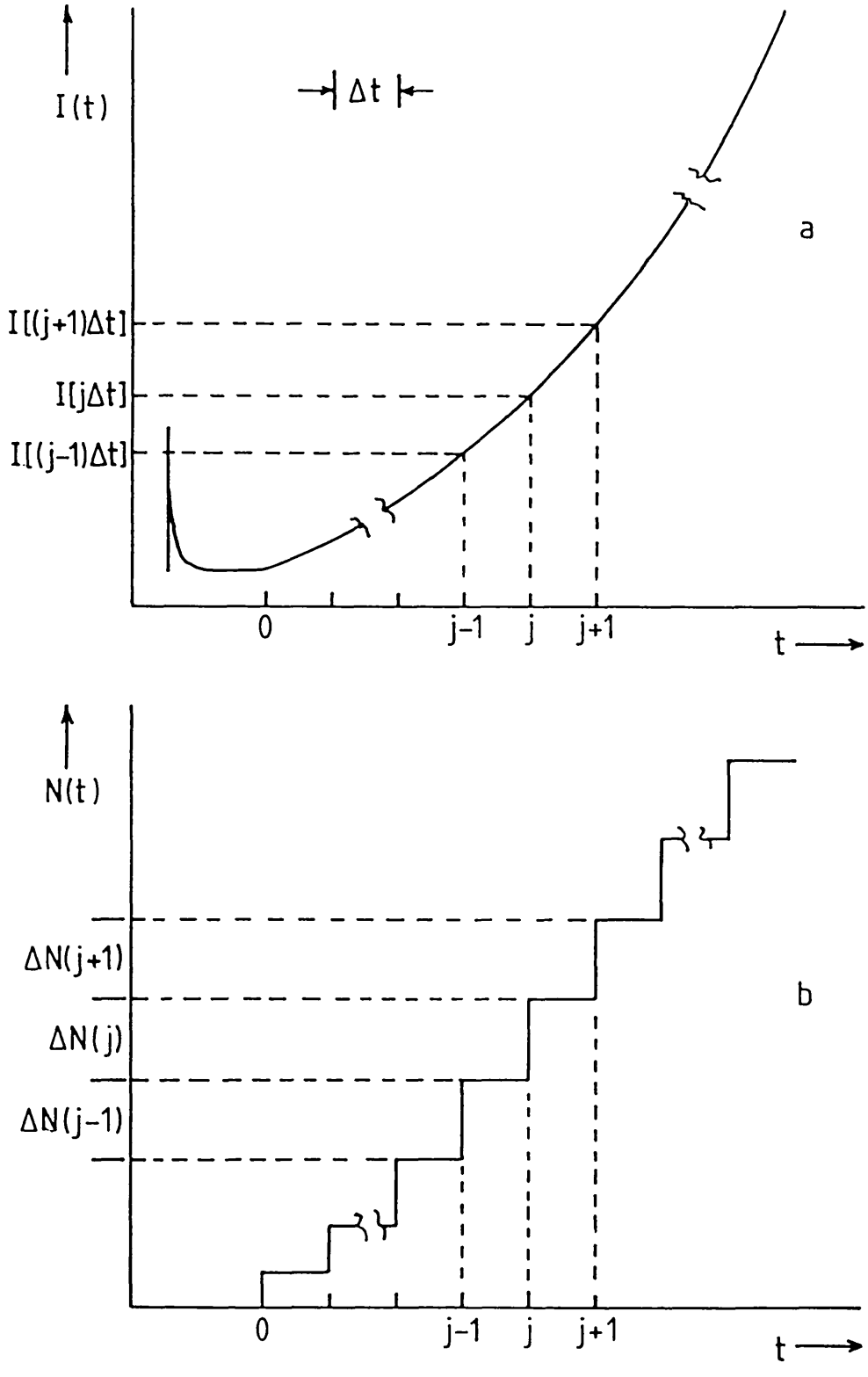

FIGURE 5.20. Representation of the method for evaluation of N(t). a) Division of experimental I(t), b) discrete N(t) curve obtained.

$$u_{\Delta N(j\Delta t)} = k\Delta t - (j-1)\Delta t \qquad 5.29$$

$$u_{\Delta N(j\Delta t)} = (k-j+1)\Delta t \qquad 5.30$$

Equation 5.27 can be written now as

$$I(k\Delta t) = \sum_{j=1}^{j=k} I_1[k-k+1)\Delta t]\ \Delta N(j\Delta t) \qquad 5.31$$

Separating the last term and solving, the following recurrent expression is obtained.

$$\Delta N(k\Delta t) = \frac{I_1(k\Delta t)}{I_1(\Delta t)} - \sum_{j=1}^{j=1-1} \Delta N(j\Delta t).I_1[(k-k+1)\Delta t]/I_1(\Delta t) \qquad 5.32$$

Replacing I_1 by the expression for the current to a growing nuclei described in terms of hemispherical diffusion (equation 5.1), equation 5.32 can be written as:

$$\Delta N(k\Delta t) = \frac{I(k\Delta t)}{B(\Delta t)^{\frac{1}{2}}} - \sum_{j=1}^{j=k-1} \Delta N(k\Delta t)(k-k+1)^{\frac{1}{2}} \qquad 5.33$$

where

$$B = zF\pi M^{\frac{1}{2}}\ (2CD)^{3/2}(1-expz\eta F/RT)^{3/2}/\rho^{\frac{1}{2}} \qquad 5.34$$

The number of nuclei at any time is then

$$N(m\Delta t) = \sum_{k=1}^{k=m} \Delta N(k\Delta t) \qquad 5.35$$

$$N(m\Delta t) = \sum_{k=1}^{k=m} \left(\frac{I(k\Delta t)}{B(\Delta t)^{\frac{1}{2}}} - \sum_{j=1}^{j=k-1} \Delta N(k\Delta t)(k-k+1)^{\frac{1}{2}}\right) \qquad 5.36$$

The values of $I(k\Delta t)$ can be obtained from the experimental I-t transients and then the values of $N(m\Delta t)$ can be calculated with the aid of a computing program developed for this purpose (see Appendix 2).

5.3.3. Results and discussion

The algorithm represented in equation 5.36 was applied to derive a N-t curve from I-t transients obtained on the nucleation of chromium on tungsten from LiCl-KCl eutectic melts containing 0.346×10^{-3} $mol.dm^{-3}$ of chromous ions (see Figure 5.21a). The resulting N-t curves obtained at different overpotentials are shown in Figure 5.21b. They present the typical characteristics observed in other systems[77,122,152-154,173]: after an initial induction time the number of nuclei grows approximately linearly with time, eventually reaching a saturation number. The rate of nuclei formation increases strongly with the applied overpotential, and so does too the final saturation nucleus density. On the other hand, the time necessary to reach a saturation value decreases with increasing overpotentials.

The N-t data obtained from Figure 5.21b, were later plotted in the dimensionless coordinates $y = N(t)/N_s$ and $x = M(t-t_o)/N_s$ in Figure 5.22 in order to compare the results with those of the models based on different limiting mechanisms for obtaining saturation nucleus densities[122] (see Section 2.3.4.). In Figure 5.22

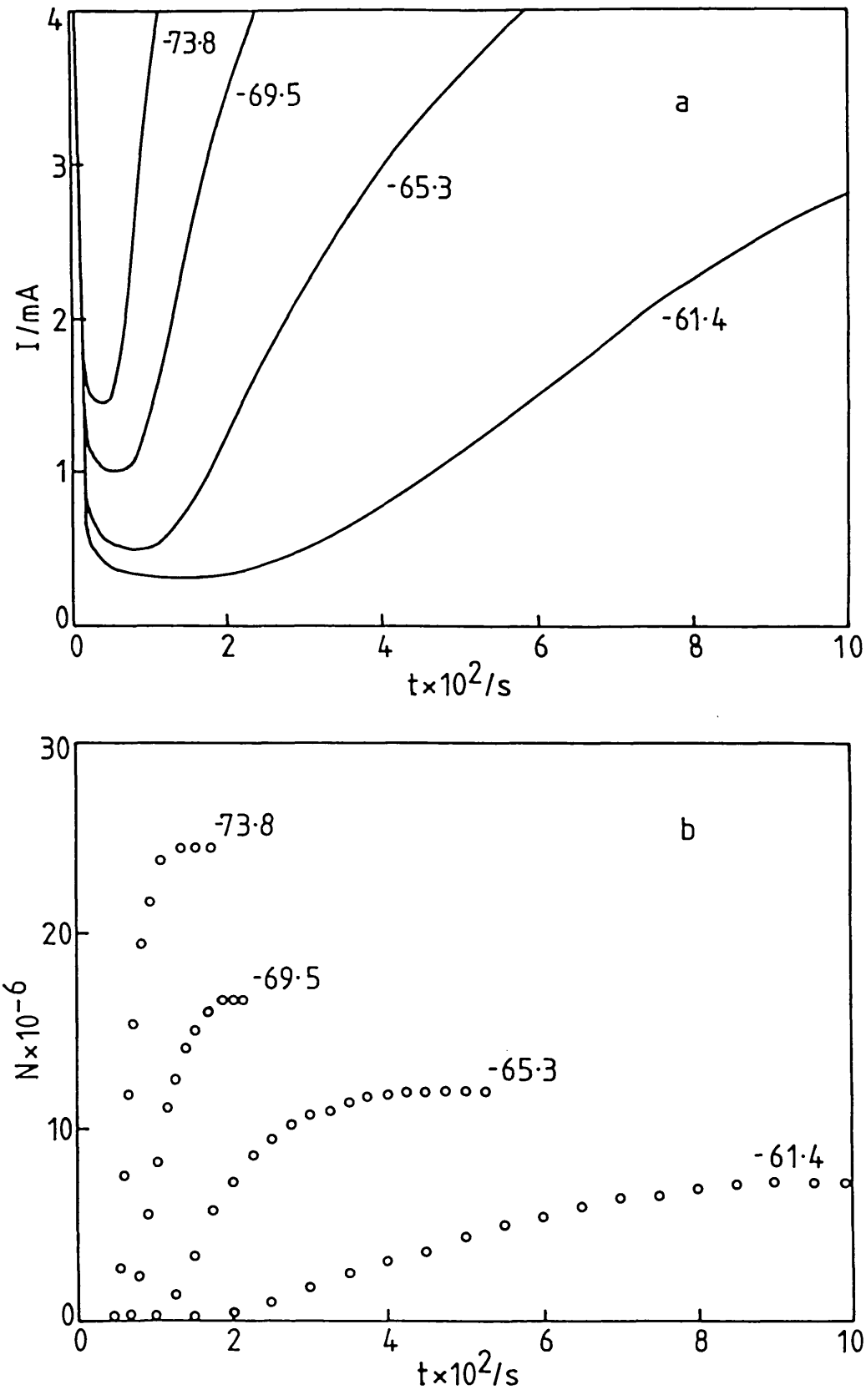

FIGURE 5.21. Evaluation of number of nuclei N versus time.
a) Potentiostatic current transient obtained on tungsten: 0.0452 cm^2, C = 0.346 $mol.dm^{-3}$ (overpotentials in mV),
b) Calculated N(t) curves.

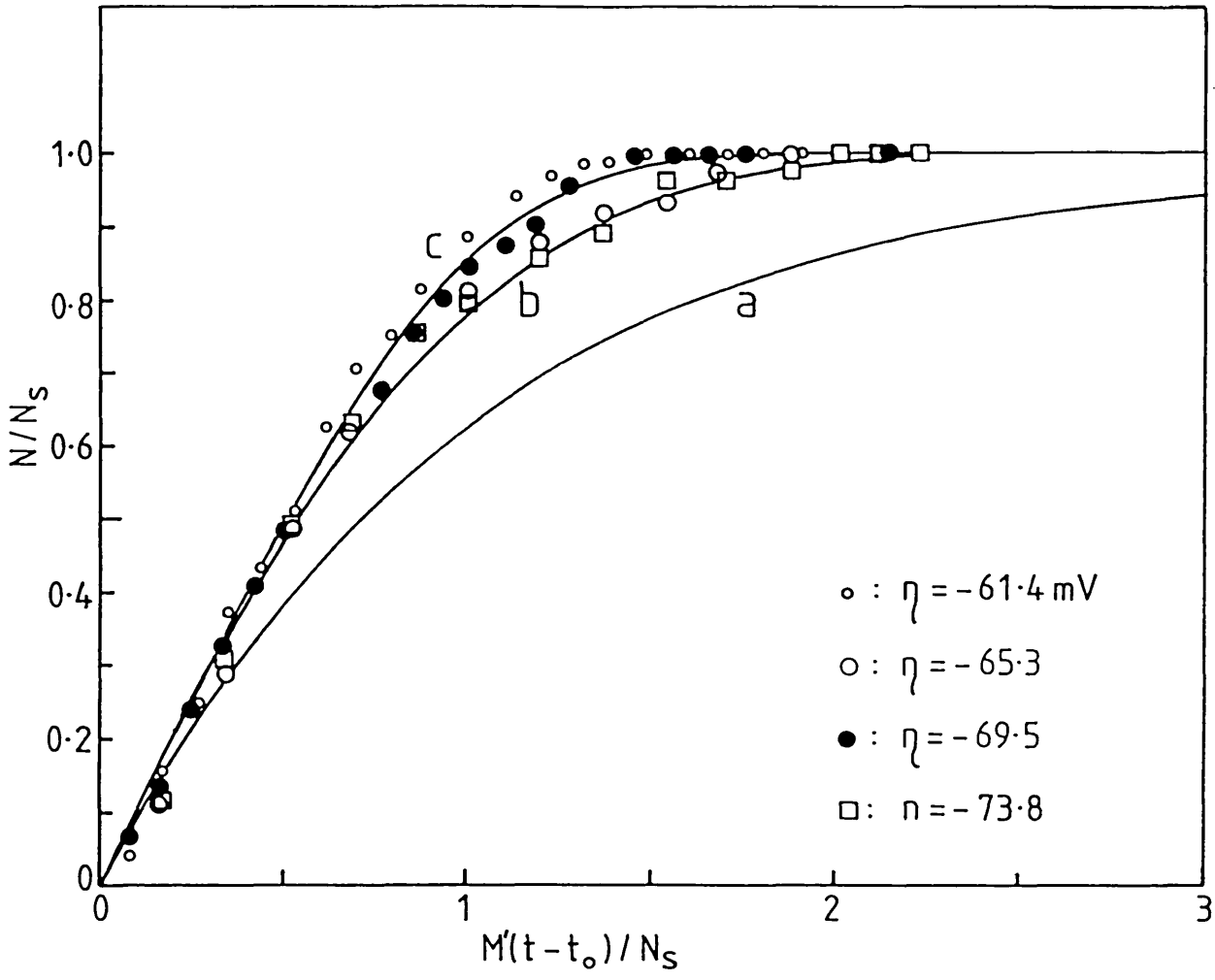

FIGURE 5.22. Comparison of calculated N-t data (from Figure 5.21b) with different nucleus saturation models.

curve a is the theoretical curve obtained when N_s is controlled by the active centres, expressed according to equation 2.84. Curves b and c (corresponding to equations 2.86 and 2.87 respectively) describe the case when the saturation mechanism is given by the overlapping of nucleation exclusion zones with constant rates of growth q = 1 and q = 1/2, respectively.

The comparison of the data with that of the theoretical models suggests that the termination of the formation of chromium nuclei is limited by overlapping of deactivation zones rather than the depletion of the active nucleation sites, even though the dispersion of the data does not permit a clear definition of the kinetics of growth of the nucleation exclusion zones. A mechanism of overlapping of exclusion zones is also more consistent with the notable increase in the saturation nuclei density with the overvoltage. Given the nature of a polycrystalline metallic surface it is difficult to attribute this change just to the increase of number of sites activated for nucleation.

The inactivating effect on nucleation that appears around the growing nuclei could be also confirmed from the observation of nuclei distributions obtained by applying a convenient double pulse technique, which is schematically shown in Figure 5.23. During the initial pulse at a low overpotential η_1 a few chromium nuclei were formed and grown for a time t_1. The magnitude of η_1 was low enough (30-50 mV) so that the formed

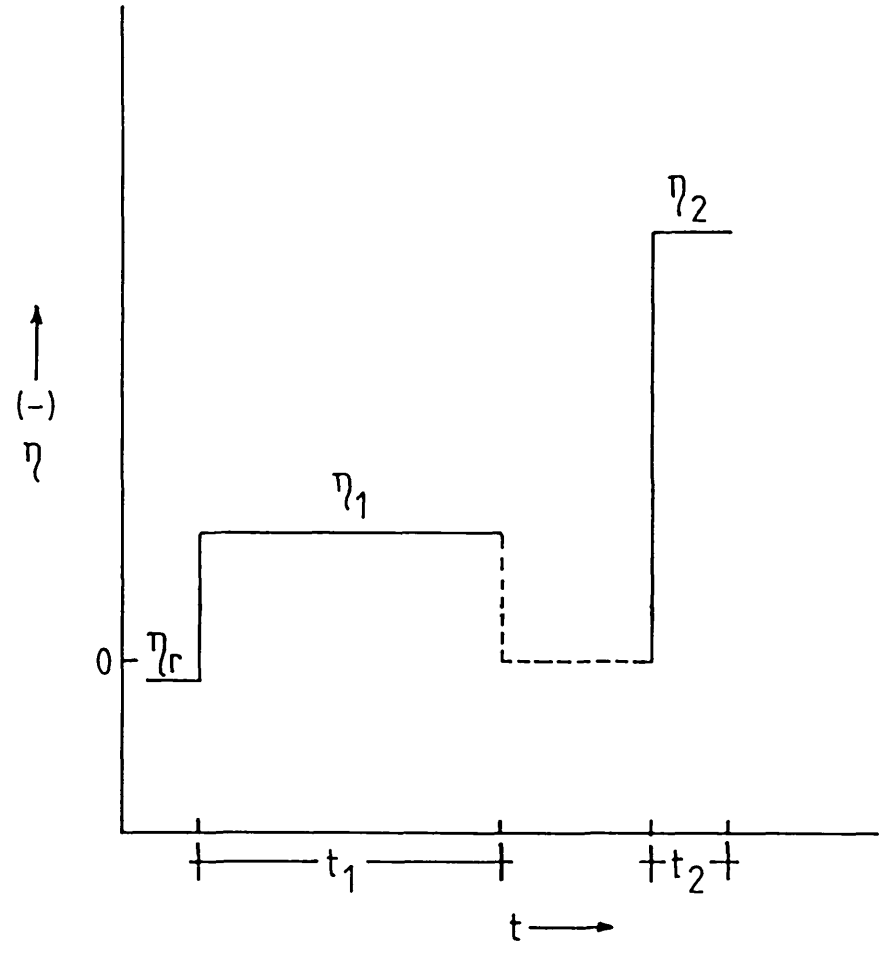

FIGURE 5.23. Step waveform applied in the characterization of nucleation exclusion zones (the broken line indicates open circuit).

nuclei were sufficiently separated from one another. A second pulse at a higher overpotential η_2 was then applied now leading to a high nuclei saturation number. A typical nuclei configuration obtained from this kind of experiment is shown in Figure 5.24, which reveals the existence of well defined inactive zones where the nucleation has been hindered in the second pulse. Average values of the nucleation exclusion zones radius r_e, defined as the distance between the edge of the central nucleus and the external boundary of the non-nucleated zone (see Figure 5.24) were determined in melts with different chromium (II) ion concentrations and at different values of η_2. The results are presented in Table 5.2. It is observed that the size of the nucleation exclusion zone at a given chromium (II) ion concentration decreases as the magnitude of η_2 increases. This tendency is related to the decrease of the induction time $\underline{t_o}$ with increasing overpotential. In other words, as the magnitude of the second overpotential η_2 increases there is less time for the exclusion area to grow. Values of the induction time $\underline{t_o}$ were estimated from potentiostatic current-time transients as the time at which the current starts rising which should correspond, approximately, to the onset of the nucleation stage. The available data on induction times $\underline{t_o}$ are plotted in Figure 5.25, from where the values in Table 5.2 were extrapolated.

Now the growth law of the exclusion zones arising in the vicinity of the chromium nuclei can be

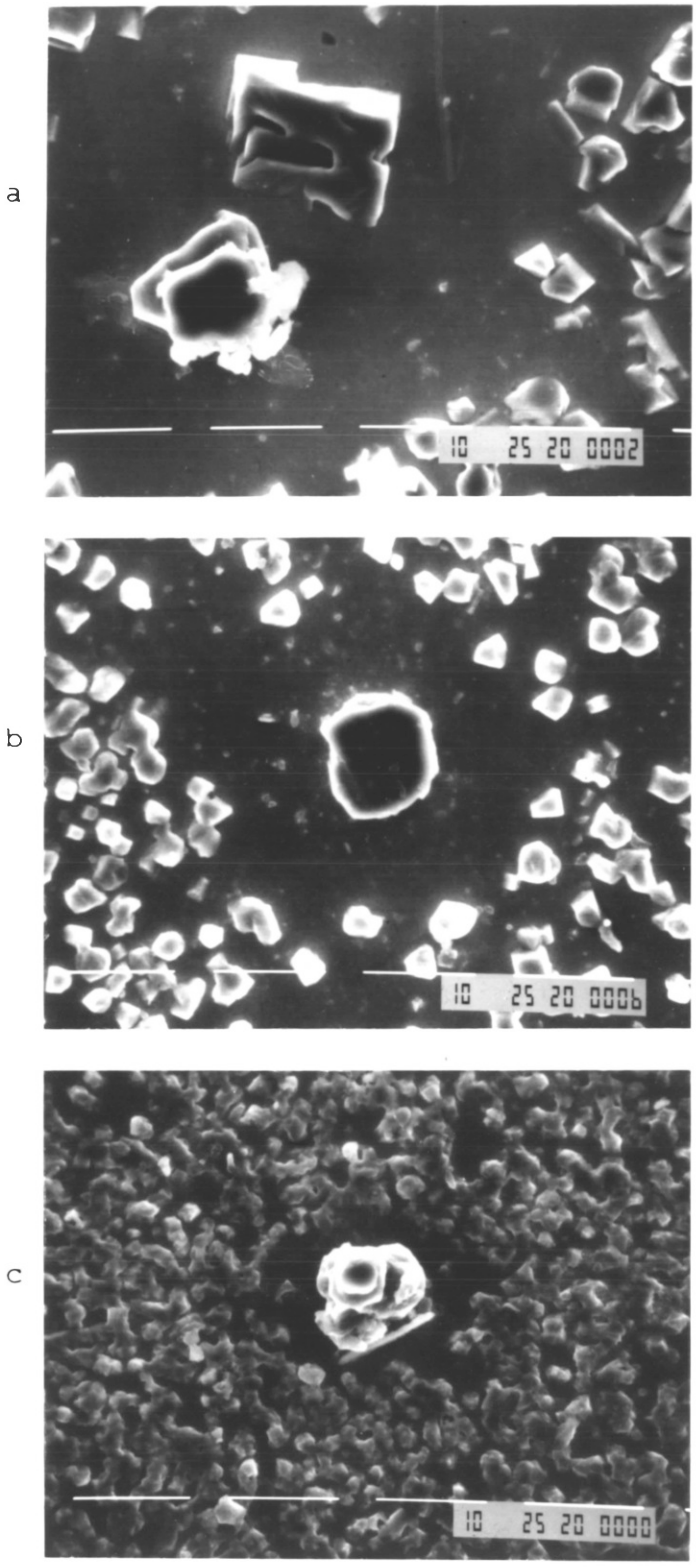

FIGURE 5.24. Screening action as a function of the applied overpotential in chromium nucleation on tungsten. $C = 0.93$ mol dm^{-3}. Values of parameters defined in Figure 5.23. t_1=10 s, η_1=-0.035 V, t_2=5 s. a) η_2=-0.044 V, b) η_2=-0.066 V, c) η_2=-0.109 V.

TABLE 5.2. Measurements related with the screening action exerted by the chromium nuclei.

$C/mol.dm^{-3}$	$\eta x10^3/V$	$r_e x10^3/cm$	$t_o x10^3/s$	$C_1/cm.s^{-1}$	$\frac{C_2 x10^3}{cm.s^{-\frac{1}{2}}}$	$\frac{C_3 x10^3}{cm.s^{-\frac{1}{2}}}$
0.346	70.6	0.43	6.1	0.071	5.51	6.5
0.931	43.7	1.58	49.8	0.032	7.1	10.8
	65.6	0.87	5.52	0.158	11.7	14.2
	109.4	0.32	0.75	0.351	11.7	12.2
1.487	69.3	0.84	3.2	0.261	14.7	17.6
	116.2	0.54	-	-	-	-
	140.2	0.21	-	-	-	-

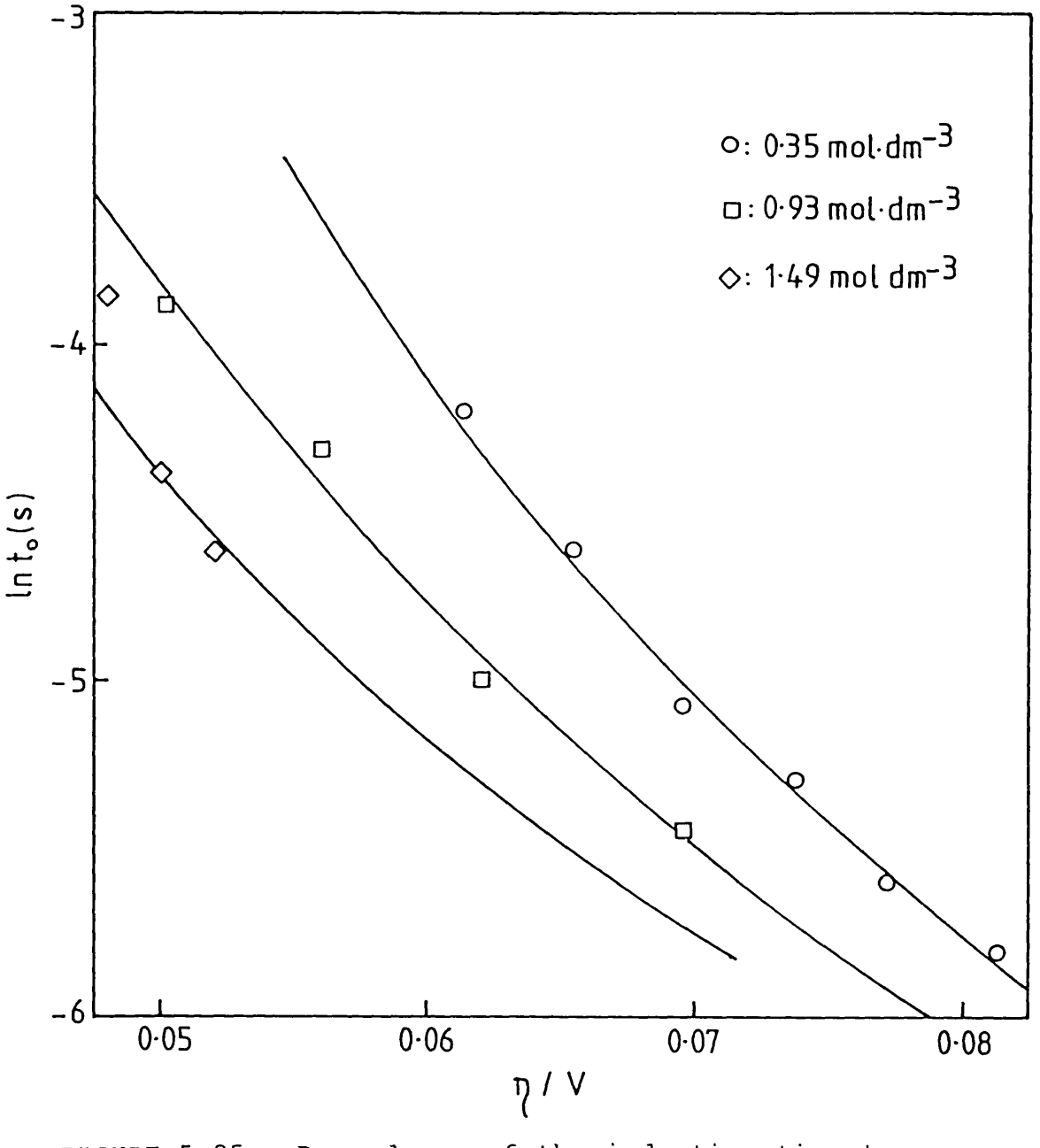

FIGURE 5.25. Dependence of the induction time t_o on the overpotential, for the case of chromium electrodeposition on tungsten.

characterized better and the relative validity of the models for q = 1/2 and q = 1 can be checked. Values of the ratios $c_1 = r_e/t_o$ and $c_2 = r_e/t_o^{\frac{1}{2}}$ were calculated (Table 5.2) and, according to the relatively more consistent values of c_2 obtained at different overpotentials in melts with 0.931 $mol.dm^{-3}$, it results that the exclusion zone growth law corresponds better to the form r_e = constant x $t^{\frac{1}{2}}$. Therefore the model for q = 1/2 is applicable in the present case, as deduced by comparison with the general expression of the zone growth low given in equation 2.81 . This kind of growth law has been observed in former studies[126,127], and it shows that the growth of the nucleation exclusion zones is related to the nucleus growth current, which also increases linearly with $t^{\frac{1}{2}}$. As the current in the present case is given by equation 5.1, a more convenient ratio is defined as $c_3 = r_e/(1-\exp znF/RT)^{1.5}t^{1.5}$, which gives a better approximation (Table 5.2).

From comparing values of c_3 at relatively similar overpotentials obtained in melts of different solute concentration, it can be seen that the growth rate constant of the exclusion zones increases with increase in concentration. It is interesting to analyze this tendency in relation to the expected values of saturation nucleus density N_s. Substituting q=1/2 in equation 2.83, the expression for N_s turns out to be

$$N_s = \Gamma(\frac{3}{2})(\frac{2S}{\pi c^2})^{\frac{1}{2}} M'^{\frac{1}{2}} \qquad 5.37$$

As $M' = I_o S$ this can be rewritten as

$$N_s = \Gamma(\frac{3}{2}) \frac{\sqrt{2}S^{1/4}}{\pi^{1/2}c} I_o^{\frac{1}{2}} \qquad 5.38$$

Earlier on in this study (see Section 5.2) it was observed that the steady state rate of chromium nucleation was not strongly dependent on concentration. Therefore, considering this and the observed dependence of nucleation exclusion zone on concentration, a decrease of N_s with increase of chromium (II) concentration is expected as a final result, according to the form of equation 5.38. This tendency was experimentally confirmed from direct counting of chromium nuclei obtained under potentiostatic conditions on tungsten and platinum electrodes, in melts of different chromium (II) ion concentration. These results are summarized in Figure 5.26 and 5.27, and some typical views of the chromium nuclei distributions are shown in Figures 5.28 and 5.29.

The values of N_s here obtained can be now compared to values reported from other systems. Some relevant information in this direction is given in Table 5.3. If the values of saturation nuclei density obtained in roughly similar conditions of concentration and overpotential are compared, it can be observed that the values reached in the present case with chromium nuclei are consistently larger than the ones obtained in other reported systems. If in principle one assumes

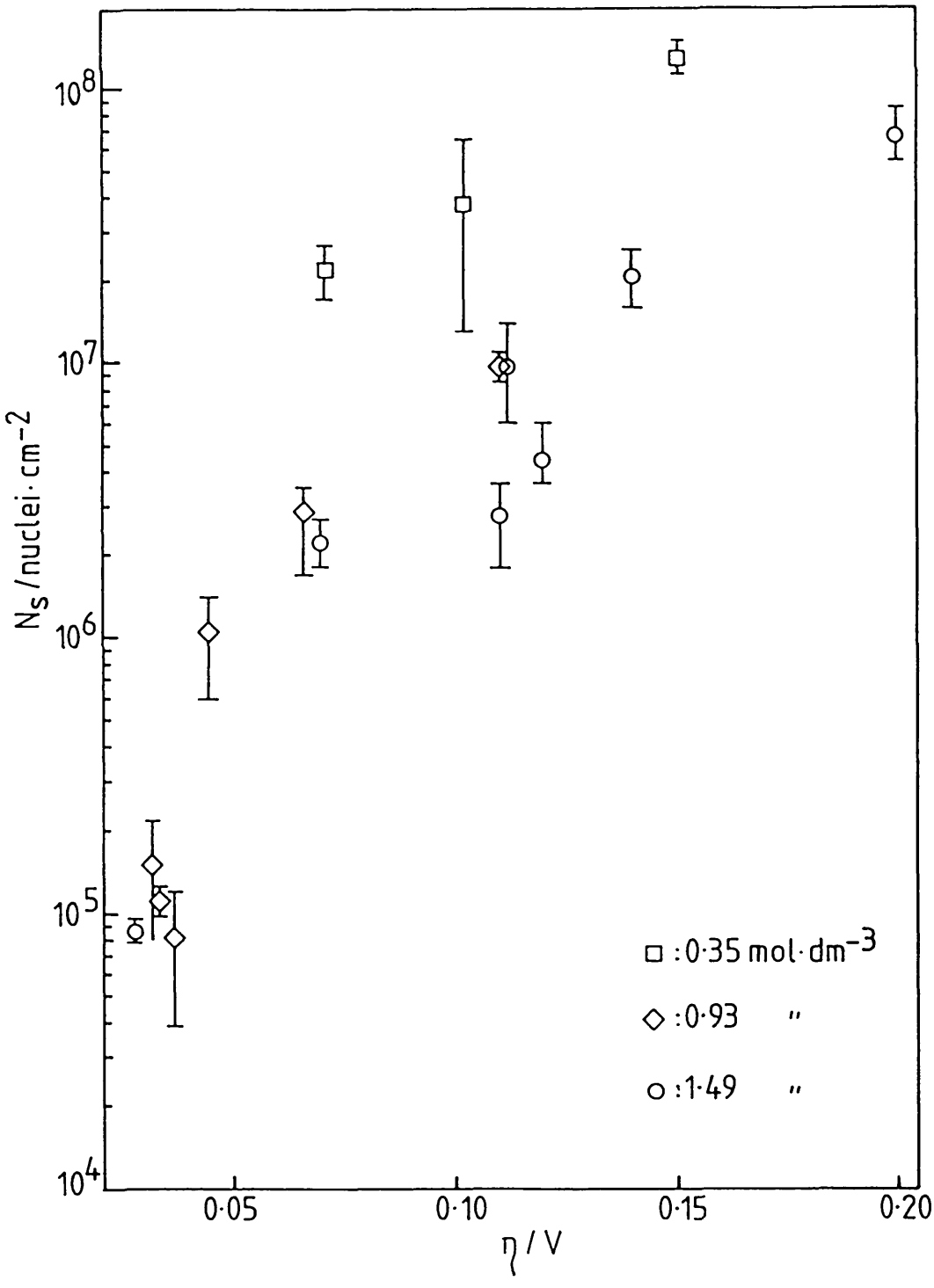

FIGURE 5.26. Experimental measurements of saturation nucleus density for the electrochemical nucleation of chromium on tungsten.

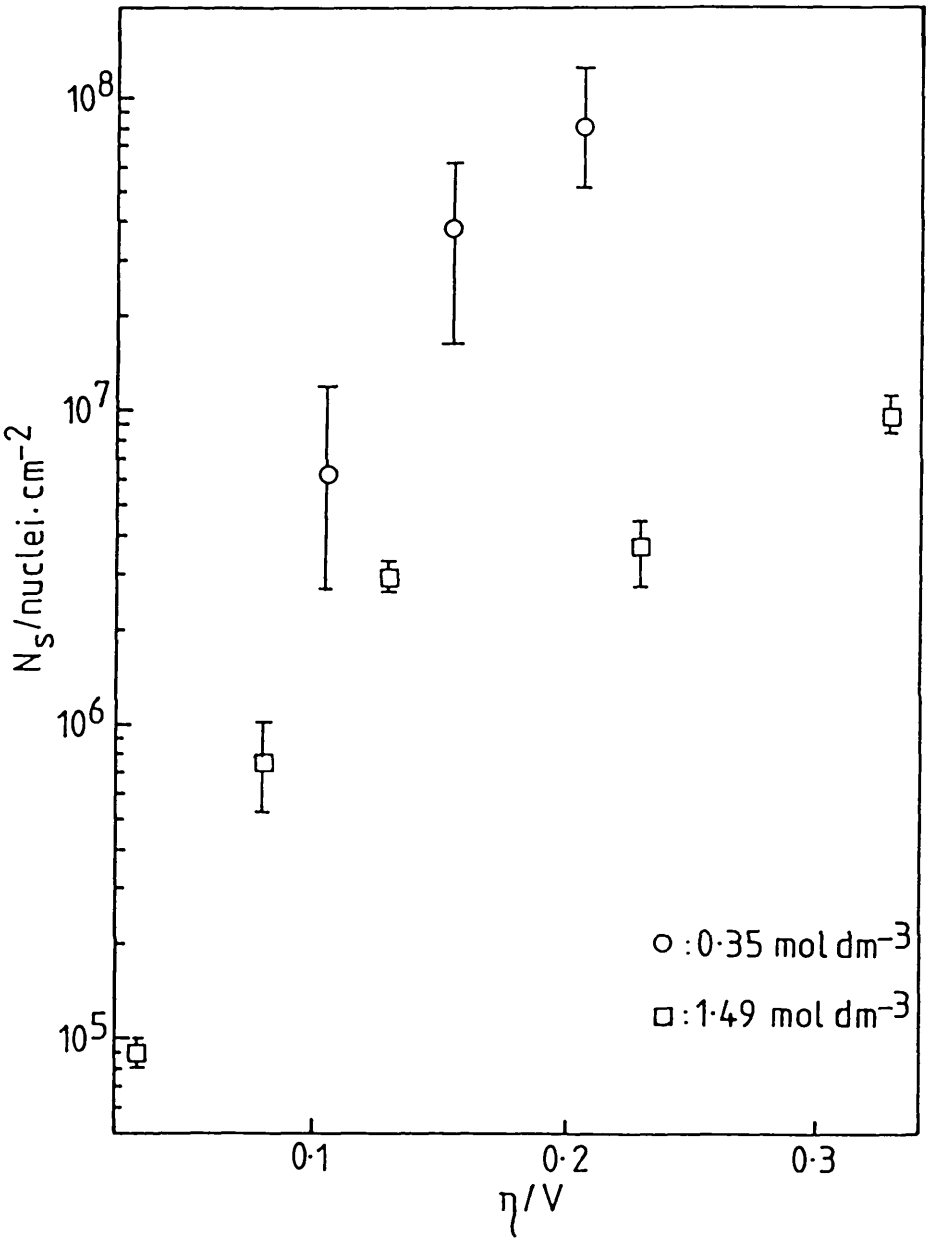

FIGURE 5.27. Experimental measurements of saturation nucleus density for the electrochemical nucleation of chromium on platinum.

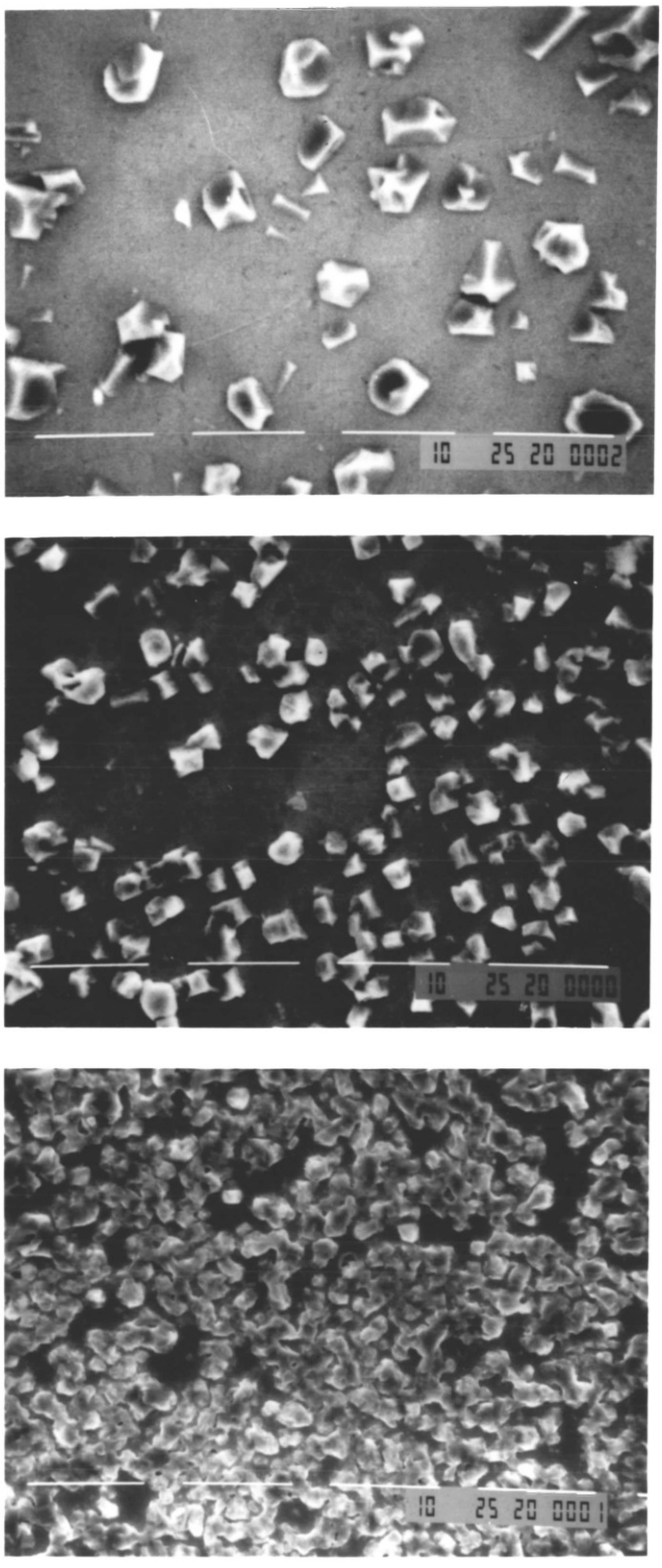

FIGURE 5.28. Saturation nucleus density obtained in the electrochemical nucleation of chromium at different overpotentials. C=0.931 mol dm^{-3}, t_N=5 s. a) η_N=-0.044 V, b) η_N=-0.066 V, c) η_N=-0.109 V (on tungsten).

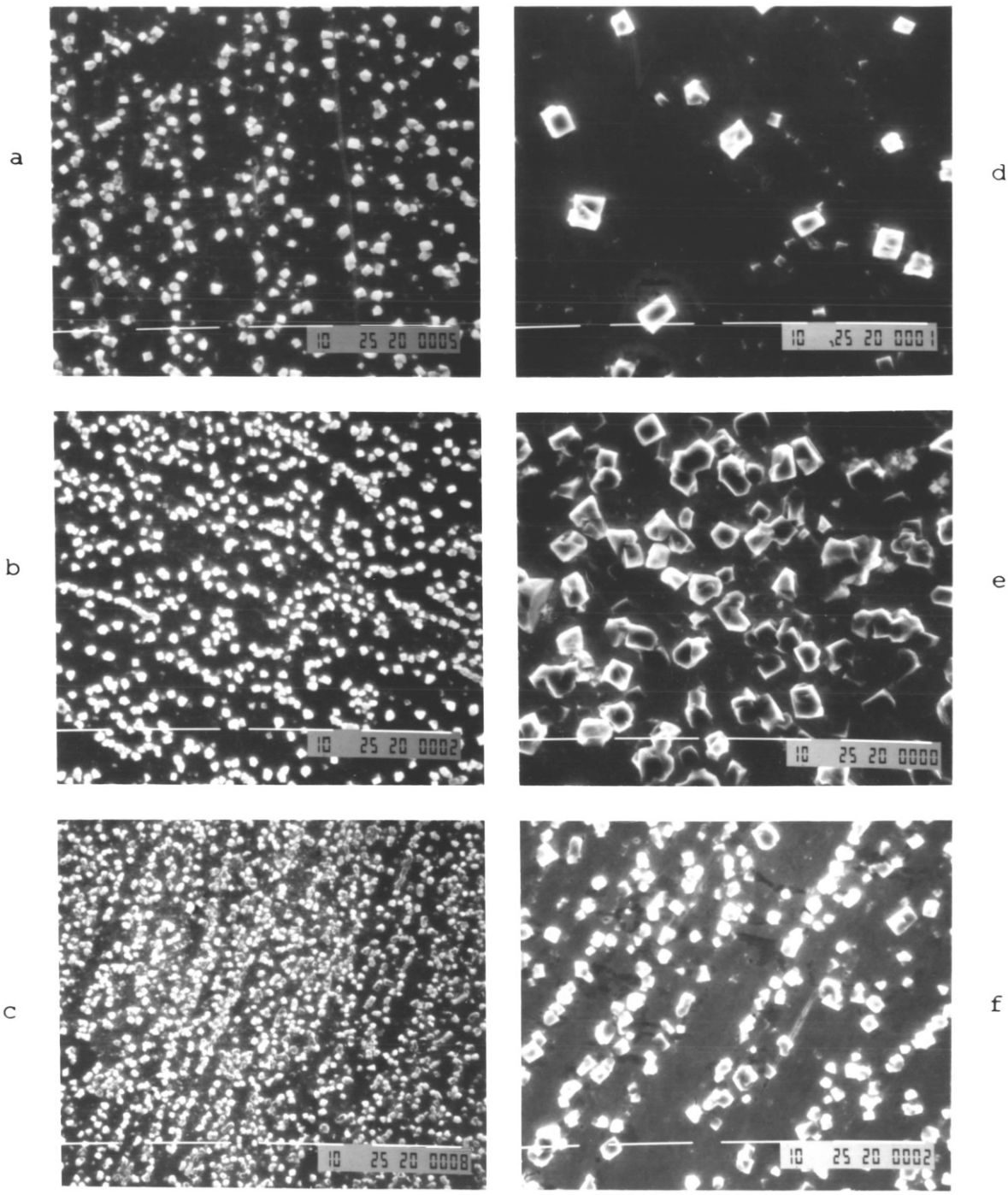

FIGURE 5.29. Saturation nucleus density obtained in the electrochemical nucleation of chromium on platinum at different overpotentials. i) C=0.346 mol dm^{-3}, t_N=1 s. a) η_N=-0.106 V, b) η_N=-0.156 V, c) η_N=-0.206 V. ii) C=1.49 mol dm^{-3}. d) η_N=-0.08 V, t_N= 1s, e) η_N =-0.23 V, t_N=0.5 s, f) η_N=-0.6 V, t_N=0.2 s.

as a first approximation that the growth rates of the nucleation exclusion zones are of the same order of magnitude in both systems, then the observed tendency can be well explained, according to equation 5.38, simply with reference to the comparatively higher values obtained for the steady state nucleation rate in the present system.

A more thorough comparison can be made with the case of Hg deposition from $Hg_2(NO_3)_2$ solutions, where values of nucleation exclusion growth rate are also provided[132]. Values obtained at 0.346 $mol.dm^{-3}$ and 0.070 V in the case of chromium nucleation (Table 5.2) can be compared with values obtained at 0.386 $mol.dm^{-3}$ and 0.083 V in the case of mercury electronucleation from aqueous solutions (Table 5.3). The dimension of the nucleation exclusion zone estimated in both cases for $t = 10^{-2}$ sec, is 6.5×10^{-5} cm and 1.24×10^{-2} cm respectively, being $t = 10^{-2}$ sec the approximate length of the nuclei formation stage (see Figure 5.21). The comparatively smaller magnitude of the nucleation exclusion effect existing in the present case is, therefore, a factor that constitutes additionally to the reaching of comparatively large saturation nucleus densities in the chromium system.

The data obtained here are not enough to define exactly the nature of the phenomenon originating the inactivating effect arising around the growing chromium nuclei. Nevertheless, the relatively low order of

TABLE 5.3. Some representative parameters determined in studies of electrochemical nucleation in aqueous systems.

Active specie	$\frac{C}{mol.dm^{-3}}$	$\frac{\eta}{V}$	$\frac{I_o}{N.s^{-1}cm^{-2}}$	$\frac{N_s}{N.cm^{-2}}$	$\frac{c}{cm.s^{-1}}$	Ref.
Ag^+	0.5	0.090	$1.96x10^5$	-	-	152
Hg^+	0.386	0.083	$1.24x10^7$	$4.3x10^4$	1.242	132
Hg^+	0.010	0.15-0.215	-	$2.4-6.9x10^4$	-	143
Hg^+	0.01	0.22-0.29	-	$0.43-2.4x10^6$	-	149
Ag^+	0.01	0.16-0.26	-	$0.75-2.5x10^6$		150
Ag^+	0.1	0.038	7.5	$0.8x10^3$	-	179

magnitude of the screening action is consistent with that expected for a system growing under diffusion control in the presence of a supporting electrolyte[127].

6. PRODUCTION OF PROTECTIVE CHROMIUM COATINGS

6.1. INTRODUCTION

This section is concerned with the application of the process of chromium electrodeposition from the LiCl-KCl eutectic, to the production of protective chromium coatings on AGR fuel cans.

The work was focused on the characterization of the mechanism of formation of chromium macrodeposits and the development of a method for the production of deposits with coherent morphology. The electrocrystallization experiments reported here were all carried out using the AGR fuel element cladding as the substrate metal.

6.2. CHROMIUM ELECTRODEPOSITS AT CONSTANT OVERPOTENTIAL

The electrocrystallization of chromium from LiCl-KCl-$CrCl_2$ melts starts with a well defined three-dimensional nucleation stage. Under potentiostatic conditions, after an initial induction period, the process begins with the simultaneous formation and growth of three-dimensional chromium nuclei. The nuclei number reaches a final saturation nuclei density, well before the complete coverage of the electrode surface is attained. This mechanism corresponds basically to the alternative path b formulated as a possible growth mechanism in Figure 2.2.

Nevertheless in the case of chromium electrocrystallization from molten LiCl-KCl-$CrCl_2$ melts the involvement of a nuclei saturation mechanism before complete coverage precludes the ready transition from island to continuous growth. In practice it was not possible to obtain a coherent chromium deposit under potentiostatic conditions. The nature of this behaviour has its origin in the specific nature of the electrocrystallization process, that can be here typified in the two curves shown in Figure 6.1. Here curve a represents the η-I polarization curve obtained for the electrodeposition of chromium on chromium and curve b represents the η-N_s relation obtained for the electronucleation of chromium on the initial substrate. According to Figure 6.1 the following situation exists:

a) On the one hand, with respect to the electronucleation process, the electrodeposition of chromium at higher overpotentials is more advisable. In this case a higher saturation nuclei density is reached (curve b) and, therefore, a better initial coverage of the surface is obtained. Nevertheless as the overpotential increases the current becomes more diffusional controlled reaching eventually the limiting current level (curve a). This fact in conjunction with the initial island growth create optimum conditions for the development of dendritic configurations[180]. The initially formed crystallites which start growing with a current controlled by hemispherical diffusion eventually develop preferentially in the direction of the solution bulk

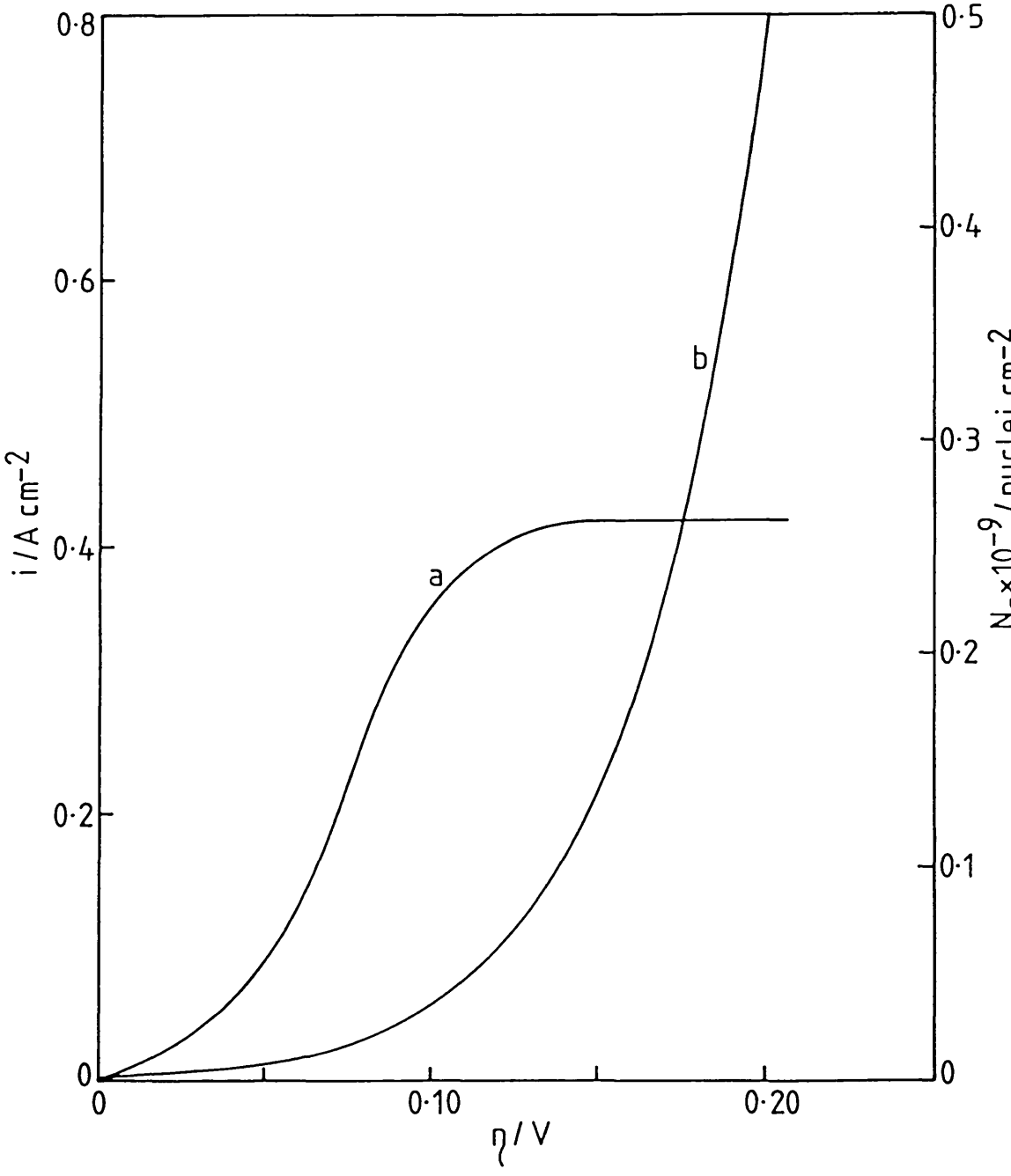

FIGURE 6.1. Example of characteristic curves in the electrocrystallization of chromium under potentiostatic conditions: tungsten, C = 0.346 mol.dm^{-3}. a) Sampled current voltammogram (sampling time: 0.1 s), b) Saturation nucleus density versus overpotential.

which provides a better supply of chromium (II) ions. At the same time nuclei growth in the horizontal direction is practically inhibited as the concentration of chromium (II) ions in the inter-nuclei melt gradually decays. Figure 6.2a illustrates well this case, showing a chromium electrodeposit with the typical dendritic growth developed out of initially formed nuclei. If the overpotential applied reaches very high values the deposit may evolve to a three-like formation, as shown in Figure 6.2b.

b) On the other hand with respect to the characteristics of the polarization curve a the electrodeposition at lower overpotential is advisable. As the deposition occur in a region far from the limit current, the diffusional overpotential becomes less important and the development of dendritic growth can be hindered or at least delayed for a longer time[180,181]. Nevertheless as the overpotential is lowered the final saturation nuclei density drastically decreases and a lower degree of coverage of the substrate is initially reached. Within the range of overpotentials permitted before reaching the limiting current region the initial degree of coverage is too low, the inter-nuclei distance too large, and the deposit does not reach a continuous structure. This situation is well exemplified in the structure of the chromium deposit shown in Figure 6.3. The growth at lower overpotential effectively prevented the development of dendrites and the deposit appeared as a continuous growth to the naked eye. Nevertheless the scanning electron micrographs showed that the

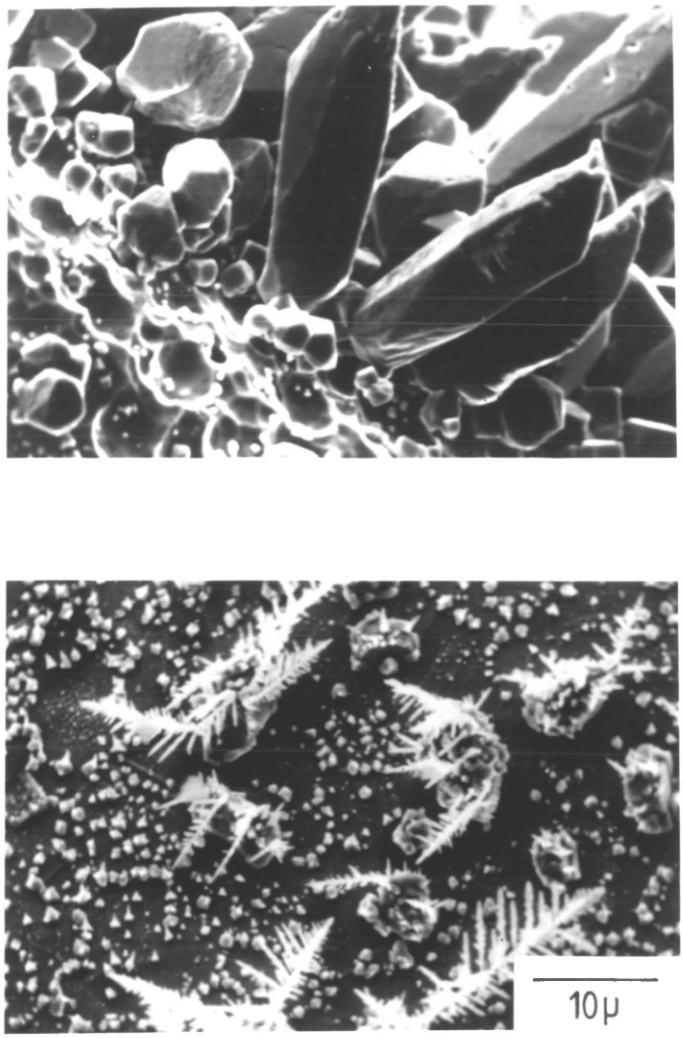

FIGURE 6.2. Typical dendritic formations obtained in chromium electrodeposits. a) dendritic deposit, C=0.354 mol dm^{-3}, η =-0.085 V. b) tree-like deposit formed on large chromium nuclei, C=0.93 mol dm^{-3}, η = -0.36 V, t = 1s.

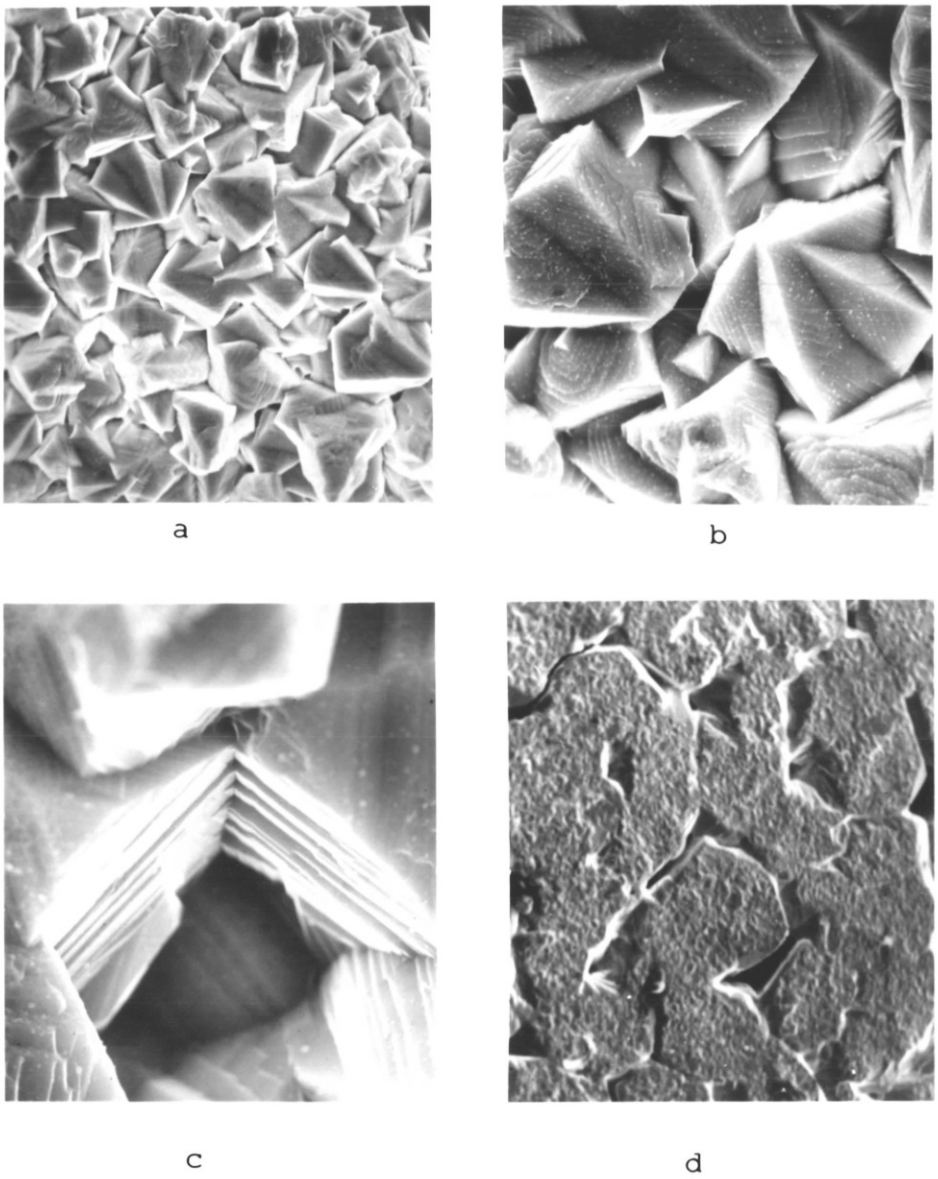

FIGURE 6.3. Chromium electrodeposits obtained at low growth overpotential (η =-0.03 V), and low chromium(II) ion concentration (C$\sim$0.14 mol dm^{-3}). a) mag. 130x, b) mag. 380x, c) mag. 1300x, d) mag. 230x.

deposit is not compact being the result of the growth of the initially formed nuclei which have eventually overlapped. The deposit has a high level of inter-crystalline space as can be observed in Figures 6.3a-b and there is an important proportion of substrate area still uncovered, as can be observed in Figures 6.3c and 6.3d, the last one showing a view of the back surface of the deposit.

From the relative positions of curve a and b in Figure 6.1 it can be seen that there is no intermediate overpotential range where both phenomena could be prevented i.e. dendrite formation and low initial coverage. In addition a change in chromium (II) ion concentration does not help in this situation as both limitations will be displaced in opposite directions with such a change. For instance an increase of concentration will result in a higher limiting current and a relative larger overpotential range will be available for deposition without dendritic formation. However, as was shown in Section 5, an increase in concentration also results in a decrease of the saturation nuclei density number, reducing at the same time the possibilities of a good initial coverage.

6.3. INITIAL PULSE METHOD

Given the intrinsic characteristics for the growth of chromium electrodeposits at constant overpotential

which prevents the production of compact structures, an alternative deposition method was proposed and studied in some detail. According to this method the conditions for deposition at the early stages of formation of the deposit were differentiated from the conditions used during the further growth and building up of the macrodeposit.

A scheme of the basic programme of overpotentials proposed is shown in Figure 6.4. Initially a large overpotential pulse (or pulses) η_N is applied for a length of time t_N. During this stage the deposition occurs mainly though nucleation and a high overpotential is used in order to reach a high saturation nuclei density which results in a good initial coverage of the substrate. Immediately after the initial pulse the overpotential is lowered to a value η_G which is applied for a time t_G enough to build up the desired thickness. During this stage deposition occurs mainly by the growth of the nuclei formed during the initial pulse.
A conveniently low overvoltage is used at this stage in order to prevent the growth of dendrites and create more favourable conditions for the coalescence of the nuclei into a continuous deposit.

6.3.1. Chromium electrogrowth with the initial pulse method

An experimental study was developed in order to determine the characteristics of the chromium electro-

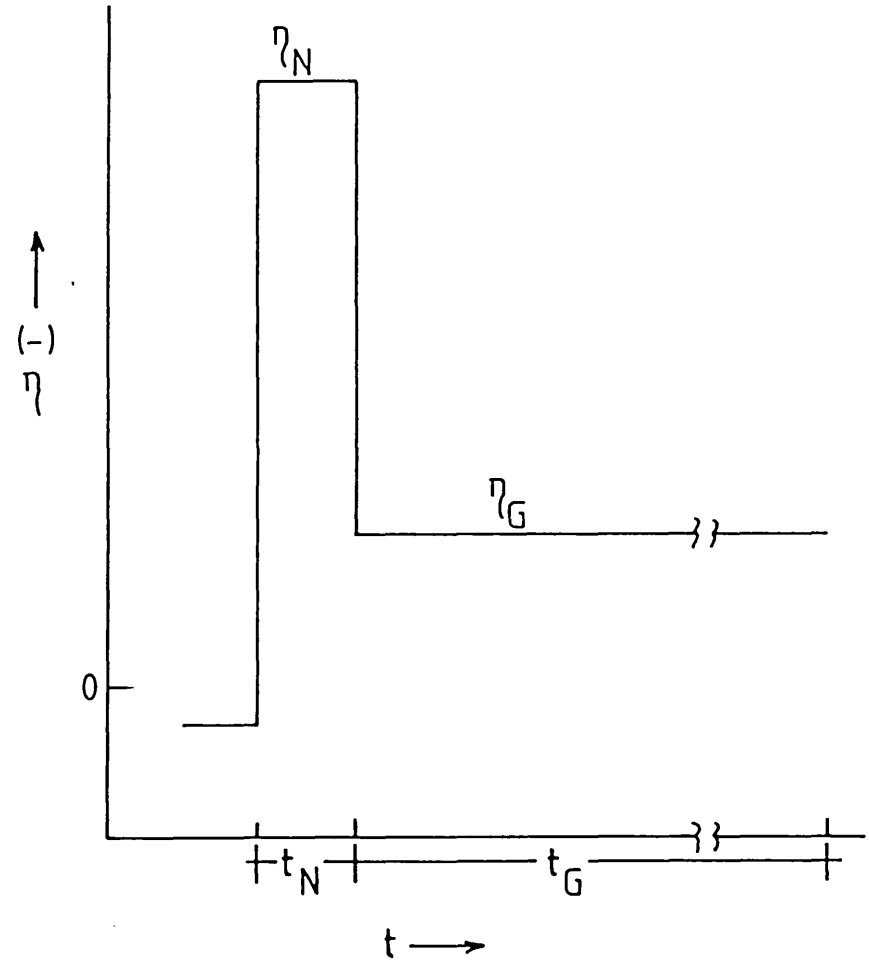

FIGURE 6.4. Basic step waveform corresponding to the initial pulse method.

growth carried out under the initial pulse method and, in this way, to evaluate its potential application to the production of protective chromium coatings. The study involved mainly the characterization of the morphological evolution of the deposit at different conditions of operation. The characterization was made using scanning electron microscopy.

The following aspects were observed.

6.3.1.1. Effect of initial nucleation pulse

The improvement of the morphological characteristics of chromium electrodeposits obtained when using an initial overpotential pulse is well illustrated in the scanning micrograph series shown in Figure 6.5. In the case of an electrodeposit obtained at constant overpotential the deposition is restricted to the growth of the few initially formed nuclei (Fig. 6.5a). Later in the process some of the nuclei have merged into a continuous layer but due to the large initial inter-nuclei distance, interstitial zones where chromium is not deposited definitely remains (Fig. 6.5b). Electrodeposition carried out in similar conditions but introducing initially 3 high overpotential pulses increases the initial nuclei coverage producing then a more even distribution of the chromium and a deposit that fully covers the substrate (Fig. 6.5c).

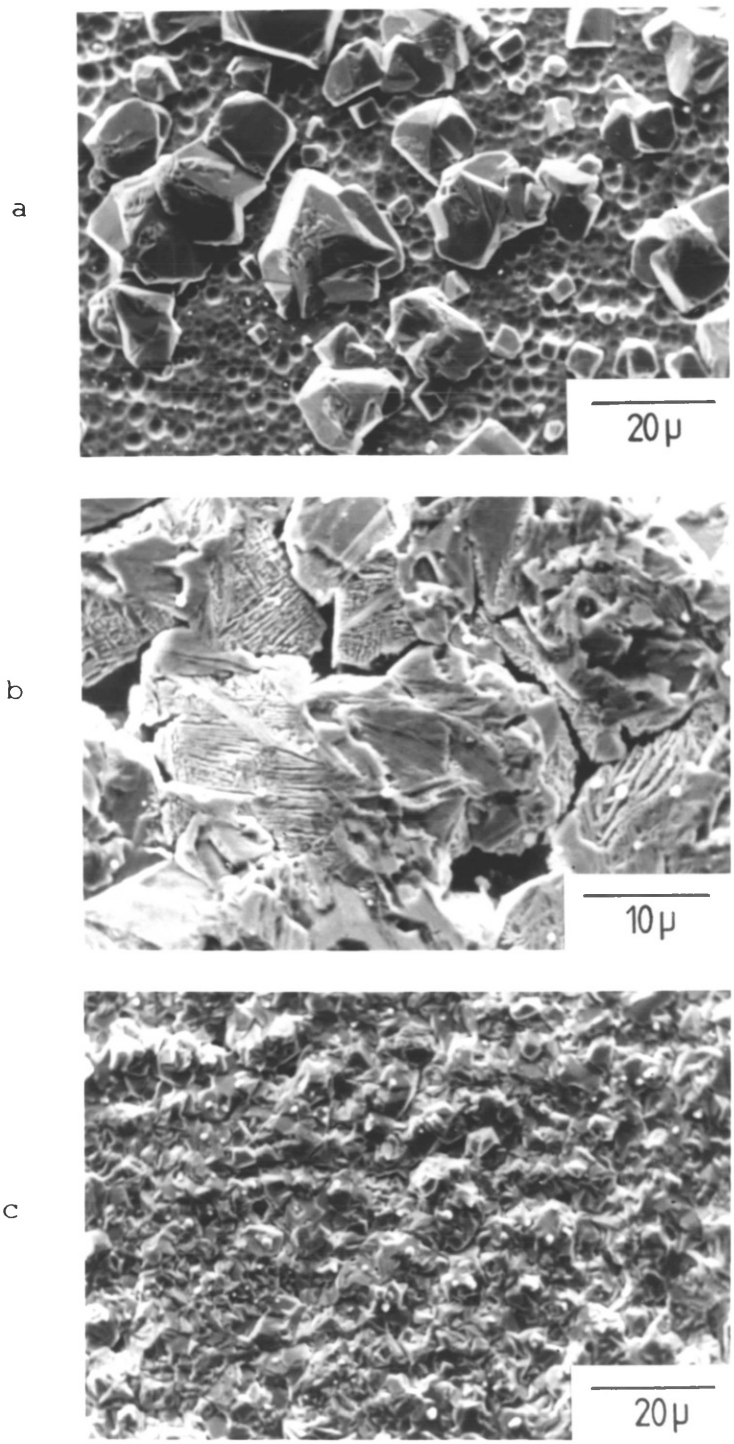

FIGURE 6.5. Influence of initial overpotential pulse on the morphology of chromium electrodeposits. C=0.93 mol dm^{-3}. a) Constant overpotential η =-0.03 V, Q=10 $C.cm^{-2}$. b) As in (a), except Q=53 $C.cm^{-2}$. c) As in (b), except starting with 3 pulses at η_N=-0.58 V, t_N=3 s.

6.3.1.2. Effect of number of initial pulses

The scanning electromicrographs in Figure 6.6. show the morphology of chromium electrodeposits obtained when using different number of nucleation pulses. The deposits in Figures 6.6a and b were obtained under the same conditions but using one and three pulses, respectively. When more than one pulse was applied a rest time was left between each pulse, necessary to homogenize the chromium (II) ion concentration near the electrode vicinity (see Figure 6.7a). The deposit in Figure 6.6c was obtained under a continuous over-potential pulse-rest cycle (see Figure 6.7b).

It can be observed that the repetition of the initial nucleation pulse does not improve the coverage provided by the first overpotential pulse, nor results in a better distribution of the chromium. Apparently the extra pulses contribute basically to enhance the growth of the initially formed nuclei while no major deposition in the internuclei zones seems to occur. This behaviour can be explained in relation to the inhibitory action that growing chromium nuclei exercise on nucleation, a phenomenon previously analysed (Section 5). In other words, as an initial nuclei number has been formed during the first pulse, the application of additional overpotential pulses will result in the rapid growth of nucleation exclusion zones arising around the initially formed nuclei, which then completely cover the internuclei area, preventing the onset of a secondary nucleation process and the improvement of the initial coverage.

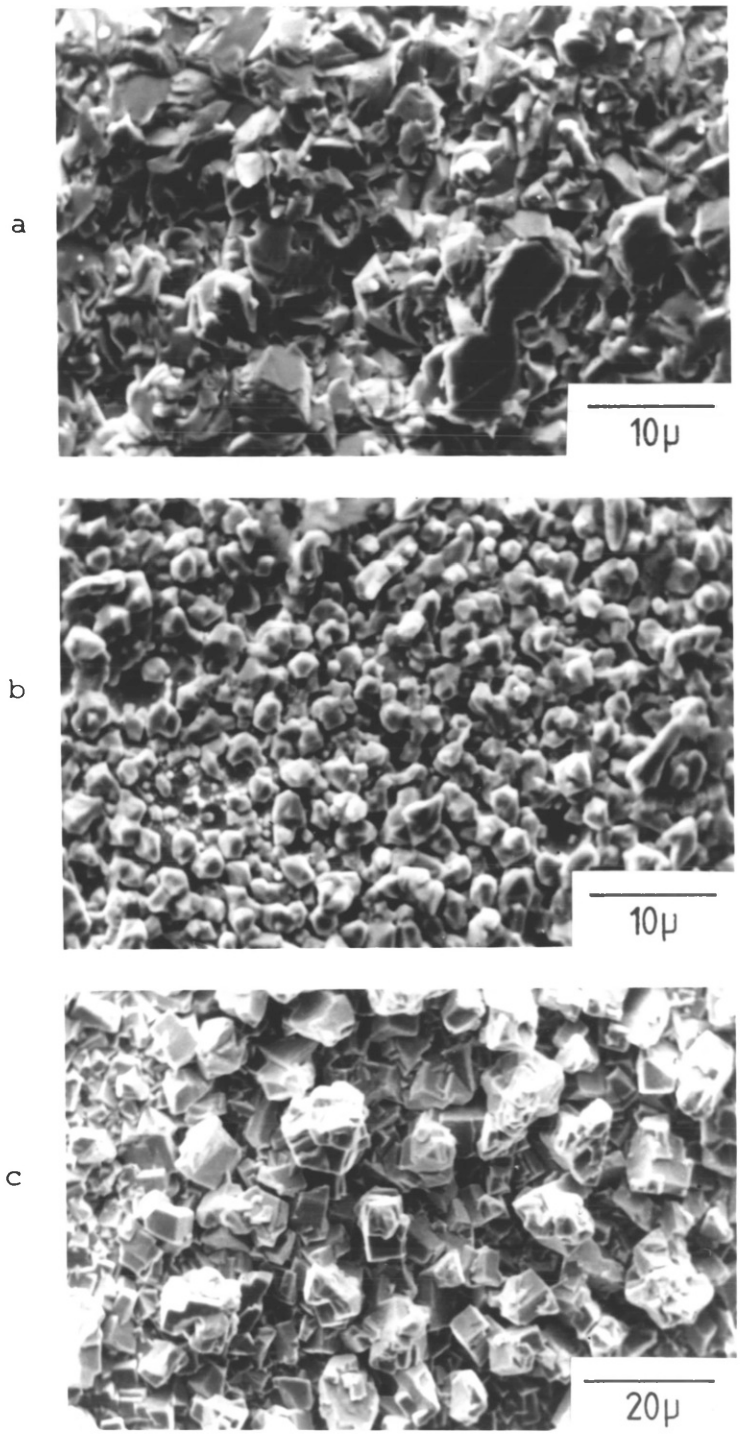

FIGURE 6.6. Effect of number of initial nucleation pulses on the morphology of the electrodeposit. a) η_N=-0.58 V, t_N=3 s, 1 pulse, η_G=-0.03 V, Q=10 C.cm^{-2}. b) As in (a), except with 3 pulses. c) Deposited under continuous pulsing. η_N=-0.58 V, t_N = 3 s, Q=29 C.cm^{-2} (C= 0.931 mol dm^{-3})

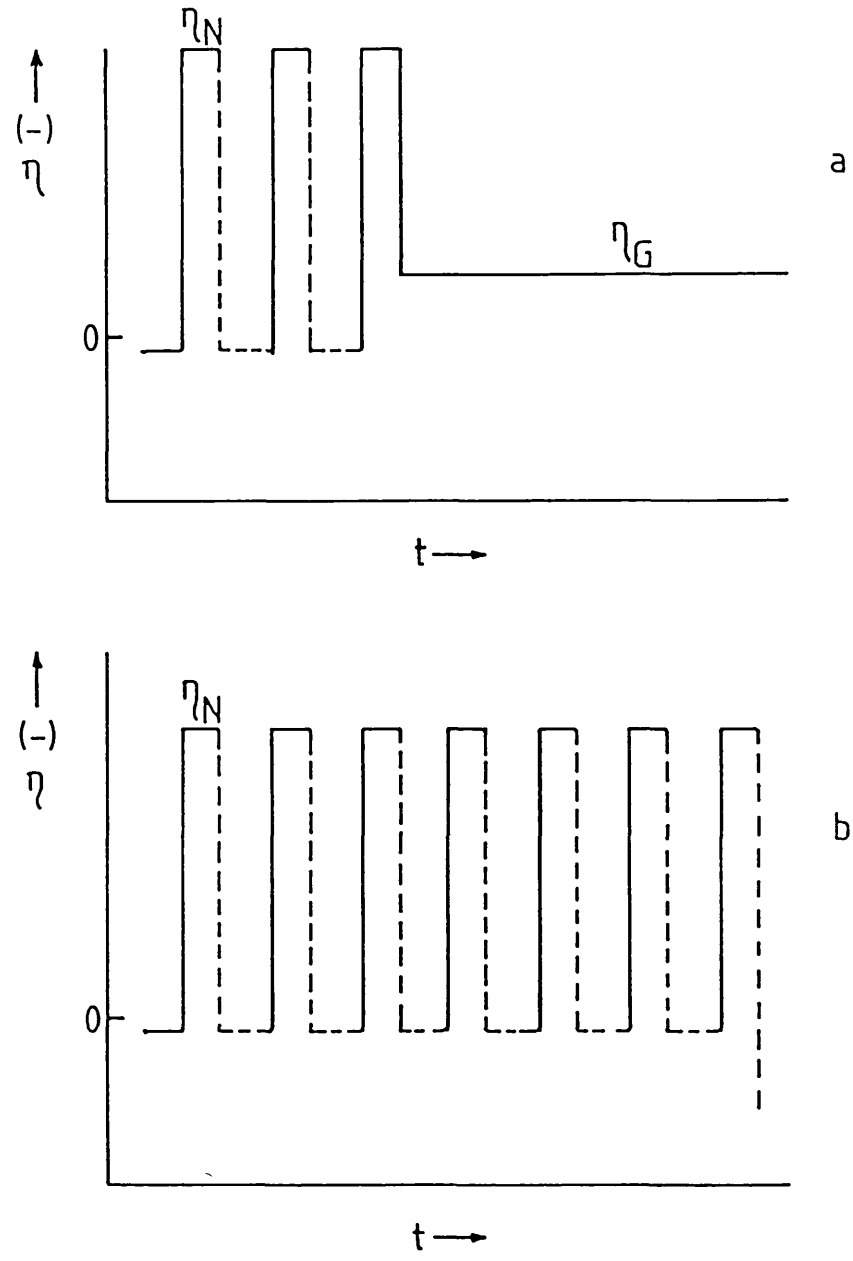

FIGURE 6.7. Other step waveforms applied in the electrodeposition of chromium a) three initial nucleation pulses, b) continuous pulsing (the broken line indicates open circuit).

If the cycle overpotential pulse-rest (Figure 6.7b) is continuously repeated the substrate surface is eventually covered but the deposition is not even and the initial nucleated morphology is maintained well into the process (see Figure 6.6c).

6.3.1.3. Effect of chromium (II) ion concentration

Given an initial nucleation pulse of a certain overpotential value a higher initial nuclei saturation number will be reached if a lower chromium (II) ion concentration is used. But even though the use of low solute concentrations is advisable with regard to the initial coverage of the substrate, it is disadvantageous with regard to the second stage of growth at low overpotential.

The scanning electromicrographs sequence in Figure 6.8 shows the evolution with time of the morphology of chromium electrodeposits obtained at relatively low chromium (II) ion concentrations. It can be observed that the use of an initial overpotential pulse produces in fact a good initial coverage of the substrate with chromium nuclei. However as the process continues the deposits evolve into a structure consisting of discrete crystals which has a high degree of interspace and does not constitute a coherent protective layer. The formation of chromium deposits of this type becomes especially noticeable when electrodepositing chromium

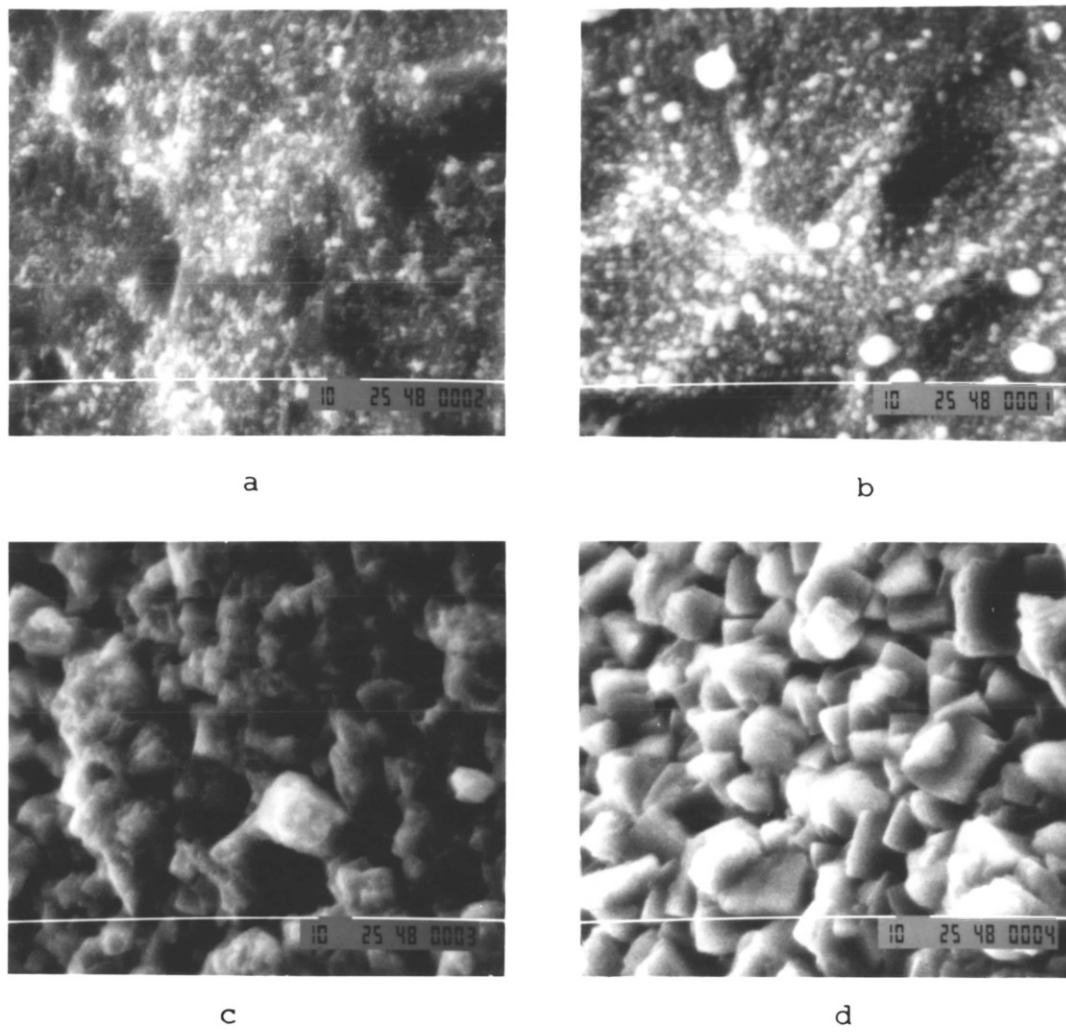

FIGURE 6.8. Growth morphology of chromium electrodeposits versus time. C=0.346 mol dm^{-3}, η_N=-0.6 V, t_N= 1 s, η_G=-0.05 V. a) t_G=0, b) t_G=0.5 min, c) t_G=4 min, d) t_G=21 min (Q=9 $C.cm^{-2}$)

at very low chromium (II) ion concentrations, as shown in Figure 6.3a-b.

The growth of chromium deposits in the form of crystals can be explained in terms of a low deposition rate/surface diffusion rate ratio. At low chromium (II) ion concentrations only a very small range of over-potential growth is available as the limiting current is low. Under these circumstances the electrodeposition rate is very low and the electrogrowth occurs close to equilibrium conditions. At the same time a high surface diffusion rate is expected in a system at this temperature[182,183], and, therefore, during the deposition there is enough time for the freshly deposited adatoms to migrate on the surface finding equilibrium sites corresponding to the crystal structure of chromium. This process can be particularly detected in the scanning micrograph in Figure 6.3b, where the growth steps of the chromium crystal are well defined.

At higher chromium (II) ion concentrations the lower saturation nuclei density obtained decreases the initial coverage of the substrate, but this situation is compensated by the improvement in the characteristics of the low overpotential growth step. At higher chromium (II) concentration the electrocrystallization occurs at higher deposition rates and therefore the possibility for the growth of discrete crystals of chromium is reduced. This behaviour is well illustrated in the scanning micrograph sequence in Figure 6.9, which

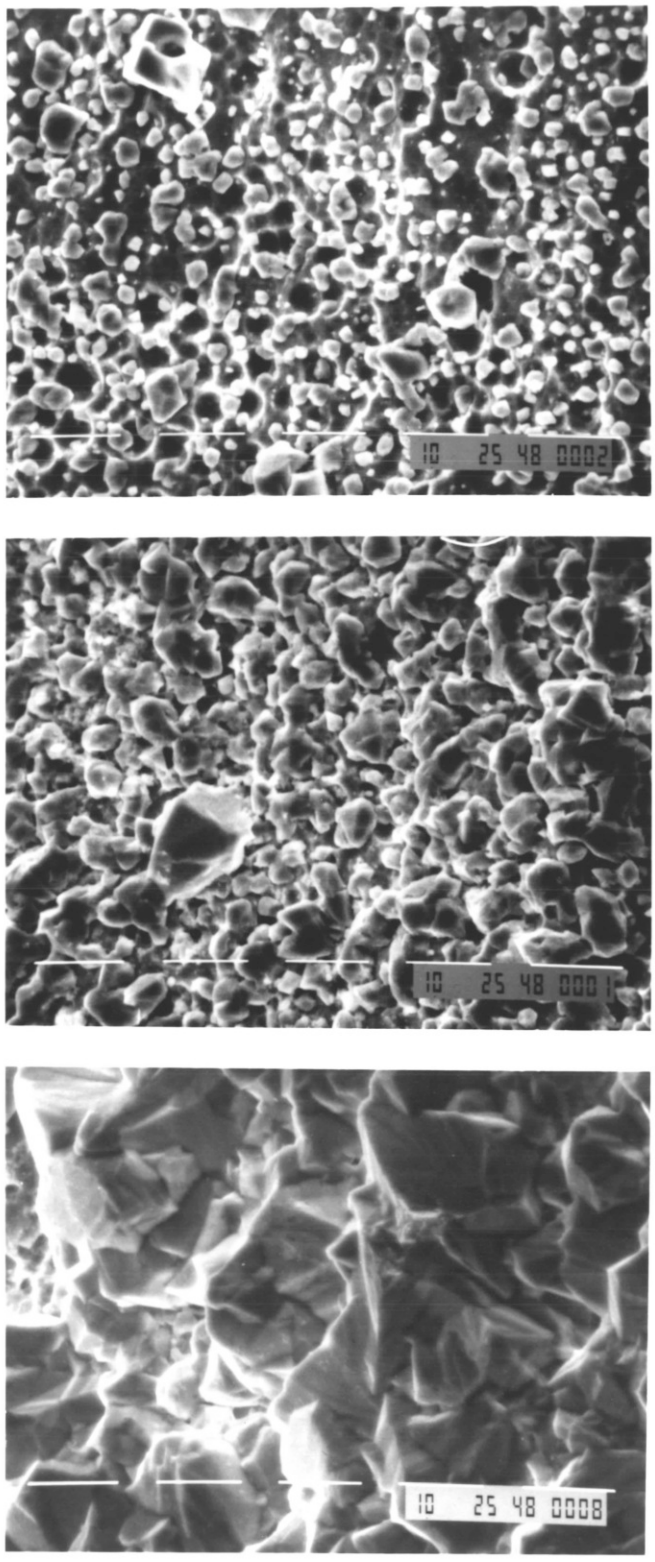

FIGURE 6.9. Growth morphology of chromium electrodeposits versus time. C=1.49 mol dm^{-3}, η_N=-0.6 V, t_N=1 s, η_G=-0.05 V. a) t_G=1.5 min, b) t_G=4.5 min, c) t_G=22 min. (Q=40.1 $C.cm^{-2}$)

shows the evolution with time of a chromium electrodeposit obtained in melts with C = 1.49 mol.dm^{-3}. The electrodeposition conditions used here are exactly the same as those corresponding to Figure 6.8, with only the concentration being different. It can be seen that now at high chromium (II) concentration the nuclei grow in the form of rounded geometries and, even if the nuclei density number is initially lower, they eventually merge into a continuous layer.

The morphology of the surface of the deposit after 22 min of deposition (Figure 6.9c) still evidences the formation of discrete crystals which indicates the strong tendency for this phenomenon to occur during the electrocrystallization of chromium in the present system. This feature can also be observed in Figure 6.10, which shows the development of a chromium electrodeposit obtained at C = 0.931 mol.dm^{-3}.

6.3.1.4. Effect of growth overpotential

After the initial nucleation pulse is applied the overpotential is set to a lower value where there are better conditions for the transition from the initial nuclei growth into a continuous deposit. The use of a low overpotential in this stage is necessary to reduce conveniently the diffusion polarization around the growing nuclei, preventing their evolution into dendrites. At the same time a low overpotential is

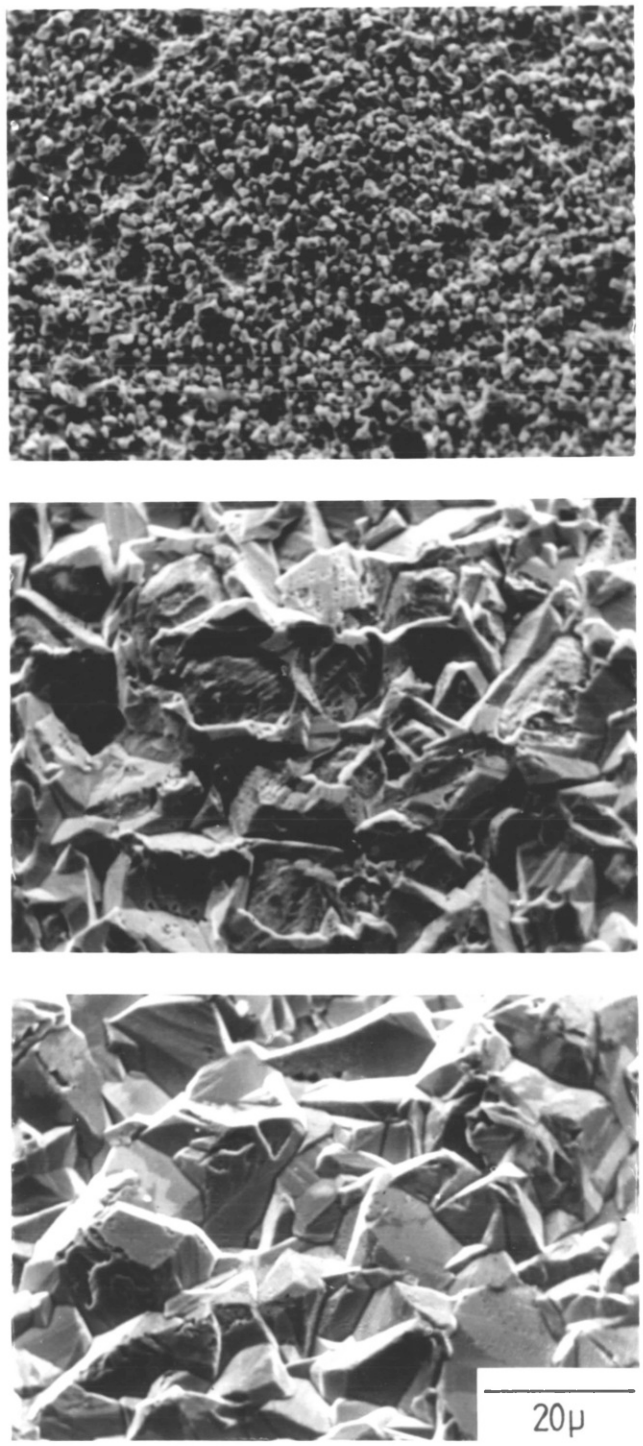

FIGURE 6.10. Growth morphology of chromium electrodeposit versus time. C=0.931 mol dm^{-3}, η_N=-0.58 V, t_N=3 s (3 pulses), η_G=-0.05 V. a) t_G=0, b) t_G=53min, c) t_G=81 min (Q=81 $C.cm^{-2}$)

necessary to minimize the trapping of melt in the inter-nuclei space, favouring the merging of the isolated nuclei. This factor can be better explained by reference to the schemes of growth morphology in Figure 6.11. On the one hand at the overpotential η_{G1} the nuclei, growing under hemispherical diffusion control, develop preferentially in the direction of the bulk of the melt which provide a good supply of chromium (II) ions. The growth in the inter-nuclei space decreases due to the poor supply of solute and eventually the inter-nuclei melt can be trapped if the nuclei frontal sides merge eventually into a continuous front. On the other hand at a conveniently low overpotential $\eta_{G2} < \eta_{G1}$ surface control predominates and the diffusion layer around each nucleus is stationary or grows very slowly, the nuclei grow at the same rate in all directions and the melt in the inter-nuclei space can be eventually displaced by the moving front of the deposit.

Considering the complexity of the transition stage of growth it is difficult to recommend a priori an acceptable value of growth overpotential to be used. A useful criterion in this direction was simply obtained out of microscopic observations on chromium electro-deposits obtained under varying growth conditions. The electron scanning micrographs in Figure 6.12 show the morphology of chromium electrodeposits obtained at high chromium (II) in concentration (1.49 $mol.dm^{-3}$), applying the same initial nucleation pulse, but grown

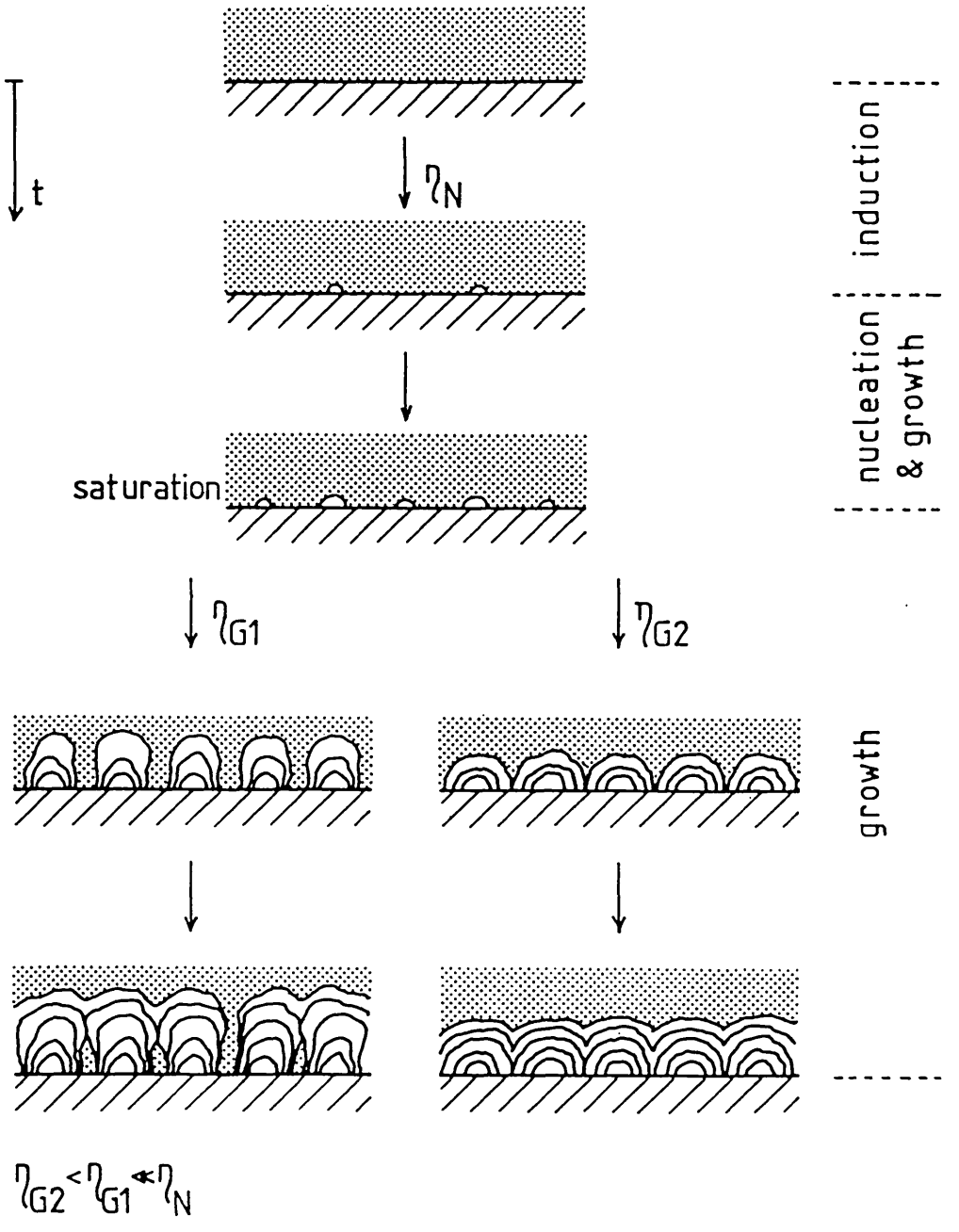

FIGURE 6.11. Schematic representation of the morphological evolution of chromium electrodeposits at different growth overpotentials.

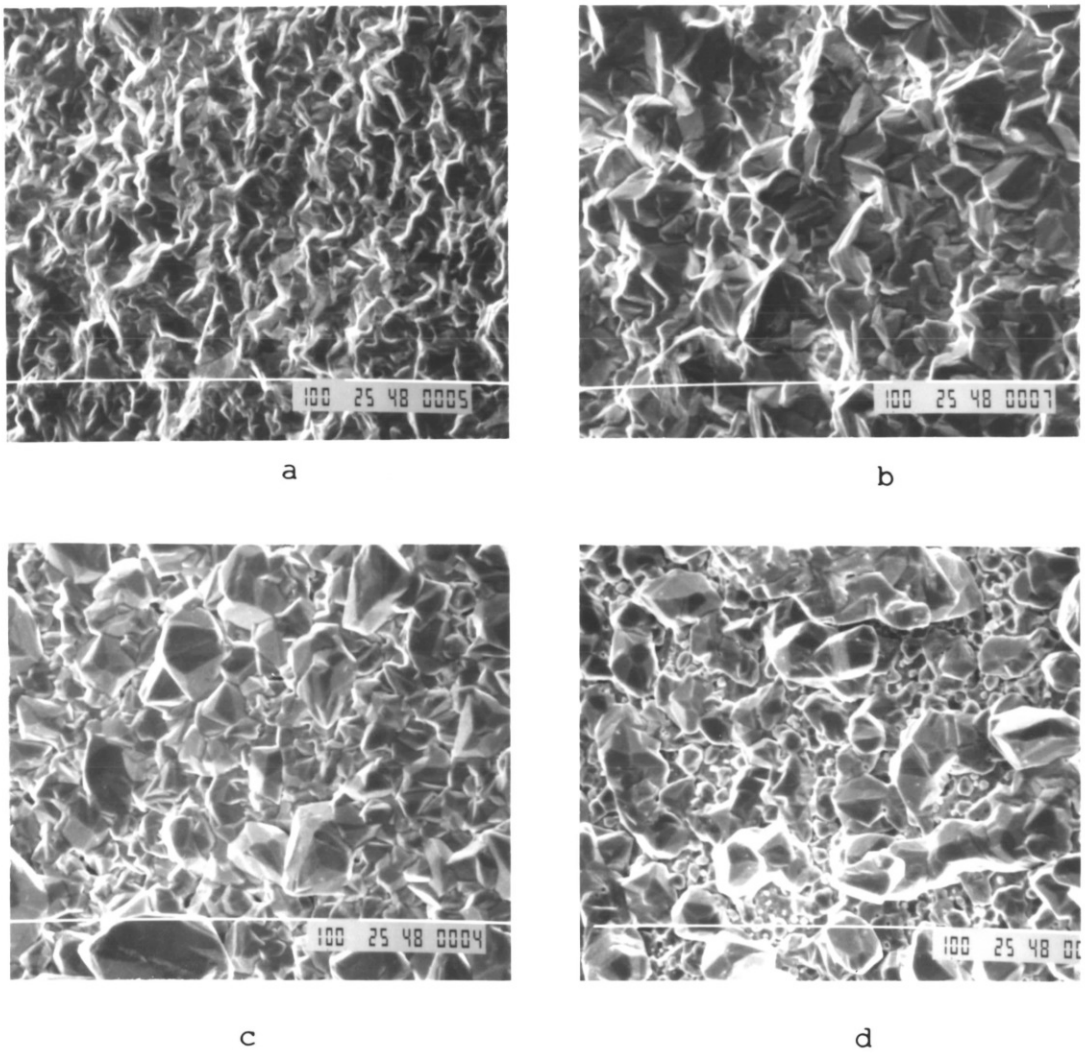

FIGURE 6.12. Morphology of chromium electrodeposits obtained at different growth overpotentials.
C = 1.49 mol dm^{-3}, η_N = -0.6 V, t_N = 1 s, Q = 40 C cm^{-2}.
a) η_G = -0.02 V, b) η_G = -0.05 V, c) η_G = -0.08 V,
d) η_G = -0.1 V

under different overpotentials. The sequence illustrates well the effect of the growth overpotential on the resultant morphology, showing the transition from a relatively even surface to a practically dendritic one as the overpotential increases in the range -0.02 V to -0.1 V. The observed morphological evolution with increasing overpotential illustrates well the corresponding increase of concentration polarization around chromium nuclei growing under hemispherical diffusion control, which leads eventually to the preferential development of some of them, at the expense of other ones, which are deprive of solute.

According to the results in Figure 6.12 only at very low growth overpotentials, say under -50 mV, can the development of protuberances be qualitatively hindered and the original nuclei merge into a coherent deposit. It would be difficult to define a similar criterion with respect to the optimum value of the growth overpotential to be used based only on electrochemical information for the system. Given the small amplitude of the imperfections of the electrode in relation to the size of the diffusional layer, the projected area of the electrode (apparent surface) quickly becomes the effective diffusional area and then the different morphological textures obtained in a small overpotential range are not clearly reflected in the resulting current[184] (e.g. see sampled-current voltammogram in Figure 6.13).

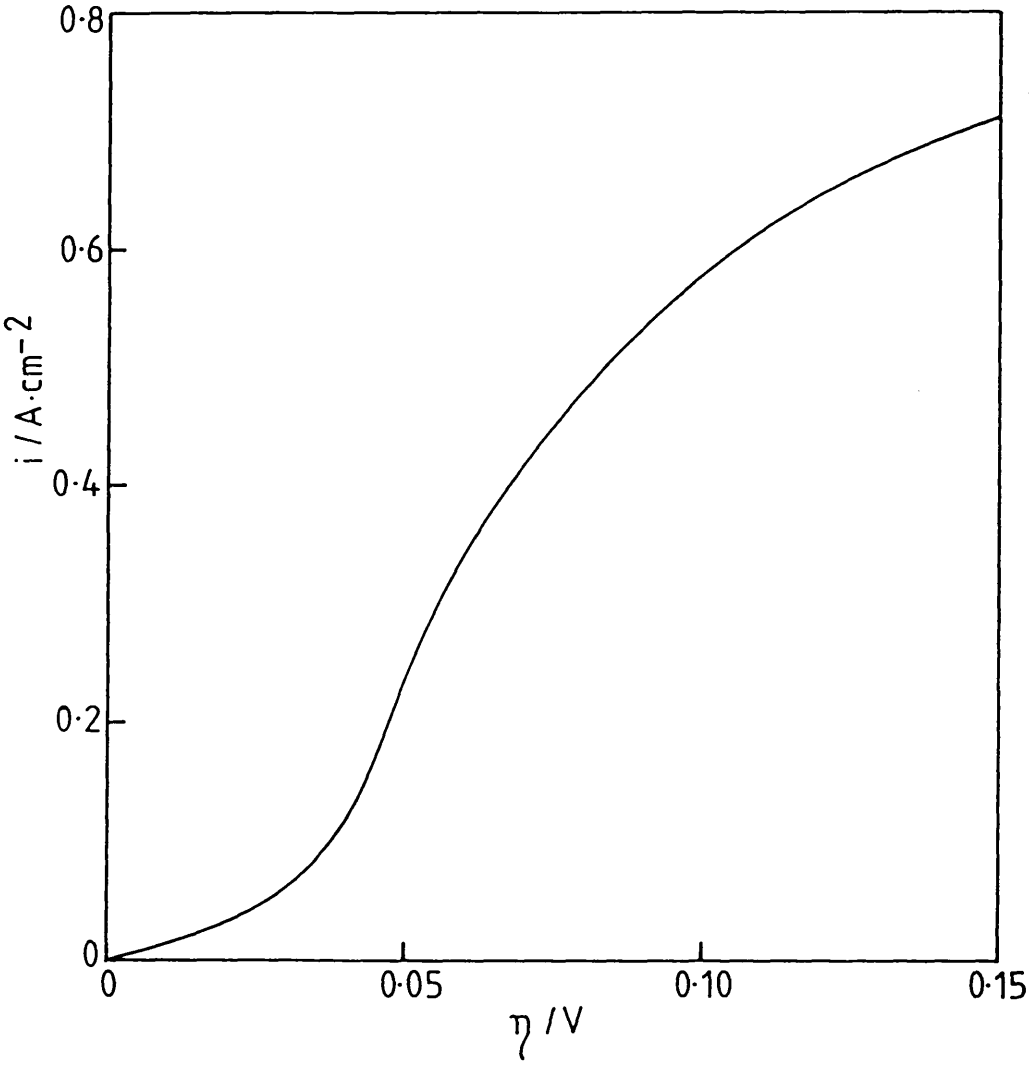

FIGURE 6.13. Sampled current voltammogram for the electrodeposition of chromium on tungsten.
C = 1.49 mol.dm^{-3}, sampling time: 1 s.

But even if the growth of continuous deposits is attainable at sufficiently low growth overpotentials, apparently more strict conditions are necessary to completely suppress the phenomenon of melt trapping in the nuclei interspace. The scanning electron micrographs in Figure 6.14 show the morphology of the back surface of chromium electrodeposits, that is the surface which is in contact with the substrate. The small holes or gaps in the surface correspond to inter-nuclei areas of the substrate that were not covered during the subsequent stage of growth of the deposit. These gaps in the substrate coverage apparently correspond to points where the melt, after being depleted of chromium (II) ions, remained trapped in the structure of the deposit. Considering the low growth overvoltages used, it seems then difficult to prevent completely the occurrence of this phenomenon, unless a strong stirring is introduced in order to improve the supply of solute to the inter-nuclei space.

6.3.2. Selection of conditions

The application of the initial pulse method modifies the development of the chromium electrogrowth, and with its application it is possible to improve the morphological characteristics of the chromium deposits. According to the characteristics observed in the electrogrowth process with this method it is possible now to define

a

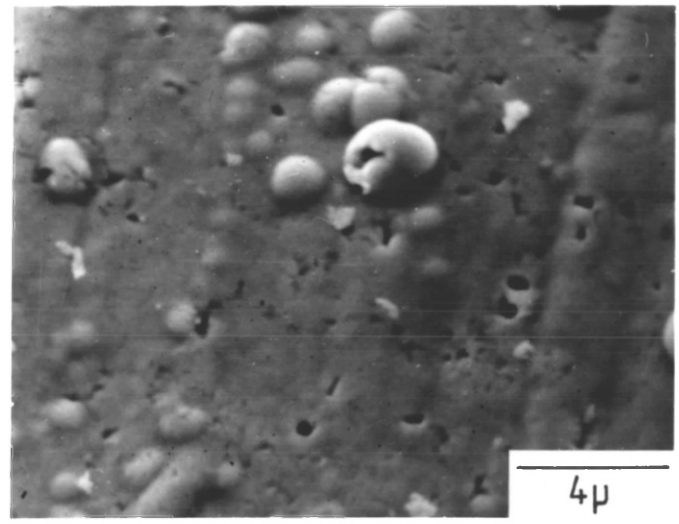

b

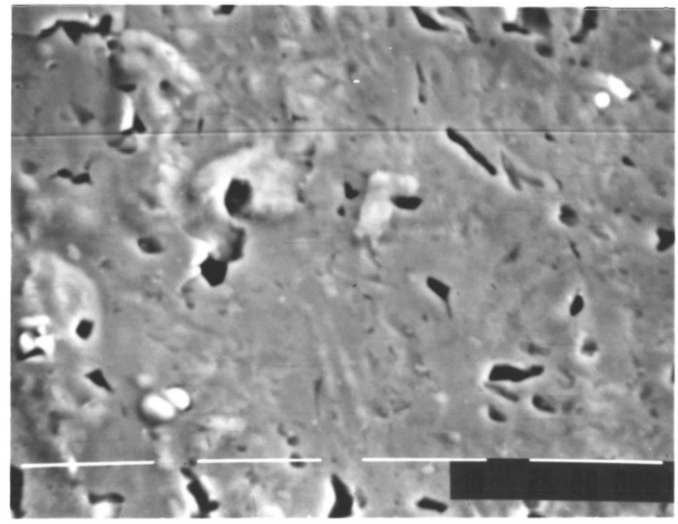

FIGURE 6.14. Scanning electron micrographs of the back surface of chromium electrodeposits. a) C = 0.77 mol dm^{-3}, η_N = -0.43 V, t_N = 5 s (2 pulses), η_G = - 0.04 V; b) C = 1.61 mol dm^{-3}, η_N = -0.6 V, t_N = 0.5 s, η_G = -0.05 V.

better the different operational parameters to be used in order to obtain the best results out of its application.

The criteria in this direction can be summarized under the following headings:

i) Use of high chromium (II) ion concentrations, preferably over 1 $mol.dm^{-3}$.

ii) Use of a nucleation overvoltage η_N as high as possible. Its value will be limited at the top end by the decomposition voltage of the melt. A typical practical range is between -0.5, -1.0 V.

iii) The nucleation pulse length t_N has to be long enough to reach the saturation nucleus density but short enough to prevent an excessive growth of the nuclei at this overpotential. A value of t_N in the range 100 μs - 1 s is considered adequate.

iv) Use of a growth overpotential η_G no greater than 50 mV, unless stirring of the melts is introduced.

A more general account of the method can be found in ref. 185.

6.3.3. Characteristics of protective chromium coatings

The development of the initial pulse method enabled the production of protective chromium coatings from the (LiCl-KCl)eut-$CrCl_2$ melts, to be attempted. Following the criteria summarised in Section 6.3.2. this method

was applied for the systematic production of chromium coatings on 20/25 NS stainless steel probes. Table 6.1 resume the typical operation conditions used in these experiments.

The obtained chromium coatings presented the following characteristics:

6.3.3.1. Morphology

The optical micrographs in Figure 6.15 correspond to cross sections of fuel can probes electrocoated with chromium, showing the typical morphological characteristics of the deposits. The chromium forms a coherent deposit, crack-free and pore-free, which fully covers the substrate surface. The chromium coatings present in general a rather uneven external surface as is well observed in the cross section in Figure 6.15c. This characteristic corresponds to the crystalline features of the surface of chromium coatings revealed in the scanning electron micrographs shown above (Fig. 6.9c, 6.10c).

The chromium coatings when etched with 1 M HCl solutions according to the procedures used for hard chromium plates[186], did not reveal any particular pattern of deposition or particular microstructure.

	A	B	C	D
Temperature, ^{o}C	450	450	450	450
C, $mol.dm^{-3}$	0.77	0.93	1.49	1.61
Nucleation overpotential, mV	-425	-600	-600	-600
Nucleation time, s	5	3	0.5	0.5
No. of nucleation pulses	2	3	1	1
Growth overpotential, mV	-35,-40	-50	-50	-40
Growth current density, $mA.cm^{-2}$	14-16	17-18	29-30	19-20
Final deposit thickness, µm	30-35	20-30	30	30

TABLE 6.1. Some typical working conditions used in the production of chromium coatings on Nb stabilized 20/25 stainless steel probes.

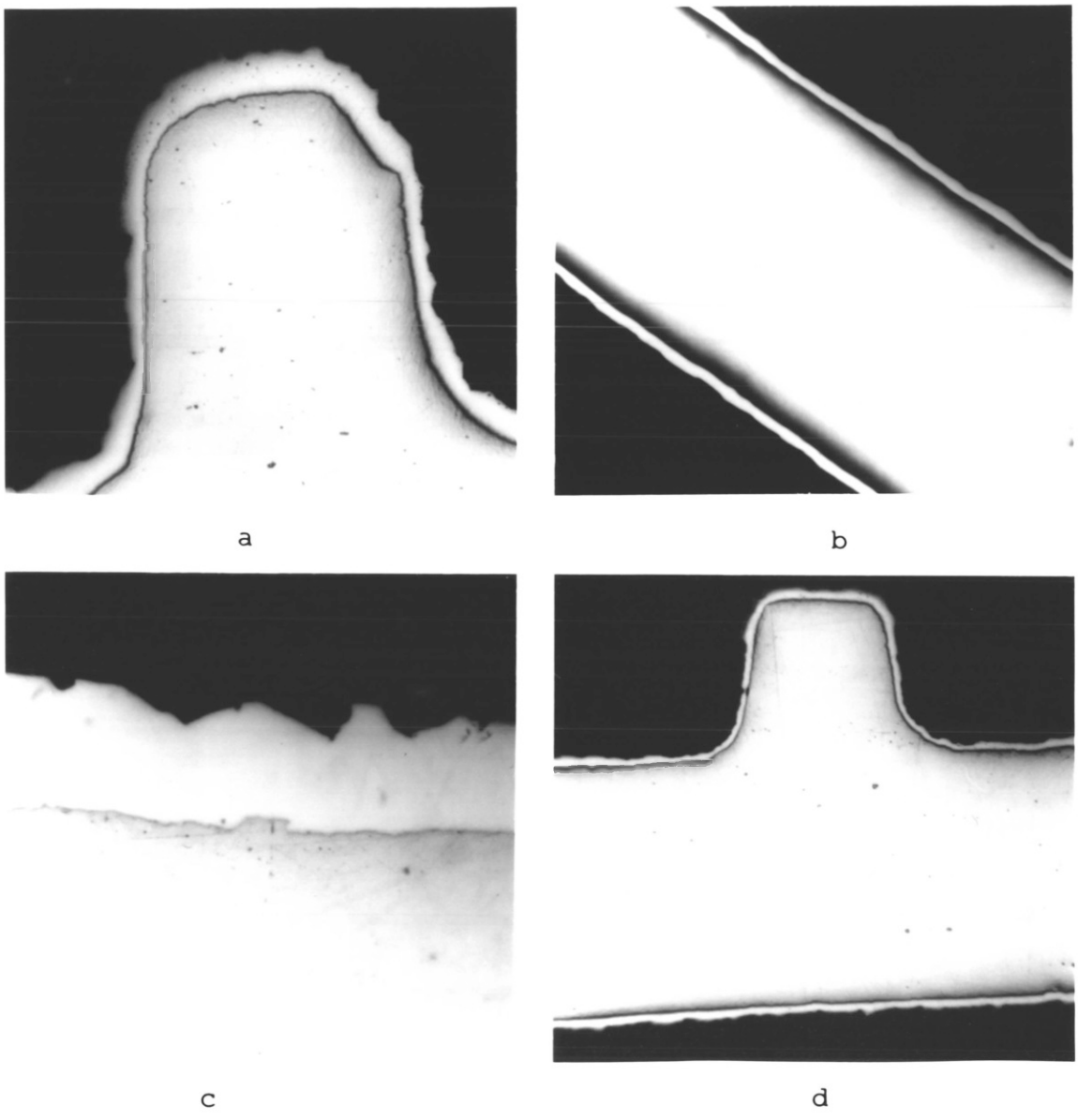

FIGURE 6.15. Optical micrographs of cross sections of chromium coatings obtained with the initial pulse method. a) C=1.61 mol dm^{-3}, η_N=-0.6 V, t_N=0.5 s, η_G=-0.05 V, thickness: ∿30 μ, mag. 160x. b) as in (a), mag. 80x. c) C=0.77 mol dm^{-3}, η_N=-0.425 V, t_N=5 s (3 pulses), η_G=-0.03 V, thickness ∿30 μ, mag. 640x. d) C=0.931 mol dm^{-3}, η_N=-0.58 V, t_N=3 s (3 pulses) η_G =-0.03 v, Thickness: ∿20 μ, mag. 80x.

6.3.3.2. Throwing power

The throwing power refers to the ability of the plating bath to produce a good distribution of the deposit on the irregularities of the substrate. Macrothrowing and microthrowing power refer to the situation of large-scale (macroscopic) or small-scale (microscopic) irregularities, respectively.

The cross-sections in Figures 6.15a and 6.15d illustrate the characteristics of the distribution of the chromium deposit around the ribs on the fuel can probe. The thickness of the chromium coating is relatively constant all over the rib profile which indicates a good macrothrowing power.

The microthrowing power is illustrated to some extent in the cross-section shown in Figure 6.15c. The good contact existing all along the deposit-substrate interface illustrates the ability to cover homogeneously all the different micro-irregularities existing on the substrate surface. This feature, extended to a smaller scale, can be observed in the scanning electron micrographs in Figures 6.16a and 6.16b, which show the typical morphology of the etched probe surface and the respective surface of the chromium deposit in contact with it (back surface). The nodular-like morphology of the coating back surface has been determined by the pitted probe surface morphology showing how the deposited chromium has filled practically all these intricate microscopic irregularities. Nevertheless according

a

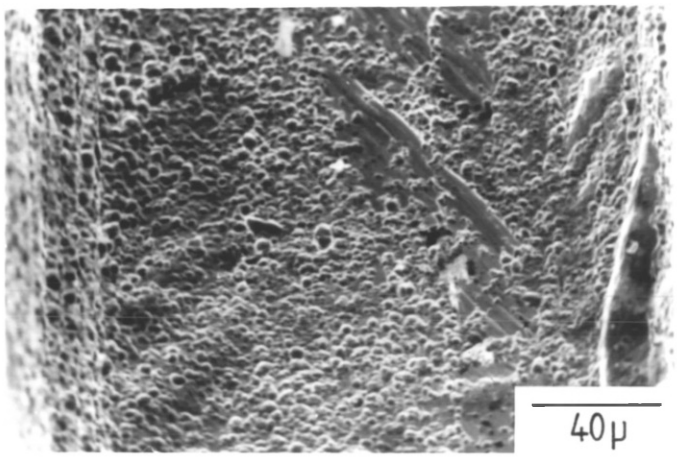

b

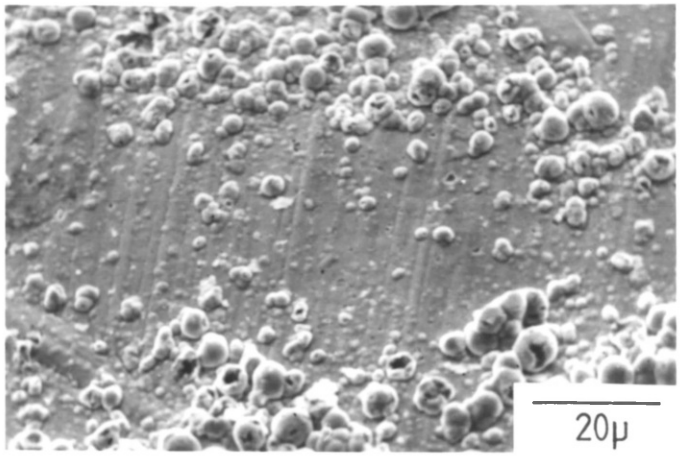

FIGURE 6.16. a) Typical features obtained on the surface of 20/25 Nb stabilized stainless steel probes after anodic etching. b) Typical features of the back surface of chromium coatings obtained on 20/25 Nb stainless steel probes.

to the microscopic gaps observed in the deposit inner surface (see Figure 6.14), one can deduce that there is still a small fraction of the substrate area where there is no deposit-substrate contact. This phenomenon was discussed before and its nature interpreted in relation to the mechanism during the initial stages of electrocrystallization.

6.3.3.3. Microhardness

Microhardness measurements using a Vicker's instrument were performed on cross-sections of chromium coatings. The values of microhardness obtained were in the range 130-280 kg/mm^2. The optical micrographs in Figure 6.17 show a typical pattern of diamond indentations obtained on a cross-section of the coating, with their respective microhardness values. The microhardness of the present deposit is much lower than that obtained in chromium electrodeposits from aqueous solutions, typically in the range 850-1000 Vickers[187].

6.3.3.4. Adherence

The adherence between the chromium coatings and the fuel can material was tested with a Sebastian Adherence Tester. For this test a special set of chromium coatings was produced on flat pieces of plate of this material (0.5 mm thickness), according to the requirements of this instrument. The application of the tester only

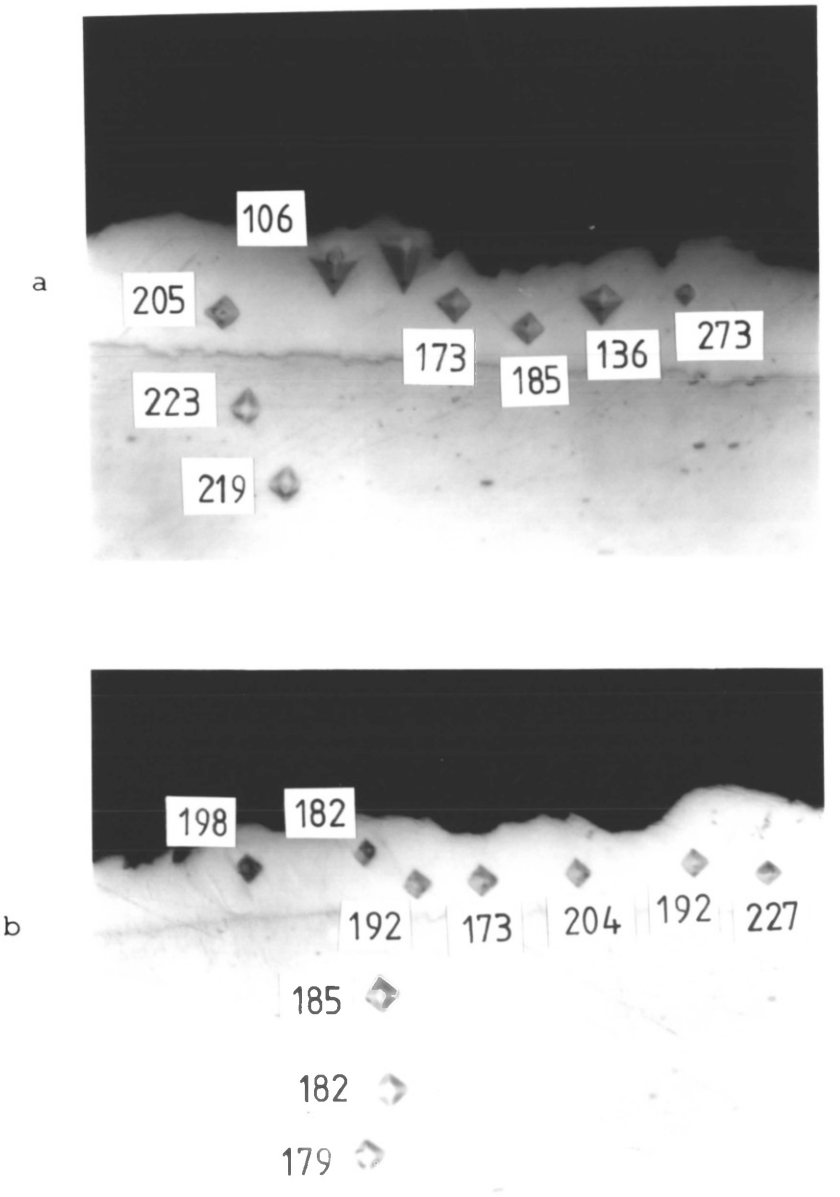

FIGURE 6.17. Typical results obtained from microhardness tests on chromium coatings. a) C=1.61 mol dm^{-3}, η_N=-0.6 V, t_N=0.5 s, η_G=-0.05 V, thickness ∿30 μ, mag. 700x. b) C=0.93 mol dm^{-3}, η_N=-0.58 V, t_N=3 s (3 pulses), η_G=-0.03 V, thickness ∿20 μ, mag. 700x. Hardness is indicated in kgf/mm^2.

permitted the conclusion that the chromium coating - 20/25 Nb stainless steel adherence was greater than 240-250 kgf/cm^2. This value corresponded to the practical upper limit of the instrument which, according to its design (see Section 4.3.5.), was given by the adherence between the pulling stud and the resin.

6.3.3.5. Chromium structure

The X-ray diffraction pattern of the deposited chromium is shown in Table 6.2, column a, which accords well with the diffraction pattern of bcc chromium, shown in column b. The body centred cubic lattice corresponds to the stable form of chromium[188]. A quantitative evaluation of the purity of the chromium deposit using a microprobe analysis technique (a JOEL T-200 SEM was used) revealed only the peaks corresponding to chromium[190].

Chromium deposit dÅ	Chromium (bcc)[189] dÅ
2.04	2.04
1.44	1.4419
	1.1774
	1.0195
	0.9120
	0.8325

TABLE 6.2. X-ray data

6.4. DISCUSSION AND CONCLUSIONS

The chromium coatings produced from $(LiCl-KCl)_{eut}$-$CrCl_2$ melts using the initial pulse method presented adequate characteristics for their use as protective coatings. The coatings were made up of a high purity, low hardness, crack-free, non-porous, well adhered chromium which fully covered the substrate with a layer of relatively constant thickness. Tests performed on 20/25 Nb stainless steel probes protected with such coatings indicated a good corrosion resistance against oxidation and carbon deposition reactions at high temperatures[191].

Several advantageous properties obtained with chromium coatings can be related to a great extent to the fact of their being produced in a molten salt bath. In the first place the good macrothrowing power observed, indicative of an even current distribution on the cathode, suggests the predominance of a secondary current distribution which is expected in a bath where polarization predominates over ohmic effects[192]. The high efficiency of chromium deposition in this bath is a factor that also contributes to the good throwing power.

The low microhardness of the chromium obtained is in agreement with its high purity[60]. This good purity can be easily achieved with a molten bath free of the most typical impurities oxygen and hydrogen, and in

addition, because of the refining properties of $LiCl-KCl-CrCl_2$ melts on chromium[47].

The good chromium-coating adherence obtained is also an expected property when depositing from molten salts and is related to the ability of these media to dissolve any oxide film or moisture film remaining from the substrate surface[9]. In the present case the good adherence tested can be also related to the method of electrodeposition used which, introducing an initial nucleation pulse, resulted in the obtaining of an improved microthrowing power and then an intimate contact between the coating and the substrate. At the same time the bond obtained in the present system between the chromium and the substrate appears to be quite strong in itself as deduced from the characterization of adherence in the electronucleation studies (see Section 5.2.4.). In addition the initial strength of this link is expected to increase during the process as a result of interdiffusion, phenomenon which has been observed to occur to some extent in this system[190].

The chromium coatings presented in general a relatively uneven external surface. This characteristic could be improved if the process of electrodeposition were carried out in conditions where the development of the crystalline features of deposit surface could be inhibited. This could be achieved by introducing stirring of the electrolytic bath, therefore making possible the application of higher growth overpotentials

and higher electrodeposition rates. (It was not possible to attempt the use of stirring in the present experiments which were all carried out in a small electrolytic cell). The electrodeposition under reversing potential conditions, method that has proved advantageous in applications in aqueous systems[193], can also, when applied at the growth stage, result in improved chromium deposit surfaces[190].

7. GENERAL CONCLUSIONS

The present study has contributed to the clarification of the mechanisms of electrocrystallization of chromium from $(LiCl-KCl)_{eut}-CrCl_2$ melts. The conclusions of the study can be summarized in the main following points:

i) The electrocrystallization of chromium on foreign substrates begins with a well defined three-dimensional nucleation process.

ii) Under potentiostatic conditions the process involves the following stages: a) induction time, b) progressive nucleation involving the simultaneous formation and growth of three dimensional nuclei, c) Reaching of a final saturation nucleus density well before the whole coverage of the substrate is reached.

iii) The growth of the three-dimensional nuclei is controlled by the diffusion of chromium (II) ions in the melt. The nucleation kinetics can be well described according to the classical theory of nucleation.

iv) The obtaining of a final saturation nucleus density is controlled by the formation of nucleation exclusion zones arising around the growing nuclei. The final saturation nucleus density is dependent on the chromium (II) ion concentration, increasing with a decrease in solute concentration, and vice versa.

v) The inherent characteristics involved in the electrocrystallization of chromium prevent the obtaining of coherent chromium macrodeposits under simple potentiostatic conditions. A method based on the introduction of initial nucleation pulses was developed enabling the production of protective chromium coatings with adequate morphological characteristics.

APPENDIX I.

Calculation of the diffusion coefficient

The current transient in Figure I.1 presents a well defined $I\text{-}t^{-\frac{1}{2}}$ dependence as is shown in Figure I.2. Cottrell's equation can be then applied, and the diffusion coefficient of chromium (II) ion calculated according to the expression

$$D = m^2 . \pi/(zFCS)^2$$

where

$$m = dI/dt^{-\frac{1}{2}}$$

corresponds to the slope in Figure I.2. In the present case $m = 1.222 \times 10^{-3}$ $A.s^{\frac{1}{2}}$, $z = 2$, $F = 96500$, $C = 0.35 \times 10^{-3}$ $mol.cm^{-3}$, $S = 0.0452$ cm^2, and we finally obtain

$$D = 1.29 \times 10^{-5} \ cm^2.s^{-1}$$

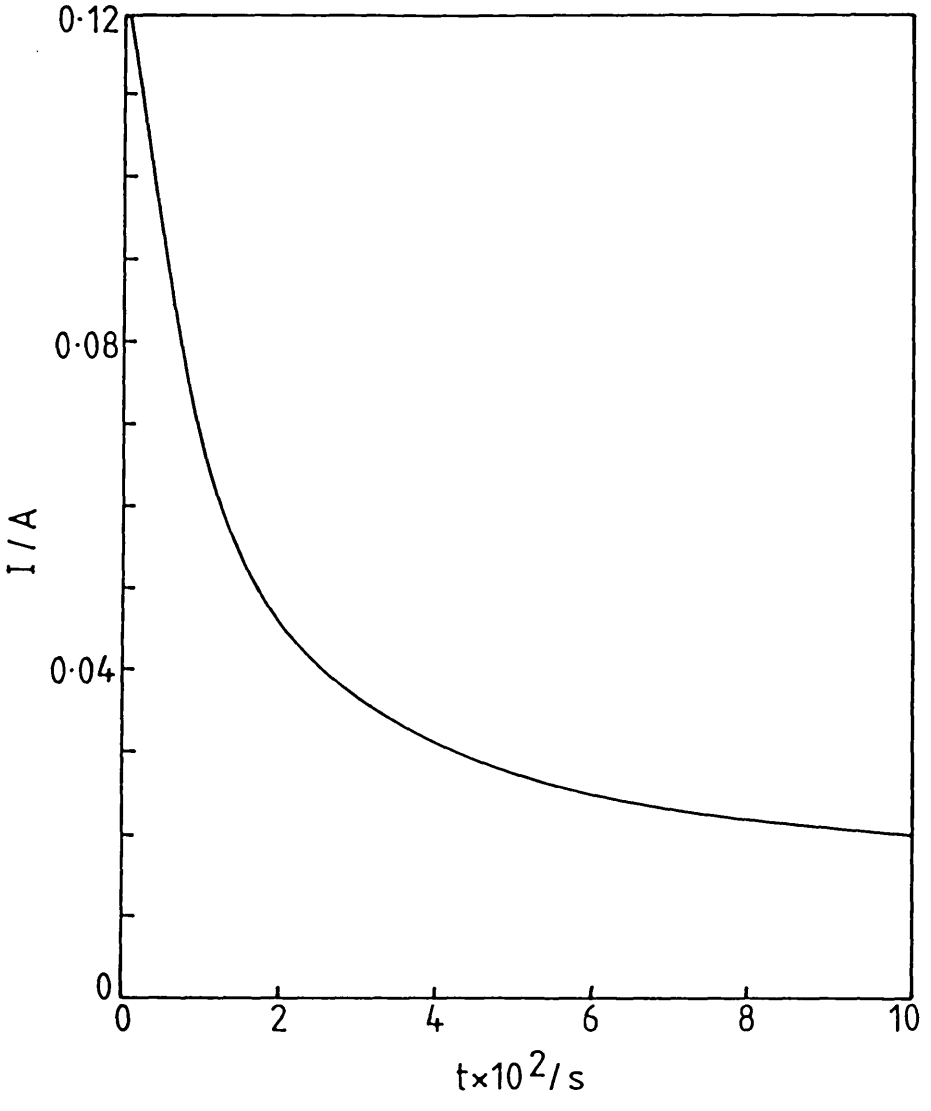

FIGURE I.1. Current decay zone of a current transient obtained at high overpotential, on tungsten: = -0.237 V, C = 0.346 mol.dm^{-3}.

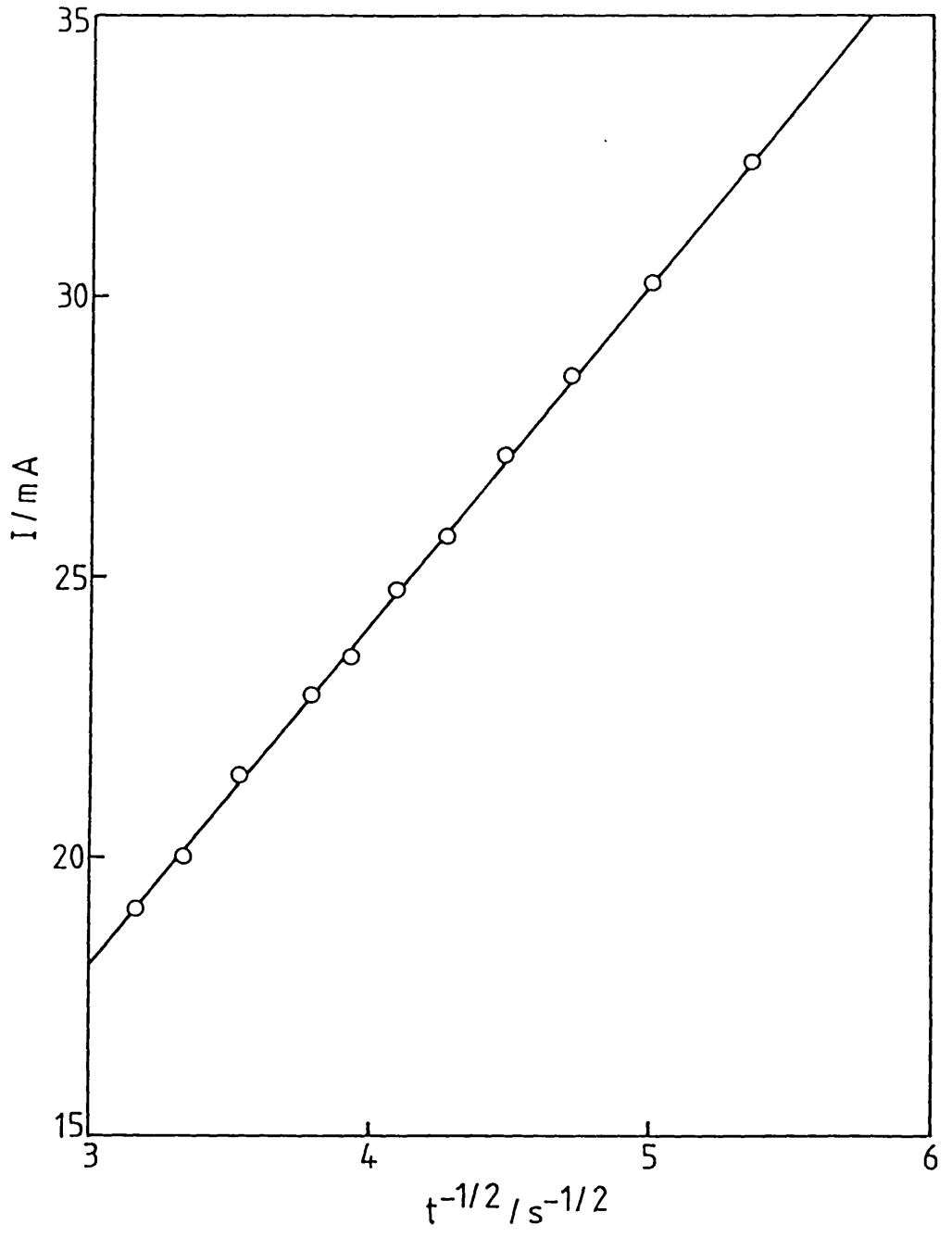

FIGURE I.2. $I\text{-}t^{-\frac{1}{2}}$ dependence for current transient in Figure I.1.

APPENDIX II.

Computing program for the calculation of nuclei numbers.

```
 1  PRINT"□"
 4 OPEN3,4
 5 OPEN1,4,1:OPEN2,4,2
 6 CMD1:LIST
 10 DIMI(200),FO(200),DE(200) ,IO(200), II(200) ,S(200) ,T(200) ,R(200)
 11 INPUT"CURVE CODE";CC$
 12 INPUT"NUMBER OF SUBDIVISIONS?";SD
 14 INPUT"SYSTEM PARAMETER?";B
 15 INPUT"OVERPOTENTIAL,VOLTS";OP
 16 INPUT"BASE I CM";IB
 18 INPUT"CM TO AMP FACTOR";TF
 20 INPUT"DELTA U?";DU
 30 INPUT"NUMBER OF POINTS =";NP
 35 PRINT
 36 PRINT"ENTER DATA"
 40 FORJ=0TONP:INPUTII(J):IO(J)=(II(J)-IB)*TF:NEXTJ
 42 AU=B*((1-EXP(32.106*OP))↑1.5)*SQR(DU/SD)
 45 A=0
 50 FORJ=0TONP-1
 55 F=(IO(J+1)-IO(J))/SD
 60 FORN=0TO(SD-1)
 61 H=J+A+N
 62 I(H)=IO(J)+N*F
 70 NEXTN
 72 A=A+SD-1
 75 NEXTJ
 77 I(NP+A)=IO(NP)
 78 L=NP+A
 82 PRINT#3,"NB      T(M),SEC   I(J),MA      DELTAN          SUM N       N/NS    "
 83 Q$="99  999.999999  9999999.9999   99999.99    99999.99    9.999"
 100 DE(1)=I(1)/AU
 110 DA=0:S(1)=DE(1):K=1
 117 S=S(1)
 120 FORK=2TOL
 121 TB=DU/SD
 125 DA=0
 130 FORN=1TOK-1
 140 DA=DA+(DE(K-N)*SQR(N+1))
 150 NEXTN
 160 DE(K)=(I(K)/AU)-DA
 162 IFDE(K)<0THENDE(K)=0
 170 S=S+DE(K)
 171 S(K)=S
 172 NEXTK
 175 FORM=1TOL:T(M)=TB*M
 176 R(M)=S(M)/S(L):NEXTM
 178 FORD=0TONP-1:M=SD+SD*D:PRINT#2,Q$
 179 PRINT#1,D+1,T(M),I(M),DE(M),S(M),R(M):NEXTD
 191 PRINT#3,"SUBDIVISION NUMBER";SD
 192 PRINT#3,"DELTA U (SEC)    ";DU
 193 PRINT#3,"CURVE CODE    ";CC$
 194 PRINT#3,"SYSTEM PARAMETER    ";B
 195 PRINT#3,"OVERPOTENTIAL,VOLTS",OP
 196 PRINT#3,"BASE I,CM",IB
 198 PRINT#3,"CM TO AMP FACTOR",TF
 200 INPUT"FANCY ANOTHER SUBDIVISION MATE Y/N";A$
 210 IFA$="N"THEN260
 220 IFA$="Y"THEN230
 230 INPUT"ENTER SUBDIVISION=";SD
 250 GOTO42
 260 INPUT"FANCY MORE DATA MATE Y/N";A$
 270 IFA$="N"THEN290
 280 IFA$="Y"THEN RUN
 290 CLOSE1,4:CLOSE4,2:CLOSE3,4
READY.
```

ACKNOWLEDGEMENTS

I would like to express my sincere thanks to my supervisor, Dr. D. Inman, for his guidance and support during this study.

I would also like to thank my colleagues in the Nuffield Group for their valuable cooperation and technical assistance.

Thanks also to Mr. G. Hicks for constant help with his glassblowing expertise, and to Miss P.R. Martins and Mr. J. Rossdale for the photographic work.

I am also grateful to Mrs. S. Greenwood for the careful typing of this thesis.

I would like to express my appreciation to my girlfriend Christa for the support and encouragement necessary for the completion of this work.

I am especially indebted to Dr. M.P. Hill and the Central Electricity Generating Board for the financial support which made this project possible.

REFERENCES

1. A.M. Emsley, M.P. Hill, in 5th Industrial Carbon and Graphite Conference, London (1978)

2. M.P. Hill (CEGB), personal communication.

3. A.H. Sully, 'Metallurgy of the rarer metals - 1: Chromium'. Butterworths Scientific Publications, London (1954).

4. Idem, ibid., pp.192.

5. F.A. Lowenheim, 'Modern Electroplating', John Wiley & Sons Inc., New York (1974).

6. A.H. Sully, op.cit., pp.191.

7. T. Healey, A.F. Brown, M.V. Speight, Phys. Met. React. Fuel. Elem., (1975) 386.

8. K. Matiasovsky, Z. Lubyova, V. Danek, Electrodepn. Surface. Treat., 1 (1972/73) 43.

9. J. Wurm, Met. Finish., 78 (1980) 37.

10. D. Inman, S.H. White, J. Appl. Electrochem., 8 (1978) 375.

11. R.S. Sethi, ibid., 9 (1979) 411.

12. W.J. Hamer, M.S. Malmberg, R. Rubin, J. Electrochem. Soc. 103 (1956) 8.

13. Idem, ibid., 112 (1965) 750.

14. H.C. Gaur, R.S. Sethi, Ind. J. Chem., 5 (1967) 485.

15. A.D. Graves, G.J. Hills, D. Inman, in ' Advances in Electrochemistry and Electrochemical Engineering' vol.4, (P. Delahay ed.). Interscience Publ., New York (1965), pp.150.

16. S. Senderoff, in 'Modern Electroplating' (F.A. Lowenheim ed.) John Wiley & Sons Inc., New York (1974), pp.473.

17. G.W. Mellors, S. Senderoff, J. Electrochem. Soc., 112 (1965) 266.

18. N.C. Cook, Sci. Amer., 221 (1969) 38.

19. G.W. Mellors, S. Senderoff, U.S. Patent 3,444,058 (1969); Plating, 51 (1964) 972.

20. S. Senderoff, G.W. Mellors, Science, 153 (1966) 1475.

21. Idem, Metall. Rev., 11 (1966) 97.

22. G.J. Janz, 'Molten Salts Handbook', Academic Press, New York (1967), pp.287.

23. G.J. Hills, D.J. Schiffrin, J. Thompson, J. Electrochem. Soc., 120 (1973) 157.

24. M.A. Steinberg, R.G. McAllen, Canadian Patent 563,495 (1958).

25. M.E. Silbert, J.T. Burwell, Canadian Patent 554,772 (1958).

26. Horizons Inc., British Patent 788,804 (1958); Chem. Abstr. 52 (1958) 8801.

27. American Electro-Metal Corp., British Patent 659,927 (1951).

28. N.C. Cook, in NATO Advanced Study Institute Conference, 'The Science and Technology of Surface Coatings', Imperial College, London (1972).

29. Idem, in Proceedings of International Conference 'Protection Against Corrosion by Metal Finishing', Basel (1966), pp.151.

30. J.C. Withers, J.E. Perry, B.A. Foschnocht, in 'Techniques of metals research', Vol.VII (R.F. Burnshah ed.), Interscience, New York (1972), pp.203.

31. S.Senderoff, Metall. Revs., 11 (1966) 97.

32. G.F. Warren, S.H. White, D. Inman, in 'Molten Salts', Electrochem. Soc., New York (1975), pp.218

33. H.A. Laitinen, W.S. Ferguson, R.A. Osteryoung, J. Electrochem. Soc., 104 (1957) 516.

34. D.W. Townsend, in 'Molten Salts', Electrochem. Soc. New York (1976), pp.388.

35. D. Inman, N.S. Wrench, Brit. Corrosion J., 1 (1966) 246.

36. W.D. Jannack, 'Rare Metal Extraction by Chemical Engineering Techniques', Pergamon, Oxford (1963), pp.274.

37. C.A. Hempel (ed), 'The Encyclopedia of Electrochemistry', Reinhold Co., New York (1964).

38. C.W. Balke, Ind. Eng. Chem. 27 (1935) 1166.

39. See ref. 16.

40. T.B. Reddy, Electrochem. Technol., 1 (1963) 325.

41. 'Ductile Chromium and its Alloys', Am. Soc. Metals, Cleveland, Ohio (1957), pp.95.

42. F.R. Cattoir, D.H. Baker Jr., U.S. Bur. Mines. Rept. of Invest. 5682 (1960).

43. A.M. Volkov, Izv. Vysshikh. Uchebn. Zaderenii, Tsven. Met., 10 (1967) 78.

44. A.K. Suri, C.K. Gupta, Surf. Techn. 5 (1977) 271.

45. F.R. Cattoir, T.A. Sullivan, U.S. Bur. Mines Rept. of Invest. 7226 (1969)

46. M. Manceaux, A. Michel, French Patent 1,320,760 (1963)

47. K.P.V. Lei, J.M. Hiegel, T.A. Sullivan, J. Less-Common Metals, 27 (1972) 353.

48. D.G. Alexander, O.N. Carlson, Trans. AIME, 245 (1969) 2592.

49. H.A. Laitinen, W.S. Fergunson, An. Chem., 30 (1958) 1266.

50. H.A. Laitinen, C.H. Liu, J. Am. Chem. Soc., 80 (1958) 1015.

51. R. Caton, H. Freund, An. Chem 36 (1964) 15.

52. T. Kuroda, T. Suzuki, J. Electrochem. Soc. Japan, 29 (1961) E-174.

53. I.I. Naryshkin, V.P. Yurkinskii, P.T. Stangrit, Elektrokhimiya 5 (1969) 1043.

54. S. Levy, W. Reinhart, J. Electrochem. Soc., 122 (1975) 200.

55. J.C.L. Legey, Ph.D. Thesis, University of London (1973).

56. D. Inman, J.C.L. Legey, R. Spencer, J. Electroanal. Chem., 61 (1975) 289.

57. R.E. Cains Jr., N.J. Grant, Trans. AIME 230 (1964) 1156.

58. J. Bigot, Mem. Sci. Rev. Met., 66 (1969) 75.

59. W.H. Smith, A.U. Seybolt, in 'Ductile Chromium and its Alloys', Am. Soc. Metals, Cleveland, Ohio (1957), pp.169.

60. A. Brenner, P. Burkhead, C. Jennings, J. Res. Nat. Bur. Stand., 40 (1948) 31.

61. C.A. Snavely, Trans. Electrochem. Soc., 92 (1947) 537.

62. J.B. Cohen, Trans. Electrochem. Soc., 86 (1944) 441.

63. A. Brenner, P. Burkhead, C.W. Jenning, Proc. Am. Electropl. Soc., 34 (1947) 32.

64. J.M. Gibbs, 'Collected Works', Longman's Green and Co., London 1928.

65. M. Volmer, A. Weber, Z. phys. Chem., 119 (1926) 277.

66. L. Farkas, ibid., 125 (1927) 236.

67. R. Kaischev, I. Stranski, ibid., B26 (1934) 317.

68. R. Becher, W. Doring, Ann. Phys., 24 (1935) 719.

69. J.B. Zeldovich, Acta Physicochim. USSR, 18 (1943)1

70. Idem, J. exp. theoret. Physics (USSR), 18 (1943)1.

71. J.I. Frenkel, 'Kinetic Theory of Liquids', Clarendon Press, Oxford (1946).

72. D. Turnbull, T.P. 2365 Metals Technology, June 1948

73. A. Kantrowitz, J. Chem. Phys. 19 (1951) 619.

74. H. Wakeshima, ibid., 22 (1954) 1614.

75. F.C. Collins, Z. Elektrochem., 59 (1955) 404.

76. D. Kashchiev, Surf. Science, 14 (1969) 209.

77. R. Kaischew, S. Toschev, I. Markov, Bulg. Acad. Sci. Comm. Chem. Dept., 11 (1969) 463.

78. S. Toschev, I. Markov, Ber. Bunsenges. Phys. Chem., 73 (1969) 184.

79. E. Bauer, Z. Kristallogr., 110 (1958) 372.

80. E. Bauer, H. Poppa, Thin Solid Films, 12 (1972)167.

81. J.A. Venables, G.L. Price, in ' Epitaxial Growth', part B, (J.W. Matthews ed.), Academic Press, New York (1975), pp.381.

82. W.A. Jesser, J.W. Matthews, Phil. Mag., 15 (1967) 1097; 17 (1968) 461; 17 (1968) 595.

83. C.T. Horng, R.W. Vook, J. Vac. Sci. Technol., 11 (1974) 140.

84. D.G. Lorg, M. Prutton, Thin Solid Films, 21 (1974) 341.

85. R. Lacmann, Z. Kristallogr., 116 (1961) 13.

86. W. Kleber, Z. Phys. Chem. NF, 53 (1967) 52.

87. S. Toschev, M. Paunov, R. Kaischew, Commun. Dept. Chem., Bulg. Acad. Sci., 1 (1968) 119.

88. I. Markov, R. Kaischew, Kristall und Technik, 11 (1976) 685.

89. Idem, Thin Solid Films, 32 (1976) 163.

90. D. Kashchiev, J. Crystal Growth, 40 (1977) 29.

91. R. Kaischew, S. Stoyanov, D. Kashchiev, ibid., 52 (1981) 3.

92. R. Kaischew, Comm. Bulg. Acad. Sci. (Phys), 1 (1950) 100.
93. R. Vook, C. Horn, J. Macur, J. Cryst. Growth, 31 (1975) 353.
94. R. Kaischew, Fortschr. Miner., 38 (1960) 7.
95. R. Kaischew, G. Bliznakov, C.R. Acad. Bulg. Sci., 1 (1949) 23.
96. U. Gradmann et al., Thin Solid Films, 34 (1976) 249.
97. I. Markov, in International Society of Electrochemistry 28th Meeting, Druzhba-Varna, Sept., 1977, Electrocrystallization (Ext. Abs.), pp.138.
98. M. Fleischmann, H.R. Thirsk, in 'Advances in Electrochemistry and Electrochemical Engineering' vol.3 (P. Delahay ed.), Interscience Publ., New York (1963), pp.195.
99. See ref. 92.
100. D.A. Vermilya, in 'Advances in Electrochemistry and Electrochemical Engineering' vol.3 (P. Delahay ed.), Interscience Publ., New York (1963), pp.211.
101. T. Erdey-Gruz, M. Volmer, Z. Phys. Chem., 157 (1931) 165.
102. G. Thompfor, M. Volmer, Ann. Phys., 33 (1938) 309.
103. D. Kashchiev, A. Milchev, Thin Solid Films, 28 (1975) 189.
104. F.F. Abraham, G.M. Pound, J. Crystal Growth, 6 (1970) 309.
105. S. Toschev, in 'Crystal Growth: an Introduction' (P. Hartman ed.), North-Holland Publ. Co. (1973), pp.149.
106. A. Milchev, in the International Society of Electrochemistry 28th Meeting, Druzhba-Varna, Sept. 1977, Electrocrystallization (Ext. Abs.), pp.122.
106. D. Walton, J. Chem. Phys., 37 (1962) 2182.
107. G. Zinsmeister, Vacuum, 16 (1966) 529.
108. R.M. Logan, Thin Solid Films, 3 (1969) 59.

109. S. Stoyanov, ibid., 18 (1973) 91.
110. A. Milchev, S. Stoyanov, R. Kaishew, ibid., 22 (1974) 255.
111. A. Milchev, S. Stoyanov, J. Electroanal. Chem., 72 (1976) 33.
112. A. Milchev, S. Stoyanov, R. Kaischew, Thin Solid Films, 22 (1974) 267.
113. Idem, Elektrokhimiya, 13 (1977) 855.
114. S. Toschev, I. Markov, Ber. Bunsenges. Phys. Chem., 73 (1969) 184.
115. A. Scheludko, M. Todorova, Comm. Bulg. Acad. SCi. (Phys.), 3 (1952) 61.
116. R. Kaischew, B. Mutaftschiew, Electrochimica Acta, 10 (1965) 643.
117. W. Kossel, Ann. Phys., 21 (1934) 457.
118. J. Frenkel, J. Phys. USSR, 9 (1945) 392.
119. W.K. Burton, N. Cabrera, F.C. Frank, Phil. Trans. Roy. Soc., A243 (1951) 299.
120. J.W. Cahn, Acta Metallurgica, 4 (1956) 449.
121. See ref. 116.
122. I. Markov, E. Stoycheva, Thin Solid Films, 35 (1976) 21.
123. B. Lewis, D.S. Campbell, J. Vac. Sci. Tech., 4 (1967) 209.
124. R.M. Logan, Thin Solid Films, 3 (1969) 59.
125. M.J. Stowell, Phil. Mag., 21 (1970) 125.
126. I. Markov, A. Boynov, S. Toschev, Electrochim. Acta, 18 (1973) 377.
127. I. Markov, S. Toschev, Electrodep. Surface Treat., 3 (1975) 385.
128. I. Markov, D. Kaschiev, J. Cryst. Growth, 13/14 (1972) 131.
129. Idem, ibid., 16 (1972) 170.
130. A.N. Kolmogoroff, Bull. Acad. Sci. USSR (Cl. Sci. Math. Nat.), 3 (1973) 355.
131. I. Markov, Thin Solid Films, 35 (1976) 11.
132. I. Markov, E. Stoycheva, ibid., 35 (1976) 21.
133. M. Fleischmann, H.R. Thirsk, op.cit., pp.172.

134. J.A. Harrison, H.R. Thirsk, in 'Electroanalytical Chemistry' vol.5 (A.J. Bard ed.), Marcel Dekker Inc., New York (1970), pp.90.
135. W.K. Behl, J. Electrochem. Soc., 118 (1971) 889.
136. Idem, ibid., 120 (1973) 1692.
137. V.M. Rudoi, V.N. Samoilenko, E.V. Kantsler, A.I. Levin, Elektrokhimiya 11 (1975) 566.
138. F. Lantelme, J.P. Hanselin, M. Chemla, Electrochimica Acta, 22 (1977) 1113.
139. Idem, J. Electroanal. Chem., 97 (1979) 49.
140. G. Gunawardena, G. Hills, I. Montenegro, Symp. Faraday Soc., 12 (1977) 90.
141. G.J. Hills, D.J. Schiffrin, J. Thompson, Electrochimica Acta, 19 (1974) 671.
142. J. Amblard, M. Froment, G. Maurin, D. Mercier, E. Trevisan-Pikacz, J. Electroanal. Chem., 134 (1982) 345.
143. G.A. Gunawardena, G.J. Hills, I. Montenegro, Electrochimica Acta, 23 (1978) 693.
144. F. Palmisano, E. Desimoni, L. Sabbatini, G. Torsi, J. Appl. Electrochem., 9 (1979) 517.
145. F. Lantelme, J. Chevalet, J. Electroanal. Chem., 121 (1981) 311.
146. N.P. Bansal, J.A. Plambeck, J. Electrochem. Soc., 126 (1977) 1036.
147. G.J. Hills, D.J. Schiffrin, J. Thompson, Electrochimica Acta, 19 (1974) 657.
148. B.R. Scharifker, Ph.D. Thesis, University of Southampton (1980).
149. G. Gunawardena, G. Hills, I. Montenegro, B. Scharifker, J. Electroanal. Chem., 138 (1982) 225.
150. G. Gunawardena, G. Hills, I. Montenegro, ibid., 138 (1982) 241.
151. G. Gunawardena, G. Hills, I. Montenegro, B. Scharifker, ibid., 138 (1982) 255.

152. A. Milchev, E. Vassileva, V. Kertov, ibid., 107 (1980) 323.
153. A. Milchev, E. Vassileva, ibid., 107 (1980) 337.
154. S. Toschev, I. Markov, Electrochimica Acta, 12 (1967) 281.
155. S. Toschev, A. Milchev, E. Vassileva, Ibid., 21 (1976) 1055.
156. H.R. Thirsk, J.A. Harrison, 'A Guide to the Study of Electrode Kinetics', Academic Press, London (1972), chap. 3.
157. J.A. Harrison, H.R. Thirsk, op.cit., pp.91.
158. P. Delahay, 'New Instrumental Methods in Electrochemistry', Interscience, New York (1954).
159. D.J. Astley, J.A. Harrison, H.R. Thirsk, Trans. Farad. Soc., 64 (1968) 192.
160. B.R. Scharifker, op.cit., chap.9.
161. F.M. Dorsey, Ind. Eng. Chem., 20 (1928) 1094.
162. A.L. L'vov, A.A. Gnilomedov, A.P. Selemenev, E.N. Protasov, Elektrokhimiya, 11 (1975) 1322.
163. C.A. Melendres, J. Electrochem. Soc., 124 (1977) 650.
164. D. Inman, Ph.D. Thesis, University of London (1957)
165. S.H. White, in 'Ionic Liquids' (D. Inman, G. Lovering ed.) Plenum Press, New York (1981), pp.185.
166. D.L. Maricle, D.N. Hume, J. Electrochem. Soc., 107 (1960) 354.
167. E. Ollard, Trans. Faraday Soc., 21 (1925/26) 81.
168. T. Berzins, P. Delahay, J. Am. Chem. Soc., 75 (1953) 555.
169. G. Mamantov, D.L. Manning, J.M. Dale, J. Electroanal. Chem., 9 (1955) 253.
170. D. Inman, Dj. Jovanovic, S.H. White, Electroanal. Chem., 43 (1973) 37.
171. S.H. White, U.M. Twardoch, in Spring Meeting of the Electrochemical Society, Extended Abstract No.789 (1983).

172. 'HP-15C Owner's Handbook', Hewlett Packard Co. (1982), pp.206.
173. S. Toschev, A. Milchev, K. Popova, I. Markov, Compt. rend. Ac. Bulg. Sc., 22 (1969) 1413.
174. D.C. Grahame, Chem. Rev.. 41 (1947) 441.
175. V.A. Kusnetsov, L.S. Zagaynova, Zh. Fiz. Khim., 35 (1961) 1640.
176. E. Gileadi, E. Kirowa-Eisner, J. Penciner, 'Interfacial Electrochemistry', Addison-Wesley Inc., Massachusetts (1975), chap. 2.
177. J. Lawrence, R. Parson, R. Payne, J. Electroanal. Chem., 16 (1968) 193.
178. L. Shtifmann, Dokl. Akad. Nauk. SSSR., 63 (1948) 709.
179. B.R. Scharifker, op.cit., chap. 7.
180. A.R. Despic, K.I. Popov, in 'Modern Aspects of Electrochemistry' vol.7 (B.E. Conway, J. O'M. Bockris ed.), Butterworth & Co., London (1972) pp.199.
181. K.I. Popov, M.D. Maksimovic, J.D. Trnjancev, J. Appl. Electrochem., 11 (1981) 239.
182. N.A. Gjostein, in 'Metal Surfaces', American Society for Metals, Metals Park, Ohio (1963), chap.4.
183. T.B. Reddy, J. Electrochem. Soc., 113 (1966) 117.
184. W.H. Reinmuth, Anal. Chem., 33 (1961) 322.
185. D. Inman, M.P. Hills, T. Vargas, UK Patent Appln. 8303622.
186. C.A. Snavely, C.L. Faust, J. Electrochem. Soc., 97 (1950) 99.
187. P. Morisset, J.W. Oswald, C.R. Draper, R. Pinner, 'Chromium Plating', Robert Draper, Teddington, Middlesex, England (1954).
188. A.H. Sully, op.cit., chap.3.
189. Data Card No. 6-0694, Power Diffraction File: Inorganic Phases, JCPDS International Centre for Diffraction Data, Pennsylvania (1980).

190. D. Inman, T. Vargas, S. Duan, P. Dudley, in Spring Meeting of the Electrochemical Society, San Francisco, California (1983), (to be published).
191. M.P. Hill (CEGB), personal communication.
192. F.A. Lowenheim, op.cit., chap. 1.
193. A.R. Despic, K.I. Popov, J. Appl. Electrochem., 1 (1971) 275.